Characterizing the molecular mechanisms of mitochondrial fusion and division in healthy and diseased cells

Brittany N. Whitley

A dissertation

submitted in partial fulfillment of the

requirements for the degree of

Doctor of Philosophy

University of Washington

2019

Reading Committee:

Suzanne Hoppins, Chair

Dana Miller

Leo Pallanck

Program Authorized to Offer Degree:

Molecular and Cellular Biology

University of Washington

Abstract

Characterizing the molecular mechanisms of mitochondrial fusion and division in healthy and diseased cells

Brittany N. Whitley

Chair of the Supervisory Committee:

Suzanne Hoppins

Department of Biochemistry

Balanced mitochondrial fusion and division activity in healthy cells typically establishes a reticular mitochondrial network that is able to support normal cellular activities. Disruptions in balanced mitochondrial dynamics can occur through regulated changes in fusion and division to mediate physiological processes such as cell division and apoptosis. Additionally, imbalanced mitochondrial dynamics have been reported as both a cause and consequence of several neurodegenerative diseases. I begin with a discussion of imbalanced mitochondrial dynamics in disease and the therapeutic potential of drugs that target the mitochondrial fusion and division machines. While the causative role of mitochondrial dynamics has only been established in a subset of diseases, I discuss our current understanding of how aberrant mitochondrial dynamics influences neurodegenerative, cardiac and metabolic diseases.

I next discuss published work in which I characterized four mutations in the gene *DNM1L*, which encodes the mitochondrial division protein Drp1. All mutations were identified by whole exome sequencing in patients with neurological defects and mitochondrial dysfunction. To determine if the mutations were sufficient to cause mitochondrial hyperfusion, I expressed each of the four mutations in human and yeast cells lacking Drp1. I also evaluated mitochondrial morphology in wild type human and yeast cells expressing each mutant to determine if the division defects were dominant as is observed in human disease. A novel mutation in the GTPase domain of Drp1, G32A, was of particular interest as a compelling causal mutation that inhibits Drp1 recruitment to mitochondria.

Finally, I investigated the mechanism of mitochondrial fusion using phosphorylation mimicking and blocking mutations at a novel Mfn1 phosphorylation site, S228. My work suggests that phosphorylation of Mfn1 S228 inhibits mitochondrial fusion by inhibiting *trans* Mfn1 interactions and nucleotide-dependent Mfn1 assembly. I also describe *in vivo* mitochondrial clustering and hyperfusion in cells expressing Mfn1 S228E and discuss a model to reconcile differences between cellular phenotypes and biochemical fusion defects. This work will also be foundational to understand how one or more signaling pathways can influence Mfn1 S228 phosphorylation to coordinate mitochondrial morphology with cellular conditions. Together, my work has provided important insights into the relationship between mitochondrial dynamics and disease, specifically DNM1L-related neurodegeneration, as well as uncovered a possible regulatory mechanism to alter mitofusin activity based on cellular conditions.

Acknowledgements

I am certain that the work presented in this dissertation would not be possible without the support and guidance of several people. Thank you to the UW MCB program and Biochemistry department for giving me the opportunity to do the science I wanted in the place I wanted to do it. Special thanks to my MCB "mom," Maia Low- I truly don't know what I would do without you.

I thank my thesis advisor, Suzanne Hoppins, for getting me exciting about mitochondria and encouraging me to step outside of my comfort zone and think like a biochemist. I am especially thankful for the wonderful group of graduate students that you brought together in the lab- Nyssa Samanas, Emily Engelhart and Stephanie Sloat. Our scientific discussions at lab meetings and in between incubations have not only aided my experiments but made me a smarter and more creative scientist. I also thank my committee members, Doug Fowler, Dana Miller, Leo Pallanck and Yasemin Sancak, for their sustained support and guidance throughout my graduate career. I want to specifically thank Yasemin for her time and resources to develop the BN-PAGE protocol in our lab. I also thank my collaborators, Gennifer Merrihew, Mike MacCoss, Ian Glass and Christina Lam, for their hard work and guidance which has been important for driving this work forward. I thank my past scientific mentors- Thomas Friedman, Robert Morell, Ruth Tincoff and Mark Haussmann. To Mark, thank you for nurturing my scientific curiosity and research skills at a point in my career where I was laser-focused on medical school. I learned so much about being a better scientist, teacher and leader from you and continue to see the effects of your mentorship today.

My life outside of the lab has remained a source of love and sanity, even in the face of difficult experiments. I began graduate school with a phenomenal group of scientists, many of whom I have

celebrated holidays and birthdays with. I especially want to thank Abby "Abadabalone" Keller, Becca "Should-we-eat-these-berries?" Martin, Sophie "Master Sophie Money (MSM)" Archambault, and Lauren "L$$" Saunders. Thank you for bringing and keeping joy in my life. Finally, I want to thank my amazingly supportive family for truly exhibiting unconditional love as I periodically went MIA in fits of PhD stress. To my mom, I never would have gotten to this point without your love, support and good genes. I dedicate this to you, my best friend and greatest person I know.

List of Figures

List of Tables

Table of Contents

Chapter One:

Chapter Two:

Chapter Four:

Chapter One:

Mitochondrial dynamics and their potential as a therapeutic target

Summary

Most of the text in this chapter has been primarily copied from a review that was published as part of a special issue on mitochondrial dynamics in Mitochondrion (Whitley et al., 2019). I have added an additional discussion section preceding the review, as well as supplemental information and discussion throughout the main text.

Mutations in the genes that encode the mitochondrial division and fusion proteins, *DNM1L*, *MFN2* and *OPA1*, have been causally linked to a series of primarily neurodegenerative disorders using cellular and animal models. Despite varying clinical presentations, these diseases typically have the most dramatic effects in metabolically active, mitochondria-dense tissues such as the brain, skeletal muscle and eye. While several novel *DNM1L* variants have been recently identified via whole exome sequencing, only three of these variants (G32A, A395D, R403C) have been experimentally validated as necessary and sufficient to cause disease (Chang et al., 2010; Fahrner et al., 2016; Waterham et al., 2007; Whitley et al., 2018). In many cases, mitochondrial morphology in patient fibroblasts is used as a proxy to infer Drp1 function across cell types, but this alone is insufficient to determine causation. The importance of establishing a causal role for *DNM1L* mutations in disease was highlighted in our recent study (Whitley et al., 2018). Whole exome sequencing identified a point mutation in *DNM1L* (Drp1 C431Y) in a patient with severe neurological dysfunction leading to death within ten months of birth. Through expression of Drp1 C431Y in human and yeast cells, we found little evidence that Drp1 C431Y dramatically altered mitochondrial shape. From this, I concluded that either our non-neuronal model system could not detect the relevant patient phenotypes in this case

or that the *DNM1L* point mutation was misidentified as the driver of disease in this patient. In chapter two, I discuss in detail our published work in which I characterized four *DNM1L* mutations in total. Future work can validate and expand upon these findings by evaluating mitochondrial morphology and function in skeletal and neuronal tissue, as well as determining the mechanism by which mutations inhibit mitochondrial division activity.

Unlike *DNM1L*-related diseases, mutations in *MFN2* are associated with a common neurodegenerative disease- Charcot Marie Tooth Type 2A (CMT2A). The specificity for Mfn2 over Mfn1 in CMT2A may result from the relatively high expression of Mfn2 in neurons. Mfn2 also performs several other cellular functions independently of Mfn1, which may or may not be dependent on its fusion activity. Current models for neurodegeneration in CMT2A hypothesize that inhibited mitochondrial fusion and/or transport drives axonal degeneration and cell death in long, peripheral neurons. Cellular models of CMT2A have variable effects ranging from mitochondrial fragmentation to clustering, suggesting that the location of point mutations on Mfn2 or the severity of the substitution may influence disease outcomes.

In the unpublished work discussed in chapter three, I describe the biochemical and cellular characterization of Mfn1 S228E as a model for the expected effects of Mfn1 S228 phosphorylation on the mitochondrial fusion activity of Mfn1. While this project is primarily intended to understand the physiological regulation of mitofusins in healthy cells, there is evidence that aberrant phosphoregulation of mitochondrial dynamic proteins is associated with disease (Ferreira et al., 2019; Roe & Qi, 2018). Based on the inhibitory role of Mfn1 S228 phosphorylation in our fusion model, I would expect that altered signaling could increase Mfn1 S228 phosphorylation to promote

mitochondrial fragmentation in diseased cells. Additionally, a specific mutation at the conserved position on Mfn2 (Mfn2 S249F) has been associated with CMT2A in two unrelated families. Future work is required, however, to determine if this mutation acts under a similar or unique mechanism to Mfn1 phosphorylation.

Abnormal mitochondrial morphology has also been observed in several human diseases with diverse genetic and environmental causes. This review aims to outline our current understanding of the relationship between aberrant mitochondrial dynamics and disease. We conclude that, even in diseases not caused by aberrant fusion or division activity, there appears to be broad therapeutic potential in reestablishing balanced mitochondrial dynamics in diseased cells. Additional mechanistic research is required, however, to understand the causative and secondary roles of mitochondrial dynamics in disease in many cases.

Introduction

Mitochondrial structure and function vary remarkably across different cell and tissue types (Kuznetsov et al., 2009). The structure of the mitochondrial network changes through fusion, division and transport based on cellular needs **(Figure 1.1)**. The balance between fusion and division is required to support the metabolic functions of mitochondria that power diverse cellular processes (Wai and Langer, 2016). For example, mitochondrial dynamics change during the cellular response to stress (Eisner et al., 2018). In some conditions that adversely impact cellular health, such as nutrient limitation (Gomes et al., 2011) or modest inhibition of cytosolic protein synthesis (Tondera et al., 2009), the mitochondrial network becomes highly interconnected, which facilitates ATP production and promotes cell survival. Mitochondria are also integrated into cell cycle progression and cell

death pathways, placing them at the heart of cellular life and death decisions (Horbay and Bilyy, 2016; Kalkavan and Green, 2018; Otera and Mihara, 2012; Salazar-Roa and Malumbres, 2017). In proliferating cells, increased mitochondrial division prior to mitosis fragments the network to facilitate mitochondrial inheritance during cell division, while decreased division upon entry to S-phase results in a more highly connected network (Mitra et al., 2009; Taguchi et al., 2007). High levels of DNA damage, on the other hand, activate apoptotic pathways and induce mitochondrial fragmentation (Frank et al., 2001; Karpinich et al., 2002). Together, the complex regulation of mitochondrial dynamics is essential to facilitate diverse cellular functions.

Mitochondrial dynamics are required during development, particularly in the heart (Dorn et al., 2015; Gong et al., 2015) and brain (Flippo and Strack, 2017), and also have a role in stem cell self-renewal and differentiation (Chen and Chan, 2017; Seo et al., 2018). Consistent with this, diseases caused by loss or dysfunction of the mitochondrial fusion or division machines are broadly characterized by developmental delays and neurodegeneration (Bertholet et al., 2016; Burté et al., 2015). Many other diseases with diverse genetic and environmental causes are associated with altered mitochondrial shape, including common neurodegenerative diseases (Gao et al., 2017), heart failure (Brown et al., 2017), diabetes (Rovira-Llopis et al., 2017), and cancer (Trotta and Chipuk, 2017). In some cases, disease-associated changes in mitochondrial structure can be attributed to altered expression of the mitochondrial fusion and division proteins. In other cases, aberrant signaling pathways are predicted to alter mitochondrial dynamics. In either case, aberrant mitochondrial structure is associated with mitochondrial dysfunction, which contributes to disease pathology.

Balanced mitochondrial fusion and division activity is associated with several aspects of mitochondrial function. The inheritance and integrity of the mitochondrial genome (mtDNA), which encodes essential components of the electron transport chain, depends on regulated changes in mitochondrial dynamics to segregate dysfunctional mitochondria from the rest of the network (Chen et al., 2010; Mishra and Chan, 2014; Burman et al., 2017; Chen and Dorn, 2013; Narendra et al., 2008; Song et al., 2015). Aberrant mitochondrial structure and accumulation of mutations in mtDNA are both reported to increase with age and have been hypothesized to contribute to declining mitochondrial and cellular function (Sun et al., 2016). In diseased cells with either excessive mitochondrial fusion or fragmentation, I expect an accumulation of mtDNA mutations over time, which should reduce respiratory capacity and ultimately cellular function. Changes in mitochondrial shape are also strongly associated with cell fate decisions. In some cases, preventing mitochondrial fragmentation can reduce cellular sensitivity to apoptotic signals (Cereghetti et al., 2010). However, cancer cells are an exception to this general trend, as mitochondrial fragmentation in cancer is associated with metabolic changes that support rapid growth and survival (Anderson et al., 2018; Inoue-Yamauchi and Oda, 2012). Through a stronger mechanistic understanding of the role of mitochondrial dynamics in disease, it will become easier to understand and exploit the potentially broad clinical applications of altering mitochondrial dynamics. In particular, treatments that re-establish the balance of fusion and division might improve cellular function and survival, leading to improved patient outcomes.

Given the critical role of mitochondrial structure and function in cellular physiology, mitochondrial dynamics have been targeted in several disease model systems utilizing both genetic and pharmacological approaches to restore balanced mitochondrial fusion and division (Archer, 2013;

Flippo and Strack, 2017; Suárez-Rivero et al., 2016; Wai and Langer, 2016). In fact, genetic manipulation to rebalance mitochondrial dynamics in a mouse model of cardiomyopathy has been shown to improve tissue function and extend lifespan (Chen et al., 2015). Genetic therapies have altered the expression of the genes encoding mitochondrial fusion and division proteins to rebalance mitochondrial dynamics. Chemical therapeutics have targeted known elements of the mitochondrial fusion and division mechanisms, including their enzymatic activity, protein-protein interactions, and post-translational modifications (PTMs). In this review, we first present an overview of the mechanisms of mitochondrial division and fusion to provide a framework for describing existing and potential therapeutic approaches. We then discuss approaches to restore mitochondrial dynamics in model systems that target abnormal expression of the mitochondrial fusion and division machines and finally the development of small molecules that affect the activity of these proteins. We conclude with a brief discussion of other potential druggable targets that could improve mitochondrial structure and function in disease states.

The mitochondrial division machine, Drp1.

Mitochondrial division requires the coordinated action of many factors (Kraus and Ryan, 2017). Division occurs primarily at mitochondria-ER contact sites (Friedman et al., 2011) where actin-mediated constriction of the mitochondria activates downstream steps in the division pathway (Moore and Holzbaur, 2018). These mitochondria-ER contact sites also couple mtDNA synthesis to mitochondrial division, facilitating the distribution of mtDNA (Lewis et al., 2016). Dynamin-related protein 1, Drp1, is a large GTPase required for mitochondrial division from yeast to mammals (Bleazard et al., 1999; Labrousse et al., 1999; Smirnova et al., 2001). Drp1 is recruited to the mitochondrial outer membrane by resident protein receptors including Mff, Fis1, MiD49, and MiD51

(Losón et al., 2013). Higher order assembly of Drp1 at mitochondrial constriction sites is stimulated by cardiolipin (Francy et al., 2017) to form large helical structures (Clinton et al., 2016; Fröhlich et al., 2013). Nucleotide binding and hydrolysis by Drp1 promote its assembly, conformational changes and disassembly to drive mitochondrial division (Kalia et al., 2018). In some cases, Dynamin-2 may also be required to further constrict the mitochondria following Drp1 (Kamerkar et al., 2018; Lee et al., 2016).

The Drp1 receptor proteins, Mff, Fis1, MiD49 and MiD51, are functionally distinct. MiD49 and MiD51 can act independently from Fis1 and Mff in Drp1 recruitment (Losón et al., 2013; Palmer et al., 2013). Loss of both MiD49 and Mff was more severe than loss of either one alone, suggesting that these receptors impact division in distinct ways (Osellame et al., 2016). MiD49 and MiD51, but not Mff, have also been implicated in cristae remodeling during apoptosis (Otera et al., 2016). Notably, the role of Fis1 in Drp1-mediated mitochondrial division has recently been challenged as new evidence suggests that Fis1 does not interact with Drp1, but with components of the fusion machine to inhibit their activity (Osellame et al., 2016; Yu et al., 2019).

Post-translational modification of Drp1 and its mitochondrial receptors, Mff and MiD49, promotes rapid changes in mitochondrial division activity based on cellular needs. Drp1 assembly and GTPase activity can be stimulated by nitrosylation of its C-terminal GTPase effector domain (Cho et al., 2009). Phosphorylation and SUMOylation of Drp1 regulate the activity and mitochondrial recruitment of cytosolic Drp1 (Otera et al., 2013). Drp1 phosphorylation by Cdk1 at S616 promotes mitochondrial fragmentation during mitosis (Taguchi et al., 2007). Other kinases such as MAPK, Cdk5 and CAMKII can also phosphorylate Drp1-S616 to promote mitochondrial division, which has been associated

with tumor growth (Kashatus et al., 2015; Serasinghe et al., 2015), as well as cell death in neurons (Guo et al., 2018) and heart (Shangcheng Xu et al., 2016). PKA-mediated phosphorylation of Drp1-S637 inhibits its activity (Chang and Blackstone, 2007; Cribbs and Strack, 2007), while calcineurin-mediated dephosphorylation of S637 promotes division by recruiting Drp1 to the mitochondria (Cereghetti et al., 2008; Cribbs and Strack, 2007). Interestingly, phosphorylation of S637 by CaMK1α (Han et al., 2008) and ROCK1 (Wang et al., 2012) increased division activity, suggesting that in addition to the site of phosphorylation, the cellular context influences how phosphorylation affects Drp1 activity.

Drp1 can also be modified by different SUMO paralogs (SUMO-1 or SUMO-2/3). During apoptosis, SUMOylation of Drp1 with SUMO-1 promotes mitochondrial division by stabilizing Drp1 on the mitochondria (Harder et al., 2004; Prudent et al., 2015; Wasiak et al., 2007). In contrast, removal of SUMO-2/3 from Drp1 by SENP3 also increased division by promoting the interaction of Drp1 with Mff (Guo et al., 2017). The interaction of Mff and Drp1 is also regulated by phosphorylation. Mitochondrial division was stimulated by AMPK-mediated phosphorylation of Mff, which promoted Drp1 recruitment to mitochondria (Toyama et al., 2016). Finally, mitochondrial division activity can be modulated by ubiquitination of Drp1 (Horn et al., 2011; H. Wang et al., 2011) and its receptor MiD49 (Cherok et al., 2017; S. Xu et al., 2016), which promotes protein turnover and therefore reduced division activity. Together, the distinct post-translational modifications of Drp1 and its receptors highlight how mitochondrial division is integrated with numerous cellular pathways.

<u>The mitochondrial fusion machines, Mitofusin and Opa1.</u>

Outer membrane fusion

Mitochondrial fusion is also mediated by dynamin-related GTPase proteins. Mitofusin 1 (Mfn1) and mitofusin 2 (Mfn2) mediate mitochondrial outer membrane fusion in vertebrates (Chen et al., 2003; Santel and Fuller, 2001). Mfn2 has also specifically been implicated in mitochondria-ER contact site formation and stability (de Brito and Scorrano, 2008; Filadi et al., 2015; Naon et al., 2016), mitochondria-lipid droplet interactions (Boutant et al., 2017), cellular proliferation (Chen et al., 2014; 2004), metabolic signaling (Bach et al., 2003; Zorzano et al., 2015), and mitophagy (McLelland et al., 2018). The topology of the Mitofusin proteins is under debate. Recent biochemical analyses are consistent with a single transmembrane domain resulting in the C-terminus residing in the intermembrane space (Mattie et al., 2018), while the structural data for the Mitofusin suggests that the C-terminus is a component of the helical bundle proximal to the GTPase domain in the cytoplasm (Cao et al., 2017; Y. Qi et al., 2016; Yan et al., 2018). Mitochondrial fusion is most efficient when both Mitofusin paralogs are present, indicating that they are functionally distinct (Chen et al., 2003; Detmer and Chan, 2007; Hoppins et al., 2011a). Mitofusin proteins are predicted to initiate fusion in a membrane tethering step through interactions between proteins on opposing membranes of a fusion pair (Hoppins et al., 2011b; Ishihara et al., 2004). Atomic resolution structures of a partial Mfn1 construct suggest that an intermolecular interface of the globular GTPase domains mediates tethering (Cao et al., 2017; Yan et al., 2018). An alternative model proposes that a helix in the mitofusin C-terminal region (HR2) acts as a mitochondrial tether (Franco et al., 2016; Koshiba et al., 2004). However, this is based primarily on data from an isolated Mfn1 HR2 domain construct, outside of the context of full-length mitofusin (Koshiba et al., 2004). Biochemical analysis indicates that Mitofusins assemble into higher order oligomers when incubated with nucleotide (Ishihara et al., 2004; Karbowski et al., 2006; Pyakurel et al., 2015; Shutt et al., 2012). Although the role of Mitofusin

assembly in membrane fusion is not well defined, visualization of tethered mitochondria by electron cryo-tomography suggests that Fzo1, the yeast Mitofusin homolog, forms a tethering ring that precedes mitochondrial outer membrane fusion (Brandt et al., 2016).

Post-translational modification of the Mitofusins regulates both protein turnover and activity. Acetylation of Mfn1 at K222 and K491 led to increased mitochondrial fragmentation and oxidative damage (Lee et al., 2014), as well as Mfn1 ubiquitination (Park et al., 2014). Deacetylation of Mfn1 in response to glucose withdrawal was associated with highly connected mitochondrial networks and improved mitochondrial function (Lee et al., 2014). Mfn1 phosphorylation at multiple sites can also inhibit fusion activity through distinct mechanisms (Ferreira et al., 2019; Pyakurel et al., 2015). Phosphorylation of Mfn1 at S86 by beta II protein kinase C (ßIIPKC) significantly increases during heart failure, which is associated with reduced in vivo GTPase activity and increased mitochondrial fragmentation (Ferreira et al., 2019). ERK phosphorylation of Mfn1 at T562 attenuated Mfn1 assembly and increased its interaction with the pro-apoptotic protein, Bak, which together inhibited fusion and promoted cell death (Pyakurel et al., 2015). Finally, mitochondrial fusion activity can be modulated by both phosphorylation of Mfn2 (Chen and Dorn, 2013) and ubiquitination (Covill-Cooke et al., 2018). Mfn2 ubiquitination has also been implicated in mitochondrial-ER contact site remodeling and increased mitophagy, although the mechanism by which ubiquitin alters mitochondrial-ER contact sites is disputed (Basso et al., 2018; McLelland et al., 2018; Sugiura et al., 2013). Therefore, PTMs of Mitofusins also serve to regulate their activity and integrate mitochondrial dynamics into a variety of cellular pathways.

Inner membrane fusion

Mitochondrial outer membrane fusion is spatially and temporally coupled to inner membrane fusion (Cipolat et al., 2004; Liu et al., 2009). The dynamin-related GTPase Optic atrophy 1 (Opa1) is required for inner membrane fusion (Olichon et al., 2003; Song et al., 2007). Multiple forms of Opa1 are found in different tissues due to alternative splicing and proteolytic processing by the inner membrane peptidases Oma1 and Yme1, which generate two topologically distinct isoforms of Opa1. The unprocessed long form (Opa1-L), is anchored to the inner membrane and the cleaved form lacks the transmembrane domain, generating short, soluble form in the intermembrane space (Opa1-S). While some studies suggest that both Opa1-L and Opa1-S are required for inner membrane fusion (Song et al., 2007), recent data indicate that Opa1-L and cardiolipin are sufficient to mediate membrane fusion (Anand et al., 2014; Ban et al., 2017). Opa1 is primarily regulated through its proteolytic cleavage by inner membrane proteases whose activities are altered by ATP and membrane potential. The increased proteolytic processing of Opa1 inhibited fusion and was proposed to function as a mechanism to sequester damaged mitochondria from the network for turnover (Ehses et al., 2009; Griparic et al., 2007; Head et al., 2009; Mishra et al., 2014; Song et al., 2007). In addition to its role in membrane fusion, Opa1 is also important for maintaining the organization and structure of the mitochondrial inner membrane (Frezza et al., 2006; Olichon et al., 2003). Therefore, modulating Opa1 activity could impact both the connectivity of the mitochondrial network and inner membrane structure, which both influence mitochondrial functions in health, such as oxidative phosphorylation, and in disease, such as membrane permeabilization during apoptotic cell death.

<u>Genetic models of disease and therapeutic approaches.</u>

Loss of fusion or division activity as the primary cause of human disease

Diseases caused by loss of fusion and division activity share common clinical features, including developmental defects and neurological dysfunction. Consistent with a vital role for mitochondrial dynamics during development, homozygous deletion of *MFN1, MFN2, OPA1 or DNM1L* in mice does not support viable embryonic development (Chen et al., 2003; Davies et al., 2007; Ishihara et al., 2009). Placental defects likely contributed to embryonic lethality in Mfn2 and Drp1 knockout mice (Chen et al., 2003; Wakabayashi et al., 2009), while cardiac and neuronal developmental defects were also observed Drp1 knockout embryos (Wakabayashi et al., 2009). The impact of imbalanced mitochondrial dynamics on neuronal development is emphasized by the perinatal lethality after pan-neuronal (Ishihara et al., 2009) or cerebellar knockout (Wakabayashi et al., 2009) of *DNM1L* in the mouse brain. While mice died primarily from a suckling defect, giant mitochondria were aggregated in neuronal cell bodies, which was associated with impaired synapse formation (Ishihara et al., 2009; Wakabayashi et al., 2009).

Human mutations in *DNM1L* impair Drp1 enzymatic activity, assembly and mitochondrial recruitment and cause a range of diseases characterized broadly by developmental delays and neurological dysfunction (Chang et al., 2010; Chao et al., 2016; Fahrner et al., 2016; Sheffer et al., 2016; Vanstone et al., 2016; Waterham et al., 2007; Whitley et al., 2018; Zaha et al., 2016). Cells isolated from patients with *de novo*, heterozygous DNM1L mutations had elongated and extensively connected mitochondria (Sheffer et al., 2016; Vanstone et al., 2016; Waterham et al., 2007; Whitley et al., 2018; Zaha et al., 2016) that mirrored the morphology observed in MEFs lacking Drp1 (Wakabayashi et al., 2009). Expression of mutant Drp1 variants in wild type cells interfered with normal division activity, consistent with the dominant inheritance pattern (Chang et al., 2010; Fahrner et al., 2016; Waterham

et al., 2007; Whitley et al., 2018). Elongated, or highly fused mitochondria are also observed in diseases caused by mutations in the genes encoding the Drp1 receptors Mff (MFF) (Koch et al., 2016; Nasca et al., 2018; Shamseldin et al., 2012) and MiD49 (MIEF2) (Bartsakoulia et al., 2018). Mutations in MFF are associated with developmental delay, Leigh Syndrome-like neuropathy (Koch et al., 2016; Nasca et al., 2018; Shamseldin et al., 2012), and cardiomyopathy (Chen et al., 2015) while a recently reported mutation in *MIEF2* was associated with skeletal muscle dysfunction instead of neuronal dysfunction (Bartsakoulia et al., 2018).

Mutations in *MFN2* cause the peripheral, sensorimotor neuropathy Charcot Marie Tooth Syndrome Type 2A (CMT2A) (Barbullushi et al., 2019; Stuppia et al., 2015; Züchner et al., 2004). In addition to altered mitochondrial fusion, some of the neuronal defects in CMT2A models have been attributed to impaired mitochondrial transport and distribution in cultured rodent (Baloh et al., 2007; Misko et al., 2010) and fly neurons (Fissi et al., 2018). Molecular characterization in model systems suggest that Mfn2 disease-associated variants may fall into unique functional classes that differently alter mitochondrial structure (Detmer and Chan, 2007; Fissi et al., 2018). In cell culture models of CMT2A, Mfn1 expression rescued morphological (Detmer and Chan, 2007) and transport (Misko et al., 2010) defects in a subset of Mfn2 CMT2A mutant variants. Recently, expression of Mfn1 was shown to rescue the neurodegenerative phenotype in mice expressing a CMT2A mutant variant of Mfn2 (Zhou et al., 2019). The promise of treating CMT2A with gene therapies that increase Mfn1 suggests that the total level of functional mitofusins may be more relevant than mitofusin identity (Mfn1 vs. Mfn2), although more work across different cell types is required to verify this relationship. Charcot Marie Tooth (CMT) disease is one of the most common inherited neurological disorders, with several distinct classes and many different genes that are mutated in patients. Gene therapies targeting

other CMT neuropathies have alleviated cellular dysfunction caused by either dominant-negative alleles (Kagiava et al., 2018) or haploinsufficiency (Sahenk et al., 2014), suggesting that targeting mitofusin levels could be a viable disease treatment for CMT2A.

Neuronal degeneration in dominant optic atrophy (DOA) is caused by mutation or heterozygous loss of *OPA1* (Alavi et al., 2009; Chun and Rizzo, 2016; Kushnareva et al., 2016; Sarzi et al., 2012). Knock-in of a common, non-functional DOA-causing *OPA1* variant, $OPA1^{delTTAG}$ caused progressive degeneration of the retinal ganglion cells (RGCs) in mice. RGC degeneration was rescued by exogenous expression of wild type *OPA1* in the surviving neurons of these $Opa1^{+/delTTAG}$ mice (Sarzi et al., 2018). Optic atrophy is also associated with a mutation in *YME1L*, which encodes one of the inner membrane proteases that cleaves Opa1-L. In this patient, *YME1L* missense mutations resulted in instability of Yme1 protein, causing improper Opa1 processing and mitochondrial fragmentation (Hartmann et al., 2016).

As exome sequencing has become more feasible and widely used, amino acid substitutions in mitochondrial fusion proteins have been associated with additional diseases. Missense mutations in *OPA1* have recently been linked to a type of parkinsonism (Carelli et al., 2015) and an *MFN2* polymorphism was associated with Alzheimer's disease in a large Korean population (Y. Kim et al., 2017). Additionally, mutations in another pro-fusion factor, *MSTO1*, have been recently associated with increased mitochondrial fragmentation, myopathy and ataxia (Gal et al., 2017; Nasca et al., 2017), providing additional support for the important role for mitochondrial dynamics in disease.

Evidence for the role of imbalanced mitochondrial dynamics in neurological disorders

Many of the diverse human diseases that are associated with aberrant mitochondrial structure and function have been recapitulated in genetic models. In neurons, mitochondrial dynamics support energy production and calcium buffering at synapses through directed and regulated transport mechanisms (Flippo and Strack, 2017). Cerebellar knockout of *DNM1L* in post-mitotic cells resulted in mitochondrial dysfunction and neuronal degeneration, leading to an age-related loss of motor coordination (Kageyama et al., 2012). Similarly, loss of Mfn2 in cerebellar neurons leads to dendrite degeneration and cell death (Chen et al., 2007). Abnormal, fragmented mitochondria are observed in neurodegenerative disease models with diverse genetic and environmental causes, including Parkinson's disease (PD) (Park et al., 2018), Huntington's disease (HD) (Reddy, 2014), Alzheimer's disease (AD) (Kandimalla and Reddy, 2016) and amyotrophic lateral sclerosis (ALS) (Smith et al., 2017). Several lines of clinical evidence support the hypothesis that mitochondrial division activity predominates over fusion activity in neurodegenerative disease. First, increased Drp1 expression and reduced Mitofusin and Opa1 mRNA and protein levels have been reported in samples obtained from the brain tissue of patients with AD (Manczak et al., 2011) and HD (Kim et al., 2010). Drp1 interactions with tau (Manczak and Reddy, 2012) and mutant huntingtin (Song et al., 2011) both stimulated its enzymatic activity. Consistent with a role in disease pathology, enhanced interactions between Drp1 and huntingtin or tau were observed in human patients with HD (Shirendeb et al., 2012) and AD (Manczak and Reddy, 2012), respectively. Finally, reduced levels of Mitofusin and Opa1 are also correlated with symptom onset and disease progression in HD (Kim et al., 2010) and ALS (Liu et al., 2013). Therefore, unbalanced mitochondrial fusion and division likely contribute to mitochondrial dysfunction and cellular degeneration in these diseased states.

Genetic approaches to decrease Drp1 expression or activity, and therefore increase mitochondrial connectivity, have been applied to a number of neurodegenerative disease models (**Table 1.1**). For example, expression of a dominant negative variant of Drp1 by neuronal adenovirus injection successfully reduced dopaminergic neuron degeneration in both genetic and environmental PD mouse models (Rappold et al., 2014). Reduction of Drp1 levels by crossing $Drp1^{+/-}$ mice with genetic mouse models of AD also reduced mitochondrial dysfunction and neurodegeneration (Kandimalla et al., 2016; Manczak et al., 2016). Inhibition of Drp1 phosphorylation (Kim et al., 2016; Yan et al., 2015) was also protective against neurodegeneration in an AD model, likely due to reduced Drp1 recruitment to mitochondria. These data highlight that aberrant mitochondrial structure and function contributes to multiple types of neuronal dysfunction and indicate that reduced Drp1 expression or activity are both appealing therapeutic approaches.

Evidence for the role of imbalanced dynamics in cardiac dysfunction

As with neurons, the high metabolic demand of the heart requires balanced mitochondrial dynamics for normal function. Heart failure in humans is associated with reduced protein levels of Mfn2 and Opa1 (Ahuja et al., 2013; Chen et al., 2009). Levels of Mfn1, Mfn2, Opa1 and Drp1 are also altered in hypertrophy-related heart failure (Fang et al., 2007; Javadov et al., 2011; Tang et al., 2014). In a screen for genetic modifiers of congestive heart failure, a mutation in *DNM1L* was associated with dilated inherited cardiomyopathy and impaired Drp1 disassembly (Ashrafian et al., 2010; Cahill et al., 2016). Additionally, several conditional knockouts of *DNM1L* in the mouse heart caused mitochondrial elongation and impaired mitochondrial function, which was associated with reduced cardiac function and survival (Ikeda et al., 2015; Ishihara et al., 2015; Kageyama et al., 2014). Mitochondrial division is also required for cardiac function after development. Cardiac-specific loss

of Drp1 in adult mice caused mitochondrial elongation and dysfunction, similar to the mitochondrial defects observed in embryonic *DNM1L* knockouts (Ikeda et al., 2015). Impaired mitochondrial fusion activity is also detrimental to cardiac function, as heart-specific knockdown (Dorn et al., 2011) and knockout (Chen et al., 2011) of the outer membrane fusion DRP led to mitochondrial fragmentation and cardiac dysfunction in flies and mice, respectively. Conditional knockout of the Mitofusins in adult mouse hearts resulted in similar cellular dysfunction and led to rapidly progressive cardiomyopathy (Chen et al., 2011). Cardiac dysfunction was also reported in $Opa1^{+/-}$ mice (Chen et al., 2012) and in a mouse model harboring a cardiac-specific deletion of the Opa1-processing protease, *YME1L*, where improper Opa1 processing was associated with cardiomyopathy and heart failure (Wai et al., 2015). Interestingly, concomitant deletion of Oma1 in the *YME1L* mutants rebalanced Opa1 processing and led to improved mitochondrial morphology and cardiac function (Wai et al., 2015). Together, these models illustrate the important role of mitochondrial fusion and division in heart development and function.

The importance of balanced mitochondrial dynamics in cardiac function is supported by genetic mouse models. The cardiomyopathy-related defects in Mff knockout mice can be significantly rescued by concomitant deletion of *MFN1* (Chen et al., 2015). Similarly, the cardiac defects in a triple knockout mouse ($Mfn1^{-/-}$, $Mfn2^{-/-}$, $Drp1^{-/-}$) are unique and less severe than any of the single knockouts (Song et al., 2017). The relationship between mitophagy and mitochondrial dynamics is unique in the heart. Specifically, loss of mitochondrial division was associated with increased mitophagy despite the highly connected network, while the fragmented mitochondria that result from loss of mitochondrial fusion were resistant to mitophagic turnover. These data suggest that in some tissues, balanced fusion and division is more important to maintain function than the absolute rate of fusion or division.

The protective effects observed in these models supports the argument that targeting the balance of mitochondrial dynamics may be a promising therapeutic approach (**Table 1.1**).

While loss of fusion activity is generally associated with mitochondrial and cardiac dysfunction, some models of *MFN1* and/or *MFN2* genetic ablation exhibit protective effects (**Table 1.1**). Cardiac-specific knockout of one or both Mitofusins was associated with attenuated cell death and increased survival during ischemic-reperfusion (IR) injury (Hall et al., 2016; Papanicolaou et al., 2011). Additionally, conditional knockdown of Mfn2 in the proximal tubules of the kidney was protective against cell death after renal IR injury (Gall et al., 2015; 2012). It could be that the loss of Mfn2 can be protective in the short-term due to increased cellular proliferation (Chen et al., 2014), while prolonged reduction of Mfn2 may lead to more serious cardiomyopathy defects due to a lack of fusion (Gall et al., 2015).

Evidence for the role of imbalanced dynamics in metabolic disease

Genetic approaches have also addressed imbalanced mitochondrial dynamics associated with metabolic sensing and signaling in type 2 diabetes (Kelley et al., 2002; Toledo et al., 2006; Williams and Caino, 2018) (**Table 1.1**). Loss of Drp1 in podocytes reduced diabetic nephropathy in mice that had already developed diabetes (Ayanga et al., 2016), suggesting that increased mitochondrial division activity or reduced mitochondrial fusion activity is associated with metabolic dysfunction. Surprisingly, while mitochondrial fragmentation is typically observed in unhealthy cells with high fat-induced insulin resistance, there appears to be an unexpectedly protective role of mitofusin deletion in adipose and liver cells. *MFN2* deletion in adipose tissue was protective against diet-induced insulin resistance (Boutant et al., 2017) and mice with a liver specific deletion of *MFN1* were

protected against high fat induced insulin resistance (Kulkarni et al., 2016). Similarly, in a distinct disease model of nonalcoholic fatty liver disease, liver-specific knockout of *OPA1* reduced the formation of giant mitochondria and partially rescued defects associated with a fatty liver (Yamada et al., 2018).

In sum, the genetic models discussed demonstrate the critical role of balanced mitochondrial dynamics during development and through adulthood. It is clear that neither fusion nor division activity is inherently healthy or pathological, but rather that the establishment of a minimal level of balanced mitochondrial fusion appears to be important for mitochondrial and cellular health. Consequently, aberrant mitochondrial dynamics are associated with tissue dysfunction in a wide range of human diseases. In these model systems, genetic approaches that re-establish balanced fusion and division indicate that genetic therapy may be a viable approach to improve patient health in disease.

Altering mitochondrial division activity with small molecules

Mitochondrial dynamics have also been rebalanced through the application of small molecules that alter Drp1 activity. In diseases characterized by excessive mitochondrial fragmentation, small molecule inhibition of Drp1 has effectively improved function and cell survival in several diverse disease models (**Table 1.2**). There appear to be two common factors that improve upon restoration of mitochondrial connectivity: mitochondrial metabolic function and reduced susceptibility to cell death signals. It is likely that by impacting these core mitochondrial functions, disease progression is slowed, and health is improved.

Both the enzymatic activity of Drp1 and its recruitment to mitochondria have been modulated by small molecules. To date, several biochemical screens for enzymatic inhibitors of Drp1 have been performed. Dynasore was an early drug identified that inhibited GTPase activity of dynamin and Drp1, but not the related DRP, MxA, or the small GTPase, Cdc42 (Macia et al., 2006). While Dynasore is not a viable therapeutic given the non-specific inhibition of both Drp1 and dynamin, its discovery established that the DRP family can be effectively targeted by small molecules. Soon after Dynasore was characterized, mdivi-1 was identified as a specific inhibitor of the yeast mitochondrial division protein, Dnm1 (Cassidy-Stone et al., 2008). Unlike Dynasore, mdivi-1 specifically inhibited the GTPase activity of Dnm1 and abolished its assembly in vitro. Furthermore, treatment of Cos7 cells with mdivi-1 resulted in mitochondrial elongation and enhanced resistance to apoptotic stimuli, which are both consistent with the conclusion that the drug inhibited mammalian Drp1 activity. While mdivi-1 has been utilized extensively in various disease models, the mechanism of mdivi-1 activity has recently been challenged (Bordt et al., 2017). This group reported that mdivi-1 did not elongate mitochondria in cell culture, but instead inhibited complex I activity and ROS generation, which could explain its therapeutic effects. The reason for the different effects on mitochondrial structure in various studies is not clear. Further characterization of mdivi-1 is required to determine its mechanism of action and its potential as a therapeutic to treat human disease.

Despite the controversial mechanism of mdivi-1, its direct or indirect effects on mitochondrial morphology can be examined to infer how changes in mitochondrial structure and function can alter disease outcomes. Therefore, we only discuss studies in which mdivi-1 has been specifically reported to restore mitochondrial morphology in disease models associated with excessive mitochondrial

division. In neurons, several lines of evidence indicate that mdivi-1 is a promising therapeutic to attenuate neuronal cell death in neurodegenerative disease and neurotoxicity models. Both apoptosis and mitophagy were inhibited by mdivi-1 treatment using in vitro genetic and environmental PD models (Alaimo et al., 2014; Cui et al., 2010; Solesio et al., 2012). Similarly, mdivi-1 treatment of in vitro neuronal models for AD restored the mitochondrial dynamic balance and alleviated mitochondrial dysfunction associated with excessive amyloid beta-induced autophagy (Gan et al., 2014; Kim et al., 2016). Furthermore, mouse models of PD and AD showed improved behavior outcomes and reduced neurodegeneration following mdivi-1 treatment (Bido et al., 2017; Wang et al., 2017), suggesting that the functional benefits of mdivi-1 treatment extend beyond the cellular level. While the mechanism of neurodegeneration in the peripheral neuropathy hereditary spastic paraplegia (HSP) is not well understood, cells derived from HSP patients had dysfunctional mitochondria, characterized by the prevalence of few, short, mitochondria with low membrane potential (Denton et al., 2018). Treatment with mdivi-1 suppressed major disease symptoms in these neurons, including neurite growth defects and neuronal cell death (Denton et al., 2018). Stress-induced neuronal apoptosis has also been observed in pediatric anesthesia models and cell death was alleviated by mdivi-1 treatment (Gao et al., 2018; Liu et al., 2017; F. Xu et al., 2016). Application of mdivi-1 also reduced neuronal death after prolonged seizure activity (Kim and Kang, 2017), traumatic brain injury (Wu et al., 2018), and spinal injury (X. Chen et al., 2018; Lin et al., 2017). Finally, the cognitive dysfunction (Zhao et al., 2018) and neuronal death caused by disrupted glucose regulation in diabetic individuals (Huang et al., 2015; S. Kim et al., 2017) can be partially rescued by mdivi-1 treatment. Together, these studies suggest that improved mitochondrial function improves disease outcome in a wide range of neurodegenerative disorders.

Mitochondrial dysfunction is a common feature of a range of cardiovascular diseases and therefore mitochondrial dynamics represent a potentially powerful therapeutic target (Brown et al., 2017). Consistent with this, mdivi-1 partially rescued cardiac dysfunction in diverse mouse cardiomyopathy models, likely due to reduced autophagy (Z. Chen et al., 2018) and apoptosis (Alam et al., 2018; Qi et al., 2018). Mitochondrial fragmentation is associated with cell death during ischemia reperfusion (IR) injury and mdivi-1 has been reported to prevent excessive cell death of both cardiac and neuronal cells during IR injuries in several model systems. In cardiac stem cells (Rosdah et al., 2017), ex vivo hearts (Sharp et al., 2014) and an in vivo mouse model (Maneechote et al., 2018), mdivi-1 treatment before, during or after cardiac IR injury was protective. Following stroke or cardiac arrest in mouse models, neuronal death and associated neurological dysfunction occur, but were rescued when mdivi-1 treatment was administered immediately after injury (Fan et al., 2017; P. Wang et al., 2018; Wu et al., 2017).

Notably, pretreatment with mdivi-1 before renal IR injury exacerbated cell death due to impaired mitophagy (Li et al., 2018), indicating that this approach is not universally effective. Further characterization of mdivi-1 and its activity in IR are needed to clarify both the drug mechanism and how it impacts the response to IR in different tissues. Nevertheless, these results suggest that modulating mitochondrial structure and function in acute injury can be a viable approach to improve IR outcomes in at least some contexts.

In addition to diseases and stress responses where mitochondrial dysfunction have been clearly implicated, mdivi-1 has been administered in a wide variety of other disorders. For example, mdivi-1 treatment has been utilized in treating bone (Wang et al., 2018) and muscle atrophy (Troncoso et

al., 2014), acetaminophen-induced liver injury (Gao et al., 2017), cisplatin-induced kidney injury (Liu et al., 2018), cisplatin-induced hair cell loss (Vargo et al., 2017) and cocksackie virus B viral infections (Sin et al., 2017). Mdivi-1 has also been reported to have anti-inflammatory effects in glial cells (Park et al., 2013), osteoblasts (Zhang et al., 2017) and peripheral blood mononuclear cells (Hecker et al., 2018). In addiction therapy, mdivi-1 was shown to blunt cocaine-seeking behavior in rats (Chandra et al., 2017). Therefore, the range of disease states that could be potentially treated by targeting mitochondrial dynamics is very broad.

Another small molecule developed to disrupt mitochondrial division activity is P110, a small peptide that specifically blocks the interaction between Drp1 and Fis1 (Qi et al., 2013). Although some Drp1 was localized to mitochondria due to interactions with other receptors, treatment of cells with P110 significantly reduced the mitochondrial population of Drp1. Consistent with a role for mitochondrial division in promoting apoptotic cell death, P110 treatment protected against cell death by inhibiting the mitochondrial recruitment of pro-apoptotic proteins, including p53, Bax and PUMA (Filichia et al., 2016; Guo et al., 2014). P110 inhibition of mitochondrial division has also improved function in many models of neurodegenerative diseases, similar to mdivi1. P110 reduced mitochondrial fragmentation and cell death in primary and iPSC-derived PD and HD patient neurons (Guo et al., 2013; Qi et al., 2013; Su and Qi, 2013). P110 treatment also prevented neuronal degeneration and motor dysfunction in mouse models for PD (Filichia et al., 2016) and HD (Guo et al., 2013). Similarly, P110 slowed neuronal degeneration and demyelination in multiple sclerosis (Luo et al., 2017). Interestingly, an enhanced interaction between Drp1 and Fis1 was observed in patient-derived fibroblasts and neurons treated with amyloid beta, a model of AD (Joshi et al., 2018a). Consistent with a pathological role for this interaction, P110 treatment of mouse models for AD rescued mitochondrial

function and cognitive defects (Joshi et al., 2018a). P110 treatment also improved locomotion and muscle structure in a mouse model for ALS (Joshi et al., 2018b). Importantly there were no observable effects on a wild type mouse, suggesting that P110 may selectively inhibit pathological division while normal physiological division activity appeared unaffected (Joshi et al., 2018b). Notably, both the neuronal and cardiac defects in a mouse model for HD can be ameliorated by P110 (Joshi et al., 2019). Consistent with this, P110 has also been described as a possible treatment for other cardiac dysfunction, including IR injury. In rat hearts, treatment with P110 after IR injury improved cardiac structure and attenuated some mitochondrial and cardiac dysfunction (Disatnik et al., 2013; Tian et al., 2017).

Together, studies assessing the application of P110 and mdivi-1 emphasize the potential of Drp1 as a therapeutic target (**Table 1.2**). Novel Drp1 GTPase inhibitors continue to be identified, highlighted by a recent study that identified compounds that inhibited Drp1 assembly and were able to restore mtDNA copy numbers in $Mfn1^{-/-}$ cells (Mallat et al., 2018). However, significantly more work is required to understand how small molecule modulation of Drp1 activity by mdivi-1, P110 or other drugs modulates disease outcomes. Moving forward, the design of effective therapeutics that target mitochondrial division will rely on improved understanding of the mechanism of mitochondrial division in normal and diseased states.

<u>Altering mitochondrial fusion activity with small molecules</u>

Chemical therapeutic approaches that target the activity and regulation of the mitochondrial fusion machines can also rebalance aberrant mitochondrial dynamics in cells (**Table 1.2**). The first small molecules that have been shown to directly modulate Mitofusin activity were small peptides

corresponding to different regions of the Mitofusins that either enhanced ($MP1^{Gly}$) or inhibited ($MP2^{Gly}$) mitochondrial fusion when added to cells in culture (Franco et al., 2016). Using a cell culture model of CMT2A, a small molecule that stimulates mitofusin activity (Chimera B-A/I) restored mitochondrial morphology and motility by activating wild-type Mitofusin (Rocha et al., 2018). These data establish that either small peptides or small molecules can directly modulate the activity of the mitochondrial fusion DRPs.

Another recently reported drug that enhanced mitochondrial fusion activity reduced cardiac apoptotic cell death in vivo. βIIPKC contributes to heart failure through phosphorylation of Mfn1, which increased its turnover and impaired mitochondrial fusion. The novel small peptide SAMβA inhibited the interaction of Mfn1 with βIIPKC, which in turn improved mitochondrial and cardiac function in a rat model for heart failure (Ferreira et al., 2019).

The GTPase activity and self-assembly of Opa1 has been modulated by the small molecule BGP-15. BGP-15 prevented mitochondrial fragmentation in lung epithelial cells treated with hydrogen peroxide (Szabo et al., 2018). However, the cytoprotective activity of BGP-15 also required Mfn1, Mfn2 and protein kinase B (AKT), suggesting that the mechanism of action is potentially more complex. Nevertheless, this suggests that modulating mitochondrial fusion could help prevent reactive oxygen species-induced cell death.

Altering the post-translational modification state of Mitofusins may be another way to alter mitochondrial fusion activity. USP30 is a deubiquitinase that removes ubiquitin from Mitofusin, which is associated with increased mitochondrial fusion and decreased mitophagy (Hou et al., 2017).

Treatment of mouse embryonic fibroblasts (MEFs) with the small molecule 15-oxospiramilactone (S3) led to increased mitochondrial connectivity and the retention of ubiquitin modifications on Mfn1 and Mfn2 that do not promote mitofusin turnover (Yue et al., 2014) through interactions with the active site of USP30 that block its deubiquitinase activity. Treatment with S3 was associated with increased mitochondrial fusion activity, ATP production and oxidative capacity of MEFs. In adult cardiomyocytes, S3 treatment was also associated with increased steady-state mitochondrial connectivity; however, cellular respiration was unchanged suggesting that the effects may be cell type specific (Zhang et al., 2017).

Screens for compounds that disrupt the balance of mitochondrial dynamics have identified other small molecules that may directly or indirectly increase mitochondrial fusion activity. Recent work established that increased pyrimidine biosynthesis correlated with increased mitochondrial connectivity and cellular resistance to stress-induced apoptosis (Miret-Casals et al., 2018). Pyrimidine biosynthesis was promoted by chemical inhibition of either dihydroorotate dehydrogenase (DHODH) or Complex III, which upregulated both Mfn1 and Mfn2 mRNA levels. The resulting increased Mitofusin protein expression corresponded to increased mitochondrial fusion and resistance of these cells to doxorubicin-induced apoptosis. Therefore, to increase mitochondrial connectivity in disease states, mitochondrial fusion could be augmented indirectly by molecules that increase protein expression to wild type levels.

In another screen to identify small molecules that alter mitochondrial morphology, hydrazone M1 (M1) restored mitochondrial fusion in Mfn1 knockout MEFs and Mfn2 knockout MEFs (Wang et al., 2012). While the mechanism of this drug is not well understood, M1 treatment increased protein

expression of ATP5A/B, subunits of the ATP synthase complex, and protected cells against apoptosis. In primary hippocampal neurons exposed to β-amyloid peptide, which has been shown to cause mitochondrial fragmentation, mitochondrial connectivity was restored and oxidative damage was inhibited following M1 treatment (Hung et al., 2018). M1 treatment is also being explored as an immune therapy because changes in mitochondrial structure have been shown to drive immune cell function (Buck et al., 2016; Du et al., 2018; Rambold and Pearce, 2018). For instance, the impaired clearance of Mycobacterium tuberculosis is associated with high levels of cholesterol and more fragmented, round mitochondria (Kaul et al., 2004) and clearance was improved by treating cholesterol-inhibited macrophages with M1 (Asalla et al., 2017). High cholesterol levels can similarly impair cellular function in pancreatic beta cells and M1 treatment restored mitochondrial morphology in culture and improved glucose-stimulated insulin secretion (Asalla et al., 2016). Although the mechanism of M1 action remains unclear, these data suggest that targeting the mitochondrial fusion machinery is a viable approach to treat a range of human diseases.

Related therapeutic approaches

Mitochondrial transport and disease

While we have emphasized therapeutic approaches that target the mitochondrial fusion and division DRPs, mitochondrial trafficking could also be modulated to improve cellular function in disease. Normal neuronal function requires mitochondrial transport from the cell body to the presynaptic terminal (Course and Wang, 2016; Devine and Kittler, 2018). Mitochondrial fusion (Misko et al., 2010) and division (Nemani et al., 2018) may influence mitochondrial trafficking, suggesting significant interplay between the different mitochondrial dynamic pathways. Indeed, aberrant mitochondrial accumulation is often observed in the cell body of neuronal models of neurodegeneration, including

CMT2A, consistent with trafficking defects (Baloh et al., 2007; Fissi et al., 2018). Mitochondria are distributed by directed and regulated transport on microtubules by kinesin and dynein motors (Pilling et al., 2006). Motor proteins attach to Miro1/2 GTPases on the mitochondrial outer membrane through the adaptor proteins TRAK1/2 (Schwarz, 2013). Deletion of *MIRO1* in mouse neurons phenocopied human upper motor neuron disease due to mitochondrial transport and distribution defects (Nguyen et al., 2014). Similarly, loss of Miro1 in mature, adult neurons caused loss of dendrite complexity and reduced neuronal survival (López-Doménech et al., 2016). Loss of Miro has also been reported in AD and ALS (Kay et al., 2018), suggesting that mitochondrial transport is altered in diverse neurodegenerative diseases.

The accumulation of functional Miro on damaged mitochondria can also be associated with Parkinson's disease progression (Hsieh et al., 2016; Shaltouki et al., 2018). In healthy cells, PINK1, Parkin and LRRK2 integrate mitochondrial function and transport by identifying dysfunctional organelles and promoting Miro degradation (Hsieh et al., 2016; Wang et al., 2011). Like Miro, defects in mitophagy caused by mutations in the genes that encode PINK1, Parkin and LRRK2 are also associated with PD (Hernandez et al., 2016). Importantly, reduction but not complete loss of Miro in a fly PD model rescued mitochondrial movement and neurodegeneration (Hsieh et al., 2016; Shaltouki et al., 2018).

Mitochondria-ER contact sites

Defective mitochondrial distribution and dynamics also affect mitochondria-endoplasmic reticulum (mito-ER) contacts, which have been implicated in Ca^{2+} and ROS signaling between the organelles (Csordas et al., 2018). Although mito-ER contacts serve various cellular functions that are likely to be

tissue specific, altered calcium signaling at mito-ER contacts has been associated with neuronal degeneration in a fly model for PD (K.-S. Lee et al., 2018). Furthermore, defects in lipid synthesis, lipid droplet regulation, and mito-ER contact formation were reported in patient-derived CMT2A cells, although it the primary driver of disease in these cells remains unclear (Larrea et al., 2019). Therefore, future experiments to evaluate the effects of drugs targeting proteins at mito-ER contact sites, such as Mfn2 and VDAC, could inform future potential therapies to modulate mitochondrial dynamics and function in diseased states (Tubbs and Rieusset, 2017).

Conclusion

Many lines of evidence indicate that aberrant mitochondrial structure and function contribute to cellular dysfunction, cell death and disease pathology. Imbalanced mitochondrial dynamics are observed in a range of diseases including neurodegenerative and cardiac disorders, all despite divergent genetic and environmental causes. Consistent with an important role for mitochondrial dynamics, mutations in the genes encoding the mitochondrial fusion and division proteins are associated with developmental defects and neurodegeneration. When fragmented mitochondrial networks are a component of disease pathophysiology, increased fusion or decreased division activity would both augment mitochondrial connectivity in these cells and would be expected to protect against deteriorating function. While excessive mitochondrial connectivity is less common in diseased states, it is observed in patients with mutations in genes encoding mitochondrial division proteins. These patients could be treated by attenuating mitochondrial fusion or increased mitochondrial division.

While the causal relationship between imbalanced mitochondrial dynamics and disease progression remains unclear in many disease models, it is apparent that therapies targeting the mitochondrial dynamics machinery are a promising tool to reduce cellular dysfunction, tissue degeneration and functional and behavioral outcomes. In this review, I have discussed several studies in which abnormally fragmented or fused mitochondrial networks have been associated with a range of diseases with varying genetic and environmental causes. In many cases, treatment with drugs that target the mitochondrial fusion and division machines to restore balanced dynamics can improve disease outcomes through unknown mechanisms. Here, I will use Parkinson's disease (PD) caused by mutations in PINK1 or parkin (Pickrell & Youle, 2015) as an example to discuss how drugs that target the mitochondrial dynamics machinery might improve disease outcomes with various causes. Significant mitochondrial fragmentation is typically observed in neurodegenerative diseases such as (PD), while the pharmacological inhibition of Drp1 activity in PD models appears to rescue mitochondrial shape, respiration and cellular function. In PD caused by defective mitochondrial turnover, cellular dysfunction could result primarily from the continued presence of damaged mitochondria and reduced mitochondrial function and/or oxidative damage in these cells (Pickrell & Youle, 2015; Burmann et al., 2012). As damaged proteins accumulate on dysfunctional mitochondria, altered cell signaling could stimulate post-translational modification of Drp1 to stimulate division and promote mitochondrial fragmentation. In this case, drugs that block Drp1 activity would be predicted to restore normal levels of division, rebalance mitochondrial morphology and improve cellular outcomes. Future work should specifically address the mechanistic relationship between mitochondrial dynamics and disease to better predict the effects of specific treatment approaches and durations. In the PD example, a causal defect in mitochondrial turnover would likely lead to mitochondrial dysfunction regardless of division activity. In this case, we might expect a short-

term improvement or delay in disease onset after drug treatment, but would not expect sustained effects from drugs targeting mitochondrial dynamics.

As with all disease interventions, therapeutics targeting mitochondria will also face delivery and specificity challenges to ameliorate pathological symptoms without inducing negative side effects. Nevertheless, both genetic and chemical approaches implemented in model systems that have rebalanced mitochondrial dynamics, the restored mitochondrial structure and function alleviates disease-associated symptoms. Research focused on dissecting the mechanism of mitochondrial fusion and division as well as understanding the integration of these processes with other cellular pathways will be essential aspects of developing effective therapeutics.

Figure/Tables

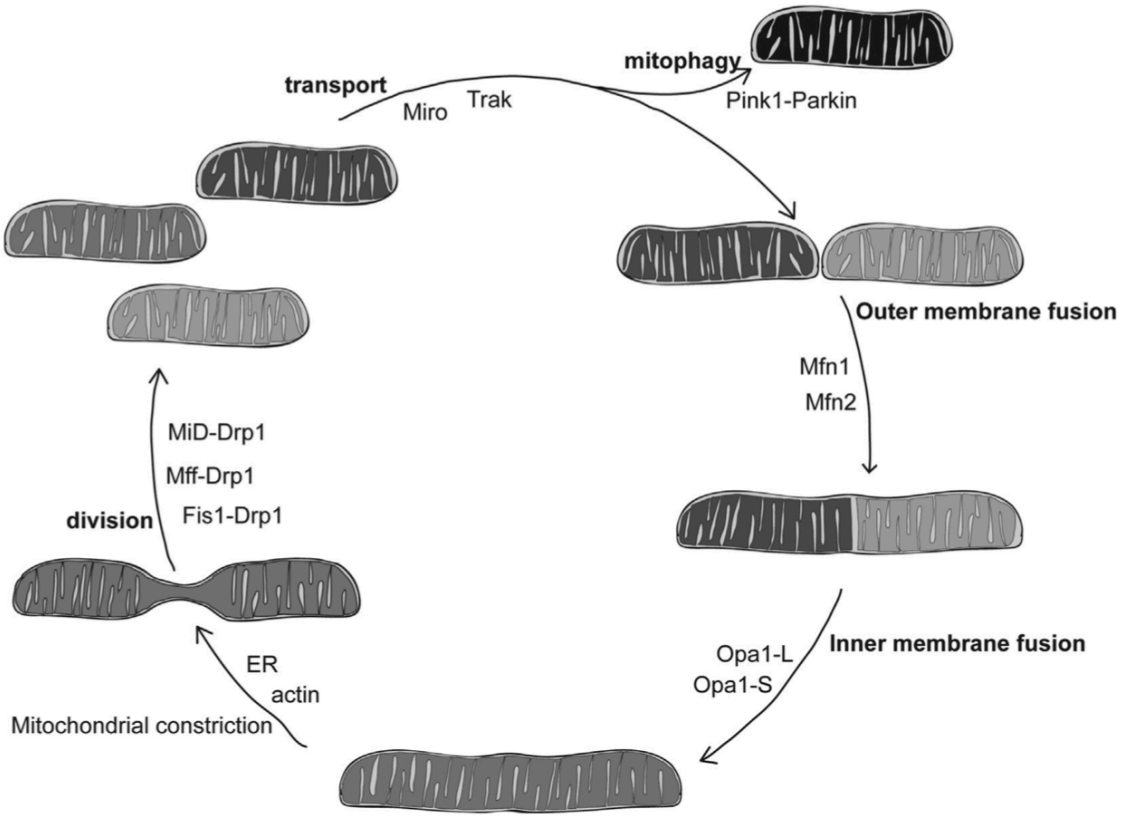

Figure 1.1. Mitochondrial fusion, division and transport mediate changes in mitochondrial structure and function.

Dynamic processes contributing to changes in mitochondrial structure are bolded. The proteins or protein-protein interactions that mediate these processes are noted inside the circle. Mitochondria are shaded to illustrate changes in membrane potential that may occur during mitochondrial fusion and division (black indicates dysfunctional mitochondria and other greys indicate normal membrane potential). Mitochondrial division supports distribution of mitochondria throughout the cell, as well as the selective degradation of dysfunctional mitochondria by mitophagy. Mitochondrial outer membrane fusion occurs first, but is coupled to mitochondrial inner membrane fusion, which allows for content mixing and promotes the formation of a connected, homogeneous network.

Table 1.1. Mitochondrial dynamics in disease models and genetic interventions.

Table 1
Mitochondrial dynamics in disease models and therapeutic approaches.

Disease model	Reference(s)	Mitochondrial morphology	Cell type	Genotype	Treatment	Outcome
Neurodegenerative disease						
Dominant optic atrophy (DOA)	Sarzi et al., 2018	Fragmented	Retinal ganglion cells (RGCs)	*OPA1*$^{+/delTTAG}$	AAV injection of WT Opa1	Attenuated loss of RGCs in DOA model
Parkinson's disease (PD)	Rappold et al., 2014		Dopaminergic neurons	*PINK1*$^{-/-}$; WT (MPTP-induced)	AAV injection of dominant negative Drp1	Restored mitochondrial shape; reduces dopaminergic degeneration
Alzheimer's disease (AD)	Manczak et al., 2016		*Ubiquitous*	*Tg2576,* APP variant	Heterozygous Drp1 knockout	Improved mitochondrial function; reduced neuronal death
	Kandimalla et al., 2016		Neurons	Tau P301L	Heterozygous Drp1 knockout	Improved mitochondrial function; reduced neuronal death
Cardiac dysfunction						
Cardiomyopathy, heart failure	Wai et al., 2015	Fragmented	Cardiomyocytes	*YME1L*$^{-/-}$	Concomitant deletion of *OMA1*	Improved mitochondrial morphology and cardiac function
	Chen et al., 2015	Heterogenous shape and abundance	*Ubiquitous*	*MFF*$^{-/-}$	Concomitant deletion of *MFN1*	Rescued mitochondrial & cardiac function; restored lifespan defects
	Song et al., 2007	Elongated in Drp1$^{-/-}$; fragmented in Mfn1$^{-/-}$, Mfn2$^{-/-}$	Cardiomyocytes	*DNM1L*$^{-/-}$ or *MFN1*$^{-/}$, *MFN2*$^{-/-}$	Triple knockout: *DNM1L*, *MFN1*, *MFN2*	Improved cardiac function partially, but created distinct abnormalities; early senescence instead of death
Ischemia reperfusion (IR) injury	Hall et al., 2016	Fragmented	Cardiomyocytes	WT	Deletion of *MFN1* and *MFN2*	Reduced cell death/increased survival
	Papanicolaou et al., 2011		Cardiomyocytes		Deletion of *MFN2*	Improved cardiac performance; protection from cell death
	Gall et al., 2015		Proximal tubules (kidney)		Deletion of *MFN2*	Improved recovery and survival after renal IR injury
Metabolic dysfunction						
Diet-induced insulin resistance	Boutant et al., 2017	Fragmented	Adipose tissue	WT	Deletion of *MFN2*	Protected against high fat induced insulin-resistance
	Kulkarni et al., 2016		Liver		Deletion of *MFN1*	Protected against high fat induced insulin-resistance; increased complex I abundance
Diabetic nephropathy	Ayanga et al., 2016		Podocytes (kidney)		Deletion of *DNM1L*	Rescued mitochondrial fragmentation; protected against mitochondrial dysfunction in diabetic neuropathy
Nonalcoholic fatty liver disease	Yamada et al., 2018	Accumulation of giant mitochondria	Liver		Deletion of *OPA1*	Reduces giant mitochondria; attenuated liver damage in fatty livers

Table 2
Small molecules altering mitochondrial fusion and division.

Drug name	Reference(s) [discovery, creation]	Effect
Division		
Dynasore	Macia et al., 2006	Inhibited GTPase activity of Dynamin 1, Dynamin 2, Drp1
mdivi-1	Cassidy-Stone et al., 2008, Bordt et al., 2017	Inhibited Drp1 (18267088) and/or Complex I (28350990)
P110	Qi et al., 2013	Inhibited GTPase activity of Drp1 and its interaction with Fis1
TAT-Drp1-SpS	Yan et al., 2015	Blocked Drp1 phosporylation by GSK3B
1H-pyrrole-2- carboxamide compounds	Mallat et al., 2018	Inhibited GTPase activity of Drp1
Fusion		
$MP1^{Gly}$	Franco et al., 2016	Stimulated Mitofusins
$MP2^{Gly}$	Franco et al., 2016	Inhibited Mitofusins
Chimera B-A/I	Rocha et al., 2018	Stimulated Mfn2
SAMβA	Ferreira et al., 2019	Inhibited interaction between Mfn1 and βIIPKC
BGP-15	Szabo et al., 2018	Stimulated GTPase activity and assembly of Opa1; activated diverse other signaling pathways
S3	Yue et al., 2014	Inhibited USP30, increased non-degradative Mitofusin ubiquitination
Leflunomide	Miret-Casals et al., 2018	Inhibited dihydorotate dehydrogenase (DHODH) or Complex III, increased Mitofusin levels
M1	Wang et al., 2012a, 2012b	Increased levels of ATP5A/B

Table 1.2. Small molecules altering mitochondrial fusion and division.

This table summarizes the existing drugs that have been implicated in the direct stimulation of mitochondrial fusion or division activity. The specific inhibition of Drp1 GTPase activity instead of other DRPs or small GTPases has been experimentally verified for mdivi-1, P110 and 1H-pyrrole-2-carboxamide compounds. The precise mechanism of activity for most of the fusion drugs, however, remains unclear.

References

Ahuja, P., Wanagat, J., Wang, Z., Wang, Y., Liem, D.A., Ping, P., Antoshechkin, I.A., Margulies, K.B., Maclellan, W.R., 2013. Divergent mitochondrial biogenesis responses in human cardiomyopathy. Circulation 127, 1957–1967. doi:10.1161/CIRCULATIONAHA.112.001219

Alaimo, A., Gorojod, R.M., Beauquis, J., Muñoz, M.J., Saravia, F., Kotler, M.L., 2014. Deregulation of mitochondria-shaping proteins Opa-1 and Drp-1 in manganese-induced apoptosis. PLoS ONE 9, e91848. doi:10.1371/journal.pone.0091848

Alam, S., Abdullah, C.S., Aishwarya, R., Miriyala, S., Panchatcharam, M., Peretik, J.M., Orr, A.W., James, J., Robbins, J., Bhuiyan, M.S., 2018. Aberrant Mitochondrial Fission Is Maladaptive in Desmin Mutation-Induced Cardiac Proteotoxicity. J Am Heart Assoc 7. doi:10.1161/JAHA.118.009289

Alavi, M.V., Fuhrmann, N., Nguyen, H.P., Yu-Wai-Man, P., Heiduschka, P., Chinnery, P.F., Wissinger, B., 2009. Subtle neurological and metabolic abnormalities in an Opa1 mouse model of autosomal dominant optic atrophy. Experimental Neurology 220, 404–409. doi:10.1016/j.expneurol.2009.09.026

Anand, R., Wai, T., Baker, M.J., Kladt, N., Schauss, A.C., Rugarli, E., Langer, T., 2014. The i-AAA protease YME1L and OMA1 cleave OPA1 to balance mitochondrial fusion and fission. J. Cell Biol. 204, 919–929. doi:10.1083/jcb.201308006

Anderson, G.R., Wardell, S.E., Cakir, M., Yip, C., Ahn, Y.-R., Ali, M., Yllanes, A.P., Chao, C.A., McDonnell, D.P., Wood, K.C., 2018. Dysregulation of mitochondrial dynamics proteins are a targetable feature of human tumors. Nat Commun 9, 1677. doi:10.1038/s41467-018-04033-x

Archer, S.L., 2013. Mitochondrial dynamics–mitochondrial fission and fusion in human diseases. N. Engl. J. Med. 369, 2236–2251. doi:10.1056/NEJMra1215233

Asalla, S., Girada, S.B., Kuna, R.S., Chowdhury, D., Kandagatla, B., Oruganti, S., Bhadra, U., Bhadra, M.P., Kalivendi, S.V., Rao, S.P., Row, A., Ibrahim, A., Ghosh, P.P., Mitra, P., 2016. Restoring Mitochondrial Function: A Small Molecule-mediated Approach to Enhance Glucose Stimulated Insulin Secretion in Cholesterol Accumulated Pancreatic beta cells. Sci Rep 6, 27513. doi:10.1038/srep27513

Asalla, S., Mohareer, K., Banerjee, S., 2017. Small Molecule Mediated Restoration of Mitochondrial Function Augments Anti-Mycobacterial Activity of Human Macrophages Subjected to Cholesterol Induced Asymptomatic Dyslipidemia. Front Cell Infect Microbiol 7, 439. doi:10.3389/fcimb.2017.00439

Ashrafian, H., Docherty, L., Leo, V., Towlson, C., Neilan, M., Steeples, V., Lygate, C.A., Hough, T., Townsend, S., Williams, D., Wells, S., Norris, D., Glyn-Jones, S., Land, J., Barbaric, I., Lalanne, Z., Denny, P., Szumska, D., Bhattacharya, S., Griffin, J.L., Hargreaves, I., Fernandez-Fuentes, N., Cheeseman, M., Watkins, H., Dear, T.N., 2010. A mutation in the mitochondrial fission gene Dnm1l leads to cardiomyopathy. PLoS Genet. 6, e1001000. doi:10.1371/journal.pgen.1001000

Ayanga, B.A., Badal, S.S., Wang, Y., Galvan, D.L., Chang, B.H., Schumacker, P.T., Danesh, F.R., 2016. Dynamin-Related Protein 1 Deficiency Improves Mitochondrial Fitness and Protects against Progression of Diabetic Nephropathy. J. Am. Soc. Nephrol. 27, 2733–2747. doi:10.1681/ASN.2015101096

Bach, D., Pich, S., Soriano, F.X., Vega, N., Baumgartner, B., Oriola, J., Daugaard, J.R., Lloberas, J., Camps, M., Zierath, J.R., Rabasa-Lhoret, R., Wallberg-Henriksson, H., Laville, M., Palacín, M., Vidal, H., Rivera, F., Brand, M., Zorzano, A., 2003. Mitofusin-2 determines mitochondrial network architecture and mitochondrial metabolism. A novel regulatory mechanism altered in obesity. J Biol Chem 278, 17190–17197. doi:10.1074/jbc.M212754200

Baloh, R.H., Schmidt, R.E., Pestronk, A., Milbrandt, J., 2007. Altered axonal mitochondrial transport in the pathogenesis of Charcot-Marie-Tooth disease from mitofusin 2 mutations. J Neurosci 27, 422–430. doi:10.1523/JNEUROSCI.4798-06.2007

Ban, T., Ishihara, T., Kohno, H., Saita, S., Ichimura, A., Maenaka, K., Oka, T., Mihara, K., Ishihara, N., 2017. Molecular basis of selective mitochondrial fusion by heterotypic action between OPA1 and cardiolipin. Nat. Cell Biol. 19, 856–863. doi:10.1038/ncb3560

Barbullushi, K., Abati, E., Rizzo, F., Bresolin, N., Comi, G.P., Corti, S., 2019. Disease Modeling and Therapeutic Strategies in CMT2A: State of the Art. Mol. Neurobiol. 1–12. doi:10.1007/s12035-019-1533-2

Bartsakoulia, M., Pyle, A., Troncoso-Chandía, D., Vial-Brizzi, J., Paz-Fiblas, M.V., Duff, J., Griffin, H., Boczonadi, V., Lochmüller, H., Kleinle, S., Chinnery, P.F., Grünert, S., Kirschner, J., Eisner, V., Horvath, R., 2018. A novel mechanism causing imbalance of mitochondrial fusion and fission in human myopathies. Hum Mol Genet 27, 1186–1195. doi:10.1093/hmg/ddy033

Basso, V., Marchesan, E., Peggion, C., Chakraborty, J., Stockum, von, S., Giacomello, M., Ottolini, D., Debattisti, V., Caicci, F., Tasca, E., Pegoraro, V., Angelini, C., Antonini, A., Bertoli, A., Brini, M.,

Ziviani, E., 2018. Regulation of ER-mitochondria contacts by Parkin via Mfn2. Pharmacol. Res. 138, 43–56. doi:10.1016/j.phrs.2018.09.006

Bertholet, A.M., Delerue, T., Millet, A.M., Moulis, M.F., David, C., Daloyau, M., Arnauné-Pelloquin, L., Davezac, N., Mils, V., Miquel, M.C., Rojo, M., Belenguer, P., 2016. Mitochondrial fusion/fission dynamics in neurodegeneration and neuronal plasticity. Neurobiol. Dis. 90, 3–19. doi:10.1016/j.nbd.2015.10.011

Bido, S., Soria, F.N., Fan, R.Z., Bezard, E., Tieu, K., 2017. Mitochondrial division inhibitor-1 is neuroprotective in the A53T-α-synuclein rat model of Parkinson's disease. Sci Rep 7, 7495. doi:10.1038/s41598-017-07181-0

Bleazard, W., McCaffery, J.M., King, E.J., Bale, S., Mozdy, A., Tieu, Q., Nunnari, J., Shaw, J.M., 1999. The dynamin-related GTPase Dnm1 regulates mitochondrial fission in yeast. Nat. Cell Biol. 1, 298–304. doi:10.1038/13014

Bordt, E.A., Clerc, P., Roelofs, B.A., Saladino, A.J., Tretter, L., Adam-Vizi, V., Cherok, E., Khalil, A., Yadava, N., Ge, S.X., Francis, T.C., Kennedy, N.W., Picton, L.K., Kumar, T., Uppuluri, S., Miller, A.M., Itoh, K., Karbowski, M., Sesaki, H., Hill, R.B., Polster, B.M., 2017. The Putative Drp1 Inhibitor mdivi-1 Is a Reversible Mitochondrial Complex I Inhibitor that Modulates Reactive Oxygen Species. Dev. Cell 40, 583–594.e6. doi:10.1016/j.devcel.2017.02.020

Boutant, M., Kulkarni, S.S., Joffraud, M., Ratajczak, J., Valera-Alberni, M., Combe, R., Zorzano, A., Cantó, C., 2017. Mfn2 is critical for brown adipose tissue thermogenic function. EMBO J 36, 1543–1558. doi:10.15252/embj.201694914

Brandt, T., Cavellini, L., Kühlbrandt, W., Cohen, M.M., 2016. A mitofusin-dependent docking ring complex triggers mitochondrial fusion in vitro. Elife 5, 36634. doi:10.7554/eLife.14618

Brown, D.A., Perry, J.B., Allen, M.E., Sabbah, H.N., Stauffer, B.L., Shaikh, S.R., Cleland, J.G.F., Colucci, W.S., Butler, J., Voors, A.A., Anker, S.D., Pitt, B., Pieske, B., Filippatos, G., Greene, S.J., Gheorghiade, M., 2017. Expert consensus document: Mitochondrial function as a therapeutic target in heart failure. Nat Rev Cardiol 14, 238–250. doi:10.1038/nrcardio.2016.203

Buck, M.D., O'Sullivan, D., Klein Geltink, R.I., Curtis, J.D., Chang, C.-H., Sanin, D.E., Qiu, J., Kretz, O., Braas, D., van der Windt, G.J.W., Chen, Q., Huang, S.C.-C., O'Neill, C.M., Edelson, B.T., Pearce, E.J., Sesaki, H., Huber, T.B., Rambold, A.S., Pearce, E.L., 2016. Mitochondrial Dynamics Controls T Cell Fate through Metabolic Programming. Cell 166, 63–76. doi:10.1016/j.cell.2016.05.035

Burman, J. L., Yu, S., Poole, A. C., Decal, R. B., & Pallanck, L. (2012). Analysis of neural subtypes reveals selective mitochondrial dysfunction in dopaminergic neurons from parkin mutants. Proceedings of the National Academy of Sciences, 109(26), 10438–10443. https://doi.org/10.1073/pnas.1120688109

Burman, J.L., Pickles, S., Wang, C., Sekine, S., Vargas, J.N.S., Zhang, Z., Youle, A.M., Nezich, C.L., Wu, X., Hammer, J.A., Youle, R.J., 2017. Mitochondrial fission facilitates the selective mitophagy of protein aggregates. J. Cell Biol. 216, 3231–3247. doi:10.1083/jcb.201612106

Burté, F., Carelli, V., Chinnery, P.F., Yu-Wai-Man, P., 2015. Disturbed mitochondrial dynamics and neurodegenerative disorders. Nat Rev Neurol 11, 11–24. doi:10.1038/nrneurol.2014.228

Cahill, T.J., Leo, V., Kelly, M., Stockenhuber, A., Kennedy, N.W., Bao, L., Cereghetti, G.M., Harper, A.R., Czibik, G., Liao, C., Bellahcene, M., Steeples, V., Ghaffari, S., Yavari, A., Mayer, A., Poulton, J., Ferguson, D.J.P., Scorrano, L., Hettiarachchi, N.T., Peers, C., Boyle, J., Hill, R.B., Simmons, A., Watkins, H., Dear, T.N., Ashrafian, H., 2016. Resistance of dynamin-related protein 1 oligomers to disassembly impairs mitophagy, resulting in myocardial inflammation and heart failure. J Biol Chem 291, 25762–25762. doi:10.1074/jbc.A115.665695

Cao, Y.-L., Meng, S., Chen, Y., Feng, J.-X., Gu, D.-D., Yu, B., Li, Y.-J., Yang, J.-Y., Liao, S., Chan, D.C., Gao, S., 2017. MFN1 structures reveal nucleotide-triggered dimerization critical for mitochondrial fusion. Nature 542, 372–376. doi:10.1038/nature21077

Carelli, V., Musumeci, O., Caporali, L., Zanna, C., La Morgia, C., Del Dotto, V., Porcelli, A.M., Rugolo, M., Valentino, M.L., Iommarini, L., Maresca, A., Barboni, P., Carbonelli, M., Trombetta, C., Valente, E.M., Patergnani, S., Giorgi, C., Pinton, P., Rizzo, G., Tonon, C., Lodi, R., Avoni, P., Liguori, R., Baruzzi, A., Toscano, A., Zeviani, M., 2015. Syndromic parkinsonism and dementia associated with OPA1 missense mutations. Ann. Neurol. 78, 21–38. doi:10.1002/ana.24410

Cassidy-Stone, A., Chipuk, J.E., Ingerman, E., Song, C., Yoo, C., Kuwana, T., Kurth, M.J., Shaw, J.T., Hinshaw, J.E., Green, D.R., Nunnari, J., 2008. Chemical inhibition of the mitochondrial division dynamin reveals its role in Bax/Bak-dependent mitochondrial outer membrane permeabilization. Dev. Cell 14, 193–204. doi:10.1016/j.devcel.2007.11.019

Cereghetti, G.M., Costa, V., Scorrano, L., 2010. Inhibition of Drp1-dependent mitochondrial fragmentation and apoptosis by a polypeptide antagonist of calcineurin. Cell Death Differ 17, 1785–1794. doi:10.1038/cdd.2010.61

Cereghetti, G.M., Stangherlin, A., Martins de Brito, O., Chang, C.R., Blackstone, C., Bernardi, P., Scorrano, L., 2008. Dephosphorylation by calcineurin regulates translocation of Drp1 to mitochondria. Proc. Natl. Acad. Sci. U.S.A. 105, 15803–15808. doi:10.1073/pnas.0808249105

Chandra, R., Engeln, M., Schiefer, C., Patton, M.H., Martin, J.A., Werner, C.T., Riggs, L.M., Francis, T.C., McGlincy, M., Evans, B., Nam, H., Das, S., Girven, K., Konkalmatt, P., Gancarz, A.M., Golden, S.A., Iñiguez, S.D., Russo, S.J., Turecki, G., Mathur, B.N., Creed, M., Dietz, D.M., Lobo, M.K., 2017. Drp1 Mitochondrial Fission in D1 Neurons Mediates Behavioral and Cellular Plasticity during Early Cocaine Abstinence. Neuron 96, 1327–1341.e6. doi:10.1016/j.neuron.2017.11.037

Chang, C.-R., Blackstone, C., 2007. Cyclic AMP-dependent protein kinase phosphorylation of Drp1 regulates its GTPase activity and mitochondrial morphology. J Biol Chem 282, 21583–21587. doi:10.1074/jbc.C700083200

Chang, C.-R., Manlandro, C.M., Arnoult, D., Stadler, J., Posey, A.E., Hill, R.B., Blackstone, C., 2010. A lethal de novo mutation in the middle domain of the dynamin-related GTPase Drp1 impairs higher order assembly and mitochondrial division. J Biol Chem 285, 32494–32503. doi:10.1074/jbc.M110.142430

Chao, Y.-H., Robak, L.A., Xia, F., Koenig, M.K., Adesina, A., Bacino, C.A., Scaglia, F., Bellen, H.J., Wangler, M.F., 2016. Missense variants in the middle domain of DNM1L in cases of infantile encephalopathy alter peroxisomes and mitochondria when assayed in Drosophila. Hum Mol Genet 25, 1846–1856. doi:10.1093/hmg/ddw059

Chen, H., Chan, D.C., 2017. Mitochondrial Dynamics in Regulating the Unique Phenotypes of Cancer and Stem Cells. Cell Metabolism 26, 39–48. doi:10.1016/j.cmet.2017.05.016

Chen, H., Detmer, S.A., Ewald, A.J., Griffin, E.E., Fraser, S.E., Chan, D.C., 2003. Mitofusins Mfn1 and Mfn2 coordinately regulate mitochondrial fusion and are essential for embryonic development. J. Cell Biol. 160, 189–200. doi:10.1083/jcb.200211046

Chen, H., McCaffery, J.M., Chan, D.C., 2007. Mitochondrial fusion protects against neurodegeneration in the cerebellum. Cell 130, 548–562. doi:10.1016/j.cell.2007.06.026

Chen, H., Ren, S., Clish, C., Jain, M., Mootha, V., McCaffery, J.M., Chan, D.C., 2015. Titration of mitochondrial fusion rescues Mff-deficient cardiomyopathy. J. Cell Biol. 211, 795–805. doi:10.1083/jcb.201507035

Chen, H., Vermulst, M., Wang, Y.E., Chomyn, A., Prolla, T.A., McCaffery, J.M., Chan, D.C., 2010. Mitochondrial fusion is required for mtDNA stability in skeletal muscle and tolerance of mtDNA mutations. Cell 141, 280–289. doi:10.1016/j.cell.2010.02.026

Chen, K.-H., Dasgupta, A., Ding, J., Indig, F.E., Ghosh, P., Longo, D.L., 2014. Role of mitofusin 2 (Mfn2) in controlling cellular proliferation. FASEB J. 28, 382–394. doi:10.1096/fj.13-230037

Chen, K.-H., Guo, X., Ma, D., Guo, Y., Li, Q., Yang, D., Li, P., Qiu, X., Wen, S., Xiao, R.-P., Tang, J., 2004. Dysregulation of HSG triggers vascular proliferative disorders. Nat. Cell Biol. 6, 872–883. doi:10.1038/ncb1161

Chen, L., Gong, Q., Stice, J.P., Knowlton, A.A., 2009. Mitochondrial OPA1, apoptosis, and heart failure. Cardiovasc. Res. 84, 91–99. doi:10.1093/cvr/cvp181

Chen, L., Liu, T., Tran, A., Lu, X., Tomilov, A.A., Davies, V., Cortopassi, G., Chiamvimonvat, N., Bers, D.M., Votruba, M., Knowlton, A.A., 2012. OPA1 mutation and late-onset cardiomyopathy: mitochondrial dysfunction and mtDNA instability. J Am Heart Assoc 1, e003012. doi:10.1161/JAHA.112.003012

Chen, X.-G., Chen, L.-H., Xu, R.-X., Zhang, H.-T., 2018. Effect evaluation of methylprednisolone plus mitochondrial division inhibitor-1 on spinal cord injury rats. Childs Nerv Syst 34, 1479–1487. doi:10.1007/s00381-018-3792-z

Chen, Y., Dorn, G.W., 2013. PINK1-phosphorylated mitofusin 2 is a Parkin receptor for culling damaged mitochondria. Science 340, 471–475. doi:10.1126/science.1231031

Chen, Y., Liu, Y., Dorn, G.W., 2011. Mitochondrial fusion is essential for organelle function and cardiac homeostasis. Circ Res 109, 1327–1331. doi:10.1161/CIRCRESAHA.111.258723

Chen, Z., Li, Y., Wang, Y., Qian, J., Ma, H., Wang, X., Jiang, G., Liu, M., An, Y., Ma, L., Kang, L., Jia, J., Yang, C., Zhang, G., Chen, Y., Gao, W., Fu, M., Huang, Z., Tang, H., Zhu, Y., Ge, J., Gong, H., Zou, Y., 2018. Cardiomyocyte-Restricted Low Density Lipoprotein Receptor-Related Protein 6 (LRP6) Deletion Leads to Lethal Dilated Cardiomyopathy Partly Through Drp1 Signaling. Theranostics 8, 627–643. doi:10.7150/thno.22177

Cherok, E., Xu, S., Li, S., Das, S., Meltzer, W.A., Zalzman, M., Wang, C., Karbowski, M., 2017. Novel regulatory roles of Mff and Drp1 in E3 ubiquitin ligase MARCH5-dependent degradation of MiD49 and Mcl1 and control of mitochondrial dynamics. Mol. Biol. Cell 28, 396–410. doi:10.1091/mbc.E16-04-0208

Cho, D.-H., Nakamura, T., Fang, J., Cieplak, P., Godzik, A., Gu, Z., Lipton, S.A., 2009. S-nitrosylation of Drp1 mediates beta-amyloid-related mitochondrial fission and neuronal injury. Science 324, 102–105. doi:10.1126/science.1171091

Chun, B.Y., Rizzo, J.F., 2016. Dominant optic atrophy: updates on the pathophysiology and clinical manifestations of the optic atrophy 1 mutation. Curr Opin Ophthalmol 27, 475–480. doi:10.1097/ICU.0000000000000314

Cipolat, S., Martins de Brito, O., Dal Zilio, B., Scorrano, L., 2004. OPA1 requires mitofusin 1 to promote mitochondrial fusion. Proc. Natl. Acad. Sci. U.S.A. 101, 15927–15932. doi:10.1073/pnas.0407043101

Clinton, R.W., Francy, C.A., Ramachandran, R., Qi, X., Mears, J.A., 2016. Dynamin-related Protein 1 Oligomerization in Solution Impairs Functional Interactions with Membrane-anchored Mitochondrial Fission Factor. J Biol Chem 291, 478–492. doi:10.1074/jbc.M115.680025

Course, M.M., Wang, Xinnan, 2016. Transporting mitochondria in neurons. F1000Res 5, 1735. doi:10.12688/f1000research.7864.1

Covill-Cooke, C., Howden, J.H., Birsa, N., Kittler, J.T., 2018. Ubiquitination at the mitochondria in neuronal health and disease. Neurochem. Int. 117, 55–64. doi:10.1016/j.neuint.2017.07.003

Cribbs, J.T., Strack, S., 2007. Reversible phosphorylation of Drp1 by cyclic AMP-dependent protein kinase and calcineurin regulates mitochondrial fission and cell death. EMBO Rep 8, 939–944. doi:10.1038/sj.embor.7401062

Csordas, G., Weaver, D., Hajnóczky, G., 2018. Endoplasmic Reticulum-Mitochondrial Contactology: Structure and Signaling Functions. Trends Cell Biol 28, 523–540. doi:10.1016/j.tcb.2018.02.009

Cui, M., Tang, X., Christian, W.V., Yoon, Y., Tieu, K., 2010. Perturbations in mitochondrial dynamics induced by human mutant PINK1 can be rescued by the mitochondrial division inhibitor mdivi-1. J Biol Chem 285, 11740–11752. doi:10.1074/jbc.M109.066662

Davies, V.J., Hollins, A.J., Piechota, M.J., Yip, W., Davies, J.R., White, K.E., Nicols, P.P., Boulton, M.E., Votruba, M., 2007. Opa1 deficiency in a mouse model of autosomal dominant optic atrophy impairs mitochondrial morphology, optic nerve structure and visual function. Hum Mol Genet 16, 1307–1318. doi:10.1093/hmg/ddm079

de Brito, O.M., Scorrano, L., 2008. Mitofusin 2 tethers endoplasmic reticulum to mitochondria. Nature 456, 605–610. doi:10.1038/nature07534

Denton, K., Mou, Y., Xu, C.-C., Shah, D., Chang, J., Blackstone, C., Li, X.-J., 2018. Impaired mitochondrial dynamics underlie axonal defects in hereditary spastic paraplegias. Hum Mol Genet 27, 2517–2530. doi:10.1093/hmg/ddy156

Detmer, S.A., Chan, D.C., 2007. Complementation between mouse Mfn1 and Mfn2 protects mitochondrial fusion defects caused by CMT2A disease mutations. J. Cell Biol. 176, 405–414. doi:10.1083/jcb.200611080

Devine, M.J., Kittler, J.T., 2018. Mitochondria at the neuronal presynapse in health and disease. Nat. Rev. Neurosci. 19, 63–80. doi:10.1038/nrn.2017.170

Disatnik, M.-H., Ferreira, J.C.B., Campos, J.C., Gomes, K.S., Dourado, P.M.M., Qi, X., Mochly-Rosen, D., 2013. Acute inhibition of excessive mitochondrial fission after myocardial infarction prevents long-term cardiac dysfunction. J Am Heart Assoc 2, e000461. doi:10.1161/JAHA.113.000461

Dorn, G.W., Clark, C.F., Eschenbacher, W.H., Kang, M.-Y., Engelhard, J.T., Warner, S.J., Matkovich, S.J., Jowdy, C.C., 2011. MARF and Opa1 control mitochondrial and cardiac function in Drosophila. Circ Res 108, 12–17. doi:10.1161/CIRCRESAHA.110.236745

Dorn, G.W., Vega, R.B., Kelly, D.P., 2015. Mitochondrial biogenesis and dynamics in the developing and diseased heart. Genes Dev. 29, 1981–1991. doi:10.1101/gad.269894.115

Du, X., Wen, J., Wang, Y., Karmaus, P.W.F., Khatamian, A., Tan, H., Li, Y., Guy, C., Nguyen, T.-L.M., Dhungana, Y., Neale, G., Peng, J., Yu, J., Chi, H., 2018. Hippo/Mst signalling couples metabolic state and immune function of CD8α+ dendritic cells. Nature 558, 141–145. doi:10.1038/s41586-018-0177-0

Ehses, S., Raschke, I., Mancuso, G., Bernacchia, A., Geimer, S., Tondera, D., Martinou, J.-C., Westermann, B., Rugarli, E.I., Langer, T., 2009. Regulation of OPA1 processing and mitochondrial fusion by m-AAA protease isoenzymes and OMA1. J. Cell Biol. 187, 1023–1036. doi:10.1083/jcb.200906084

Eisner, V., Picard, M., Hajnóczky, G., 2018. Mitochondrial dynamics in adaptive and maladaptive cellular stress responses. Nat. Cell Biol. 20, 755–765. doi:10.1038/s41556-018-0133-0

Fahrner, J.A., Liu, R., Perry, M.S., Klein, J., Chan, D.C., 2016. A novel de novo dominant negative mutation in DNM1Limpairs mitochondrial fission and presents as childhood epileptic encephalopathy. Am. J. Med. Genet. A 170, 2002–2011. doi:10.1002/ajmg.a.37721

Fan, L.-F., He, P.-Y., Peng, Y.-C., Du, Q.-H., Ma, Y.-J., Jin, J.-X., Xu, H.-Z., Li, J.-R., Wang, Z.-J., Cao, S.-L., Li, T., Yan, F., Gu, C., Wang, L., Chen, G., 2017. Mdivi-1 ameliorates early brain injury after subarachnoid hemorrhage via the suppression of inflammation-related blood-brain barrier

disruption and endoplasmic reticulum stress-based apoptosis. Free Radic. Biol. Med. 112, 336–349. doi:10.1016/j.freeradbiomed.2017.08.003

Fang, L., Moore, X.-L., Gao, X.-M., Dart, A.M., Lim, Y.L., Du, X.-J., 2007. Down-regulation of mitofusin-2 expression in cardiac hypertrophy in vitro and in vivo. Life Sci. 80, 2154–2160. doi:10.1016/j.lfs.2007.04.003

Ferreira, J.C.B., Campos, J.C., Qvit, N., Qi, X., Bozi, L.H.M., Bechara, L.R.G., Lima, V.M., Queliconi, B.B., Disatnik, M.-H., Dourado, P.M.M., Kowaltowski, A.J., Mochly-Rosen, D., 2019. A selective inhibitor of mitofusin 1-βIIPKC association improves heart failure outcome in rats. Nat Commun 10, 329. doi:10.1038/s41467-018-08276-6

Filadi, R., Greotti, E., Turacchio, G., Luini, A., Pozzan, T., Pizzo, P., 2015. Mitofusin 2 ablation increases endoplasmic reticulum-mitochondria coupling. Proc. Natl. Acad. Sci. U.S.A. 112, E2174–81. doi:10.1073/pnas.1504880112

Filichia, E., Hoffer, B., Qi, X., Luo, Y., 2016. Inhibition of Drp1 mitochondrial translocation provides neural protection in dopaminergic system in a Parkinson's disease model induced by MPTP. Sci Rep 6, 32656. doi:10.1038/srep32656

Fissi, El, N., Rojo, M., Aouane, A., Karatas, E., Poliacikova, G., David, C., Royet, J., Rival, T., 2018. Mitofusin gain and loss of function drive pathogenesis in Drosophila models of CMT2A neuropathy. EMBO Rep 19, e45241. doi:10.15252/embr.201745241

Flippo, K.H., Strack, S., 2017. Mitochondrial dynamics in neuronal injury, development and plasticity. Journal of Cell Science 130, 671–681. doi:10.1242/jcs.171017

Franco, A., Kitsis, R.N., Fleischer, J.A., Gavathiotis, E., Kornfeld, O.S., Gong, G., Biris, N., Benz, A., Qvit, N., Donnelly, S.K., Chen, Y., Mennerick, S., Hodgson, L., Mochly-Rosen, D., Dorn, G.W., 2016. Correcting mitochondrial fusion by manipulating mitofusin conformations. Nature 540, 74–79. doi:10.1038/nature20156

Francy, C.A., Clinton, R.W., Fröhlich, C., Murphy, C., Mears, J.A., 2017. Cryo-EM Studies of Drp1 Reveal Cardiolipin Interactions that Activate the Helical Oligomer. Sci Rep 7, 10744. doi:10.1038/s41598-017-11008-3

Frank, S., Gaume, B., Bergmann-Leitner, E.S., Leitner, W.W., Robert, E.G., Catez, F., Smith, C.L., Youle, R.J., 2001. The role of dynamin-related protein 1, a mediator of mitochondrial fission, in apoptosis. Dev. Cell 1, 515–525.

Frezza, C., Cipolat, S., Martins de Brito, O., Micaroni, M., Beznoussenko, G.V., Rudka, T., Bartoli, D., Polishuck, R.S., Danial, N.N., De Strooper, B., Scorrano, L., 2006. OPA1 controls apoptotic cristae remodeling independently from mitochondrial fusion. Cell 126, 177–189. doi:10.1016/j.cell.2006.06.025

Friedman, J.R., Lackner, L.L., West, M., DiBenedetto, J.R., Nunnari, J., Voeltz, G.K., 2011. ER tubules mark sites of mitochondrial division. Science 334, 358–362. doi:10.1126/science.1207385

Fröhlich, C., Grabiger, S., Schwefel, D., Faelber, K., Rosenbaum, E., Mears, J., Rocks, O., Daumke, O., 2013. Structural insights into oligomerization and mitochondrial remodelling of dynamin 1-like protein. EMBO J 32, 1280–1292. doi:10.1038/emboj.2013.74

Gal, A., Balicza, P., Weaver, D., Naghdi, S., Joseph, S.K., Varnai, P., Gyuris, T., Horváth, A., Nagy, L., Seifert, E.L., Molnar, M.J., Hajnóczky, G., 2017. MSTO1 is a cytoplasmic pro-mitochondrial fusion protein, whose mutation induces myopathy and ataxia in humans. EMBO Mol Med 9, 967–984. doi:10.15252/emmm.201607058

Gall, J.M., Wang, Z., Bonegio, R.G., Havasi, A., Liesa, M., Vemula, P., Borkan, S.C., 2015. Conditional knockout of proximal tubule mitofusin 2 accelerates recovery and improves survival after renal ischemia. J. Am. Soc. Nephrol. 26, 1092–1102. doi:10.1681/ASN.2014010126

Gall, J.M., Wang, Z., Liesa, M., Molina, A., Havasi, A., Schwartz, J.H., Shirihai, O., Borkan, S.C., Bonegio, R.G.B., 2012. Role of mitofusin 2 in the renal stress response. PLoS ONE 7, e31074. doi:10.1371/journal.pone.0031074

Gan, X., Huang, S., Wu, L., Wang, Y., Hu, G., Li, G., Zhang, H., Yu, H., Swerdlow, R.H., Chen, J.X., Yan, S.S., 2014. Inhibition of ERK-DLP1 signaling and mitochondrial division alleviates mitochondrial dysfunction in Alzheimer's disease cybrid cell. Biochim. Biophys. Acta 1842, 220–231. doi:10.1016/j.bbadis.2013.11.009

Gao, Jie, Luo, A., Yan, J., Fang, X., Tang, X., Zhao, Y., Li, S., 2018. Mdivi-1 pretreatment mitigates isoflurane-induced cognitive deficits in developmental rats. Am J Transl Res 10, 432–443.

Gao, Ju, Wang, L., Liu, J., Xie, F., Su, B., Wang, X., 2017. Abnormalities of Mitochondrial Dynamics in Neurodegenerative Diseases. Antioxidants (Basel) 6, 25. doi:10.3390/antiox6020025

Gao, Yan, Chu, S., Zhang, Z., Zuo, W., Xia, C., Ai, Q., Luo, P., Cao, P., Chen, N., 2017. Early Stage Functions of Mitochondrial Autophagy and Oxidative Stress in Acetaminophen-Induced Liver Injury. J. Cell. Biochem. 118, 3130–3141. doi:10.1002/jcb.25788

Gomes, L.C., Di Benedetto, G., Scorrano, L., 2011. During autophagy mitochondria elongate, are spared from degradation and sustain cell viability. Nat. Cell Biol. 13, 589–598. doi:10.1038/ncb2220

Gong, G., Song, M., Csordas, G., Kelly, D.P., Matkovich, S.J., Dorn, G.W.I., 2015. Parkin-mediated mitophagy directs perinatal cardiac metabolic maturation in mice. Science 350, -aad2459. doi:10.1126/science.aad2459

Griparic, L., Kanazawa, T., van der Bliek, A.M., 2007. Regulation of the mitochondrial dynamin-like protein Opa1 by proteolytic cleavage. J. Cell Biol. 178, 757–764. doi:10.1083/jcb.200704112

Guo, C., Wilkinson, K.A., Evans, A.J., Rubin, P.P., Henley, J.M., 2017. SENP3-mediated deSUMOylation of Drp1 facilitates interaction with Mff to promote cell death. Sci Rep 7, 43811. doi:10.1038/srep43811

Guo, M.-Y., Shang, L., Hu, Y.-Y., Jiang, L.-P., Wan, Y.-Y., Zhou, Q.-Q., Zhang, K., Liao, H.-F., Yi, J.-L., Han, X.-J., 2018. The role of Cdk5-mediated Drp1 phosphorylation in Aβ1-42 induced mitochondrial fission and neuronal apoptosis. J. Cell. Biochem. 119, 4815–4825. doi:10.1002/jcb.26680

Guo, X., Disatnik, M.-H., Monbureau, M., Shamloo, M., Mochly-Rosen, D., Qi, X., 2013. Inhibition of mitochondrial fragmentation diminishes Huntington's disease-associated neurodegeneration. J. Clin. Invest. 123, 5371–5388. doi:10.1172/JCI70911

Guo, X., Sesaki, H., Qi, X., 2014. Drp1 stabilizes p53 on the mitochondria to trigger necrosis under oxidative stress conditions in vitro and in vivo. Biochem. J. 461, 137–146. doi:10.1042/BJ20131438

Hall, A.R., Burke, N., Dongworth, R.K., Kalkhoran, S.B., Dyson, A., Vicencio, J.M., Dorn, G.W., Yellon, D.M., Hausenloy, D.J., 2016. Hearts deficient in both Mfn1 and Mfn2 are protected against acute myocardial infarction. Cell Death Dis 7, e2238–e2238. doi:10.1038/cddis.2016.139

Han, X.-J., Lu, Y.-F., Li, S.-A., Kaitsuka, T., Sato, Y., Tomizawa, K., Nairn, A.C., Takei, K., Matsui, H., Matsushita, M., 2008. CaM kinase I alpha-induced phosphorylation of Drp1 regulates mitochondrial morphology. J. Cell Biol. 182, 573–585. doi:10.1083/jcb.200802164

Harder, Z., Zunino, R., McBride, H., 2004. Sumo1 conjugates mitochondrial substrates and participates in mitochondrial fission. Curr. Biol. 14, 340–345. doi:10.1016/j.cub.2004.02.004

Hartmann, B., Wai, T., Hu, H., MacVicar, T., Musante, L., Fischer-Zirnsak, B., Stenzel, W., Gräf, R., van den Heuvel, L., Ropers, H.-H., Wienker, T.F., Hübner, C., Langer, T., Kaindl, A.M., 2016. Homozygous YME1L1 mutation causes mitochondriopathy with optic atrophy and mitochondrial network fragmentation. Elife 5, 919. doi:10.7554/eLife.16078

Head, B., Griparic, L., Amiri, M., Gandre-Babbe, S., van der Bliek, A.M., 2009. Inducible proteolytic inactivation of OPA1 mediated by the OMA1 protease in mammalian cells. J. Cell Biol. 187, 959–966. doi:10.1083/jcb.200906083

Hecker, M., Sommer, N., Foch, S., Hecker, A., Hackstein, H., Witzenrath, M., Weissmann, N., Seeger, W., Mayer, K., 2018. Resolvin E1 and its precursor 18R-HEPE restore mitochondrial function in inflammation. Biochim Biophys Acta Mol Cell Biol Lipids 1863, 1016–1028. doi:10.1016/j.bbalip.2018.06.011

Hernandez, D.G., Reed, X., Singleton, A.B., 2016. Genetics in Parkinson disease: Mendelian versus non-Mendelian inheritance. J. Neurochem. 139 Suppl 1, 59–74. doi:10.1111/jnc.13593

Hoppins, S., Collins, S.R., Cassidy-Stone, A., Hummel, E., DeVay, R.M., Lackner, L.L., Westermann, B., Schuldiner, M., Weissman, J.S., Nunnari, J., 2011a. A mitochondrial-focused genetic interaction map reveals a scaffold-like complex required for inner membrane organization in mitochondria. J. Cell Biol. 195, 323–340. doi:10.1083/jcb.201107053

Hoppins, S., Edlich, F., Cleland, M.M., Banerjee, S., McCaffery, J.M., Youle, R.J., Nunnari, J., 2011b. The soluble form of Bax regulates mitochondrial fusion via MFN2 homotypic complexes. Molecular Cell 41, 150–160. doi:10.1016/j.molcel.2010.11.030

Horbay, R., Bilyy, R., 2016. Mitochondrial dynamics during cell cycling. Apoptosis 21, 1327–1335. doi:10.1007/s10495-016-1295-5

Horn, S.R., Thomenius, M.J., Johnson, E.S., Freel, C.D., Wu, J.Q., Coloff, J.L., Yang, C.-S., Tang, W., An, J., Ilkayeva, O.R., Rathmell, J.C., Newgard, C.B., Kornbluth, S., 2011. Regulation of mitochondrial morphology by APC/CCdh1-mediated control of Drp1 stability. Mol. Biol. Cell 22, 1207–1216. doi:10.1091/mbc.E10-07-0567

Hou, J., Eldeeb, M., Wang, X., 2017. Beyond Deubiquitylation: USP30-Mediated Regulation of Mitochondrial Homeostasis. Adv. Exp. Med. Biol. 1038, 133–148. doi:10.1007/978-981-10-6674-0_10

Hsieh, C.-H., Shaltouki, A., Gonzalez, A.E., Bettencourt da Cruz, A., Burbulla, L.F., St Lawrence, E., Schüle, B., Krainc, D., Palmer, T.D., Wang, X., 2016. Functional Impairment in Miro Degradation and Mitophagy Is a Shared Feature in Familial and Sporadic Parkinson's Disease. Cell Stem Cell 19, 709–724. doi:10.1016/j.stem.2016.08.002

Huang, S., Wang, Y., Gan, X., Fang, D., Zhong, C., Wu, L., Hu, G., Sosunov, A.A., McKhann, G.M., Yu, H., Yan, S.S., 2015. Drp1-mediated mitochondrial abnormalities link to synaptic injury in diabetes model. Diabetes 64, 1728–1742. doi:10.2337/db14-0758

Hung, C.H.-L., Cheng, S.S.-Y., Cheung, Y.-T., Wuwongse, S., Zhang, N.Q., Ho, Y.-S., Lee, S.M.-Y., Chang, R.C.-C., 2018. A reciprocal relationship between reactive oxygen species and mitochondrial dynamics in neurodegeneration. Redox Biol 14, 7–19. doi:10.1016/j.redox.2017.08.010

Ikeda, Y., Shirakabe, A., Maejima, Y., Zhai, P., Sciarretta, S., Toli, J., Nomura, M., Mihara, K., Egashira, K., Ohishi, M., Abdellatif, M., Sadoshima, J., 2015. Endogenous Drp1 mediates mitochondrial autophagy and protects the heart against energy stress. Circ Res 116, 264–278. doi:10.1161/CIRCRESAHA.116.303356

Inoue-Yamauchi, A., Oda, H., 2012. Depletion of mitochondrial fission factor DRP1 causes increased apoptosis in human colon cancer cells. Biochem. Biophys. Res. Commun. 421, 81–85. doi:10.1016/j.bbrc.2012.03.118

Ishihara, N., Eura, Y., Mihara, K., 2004. Mitofusin 1 and 2 play distinct roles in mitochondrial fusion reactions via GTPase activity. J Cell Sci 117, 6535–6546. doi:10.1242/jcs.01565

Ishihara, N., Nomura, M., Jofuku, A., Kato, H., Suzuki, S.O., Masuda, K., Otera, H., Nakanishi, Y., Nonaka, I., Goto, Y.-I., Taguchi, N., Morinaga, H., Maeda, M., Takayanagi, R., Yokota, S., Mihara,

K., 2009. Mitochondrial fission factor Drp1 is essential for embryonic development and synapse formation in mice. Nat. Cell Biol. 11, 958–966. doi:10.1038/ncb1907

Ishihara, T., Ban-Ishihara, R., Maeda, M., Matsunaga, Y., Ichimura, A., Kyogoku, S., Aoki, H., Katada, S., Nakada, K., Nomura, M., Mizushima, N., Mihara, K., Ishihara, N., 2015. Dynamics of mitochondrial DNA nucleoids regulated by mitochondrial fission is essential for maintenance of homogeneously active mitochondria during neonatal heart development. Mol. Cell. Biol. 35, 211–223. doi:10.1128/MCB.01054-14

Javadov, S., Rajapurohitam, V., Kilić, A., Hunter, J.C., Zeidan, A., Said Faruq, N., Escobales, N., Karmazyn, M., 2011. Expression of mitochondrial fusion-fission proteins during post-infarction remodeling: the effect of NHE-1 inhibition. Basic Res. Cardiol. 106, 99–109. doi:10.1007/s00395-010-0122-3

Joshi, A.U., Ebert, A.E., Haileselassie, B., Mochly-Rosen, D., 2019. Drp1/Fis1-mediated mitochondrial fragmentation leads to lysosomal dysfunction in cardiac models of Huntington's disease. J Mol Cell Cardiol 127, 125–133. doi:10.1016/j.yjmcc.2018.12.004

Joshi, A.U., Saw, N.L., Shamloo, M., Mochly-Rosen, D., 2018a. Drp1/Fis1 interaction mediates mitochondrial dysfunction, bioenergetic failure and cognitive decline in Alzheimer's disease. Oncotarget 9, 6128–6143. doi:10.18632/oncotarget.23640

Joshi, A.U., Saw, N.L., Vogel, H., Cunnigham, A.D., Shamloo, M., Mochly-Rosen, D., 2018b. Inhibition of Drp1/Fis1 interaction slows progression of amyotrophic lateral sclerosis. EMBO Mol Med 10, e8166. doi:10.15252/emmm.201708166

Kageyama, Y., Hoshijima, M., Seo, K., Bedja, D., Sysa-Shah, P., Andrabi, S.A., Chen, W., Höke, A., Dawson, V.L., Dawson, T.M., Gabrielson, K., Kass, D.A., Iijima, M., Sesaki, H., 2014. Parkin-independent mitophagy requires Drp1 and maintains the integrity of mammalian heart and brain. EMBO J 33, 2798–2813. doi:10.15252/embj.201488658

Kageyama, Y., Zhang, Z., Roda, R., Fukaya, M., Wakabayashi, J., Wakabayashi, N., Kensler, T.W., Reddy, P.H., Iijima, M., Sesaki, H., 2012. Mitochondrial division ensures the survival of postmitotic neurons by suppressing oxidative damage. J. Cell Biol. 197, 535–551. doi:10.1083/jcb.201110034

Kagiava, A., Karaiskos, C., Richter, J., Tryfonos, C., Lapathitis, G., Sargiannidou, I., Christodoulou, C., Kleopa, K.A., 2018. Intrathecal gene therapy in mouse models expressing CMT1X mutations. Hum Mol Genet 27, 1460–1473. doi:10.1093/hmg/ddy056

Kalia, R., Wang, R.Y.-R., Yusuf, A., Thomas, P.V., Agard, D.A., Shaw, J.M., Frost, A., 2018. Structural basis of mitochondrial receptor binding and constriction by DRP1. Nature 558, 401–405. doi:10.1038/s41586-018-0211-2

Kalkavan, H., Green, D.R., 2018. MOMP, cell suicide as a BCL-2 family business. Cell Death Differ 25, 46–55. doi:10.1038/cdd.2017.179

Kamerkar, S.C., Kraus, F., Sharpe, A.J., Pucadyil, T.J., Ryan, M.T., 2018. Dynamin-related protein 1 has membrane constricting and severing abilities sufficient for mitochondrial and peroxisomal fission. Nat Commun 9, 5239. doi:10.1038/s41467-018-07543-w

Kandimalla, R., Manczak, M., Fry, D., Suneetha, Y., Sesaki, H., Reddy, P.H., 2016. Reduced dynamin-related protein 1 protects against phosphorylated Tau-induced mitochondrial dysfunction and synaptic damage in Alzheimer's disease. Hum Mol Genet 25, 4881–4897. doi:10.1093/hmg/ddw312

Kandimalla, R., Reddy, P.H., 2016. Multiple faces of dynamin-related protein 1 and its role in Alzheimer's disease pathogenesis. Biochim. Biophys. Acta 1862, 814–828. doi:10.1016/j.bbadis.2015.12.018

Karbowski, M., Norris, K.L., Cleland, M.M., Jeong, S.-Y., Youle, R.J., 2006. Role of Bax and Bak in mitochondrial morphogenesis. Nature 443, 658–662. doi:10.1038/nature05111

Karpinich, N.O., Tafani, M., Rothman, R.J., Russo, M.A., Farber, J.L., 2002. The course of etoposide-induced apoptosis from damage to DNA and p53 activation to mitochondrial release of cytochrome c. J Biol Chem 277, 16547–16552. doi:10.1074/jbc.M110629200

Kashatus, J.A., Nascimento, A., Myers, L.J., Sher, A., Byrne, F.L., Hoehn, K.L., Counter, C.M., Kashatus, D.F., 2015. Erk2 phosphorylation of Drp1 promotes mitochondrial fission and MAPK-driven tumor growth. Molecular Cell 57, 537–551. doi:10.1016/j.molcel.2015.01.002

Kaul, D., Anand, P.K., Verma, I., 2004. Cholesterol-sensor initiates M. tuberculosis entry into human macrophages. Mol. Cell. Biochem. 258, 219–222.

Kay, L., Pienaar, I.S., Cooray, R., Black, G., Soundararajan, M., 2018. Understanding Miro GTPases: Implications in the Treatment of Neurodegenerative Disorders. Mol. Neurobiol. 55, 7352–7365. doi:10.1007/s12035-018-0927-x

Kelley, D.E., He, J., Menshikova, E.V., Ritov, V.B., 2002. Dysfunction of mitochondria in human skeletal muscle in type 2 diabetes. Diabetes 51, 2944–2950.

Kim, D.I., Lee, K.H., Gabr, A.A., Choi, G.E., Kim, J.S., Ko, S.H., Han, H.J., 2016. Aβ-Induced Drp1 phosphorylation through Akt activation promotes excessive mitochondrial fission leading to neuronal apoptosis. Biochim. Biophys. Acta 1863, 2820–2834. doi:10.1016/j.bbamcr.2016.09.003

Kim, J., Moody, J.P., Edgerly, C.K., Bordiuk, O.L., Cormier, K., Smith, K., Beal, M.F., Ferrante, R.J., 2010. Mitochondrial loss, dysfunction and altered dynamics in Huntington's disease. Hum Mol Genet 19, 3919–3935. doi:10.1093/hmg/ddq306

Kim, J.-E., Kang, T.-C., 2017. p47Phox/CDK5/DRP1-Mediated Mitochondrial Fission Evokes PV Cell Degeneration in the Rat Dentate Gyrus Following Status Epilepticus. Front Cell Neurosci 11, 267. doi:10.3389/fncel.2017.00267

Kim, S., Kim, C., Park, S., 2017. Mdivi-1 Protects Adult Rat Hippocampal Neural Stem Cells against Palmitate-Induced Oxidative Stress and Apoptosis. Int J Mol Sci 18, 1947. doi:10.3390/ijms18091947

Kim, Y.J., Park, J.K., Kang, W.S., Kim, S.K., Han, C., Na, H.R., Park, H.J., Kim, J.W., Kim, Y.Y., Park, M.H., Paik, J.-W., 2017. Association between Mitofusin 2 Gene Polymorphisms and Late-Onset Alzheimer's Disease in the Korean Population. Psychiatry Investig 14, 81–85. doi:10.4306/pi.2017.14.1.81

Koch, J., Feichtinger, R.G., Freisinger, P., Pies, M., Schrödl, F., Iuso, A., Sperl, W., Mayr, J.A., Prokisch, H., Haack, T.B., 2016. Disturbed mitochondrial and peroxisomal dynamics due to loss of MFF causes Leigh-like encephalopathy, optic atrophy and peripheral neuropathy. J. Med. Genet. 53, 270–278. doi:10.1136/jmedgenet-2015-103500

Koshiba, T., Detmer, S.A., Kaiser, J.T., Chen, H., McCaffery, J.M., Chan, D.C., 2004. Structural basis of mitochondrial tethering by mitofusin complexes. Science 305, 858–862. doi:10.1126/science.1099793

Kraus, F., Ryan, M.T., 2017. The constriction and scission machineries involved in mitochondrial fission. Journal of Cell Science 130, 2953–2960. doi:10.1242/jcs.199562

Kulkarni, S.S., Joffraud, M., Boutant, M., Ratajczak, J., Gao, A.W., Maclachlan, C., Hernández-Alvarez, M.I., Raymond, F., Metairon, S., Descombes, P., Houtkooper, R.H., Zorzano, A., Cantó, C., 2016. Mfn1 Deficiency in the Liver Protects Against Diet-Induced Insulin Resistance and Enhances the Hypoglycemic Effect of Metformin. Diabetes 65, 3552–3560. doi:10.2337/db15-1725

Kushnareva, Y., Seong, Y., Andreyev, A.Y., Kuwana, T., Kiosses, W.B., Votruba, M., Newmeyer, D.D., 2016. Mitochondrial dysfunction in an Opa1(Q285STOP) mouse model of dominant optic atrophy

results from Opa1 haploinsufficiency. Cell Death Dis 7, e2309–e2309. doi:10.1038/cddis.2016.160

Kuznetsov, A.V., Hermann, M., Saks, V., Hengster, P., Margreiter, R., 2009. The cell-type specificity of mitochondrial dynamics. Int. J. Biochem. Cell Biol. 41, 1928–1939. doi:10.1016/j.biocel.2009.03.007

Labrousse, A.M., Zappaterra, M.D., Rube, D.A., van der Bliek, A.M., 1999. C. elegans dynamin-related protein DRP-1 controls severing of the mitochondrial outer membrane. Molecular Cell 4, 815–826.

Larrea, D., Pera, M., Gonelli, A., Cabrera, R.Q., Akman, H.O., Guardia-Laguarta, C., Velasco, K.R., Area-Gomez, E., Dal Bello, F., De Stefani, D., Horvath, R., Shy, M.E., Schon, E.A., Giacomello, M., 2019. MFN2 mutations in Charcot-Marie-Tooth disease alter mitochondria-associated ER membrane function but do not impair bioenergetics. Hum Mol Genet 51, 181. doi:10.1093/hmg/ddz008

Lee, J.-Y., Kapur, M., Li, M., Choi, M.-C., Choi, S., Kim, H.-J., Kim, I., Lee, E., Taylor, J.P., Yao, T.-P., 2014. MFN1 deacetylation activates adaptive mitochondrial fusion and protects metabolically challenged mitochondria. J Cell Sci 127, 4954–4963. doi:10.1242/jcs.157321

Lee, J.E., Westrate, L.M., Wu, H., Page, C., Voeltz, G.K., 2016. Multiple dynamin family members collaborate to drive mitochondrial division. Nature 540, 139–143. doi:10.1038/nature20555

Lee, K.-S., Huh, S., Lee, S., Wu, Z., Kim, A.-K., Kang, H.-Y., Lu, B., 2018. Altered ER-mitochondria contact impacts mitochondria calcium homeostasis and contributes to neurodegeneration in vivo in disease models. Proc. Natl. Acad. Sci. U.S.A. 115, E8844–E8853. doi:10.1073/pnas.1721136115

Lewis, S.C., Uchiyama, L.F., Nunnari, J., 2016. ER-mitochondria contacts couple mtDNA synthesis with mitochondrial division in human cells. Science 353, aaf5549. doi:10.1126/science.aaf5549

Li, N., Wang, H., Jiang, C., Zhang, M., 2018. Renal ischemia/reperfusion-induced mitophagy protects against renal dysfunction via Drp1-dependent-pathway. Exp Cell Res 369, 27–33. doi:10.1016/j.yexcr.2018.04.025

Lin, H., Zhao, L., Ma, X., Wang, B.-C., Deng, X.-Y., Cui, M., Chen, S.-F., Shao, Z.-W., 2017. Drp1 mediates compression-induced programmed necrosis of rat nucleus pulposus cells by promoting mitochondrial translocation of p53 and nuclear translocation of AIF. Biochem. Biophys. Res. Commun. 487, 181–188. doi:10.1016/j.bbrc.2017.04.037

Liu, W., Yamashita, T., Tian, F., Morimoto, N., Ikeda, Y., Deguchi, K., Abe, K., 2013. Mitochondrial fusion and fission proteins expression dynamically change in a murine model of amyotrophic lateral sclerosis. Curr Neurovasc Res 10, 222–230.

Liu, X., Weaver, D., Shirihai, O., Hajnóczky, G., 2009. Mitochondrial "kiss-and-run": interplay between mitochondrial motility and fusion-fission dynamics. EMBO J 28, 3074–3089. doi:10.1038/emboj.2009.255

Liu, Y., Yan, Y., Inagaki, Y., Logan, S., Bosnjak, Z.J., Bai, X., 2017. Insufficient Astrocyte-Derived Brain-Derived Neurotrophic Factor Contributes to Propofol-Induced Neuron Death Through Akt/Glycogen Synthase Kinase 3β/Mitochondrial Fission Pathway. Anesth. Analg. 125, 241–254. doi:10.1213/ANE.0000000000002137

Liu, Z., Li, H., Su, J., Xu, S., Zhu, F., Ai, J., Hu, Z., Zhou, M., Tian, J., Su, Z., Yang, P., Nie, J., 2018. Numb Depletion Promotes Drp1-Mediated Mitochondrial Fission and Exacerbates Mitochondrial Fragmentation and Dysfunction in Acute Kidney Injury. Antioxid Redox Signal ars.2017.7432. doi:10.1089/ars.2017.7432

Losón, O.C., Song, Z., Chen, H., Chan, D.C., 2013. Fis1, Mff, MiD49, and MiD51 mediate Drp1 recruitment in mitochondrial fission. Mol. Biol. Cell 24, 659–667. doi:10.1091/mbc.E12-10-0721

López-Doménech, G., Higgs, N.F., Vaccaro, V., Roš, H., Arancibia-Cárcamo, I.L., MacAskill, A.F., Kittler, J.T., 2016. Loss of Dendritic Complexity Precedes Neurodegeneration in a Mouse Model with Disrupted Mitochondrial Distribution in Mature Dendrites. Cell Rep 17, 317–327. doi:10.1016/j.celrep.2016.09.004

Luo, F., Herrup, K., Qi, X., Yang, Y., 2017. Inhibition of Drp1 hyper-activation is protective in animal models of experimental multiple sclerosis. Experimental Neurology 292, 21–34. doi:10.1016/j.expneurol.2017.02.015

Macia, E., Ehrlich, M., Massol, R., Boucrot, E., Brunner, C., Kirchhausen, T., 2006. Dynasore, a cell-permeable inhibitor of dynamin. Dev. Cell 10, 839–850. doi:10.1016/j.devcel.2006.04.002

Mallat, A., Uchiyama, L.F., Lewis, S.C., Fredenburg, R.A., Terada, Y., Ji, N., Nunnari, J., Tseng, C.C., 2018. Discovery and characterization of selective small molecule inhibitors of the mammalian mitochondrial division dynamin, DRP1. Biochem. Biophys. Res. Commun. 499, 556–562. doi:10.1016/j.bbrc.2018.03.189

Manczak, M., Calkins, M.J., Reddy, P.H., 2011. Impaired mitochondrial dynamics and abnormal interaction of amyloid beta with mitochondrial protein Drp1 in neurons from patients with Alzheimer's disease: implications for neuronal damage. Hum Mol Genet 20, 2495–2509. doi:10.1093/hmg/ddr139

Manczak, M., Kandimalla, R., Fry, D., Sesaki, H., Reddy, P.H., 2016. Protective effects of reduced dynamin-related protein 1 against amyloid beta-induced mitochondrial dysfunction and synaptic damage in Alzheimer's disease. Hum Mol Genet 25, 5148–5166. doi:10.1093/hmg/ddw330

Manczak, M., Reddy, P.H., 2012. Abnormal interaction between the mitochondrial fission protein Drp1 and hyperphosphorylated tau in Alzheimer's disease neurons: implications for mitochondrial dysfunction and neuronal damage. Hum Mol Genet 21, 2538–2547. doi:10.1093/hmg/dds072

Maneechote, C., Palee, S., Kerdphoo, S., Jaiwongkam, T., Chattipakorn, S.C., Chattipakorn, N., 2018. Differential temporal inhibition of mitochondrial fission by Mdivi-1 exerts effective cardioprotection in cardiac ischemia/reperfusion injury. Clin. Sci. 132, 1669–1683. doi:10.1042/CS20180510

Mattie, S., Riemer, J., Wideman, J.G., McBride, H.M., 2018. A new mitofusin topology places the redox-regulated C terminus in the mitochondrial intermembrane space. J. Cell Biol. 217, 507–515. doi:10.1083/jcb.201611194

McLelland, G.-L., Goiran, T., Yi, W., Dorval, G., Chen, C.X., Lauinger, N.D., Krahn, A.I., Valimehr, S., Rakovic, A., Rouiller, I., Durcan, T.M., Trempe, J.-F., Fon, E.A., 2018. Mfn2 ubiquitination by PINK1/parkin gates the p97-dependent release of ER from mitochondria to drive mitophagy. Elife 7, e16038. doi:10.7554/eLife.32866

Miret-Casals, L., Sebastián, D., Brea, J., Rico-Leo, E.M., Palacín, M., Fernández-Salguero, P.M., Loza, M.I., Albericio, F., Zorzano, A., 2018. Identification of New Activators of Mitochondrial Fusion Reveals a Link between Mitochondrial Morphology and Pyrimidine Metabolism. Cell Chem Biol 25, 268–278.e4. doi:10.1016/j.chembiol.2017.12.001

Mishra, P., Carelli, V., Manfredi, G., Chan, D.C., 2014. Proteolytic cleavage of Opa1 stimulates mitochondrial inner membrane fusion and couples fusion to oxidative phosphorylation. Cell Metabolism 19, 630–641. doi:10.1016/j.cmet.2014.03.011

Mishra, P., Chan, D.C., 2014. Mitochondrial dynamics and inheritance during cell division, development and disease. Nat Rev Mol Cell Biol 15, 634–646. doi:10.1038/nrm3877

Misko, A., Jiang, S., Wegorzewska, I., Milbrandt, J., Baloh, R.H., 2010. Mitofusin 2 is necessary for transport of axonal mitochondria and interacts with the Miro/Milton complex. J Neurosci 30, 4232–4240. doi:10.1523/JNEUROSCI.6248-09.2010

Mitra, K., Wunder, C., Roysam, B., Lin, G., Lippincott-Schwartz, J., 2009. A hyperfused mitochondrial state achieved at G1-S regulates cyclin E buildup and entry into S phase. Proc. Natl. Acad. Sci. U.S.A. 106, 11960–11965. doi:10.1073/pnas.0904875106

Moore, A.S., Holzbaur, E.L.F., 2018. Mitochondrial-cytoskeletal interactions: dynamic associations that facilitate network function and remodeling. Curr Opin Physiol 3, 94–100. doi:10.1016/j.cophys.2018.03.003

Naon, D., Zaninello, M., Giacomello, M., Varanita, T., Grespi, F., Lakshminaranayan, S., Serafini, A., Semenzato, M., Herkenne, S., Hernández-Alvarez, M.I., Zorzano, A., De Stefani, D., Dorn, G.W., Scorrano, L., 2016. Critical reappraisal confirms that Mitofusin 2 is an endoplasmic reticulum-mitochondria tether. Proc. Natl. Acad. Sci. U.S.A. 113, 11249–11254. doi:10.1073/pnas.1606786113

Narendra, D., Tanaka, A., Suen, D.-F., Youle, R.J., 2008. Parkin is recruited selectively to impaired mitochondria and promotes their autophagy. J. Cell Biol. 183, 795–803. doi:10.1083/jcb.200809125

Nasca, A., Nardecchia, F., Commone, A., Semeraro, M., Legati, A., Garavaglia, B., Ghezzi, D., Leuzzi, V., 2018. Clinical and Biochemical Features in a Patient With Mitochondrial Fission Factor Gene Alteration. Front Genet 9, 625. doi:10.3389/fgene.2018.00625

Nasca, A., Scotton, C., Zaharieva, I., Neri, M., Selvatici, R., Magnusson, O.T., Gal, A., Weaver, D., Rossi, R., Armaroli, A., Pane, M., Phadke, R., Sarkozy, A., Muntoni, F., Hughes, I., Cecconi, A., Hajnóczky, G., Donati, A., Mercuri, E., Zeviani, M., Ferlini, A., Ghezzi, D., 2017. Recessive mutations in MSTO1 cause mitochondrial dynamics impairment, leading to myopathy and ataxia. Hum. Mutat. 38, 970–977. doi:10.1002/humu.23262

Nemani, N., Carvalho, E., Tomar, D., Dong, Z., Ketschek, A., Breves, S.L., Jaña, F., Worth, A.M., Heffler, J., Palaniappan, P., Tripathi, A., Subbiah, R., Riitano, M.F., Seelam, A., Manfred, T., Itoh, K., Meng, S., Sesaki, H., Craigen, W.J., Rajan, S., Shanmughapriya, S., Caplan, J., Prosser, B.L., Gill, D.L., Stathopulos, P.B., Gallo, G., Chan, D.C., Mishra, P., Madesh, M., 2018. MIRO-1 Determines Mitochondrial Shape Transition upon GPCR Activation and Ca2+ Stress. Cell Rep 23, 1005–1019. doi:10.1016/j.celrep.2018.03.098

Nguyen, T.T., Oh, S.S., Weaver, D., Lewandowska, A., Maxfield, D., Schuler, M.-H., Smith, N.K., Macfarlane, J., Saunders, G., Palmer, C.A., Debattisti, V., Koshiba, T., Pulst, S., Feldman, E.L., Hajnóczky, G., Shaw, J.M., 2014. Loss of Miro1-directed mitochondrial movement results in a novel murine model for neuron disease. Proc. Natl. Acad. Sci. U.S.A. 111, E3631–40. doi:10.1073/pnas.1402449111

Olichon, A., Baricault, L., Gas, N., Guillou, E., Valette, A., Belenguer, P., Lenaers, G., 2003. Loss of OPA1 perturbates the mitochondrial inner membrane structure and integrity, leading to cytochrome c release and apoptosis. J Biol Chem 278, 7743–7746. doi:10.1074/jbc.C200677200

Osellame, L.D., Singh, A.P., Stroud, D.A., Palmer, C.S., Stojanovski, D., Ramachandran, R., Ryan, M.T., 2016. Cooperative and independent roles of the Drp1 adaptors Mff, MiD49 and MiD51 in mitochondrial fission. Journal of Cell Science 129, 2170–2181. doi:10.1242/jcs.185165

Otera, H., Ishihara, N., Mihara, K., 2013. New insights into the function and regulation of mitochondrial fission. Biochim. Biophys. Acta 1833, 1256–1268. doi:10.1016/j.bbamcr.2013.02.002

Otera, H., Mihara, K., 2012. Mitochondrial dynamics: functional link with apoptosis. Int J Cell Biol 2012, 821676–10. doi:10.1155/2012/821676

Otera, H., Miyata, N., Kuge, O., Mihara, K., 2016. Drp1-dependent mitochondrial fission via MiD49/51 is essential for apoptotic cristae remodeling. J. Cell Biol. 212, 531–544. doi:10.1083/jcb.201508099

Palmer, C.S., Elgass, K.D., Parton, R.G., Osellame, L.D., Stojanovski, D., Ryan, M.T., 2013. Adaptor proteins MiD49 and MiD51 can act independently of Mff and Fis1 in Drp1 recruitment and are specific for mitochondrial fission. J Biol Chem 288, 27584–27593. doi:10.1074/jbc.M113.479873

Papanicolaou, K.N., Khairallah, R.J., Ngoh, G.A., Chikando, A., Luptak, I., O'Shea, K.M., Riley, D.D., Lugus, J.J., Colucci, W.S., Lederer, W.J., Stanley, W.C., Walsh, K., 2011. Mitofusin-2 maintains mitochondrial structure and contributes to stress-induced permeability transition in cardiac myocytes. Mol. Cell. Biol. 31, 1309–1328. doi:10.1128/MCB.00911-10

Park, J., Choi, H., Min, J.-S., Park, S.-J., Kim, J.-H., Park, H.-J., Kim, B., Chae, J.-I., Yim, M., Lee, D.-S., 2013. Mitochondrial dynamics modulate the expression of pro-inflammatory mediators in microglial cells. J. Neurochem. 127, 221–232. doi:10.1111/jnc.12361

Park, J.-S., Davis, R.L., Sue, C.M., 2018. Mitochondrial Dysfunction in Parkinson's Disease: New Mechanistic Insights and Therapeutic Perspectives. Curr Neurol Neurosci Rep 18, 21. doi:10.1007/s11910-018-0829-3

Park, Y.-Y., Nguyen, O.T.K., Kang, H., Cho, H., 2014. MARCH5-mediated quality control on acetylated Mfn1 facilitates mitochondrial homeostasis and cell survival. Cell Death Dis 5, e1172–e1172. doi:10.1038/cddis.2014.142

Pickles, S., Vigié, P., Youle, R.J., 2018. Mitophagy and Quality Control Mechanisms in Mitochondrial Maintenance. Curr. Biol. 28, R170–R185. doi:10.1016/j.cub.2018.01.004

Pickrell, A. M., & Youle, R. J. (2015). The Roles of PINK1, Parkin, and Mitochondrial Fidelity in Parkinson's Disease. Neuron, 85(2), 257–273. https://doi.org/10.1016/j.neuron.2014.12.007

Pilling, A.D., Horiuchi, D., Lively, C.M., Saxton, W.M., 2006. Kinesin-1 and Dynein are the primary motors for fast transport of mitochondria in Drosophila motor axons. Mol. Biol. Cell 17, 2057–2068. doi:10.1091/mbc.e05-06-0526

Prudent, J., Zunino, R., Sugiura, A., Mattie, S., Shore, G.C., McBride, H.M., 2015. MAPL SUMOylation of Drp1 Stabilizes an ER/Mitochondrial Platform Required for Cell Death. Molecular Cell 59, 941–955. doi:10.1016/j.molcel.2015.08.001

Pyakurel, A., Savoia, C., Hess, D., Scorrano, L., 2015. Extracellular regulated kinase phosphorylates mitofusin 1 to control mitochondrial morphology and apoptosis. Molecular Cell 58, 244–254. doi:10.1016/j.molcel.2015.02.021

Qi, J., Wang, F., Yang, P., Wang, X., Xu, R., Chen, J., Yuan, Y., Lu, Z., Duan, J., 2018. Mitochondrial Fission Is Required for Angiotensin II-Induced Cardiomyocyte Apoptosis Mediated by a Sirt1-p53 Signaling Pathway. Front Pharmacol 9, 176. doi:10.3389/fphar.2018.00176

Qi, X., Qvit, N., Su, Y.-C., Mochly-Rosen, D., 2013. A novel Drp1 inhibitor diminishes aberrant mitochondrial fission and neurotoxicity. Journal of Cell Science 126, 789–802. doi:10.1242/jcs.114439

Qi, Y., Yan, L., Yu, C., Guo, X., Zhou, X., Hu, X., Huang, X., 2016. Structures of human mitofusin 1 provide insight into mitochondrial tethering. jcb.rupress.org.

Rambold, A.S., Pearce, E.L., 2018. Mitochondrial Dynamics at the Interface of Immune Cell Metabolism and Function. Trends Immunol. 39, 6–18. doi:10.1016/j.it.2017.08.006

Rappold, P.M., Cui, M., Grima, J.C., Fan, R.Z., de Mesy-Bentley, K.L., Chen, L., Zhuang, X., Bowers, W.J., Tieu, K., 2014. Drp1 inhibition attenuates neurotoxicity and dopamine release deficits in vivo. Nat Commun 5, 5244. doi:10.1038/ncomms6244

Reddy, P.H., 2014. Increased mitochondrial fission and neuronal dysfunction in Huntington's disease: implications for molecular inhibitors of excessive mitochondrial fission. Drug Discov. Today 19, 951–955. doi:10.1016/j.drudis.2014.03.020

Rocha, A.G., Franco, A., Krezel, A.M., Rumsey, J.M., Alberti, J.M., Knight, W.C., Biris, N., Zacharioudakis, E., Janetka, J.W., Baloh, R.H., Kitsis, R.N., Mochly-Rosen, D., Townsend, R.R., Gavathiotis, E., Dorn, G.W., 2018. MFN2 agonists reverse mitochondrial defects in preclinical models of Charcot-Marie-Tooth disease type 2A. Science 360, 336–341. doi:10.1126/science.aao1785

Roe, A. J., & Qi, X. (2018). Drp1 phosphorylation by MAPK1 causes mitochondrial dysfunction in cell culture model of Huntington's disease. Biochemical and Biophysical Research Communications, 496(2), 706–711. https://doi.org/10.1016/j.bbrc.2018.01.114

Rosdah, A.A., Bond, S.T., Sivakumaran, P., Hoque, A., Oakhill, J.S., Drew, B.G., Delbridge, L.M.D., Lim, S.Y., 2017. Mdivi-1 Protects Human W8B2+ Cardiac Stem Cells from Oxidative Stress and Simulated Ischemia-Reperfusion Injury. Stem Cells Dev. 26, 1771–1780. doi:10.1089/scd.2017.0157

Rovira-Llopis, S., Bañuls, C., Diaz-Morales, N., Hernandez-Mijares, A., Rocha, M., Victor, V.M., 2017. Mitochondrial dynamics in type 2 diabetes: Pathophysiological implications. Redox Biol 11, 637–645. doi:10.1016/j.redox.2017.01.013

Sahenk, Z., Galloway, G., Clark, K.R., Malik, V., Rodino-Klapac, L.R., Kaspar, B.K., Chen, L., Braganza, C., Montgomery, C., Mendell, J.R., 2014. AAV1.NT-3 gene therapy for charcot-marie-tooth neuropathy. Mol. Ther. 22, 511–521. doi:10.1038/mt.2013.250

Salazar-Roa, M., Malumbres, M., 2017. Fueling the Cell Division Cycle. Trends Cell Biol 27, 69–81. doi:10.1016/j.tcb.2016.08.009

Santel, A., Fuller, M.T., 2001. Control of mitochondrial morphology by a human mitofusin. J Cell Sci 114, 867–874.

Sarzi, E., Angebault, C., Seveno, M., Gueguen, N., Chaix, B., Bielicki, G., Boddaert, N., Mausset-Bonnefont, A.-L., Cazevieille, C., Rigau, V., Renou, J.-P., Wang, J., Delettre, C., Brabet, P., Puel, J.-L., Hamel, C.P., Reynier, P., Lenaers, G., 2012. The human OPA1delTTAG mutation induces premature age-related systemic neurodegeneration in mouse. Brain 135, 3599–3613. doi:10.1093/brain/aws303

Sarzi, E., Seveno, M., Piro-Mégy, C., Elzière, L., Quilès, M., Péquignot, M., Müller, A., Hamel, C.P., Lenaers, G., Delettre, C., 2018. OPA1 gene therapy prevents retinal ganglion cell loss in a Dominant Optic Atrophy mouse model. Sci Rep 8, 2468. doi:10.1038/s41598-018-20838-8

Schwarz, T.L., 2013. Mitochondrial trafficking in neurons. Cold Spring Harb Perspect Biol 5, a011304–a011304. doi:10.1101/cshperspect.a011304

Seo, B.J., Yoon, S.H., Do, J.T., 2018. Mitochondrial Dynamics in Stem Cells and Differentiation. Int J Mol Sci 19, 3893. doi:10.3390/ijms19123893

Serasinghe, M.N., Wieder, S.Y., Renault, T.T., Elkholi, R., Asciolla, J.J., Yao, J.L., Jabado, O., Hoehn, K., Kageyama, Y., Sesaki, H., Chipuk, J.E., 2015. Mitochondrial division is requisite to RAS-induced transformation and targeted by oncogenic MAPK pathway inhibitors. Molecular Cell 57, 521–536. doi:10.1016/j.molcel.2015.01.003

Shaltouki, A., Hsieh, C.-H., Kim, M.J., Wang, X., 2018. Alpha-synuclein delays mitophagy and targeting Miro rescues neuron loss in Parkinson's models. Acta Neuropathol. 136, 607–620. doi:10.1007/s00401-018-1873-4

Shamseldin, H.E., Alshammari, M., Al-Sheddi, T., Salih, M.A., Alkhalidi, H., Kentab, A., Repetto, G.M., Hashem, M., Alkuraya, F.S., 2012. Genomic analysis of mitochondrial diseases in a

consanguineous population reveals novel candidate disease genes. J. Med. Genet. 49, 234–241. doi:10.1136/jmedgenet-2012-100836

Sharp, W.W., Fang, Y.H., Han, M., Zhang, H.J., Hong, Z., Banathy, A., Morrow, E., Ryan, J.J., Archer, S.L., 2014. Dynamin-related protein 1 (Drp1)-mediated diastolic dysfunction in myocardial ischemia-reperfusion injury: therapeutic benefits of Drp1 inhibition to reduce mitochondrial fission. FASEB J. 28, 316–326. doi:10.1096/fj.12-226225

Sheffer, R., Douiev, L., Edvardson, S., Shaag, A., Tamimi, K., Soiferman, D., Meiner, V., Saada, A., 2016. Postnatal microcephaly and pain insensitivity due to a de novo heterozygous DNM1L mutation causing impaired mitochondrial fission and function. Am. J. Med. Genet. A 170, 1603–1607. doi:10.1002/ajmg.a.37624

Shirendeb, U.P., Calkins, M.J., Manczak, M., Anekonda, V., Dufour, B., McBride, J.L., Mao, P., Reddy, P.H., 2012. Mutant huntingtin"s interaction with mitochondrial protein Drp1 impairs mitochondrial biogenesis and causes defective axonal transport and synaptic degeneration in Huntington"s disease. Hum Mol Genet 21, 406–420. doi:10.1093/hmg/ddr475

Shutt, T., Geoffrion, M., Milne, R., McBride, H.M., 2012. The intracellular redox state is a core determinant of mitochondrial fusion. EMBO Rep 13, 909–915. doi:10.1038/embor.2012.128

Sin, J., McIntyre, L., Stotland, A., Feuer, R., Gottlieb, R.A., 2017. Coxsackievirus B Escapes the Infected Cell in Ejected Mitophagosomes. J. Virol. 91, 1201. doi:10.1128/JVI.01347-17

Smirnova, E., Griparic, L., Shurland, D.L., van der Bliek, A.M., 2001. Dynamin-related protein Drp1 is required for mitochondrial division in mammalian cells. Mol. Biol. Cell 12, 2245–2256. doi:10.1091/mbc.12.8.2245

Smith, E.F., Shaw, P.J., De Vos, K.J., 2017. The role of mitochondria in amyotrophic lateral sclerosis. Neurosci. Lett. doi:10.1016/j.neulet.2017.06.052

Solesio, M.E., Saez-Atienzar, S., Jordán, J., Galindo, M.F., 2012. Characterization of mitophagy in the 6-hydoxydopamine Parkinson's disease model. Toxicol. Sci. 129, 411–420. doi:10.1093/toxsci/kfs218

Song, M., Franco, A., Fleischer, J.A., Zhang, L., Dorn, G.W., 2017. Abrogating Mitochondrial Dynamics in Mouse Hearts Accelerates Mitochondrial Senescence. Cell Metabolism 26, 872–883.e5. doi:10.1016/j.cmet.2017.09.023

Song, M., Mihara, K., Chen, Y., Scorrano, L., Dorn, G.W., 2015. Mitochondrial fission and fusion factors reciprocally orchestrate mitophagic culling in mouse hearts and cultured fibroblasts. Cell Metabolism 21, 273–286. doi:10.1016/j.cmet.2014.12.011

Song, W., Chen, J., Petrilli, A., Liot, G., Klinglmayr, E., Zhou, Y., Poquiz, P., Tjong, J., Pouladi, M.A., Hayden, M.R., Masliah, E., Ellisman, M., Rouiller, I., Schwarzenbacher, R., Bossy, B., Perkins, G., Bossy-Wetzel, E., 2011. Mutant huntingtin binds the mitochondrial fission GTPase dynamin-related protein-1 and increases its enzymatic activity. Nat Med 17, 377–382. doi:10.1038/nm.2313

Song, Z., Chen, H., Fiket, M., Alexander, C., Chan, D.C., 2007. OPA1 processing controls mitochondrial fusion and is regulated by mRNA splicing, membrane potential, and Yme1L. J. Cell Biol. 178, 749–755. doi:10.1083/jcb.200704110

Stuppia, G., Rizzo, F., Riboldi, G., Del Bo, R., Nizzardo, M., Simone, C., Comi, G.P., Bresolin, N., Corti, S., 2015. MFN2-related neuropathies: Clinical features, molecular pathogenesis and therapeutic perspectives. J. Neurol. Sci. 356, 7–18. doi:10.1016/j.jns.2015.05.033

Su, Y.-C., Qi, X., 2013. Inhibition of excessive mitochondrial fission reduced aberrant autophagy and neuronal damage caused by LRRK2 G2019S mutation. Hum Mol Genet 22, 4545–4561. doi:10.1093/hmg/ddt301

Suárez-Rivero, J.M., Villanueva-Paz, M., la Cruz-Ojeda, de, P., la Mata, de, M., Cotán, D., Oropesa-Ávila, M., de Lavera, I., Álvarez-Córdoba, M., Luzón-Hidalgo, R., Sánchez-Alcázar, J.A., 2016. Mitochondrial Dynamics in Mitochondrial Diseases. Diseases 5, 1. doi:10.3390/diseases5010001

Sugiura, A., Nagashima, S., Tokuyama, T., Amo, T., Matsuki, Y., Ishido, S., Kudo, Y., McBride, H.M., Fukuda, T., Matsushita, N., Inatome, R., Yanagi, S., 2013. MITOL Regulates Endoplasmic Reticulum-Mitochondria Contacts via Mitofusin2. Molecular Cell 51, 20–34. doi:10.1016/j.molcel.2013.04.023

Sun, N., Youle, R.J., Finkel, T., 2016. The Mitochondrial Basis of Aging. Molecular Cell 61, 654–666. doi:10.1016/j.molcel.2016.01.028

Szabo, A., Sumegi, K., Fekete, K., Hocsak, E., Debreceni, B., Setalo, G., Kovacs, K., Deres, L., Kengyel, A., Kovacs, D., Mandl, J., Nyitrai, M., Febbraio, M.A., Gallyas, F., Sumegi, B., 2018. Activation of mitochondrial fusion provides a new treatment for mitochondria-related diseases. Biochem. Pharmacol. 150, 86–96. doi:10.1016/j.bcp.2018.01.038

Taguchi, N., Ishihara, N., Jofuku, A., Oka, T., Mihara, K., 2007. Mitotic phosphorylation of dynamin-related GTPase Drp1 participates in mitochondrial fission. J Biol Chem 282, 11521–11529. doi:10.1074/jbc.M607279200

Tang, Y., Mi, C., Liu, J., Gao, F., Long, J., 2014. Compromised mitochondrial remodeling in compensatory hypertrophied myocardium of spontaneously hypertensive rat. Cardiovasc. Pathol. 23, 101–106. doi:10.1016/j.carpath.2013.11.002

Tian, L., Neuber-Hess, M., Mewburn, J., Dasgupta, A., Dunham-Snary, K., Wu, D., Chen, K.-H., Hong, Z., Sharp, W.W., Kutty, S., Archer, S.L., 2017. Ischemia-induced Drp1 and Fis1-mediated mitochondrial fission and right ventricular dysfunction in pulmonary hypertension. J. Mol. Med. 95, 381–393. doi:10.1007/s00109-017-1522-8

Toledo, F.G.S., Watkins, S., Kelley, D.E., 2006. Changes induced by physical activity and weight loss in the morphology of intermyofibrillar mitochondria in obese men and women. J. Clin. Endocrinol. Metab. 91, 3224–3227. doi:10.1210/jc.2006-0002

Tondera, D., Grandemange, S., Jourdain, A., Karbowski, M., Mattenberger, Y., Herzig, S., Da Cruz, S., Clerc, P., Raschke, I., Merkwirth, C., Ehses, S., Krause, F., Chan, D.C., Alexander, C., Bauer, C., Youle, R., Langer, T., Martinou, J.-C., 2009. SLP-2 is required for stress-induced mitochondrial hyperfusion. EMBO J 28, 1589–1600. doi:10.1038/emboj.2009.89

Toyama, E.Q., Herzig, S., Courchet, J., Lewis, T.L., Losón, O.C., Hellberg, K., Young, N.P., Chen, H., Polleux, F., Chan, D.C., Shaw, R.J., 2016. Metabolism. AMP-activated protein kinase mediates mitochondrial fission in response to energy stress. Science 351, 275–281. doi:10.1126/science.aab4138

Troncoso, R., Paredes, F., Parra, V., Gatica, D., Vásquez-Trincado, C., Quiroga, C., Bravo-Sagua, R., López-Crisosto, C., Rodriguez, A.E., Oyarzún, A.P., Kroemer, G., Lavandero, S., 2014. Dexamethasone-induced autophagy mediates muscle atrophy through mitochondrial clearance. Cell Cycle 13, 2281–2295. doi:10.4161/cc.29272

Trotta, A.P., Chipuk, J.E., 2017. Mitochondrial dynamics as regulators of cancer biology. Cell Mol Life Sci 74, 1999–2017. doi:10.1007/s00018-016-2451-3

Tubbs, E., Rieusset, J., 2017. Metabolic signaling functions of ER-mitochondria contact sites: role in metabolic diseases. J. Mol. Endocrinol. 58, R87–R106. doi:10.1530/JME-16-0189

Vanstone, J.R., Smith, A.M., McBride, S., Naas, T., Holcik, M., Antoun, G., Harper, M.-E., Michaud, J., Sell, E., Chakraborty, P., Tetreault, M., Care4Rare Consortium, Majewski, J., Baird, S., Boycott, K.M., Dyment, D.A., MacKenzie, A., Lines, M.A., 2016. DNM1L-related mitochondrial fission defect presenting as refractory epilepsy. Eur. J. Hum. Genet. 24, 1084–1088. doi:10.1038/ejhg.2015.243

Vargo, J.W., Walker, S.N., Gopal, S.R., Deshmukh, A.R., McDermott, B.M., Alagramam, K.N., Stepanyan, R., 2017. Inhibition of Mitochondrial Division Attenuates Cisplatin-Induced Toxicity in the Neuromast Hair Cells. Front Cell Neurosci 11, 393. doi:10.3389/fncel.2017.00393

Wai, T., García-Prieto, J., Baker, M.J., Merkwirth, C., Benit, P., Rustin, P., Rupérez, F.J., Barbas, C., Ibañez, B., Langer, T., 2015. Imbalanced OPA1 processing and mitochondrial fragmentation cause heart failure in mice. Science 350, aad0116-aad0116. doi:10.1126/science.aad0116

Wai, T., Langer, T., 2016. Mitochondrial Dynamics and Metabolic Regulation. Trends Endocrinol. Metab. 27, 105–117. doi:10.1016/j.tem.2015.12.001

Wakabayashi, J., Zhang, Z., Wakabayashi, N., Tamura, Y., Fukaya, M., Kensler, T.W., Iijima, M., Sesaki, H., 2009. The dynamin-related GTPase Drp1 is required for embryonic and brain development in mice. J. Cell Biol. 186, 805–816. doi:10.1083/jcb.200903065

Wang, Danling, Wang, J., Bonamy, G.M.C., Meeusen, S., Brusch, R.G., Turk, C., Yang, P., Schultz, P.G., 2012. A small molecule promotes mitochondrial fusion in mammalian cells. Angew. Chem. Int. Ed. Engl. 51, 9302–9305. doi:10.1002/anie.201204589

Wang, Hongxia, Song, P., Du, L., Tian, W., Yue, W., Liu, M., Li, D., Wang, B., Zhu, Y., Cao, C., Zhou, J., Chen, Q., 2011. Parkin ubiquitinates Drp1 for proteasome-dependent degradation: implication of dysregulated mitochondrial dynamics in Parkinson disease. J Biol Chem 286, 11649–11658. doi:10.1074/jbc.M110.144238

Wang, Huan, Yi, J., Li, X., Xiao, Y., Dhakal, K., Zhou, J., 2018. ALS-associated mutation SOD1G93A leads to abnormal mitochondrial dynamics in osteocytes. Bone 106, 126–138. doi:10.1016/j.bone.2017.10.010

Wang, Peng, Li, Y., Yang, Z., Yu, T., Zheng, G., Fang, X., Huang, Z., Jiang, L., Tang, W., 2018. Inhibition of dynamin-related protein 1 has neuroprotective effect comparable with therapeutic hypothermia in a rat model of cardiac arrest. Transl Res 194, 68–78. doi:10.1016/j.trsl.2018.01.002

Wang, Wenjian, Wang, Y., Long, J., Wang, J., Haudek, S.B., Overbeek, P., Chang, B.H.J., Schumacker, P.T., Danesh, F.R., 2012. Mitochondrial fission triggered by hyperglycemia is mediated by ROCK1 activation in podocytes and endothelial cells. Cell Metabolism 15, 186–200. doi:10.1016/j.cmet.2012.01.009

Wang, Wenzhang, Yin, J., Ma, X., Zhao, F., Siedlak, S.L., Wang, Z., Torres, S., Fujioka, H., Xu, Y., Perry, G., Zhu, X., 2017. Inhibition of mitochondrial fragmentation protects against Alzheimer's disease in rodent model. Hum Mol Genet 26, 4118–4131. doi:10.1093/hmg/ddx299

Wang, Xinnan, Winter, D., Ashrafi, G., Schlehe, J., Wong, Y.L., Selkoe, D., Rice, S., Steen, J., LaVoie, M.J., Schwarz, T.L., 2011. PINK1 and Parkin target Miro for phosphorylation and degradation to arrest mitochondrial motility. Cell 147, 893–906. doi:10.1016/j.cell.2011.10.018

Wasiak, S., Zunino, R., McBride, H.M., 2007. Bax/Bak promote sumoylation of DRP1 and its stable association with mitochondria during apoptotic cell death. J. Cell Biol. 177, 439–450. doi:10.1083/jcb.200610042

Waterham, H.R., Koster, J., van Roermund, C.W.T., Mooyer, P.A.W., Wanders, R.J.A., Leonard, J.V., 2007. A lethal defect of mitochondrial and peroxisomal fission. N. Engl. J. Med. 356, 1736–1741. doi:10.1056/NEJMoa064436

Whitley, B.N., Lam, C., Cui, H., Haude, K., Bai, R., Escobar, L., Hamilton, A., Brady, L., Tarnopolsky, M.A., Dengle, L., Picker, J., Lincoln, S., Lackner, L.L., Glass, I.A., Hoppins, S., 2018. Aberrant Drp1-mediated mitochondrial division presents in humans with variable outcomes. Hum Mol Genet 27, 3710–3719. doi:10.1093/hmg/ddy287

Williams, M., Caino, M.C., 2018. Mitochondrial Dynamics in Type 2 Diabetes and Cancer. Front Endocrinol (Lausanne) 9, 211. doi:10.3389/fendo.2018.00211

Wu, P., Li, Y., Zhu, S., Wang, C., Dai, J., Zhang, G., Zheng, B., Xu, S., Wang, L., Zhang, T., Zhou, P., Zhang, J.H., Shi, H., 2017. Mdivi-1 Alleviates Early Brain Injury After Experimental Subarachnoid Hemorrhage in Rats, Possibly via Inhibition of Drp1-Activated Mitochondrial Fission and Oxidative Stress. Neurochem. Res. 42, 1449–1458. doi:10.1007/s11064-017-2201-4

Wu, Q., Gao, C., Wang, H., Zhang, X., Li, Q., Gu, Z., Shi, X., Cui, Y., Wang, T., Chen, X., Wang, X., Luo, C., Tao, L., 2018. Mdivi-1 alleviates blood-brain barrier disruption and cell death in experimental traumatic brain injury by mitigating autophagy dysfunction and mitophagy activation. Int. J. Biochem. Cell Biol. 94, 44–55. doi:10.1016/j.biocel.2017.11.007

Xu, Fenglian, Armstrong, R., Urrego, D., Qazzaz, M., Pehar, M., Armstrong, J.N., Shutt, T., Syed, N., 2016. The mitochondrial division inhibitor Mdivi-1 rescues mammalian neurons from anesthetic-induced cytotoxicity. Mol Brain 9, 35. doi:10.1186/s13041-016-0210-x

Xu, Shan, Cherok, E., Das, S., Li, S., Roelofs, B.A., Ge, S.X., Polster, B.M., Boyman, L., Lederer, W.J., Wang, C., Karbowski, M., 2016. Mitochondrial E3 ubiquitin ligase MARCH5 controls mitochondrial fission and cell sensitivity to stress-induced apoptosis through regulation of MiD49 protein. Mol. Biol. Cell 27, 349–359. doi:10.1091/mbc.E15-09-0678

Xu, Shangcheng, Wang, P., Zhang, H., Gong, G., Gutierrez Cortes, N., Zhu, W., Yoon, Y., Tian, R., Wang, W., 2016. CaMKII induces permeability transition through Drp1 phosphorylation during chronic β-AR stimulation. Nat Commun 7, 13189. doi:10.1038/ncomms13189

Yamada, T., Murata, D., Adachi, Y., Itoh, K., Kameoka, S., Igarashi, A., Kato, T., Araki, Y., Huganir, R.L., Dawson, T.M., Yanagawa, T., Okamoto, K., Iijima, M., Sesaki, H., 2018. Mitochondrial Stasis Reveals p62-Mediated Ubiquitination in Parkin-Independent Mitophagy and Mitigates Nonalcoholic Fatty Liver Disease. Cell Metabolism 28, 588–604.e5. doi:10.1016/j.cmet.2018.06.014

Yan, J., Liu, X.-H., Han, M.-Z., Wang, Y.-M., Sun, X.-L., Yu, N., Li, T., Su, B., Chen, Z.-Y., 2015. Blockage of GSK3β-mediated Drp1 phosphorylation provides neuroprotection in neuronal and mouse models of Alzheimer's disease. Neurobiol. Aging 36, 211–227. doi:10.1016/j.neurobiolaging.2014.08.005

Yan, L., Qi, Y., Huang, X., Yu, C., Lan, L., Guo, X., Rao, Z., Hu, J., Lou, Z., 2018. Structural basis for GTP hydrolysis and conformational change of MFN1 in mediating membrane fusion. Nat. Struct. Mol. Biol. 25, 233–243. doi:10.1038/s41594-018-0034-8

Yu, R., Jin, S.-B., Lendahl, U., Nistér, M., Zhao, J., 2019. Human Fis1 regulates mitochondrial dynamics through inhibition of the fusion machinery. EMBO J. doi:10.15252/embj.201899748

Yue, W., Chen, Z., Liu, H., Yan, C., Chen, M., Feng, D., Yan, C., Wu, H., Du, L., Wang, Y., Liu, J., Huang, X., Xia, L., Liu, L., Wang, X., Jin, H., Wang, J., Song, Z., Hao, X., Chen, Q., 2014. A small natural molecule promotes mitochondrial fusion through inhibition of the deubiquitinase USP30. Cell Res. 24, 482–496. doi:10.1038/cr.2014.20

Zaha, K., Matsumoto, H., Itoh, M., Saitsu, H., Kato, K., Kato, M., Ogata, S., Murayama, K., Kishita, Y., Mizuno, Y., Kohda, M., Nishino, I., Ohtake, A., Okazaki, Y., Matsumoto, N., Nonoyama, S., 2016. DNM1L-related encephalopathy in infancy with Leigh syndrome-like phenotype and suppression-burst. Clin. Genet. 90, 472–474. doi:10.1111/cge.12805

Zhang, H., Wang, P., Bisetto, S., Yoon, Y., Chen, Q., Sheu, S.-S., Wang, W., 2017. A novel fission-independent role of dynamin-related protein 1 in cardiac mitochondrial respiration. Cardiovasc. Res. 113, 160–170. doi:10.1093/cvr/cvw212

Zhang, L., Gan, X., He, Y., Zhu, Z., Zhu, J., Yu, H., 2017. Drp1-dependent mitochondrial fission mediates osteogenic dysfunction in inflammation through elevated production of reactive oxygen species. PLoS ONE 12, e0175262. doi:10.1371/journal.pone.0175262

Zhao, Y., Sun, X., Qi, X., 2018. Inhibition of Drp1 hyperactivation reduces neuropathology and behavioral deficits in zQ175 knock-in mouse model of Huntington's disease. Biochem. Biophys. Res. Commun. 507, 319–323. doi:10.1016/j.bbrc.2018.11.031

Zhou, Y., Carmona, S., Muhammad, A.K.M.G., Bell, S., Landeros, J., Vazquez, M., Ho, R., Franco, A., Bin Lu, Dorn, G.W., Wang, S., Lutz, C.M., Baloh, R.H., 2019. Restoring mitofusin balance prevents axonal degeneration in a Charcot-Marie-Tooth type 2A model. J. Clin. Invest. 129, 11. doi:10.1172/JCI124194

Zorzano, A., Hernández-Alvarez, M.I., Sebastián, D., Muñoz, J.P., 2015. Mitofusin 2 as a driver that controls energy metabolism and insulin signaling. Antioxid Redox Signal 22, 1020–1031. doi:10.1089/ars.2014.6208

Züchner, S., Mersiyanova, I.V., Muglia, M., Bissar-Tadmouri, N., Rochelle, J., Dadali, E.L., Zappia, M., Nelis, E., Patitucci, A., Senderek, J., Parman, Y., Evgrafov, O., Jonghe, P.D., Takahashi, Y., Tsuji, S., Pericak-Vance, M.A., Quattrone, A., Battaloglu, E., Polyakov, A.V., Timmerman, V., Schröder, J.M., Vance, J.M., Battologlu, E., 2004. Mutations in the mitochondrial GTPase mitofusin 2 cause Charcot-Marie-Tooth neuropathy type 2A. Nature Genetics 36, 449–451. doi:10.1038/ng1341

Chapter Two:

Aberrant Drp1-mediated mitochondrial division presents in humans with variable outcomes

Summary

The work in this chapter has been published in Human Molecular Genetics (Whitley et al., 2018). Our lab was approached by a clinician from Seattle Children's Hospital who had a patient with severe neurological and developmental abnormalities associated with a mutation in *DNM1L.* This mutation, along with three additional mutations in four patients, was identified by whole exome sequencing performed by GeneDx. I evaluated mitochondrial and peroxisomal morphology in primary fibroblasts from the patient harboring the G32A mutation to determine if the mutation and cellular dysfunction are associated with Drp1 dysfunction. I then evaluated mitochondrial morphology in mammalian and yeast cells to understand the causal role of these *DNM1L* mutations on mitochondrial dynamics and the possible implications for disease.

Introduction

Mitochondrial function is essential for many cellular processes. In addition to their canonical role in energy production and metabolism, mitochondria also contribute to lipid biosynthesis, iron cluster formation and other cellular pathways including autophagy, inflammasome activation, telomere maintenance and apoptotic cell death (1, 2). Mitochondria exist as a complex and dynamic network that moves, fuses and divides (3, 4). These processes are mediated by conserved protein families and are essential for mitochondrial distribution and quality control.

Mitochondrial division requires the coordinated action of several factors. The actin cytoskeleton and endoplasmic reticulum both contribute early in the process of division, cooperating to constrict the diameter of mitochondria (5, 6). Further constriction of mitochondria is driven by Drp1, a mechanochemical enzyme encoded by the *DNM1L* gene (7). The protein is found in the cytosol and is recruited to mitochondria by protein receptors embedded in the mitochondrial outer membrane. There are several different receptors including Mff, Fis1, MiD49 and MiD51 (5). The functional role of each receptor is not clear, but there is evidence to suggest that they can work both cooperatively and independently (8–11). Drp1 assembly is mediated by the stalk domain, which forms a helical bundle that extends from the globular GTPase domain and has multiple interaction surfaces (**Figure 2.1**) (12, 13). In the cytosol, Drp1 is a dimer and recruitment to mitochondria by receptors stimulates higher order assembly of Drp1. Following assembly of a Drp1 ring or helix on the mitochondrial surface, GTP binding and hydrolysis drive conformational changes that are coupled to constriction and disassembly (14, 15). The final step of mitochondrial division in vertebrates requires a related enzyme, dynamin-2, which works by a mechanism similar to Drp1 and constricts the mitochondria to the very narrow diameter required for separation of membranes (16). Interestingly, many components of the mitochondrial division machine have also been shown to be required for division of peroxisomes (17, 18).

Perturbations in mitochondrial division affect cell and organism health. Impaired mitochondrial fusion results in fragmentation of the mitochondrial network, due to ongoing division (19). In contrast, loss of division results in unopposed fusion, causing excessive extension of tubules and interconnection of the network (20). In both cases, mitochondrial distribution and function are

compromised. Indeed, loss of Drp1 is embryonic lethal in mice and tissue-specific knock out in the cerebellum is catastrophic, resulting in death within one day of birth (21, 22).

Several heterozygous *de novo* missense mutations in *DNM1L* have been reported in humans (MIM #614388 and 610708). All variants associated with premature death in humans have thus far reported to be in the stalk domain (23–25). These patients all presented with CNS dysgenesis and neurodegeneration manifesting as hypotonia, developmental regression and an abnormal MRI of the brain. Some pathological variants in the stalk domain of Drp1 support life, but present with seizures and developmental delay. For example, a variant in the stalk domain (G362D) was identified in a patient who presented with global developmental delay at six months of age and refractory epilepsy at one year (26). Another variant within the stalk domain (R403C) was reported in two unrelated individuals who presented with later onset refractory epilepsy, encephalopathy, developmental regression and myoclonus (27). There are also reports of mutations in the GTPase domain that cause autosomal dominant optic atrophy (E2A and A192E) or hypotonia and developmental delay (T115M) (28, 29). The dominant inheritance pattern and the molecular characterization of a few mutant variants together suggest that disease variants have limited protein function and also interfere with the function of wild type Drp1 in heterozygous patients, likely through heterotypic complex formation (27, 30).

Here we describe five patients with mutations in *DNM1L*. We report two novel *de novo* heterozygous missense mutations, one in the stalk that was associated with patient death within a year of birth (C431Y) and one in the GTPase domain (G32A). In addition, two patients were identified with a pathogenic variant that has been previously reported (R403C). Finally, we report a more modest

impact for a missense variant at position A395, compatible with survival (A395G), in contrast to the lethal variant that introduces a charge at that position (A395D). We have also performed functional characterization of each variant to gain insight into the pathophysiology of diseases associated with Drp1 variants. Our data suggests that different variants have unique molecular consequences that lead to a range of disease states.

Results

Clinical phenotypes of individuals with pathogenic variants in DNML1 varied significantly between genotypes.

All five individuals presented with hypotonia and developmental delays and/or regression. The degree of cognitive delay varied among individuals. Half of the individuals were documented to have seizures, but only the individual with the G32A variant exhibited significant ocular involvement. Brain MRI abnormalities and biochemical markers including lactate and very long chain fatty acids were variably abnormal (Supplementary Patient Information in Whitley et al., 2018). To date, there has not yet been a specific, common disorder linked to mutations in *DNM1L*. The variation in disease traits among affected individuals could be due to differential effects of specific mutations on Drp1 function. For example, it is possible that mutations in the stalk region of Drp1 have a more dramatic neurological phenotype than mutations in the bundle signaling element (BSE). Alternatively, it is possible that patients with *DNM1L* mutations have enhancing or suppressing mutations in other mitochondrial proteins that lead to differential effects on mitochondrial function. A more thorough genetic and cellular analysis will be important to fully understand the variations in human disease.

Drp1 G32A patient fibroblast mitochondria are dramatically hyperfused.

In fibroblast cells, the mitochondrial network is composed of many tubular organelles distributed throughout the cell. Loss of division activity by deletion or mutation of Drp1 results in dramatic mitochondrial elongation and interconnection due to unopposed mitochondrial fusion (7, 21, 22). To determine if the novel mutation identified in Patient 4 (G32A) altered mitochondrial structure, we visualized mitochondria in patient-derived primary fibroblasts. Indeed, we observed a highly connected mitochondrial network in the patient cells compared to age-matched control fibroblasts (**Figure 2.2**). Many regions of the network formed net-like structures that are characteristic of defective Drp1 function and loss of mitochondrial division (**Figure 2.2A, inset**).

Drp1 has also been implicated in peroxisome division and abundance (31). Peroxisome biosynthesis includes elongation of the organelle, which is followed by Drp1-mediated division. Two reported variants in the stalk of Drp1, G362D and A395D, cause peroxisome elongation in patient fibroblasts, consistent with reduced division activity (23, 26). To determine if Drp1-G32A similarly affects peroxisome morphology, we visualized peroxisomes in fibroblasts from Patient 4 and the age-matched control. The observed peroxisome length and number were indistinguishable between control and patient cells, indicating that peroxisome division is not notably altered in the patient fibroblasts (**Figure 2.3**).

Drp1 mutant alleles cannot restore normal mitochondrial morphology in Drp1 null cells.

To determine how the identified *DNM1L* mutations affected Drp1-mediated mitochondrial division, we assessed the ability of each mutant to rescue the mitochondrial morphology defect in cells lacking Drp1. HCT116 cells lacking Drp1 ($Drp1^{-/-}$) have an extensively interconnected mitochondrial

network (**Figure 2.4, empty**) (32). Expression of human Drp1 in Drp1$^{-/-}$ cells resulted in the restoration of some shorter mitochondrial tubules (**Figure 2.4, WT**). As controls for Drp1 function, we also included two well-characterized mutants that do not support mitochondrial division, Drp1-K38A and Drp1-G350D, throughout our analysis. Drp1-K38A abolishes GTPase activity by changing a key catalytic residue in the P-loop, which forms the GTP-binding pocket (33). Drp1-G350D is a variant in the stalk domain similar to a previously reported lethal mutation (G350R) and a well-characterized mutation in the yeast division protein, Dnm1 (G385D), which interferes with higher-order self-assembly (24, 34, 35). As expected, in Drp1 null cells expressing Drp1-K38A or Drp1-G350D, mitochondria remained extensively hyperfused, indicating no Drp1-dependent mitochondrial division (**Figure 2.4**).

Similar to Drp1-K38A, Drp1-G32A changes a conserved residue in the nucleotide-binding domain of Drp1. Mitochondria in Drp1$^{-/-}$ cells expressing Drp1-G32A remained hyperfused, as in Drp1-K38A-expressing cells (**Figure 2.4**). Drp1$^{-/-}$ cells expressing Drp1-R403C and Drp1-C431Y also showed no rescue, with hyperfused mitochondria in >95% of cells (**Figure 2.4**). Consistent with previously reported data, the Drp1-R403C variant was similarly unable to restore wild type mitochondria morphology in Drp1-null cells (**Figure 2.4**) (27). Interestingly, ~75% of cells expressing Drp1-A395G had mitochondria with a reticular morphology, similar to wild type cells. This suggests that Drp1-A395G supports division activity and may have a less dramatic effect on mitochondrial dynamics than the other substitutions evaluated here.

These variants are at positions that are fully conserved in the members of the dynamin-related protein family that mediate membrane scission events, consistent with critical function. To explore

the impact on conserved function, we characterized the variants in Dnm1, the S. cerevisiae mitochondrial division machine. While Drp1 and Dnm1 are very similar, Drp1 cannot restore division in yeast, consistent with unique mechanisms in each organism (11). To determine if the *de novo* patient mutations alter a fundamental and conserved property intrinsic to the division activity of Drp1 and separate from its regulation or interaction with other proteins, we made the analogous mutations in yeast dnm1 and expressed these in Δdnm1 cells to assess Dnm1-mediated mitochondrial division activity. In wild type yeast, mitochondria are localized to the cell cortex in an extended, branched network (**Figure 2.5, branched**). In contrast, mitochondria in yeast cells lacking Dnm1 form a net-like structure (**Figure 2.5, hyperfused**). Expression of wild type Dnm1-GFP resulted in a more branched network compared to Δdnm1 yeast, consistent with restoration of mitochondrial division. Dnm1-K41A (Drp1 K38A) and Dnm1-G385D (Drp1-G350D) expression in Δdnm1 yeast did not change the mitochondrial network compared to empty vector controls, consistent with their characterization as non-functional variants (34, 36).

As we observed with the human Drp1 mutants, none of the mutations in yeast Dnm1 fully rescued mitochondrial division activity (**Figure 2.5)**. Dnm1-G35A (Drp1-G32A) exhibited the most severe phenotype, with virtually no branched networks, consistent with no division activity. Drp1 stalk domain mutants, Dnm1-A430G (Drp1-A395G) and Dnm1-C466Y (Drp1-C431Y), each showed moderate rescue of division activity in Δdnm1 yeast, although not as much as wild type Dnm1. In contrast, cells expressing Dnm1-R438C (Drp1 R403C) had almost no branched mitochondrial networks, indicating that the R403C mutation also disrupts a conserved function of the mitochondrial division machine. Most notably, the morphological results were distinct between yeast and human cells for Drp1-C431Y/Dnm1-C466Y. This could suggest a smaller role for this mutation in causing

disease, or that this region of Drp1 is perhaps less sensitive to altered assembly/recruitment in human cells. The isolation of patient cells and the evaluation of mitochondrial morphology can also provide evidence into the causal role of this mutation in disease.

The dominant-negative effects on mitochondrial division by Drp1 variants.

Given that the mutations were heterozygous in patients, we set out to assess whether our identified mutant alleles exert a dominant negative effect, which would interfere with the function of the wild type Drp1. Indeed, the extensive mitochondrial hyperfusion observed in Patient 4 fibroblasts suggests that the G32A allele is dominant-negative (**Figure 2.2**). Previous work indicates that overexpression of Drp1-A395D and Drp1-R403C mutants in wild type cells inhibits normal division activity (27, 30). We expressed Drp1-GFP mutants by transient transfection with a fluorescent mitochondrial matrix marker in wild type HCT116 cells, which have normal mitochondrial division activity, and scored mitochondrial morphology. We also examined Drp1-GFP assembly and subcellular localization as a proxy for mitochondrial recruitment and higher order assembly.

Cells expressing the mitochondrial matrix marker alone or wild type GFP-Drp1 maintained a reticular mitochondrial network and we observed localization of several GFP-Drp1 foci on mitochondria (Fig. 5). Expression of either GFP-Drp1-K38A or GFP-Drp1-G350D resulted in a hyperfused mitochondrial network, as expected for dominant negative mutants (**Figure 2.6, hyperfused**). GFP-Drp1-K38A formed abnormally large foci that colocalized with mitochondria while GFP-Drp1-G350D remained completely cytosolic. These data indicate that, while both block activity of the Drp1-WT, these mutations affect different steps in the division pathway, including recruitment to mitochondria and higher order Drp1 assembly. GFP-Drp1-G32A also had very strong dominant negative effects,

increasing the amount of hyperfused mitochondria from 18.5% in cells expressing Drp1-WT to 86.2% in cells expressing the mutant (**Figure 2.6**). GFP-Drp1-K38A forms some foci in cells, GFP-Drp1-G32A remained completely cytosolic, and formed no foci on mitochondria, indicating that GFP-Drp1-G32A has defects in mitochondrial localization and higher order assembly. GFP-Drp1-A395G and GFP-Drp1-C431Y had a less severe impact on Drp1-WT function, averaging a 1.9-fold increase the number of cells with hyperfused mitochondria compared to cells expressing GFP-Drp1-WT or the mitochondrial matrix marker alone (**Figure 2.6**). Because these two substitutions also had the most subtle effects in the human and yeast rescue experiments, respectively, it is not clear that Drp1 activity in these cells is the primary driver of disease. Consistent with this, these mutants show only minor defects in mitochondrial recruitment and higher order assembly in the presence of wild type Drp1, as all cells expressing these variants show some GFP-Drp1 foci colocalized with mitochondria. Of the stalk domain variants, GFP-Drp1-R403C had stronger dominant negative effects, but GFP-Drp1 recruitment was indistinguishable from the wild type GFP-Drp1 (**Figure 2.6**).

To determine if the dominant negative properties of these mutants are conserved, we expressed Dnm1 in wild type (W303) yeast. Mitochondria in wild type yeast cells expressing Dnm1 are mostly reticular and branched. In contrast, expression of Dnm1-K41A (Drp1-K38A) or Dnm1-G385D (Drp1-G350D) resulted in mitochondria that are highly connected or hyperfused, with a more dramatic phenotype in G385D-expressing cells (**Figure 2.7**). Once again, Dnm1-G35A (Drp1-G32A) was the most potent dominant negative allele from this group of patient variants, with 75% of cells having hyperfused mitochondria compared to 10% with Dnm1-WT (Fig. 6). In contrast, the stalk domain mutants were only mildly dominant negative, and shifted the population of cells with hyperfused mitochondria from 12% with expression of Dnm1-WT to 15-30% with the mutant proteins (**Figure 2.7**).

Together, these data indicate that all mutant alleles are loss of function, as they cannot fully restore mitochondrial division activity in cells lacking Drp1/Dnm1. Further, Drp1-G32A and Drp1-R403C both demonstrate a robust dominant negative phenotype, indicating that the mutants interfere with the function of the wild type protein. In these model cells, the A395G and C431Y variants are partially dominant negative by comparison.

Drp1 mutant alleles interact with wild type Drp1.

The dominant negative activity of Drp1/Dnm1 variants suggests that the mutant Drp1 interacts with wild type Drp1 to inhibit normal division activity. To test this, we assessed direct interactions of the mutants with wild type Drp1 using a yeast two-hybrid assay. Wild type Drp1 interacts with itself, as indicated by growth of cells expressing AD-Drp1 and BD-Drp1 (**Figure 2.8**). Drp1-G350D and Drp1-A395D did not interact with Drp1-WT in this assay, consistent with previously published data (30, 37). Given the strong inhibition of Drp1 activity in wild type cells upon expression of these mutants, these data indicate that the yeast two hybrid does not detect the interaction interface that allows these mutants to assemble with wild type protein. In contrast, Drp1-K38A and all of the de novo mutants described here interact with Drp1-WT, consistent with dominant negative effects.

Discussion

Mitochondria are complex and dynamic organelles, constantly changing their overall structure and organization through the coordination of mitochondrial division, fusion and transport. Genetic models that abolish genes encoding proteins required for mitochondrial dynamics illustrate that these activities are required for normal development (21, 22). Furthermore, mutations in *DNM1L* have been reported in patients causing a range of disease states including early lethality, seizures,

developmental delay and dominant optic atrophy. Given the spectrum of observed disease outcomes in affected individuals, it is important to fully characterize new disease-associated alleles, to address the dearth in our knowledge of how changes in Drp1 function alter physiology. In this particular condition, this information is of paramount importance for accurate interpretation of *DNM1L* variants and diagnosis, given the paucity of characteristic and consistent clinical and/or biochemical markers of *DNM1L*-related disease.

Herein, we report the identification of five patients with pathogenic or likely pathogenic variants mutations in the gene *DNM1L* gene, including a possible variant in the stalk domain associated with early death (C431Y; Patient 1), a previously reported variant (R403C; Patients 2 & 3), a novel missense variant in the GTPase domain (G32A; Patient 4) and a novel missense variant at a previously reported residue (A395G; Patient 5).

All of these variants are of highly conserved amino acids within the dynamin family and were not observed in the general public databases (gnomAD, Exome Sequencing Project). *In silico* analysis (Provean, MutTaster, SIFTnew, CADD, Phylo P, PolyPhen-2) predicts that all of these variants are probably damaging to the protein structure/function. To further investigate the functional consequences of these variants, we performed a molecular analysis for their effects upon mitochondrial division in vertebrates and S. cerevisiae. The analysis in each model system was internally consistent, indicating that the highly conserved function of the mitochondrial division machine was altered, rather than regulatory pathways or interactions with other proteins. Interestingly, not all alleles exhibit the same strong dominant negative phenotype in the model systems tested here, unlike previously reported disease alleles (27, 30). The fact that the variants

with partial dominant negative activity do not restore mitochondrial division in cells lacking Drp1 or Dnm1 raises the possibility that the pathophysiology of these diseases includes haploinsufficiency. However, we cannot exclude that the model systems do not fully recapitulate the complexity of human tissues affected in these patients.

Interestingly, our molecular analysis of Drp1-C431Y is discordant with the early death of Patient 1, as the allele is null, but is not the most robust dominant negative activity in the HCT116 and S. cerevisiae cells tested here. This suggests that the defect caused by Drp1-C431Y is minimized in these models but is catastrophic in the context of a specialized cell or tissue type, such as post mitotic neurons. Of significance, this position maps to an assembly interface identified in the crystal structure of Drp1. Other variants in this region (E426A & R430D) were characterized in vitro and were indistinguishable from Drp1-WT in their ability to self-assemble, interact with liposomes and hydrolyze GTP (13). In contrast, these mutants did not tubulate liposomes in vitro, indicative of a defect in the formation of stable, membrane-anchored assemblies that can constrict mitochondria. While C431 is not implicated in the formation of intramolecular bonds as E426 and E430 are, the mutation to tyrosine could alter the integrity of the interface and impact assembly.

Consistent with previous reports, Patient 2 and Patient 3 (R403C) both presented with seizures and developmental regression. Our functional characterization of Drp1-R403C demonstrates that this mutant cannot support mitochondrial division and is dominant negative (27). Interestingly, this position falls within a highly conserved loop in the dynamin family. One very well characterized mutation in dynamin also falls in this loop and completely abrogates assembly (38).

In both vertebrate cells and in S. cerevisiae, Drp1-G32A had the most robust dominant negative phenotype. The complete lack of GFP foci in cells is consistent with an inability to assembly into higher order structures and there is no apparent recruitment to mitochondria. Patient 4 also presented with optic atrophy. Autosomal dominant optic atrophy was previously reported in patients identified with de novo variants in the GTPase domain of Drp1 (28), suggesting that the functional defects associated with variants in this region are distinctly detrimental in this tissue, specifically at the level of ganglion cells. Additionally, this patient was shown to have pure progressive sensory neuropathy, which is likely a major contributor to her ataxia. To our knowledge, pure sensory neuropathy has not been reported previously in *DNM1L*-associated disorders although findings attributable to an underlying neuropathy including ataxia, absent deep tendon reflexes, and pain insensitivity have been reported (39). However, sensory neuropathy is well documented in a known mitochondrial fission defect causing Charcot Marie Tooth syndrome (40).

The first report of a disease-associated mutation in *DNM1L* was a lethal variant, Drp1-A395D. This is a dramatic alteration, from a small and neutral amino acid to a large, branched and charged residue. Drp1-A395D was dominant negative in cells and was predicted to disrupt the assembly of Drp1 required for mitochondrial division (30). In contrast, we report a relatively modest change (alanine to glycine) that has a more modest impact on Drp1 function. These data reveal that, while this site is sensitive to changes, the overall impact on Drp1 function can be grossly different dependent on the characteristics of the precise amino acid substitution.

Materials and Methods

Research subjects

The guardians of the individuals participating in this study gave written, informed consent through journal publication consents or as part of clinical protocols or waivers approved by the Institutional Review Boards of the respective home institutions. DNA was harvested from peripheral whole blood. Fibroblast cultures were established from forearm full thickness skin punch biopsies or quadriceps muscle biopsies obtained for diagnostic purposes. Mitochondrial respiratory chain analysis, when performed, occurred in a clinical laboratory using previously described methods (41, 42).

Whole exome sequencing

Clinical whole exome sequencing (WES) testing was performed for all patients and their parents as described (43). A trio-based design was utilized for WES. Genomic DNA from either whole blood or fibroblasts was extracted and isolated from the affected patient and their parents using standard methods. DNA libraries were generated using the SureSelect Human All Exon V4 or Clinical Research Exome kit (Agilent Technologies, Santa Clara, California, USA). Data were mapped to the NCBI hg19/GRCh37 human genome reference sequence and analyzed using GeneDx's XomeAnalyzer, an interface for variant annotation, filtering, and viewing. The mean depth coverage for the DNM1L gene was 96x, and 100% of the coding region and the adjacent intronic regions were covered at ≥10x. Variants identified by WES were evaluated and classified according to published guidelines (44). Whole mitochondrial genome sequencing analysis in DNA extracted from whole blood was performed for patients 3-5; mitochondrial DNA sequence was assembled and analyzed relative to the revised Cambridge Reference Sequence (rCRS) and MITOMAP database

(http://www.mitomap.org) in combination with concurrent matrilineal relative testing. Identified sequence changes of interest were confirmed via Sanger sequencing, and segregation analysis was performed for family members.

Plasmids and Strains

pcDNA3.1 GFP-Drp1-SV3 (7) and pHS20 Dnm1-GFP (45) were used to transfect mammalian and yeast cells, respectively. To construct yeast-two-hybrid plasmids, splice variant 3 (SV3) of human dynamin-like protein (699 amino acids, NCBI NP_005681.2) was inserted into pGBKT7 and pGADT7 plasmids. Drp1 SV3 was PCR amplified (forward primer – 5′-CGCGGATCCATGGAGGCGCTAATTCCTGTC-3′ and reverse primer – 5′-ACGCGTCGACTCACCAAAGATGAGTCTCCCGGA-3′) and inserted into pGAD-C1 using BamHI/SalI sites. Drp1 SV3 was then excised from pGAD-C1 using EcoRI/SalI sites and inserted into pGBKT7 using EcoRI/SalI sites and pGADT7 using EcoRI/XhoI sites.

Drp1 mutations were introduced by overlapping PCR mutagenesis with Gibson assembly. To generate mutants for yeast transformation, site-directed mutagenesis PCR of pHS20 Dnm1-GFP was followed by yeast-mediated assembly. Specifically, yeast were transformed with PCR products encoding both halves of the target plasmid with overlapping ends and incubated at 30°C for 2 days. To extract the plasmid, yeast were pelleted from liquid cultures and resuspended in 67mM KH_2PO_4 with 2.5mM Zymolase and incubated at 37°C for one hour. DNA was isolated with GeneJet Miniprep kit and this was transformed into E. coli strain DH5alpha. All plasmids were verified by sequencing.

W303 wild type (ade2-1; leu2-3; his3-11, 15; trp1-1; ura3-1; can1-100) and Δdnm1::KANMX6 yeast (36) were transformed to image mitochondrial morphology. For yeast-two-hybrid analysis, bait and prey constructs were co-transformed into PJ69-4A yeast (MATa trp1-901; leu2-3,112; ura3-52; his3-200; gal4Δ; gal80Δ; GAL2-ADE2; LYS2::GAL1-HIS3; met2::GAL7-lacZ).

Yeast two hybrid

Drp1-SV3 pGADT7 variants (prey) were cotransformed with WT-Drp1 pGBKT7 (bait) into PJ64-4A yeast. Transformants were selected on plates lacking leucine and tryptophan. Serial dilutions of yeast were plated on leucine, tryptophan, histidine and adenine deficient plates to assess protein-protein interactions at 30°C for 2 days. Each experiment was repeated three times.

Cell Culture

All cells were grown at 37°C with 5% CO2 and cultured in DMEM (Thermo Fisher Scientific) containing 1X Glutamax (Thermo Fisher Scientific) with 10% FBS (Seradigm) and 1% penicillin/streptomycin (Thermo Fisher Scientific). Primary human fibroblasts were obtained by skin biopsy. Control fibroblasts were collected from an age-matched, healthy female subject. Wild type and Drp1-null HCT116 cells were a gift from Richard Youle (32) (NIH, Bethesda, Maryland).

Transfection and microscopy

All cells were plated in No 1.5 glass-bottomed dishes (MatTek). Human fibroblasts were incubated with 0.1 g/mL Mitotracker Red CMX Ros for 30 minutes before imaging, washed and incubated with complete media for at least 30 minutes prior to imaging. For peroxisome staining, fibroblasts were incubated with 30PPC (parts per cell) of Cell-Light Peroxisome-GFP (Life Technologies) for 16

hr at 37°C before imaging. Drp1-null HCT116 cells were plated at $5x10^5$ cells per well in a 6-well dish. The following day, 3 g Drp1-GFP was transfected using Lipofectamine 3000, according to manufacturer's instructions. Cells were split into glass-bottomed dish 16-24 hr post-transfection. Drp1-null HCT116 cells were stained with 0.1 g/mL MitoTracker Red CMX Ros and imaged 48 hr post-transfection at 37°C with 5% CO_2. Cells expressing similar levels of Drp1-GFP protein were chosen to score mitochondrial morphology (GFP pixel intensity between 9,000 and 15,000 units). Wild type HCT116 cells were plated at $4x10^5$ cells per dish. The following day, 50 ng mitochondrial matrix targeted dsRed (mitoRed) and 300 ng Drp1-GFP were transfected with Lipofectamine 2000, according to manufacturer's instructions. Wild type HCT116 were imaged 16-24 hr post-transfection at 37°C with 5% CO_2. A Z-series with a step size of 0.3 microns was collected with a Nikon Ti-E widefield microscope with a 63X NA 1.4 oil objective (Nikon), a solid-state light source (Spectra X, Lumencor), and a sCMOS camera (Zyla 5.5 Megapixel). Each mutant was transfected and imaged on at least three separate occasions (n>100 cells per experiment).

Single colony yeast transformants were grown overnight at 30°C in SC-Leu-Ura + 2% w/v dextrose to mid-log phase. Yeast cells were sonicated (Fisher Sonic Dismembrator Model 100) at setting 1 for one second to separate progeny and recovered at least 1 hr at 30°C before imaging. Cells were concentrated by centrifugation and mounted on a 3% low melt agarose pad. All yeast cells were imaged at room temperature using 100x/1.2oil objective with 1.5X magnification. Three independent yeast clones from two separate transformations were imaged.

Image Analysis

Images were deconvolved using 8 iterations of 3D Landweber or 3D blind deconvolution (Nikon).

Deconvolved images were analyzed using Nikon Elements software. Maximum intensity projections were created using ImageJ Software (NIH). Mitochondrial morphology in mammalian cells was scored, unblinded, as follows: hyperfused indicates that the entire mitochondrial network was highly connected, with few mitochondrial tips and lacking any mitochondrial fragments (defined as mitochondria less than 2 microns in length); reticular indicates that fewer than 30% of the mitochondria were fragments; fragmented indicates that more than 30% of the mitochondria were less than 2 microns in length.

Yeast mitochondria were categorized as hyperfused, branched or fragmented as follows: hyperfused mitochondria included single, elongated tubes and net structures; branched mitochondria indicate a multi-nodal connected network distributed throughout the cell with >2 mitochondria tips; and fragmented mitochondria were disconnected in short puncta of 0.5 microns or less.

Figures/Table

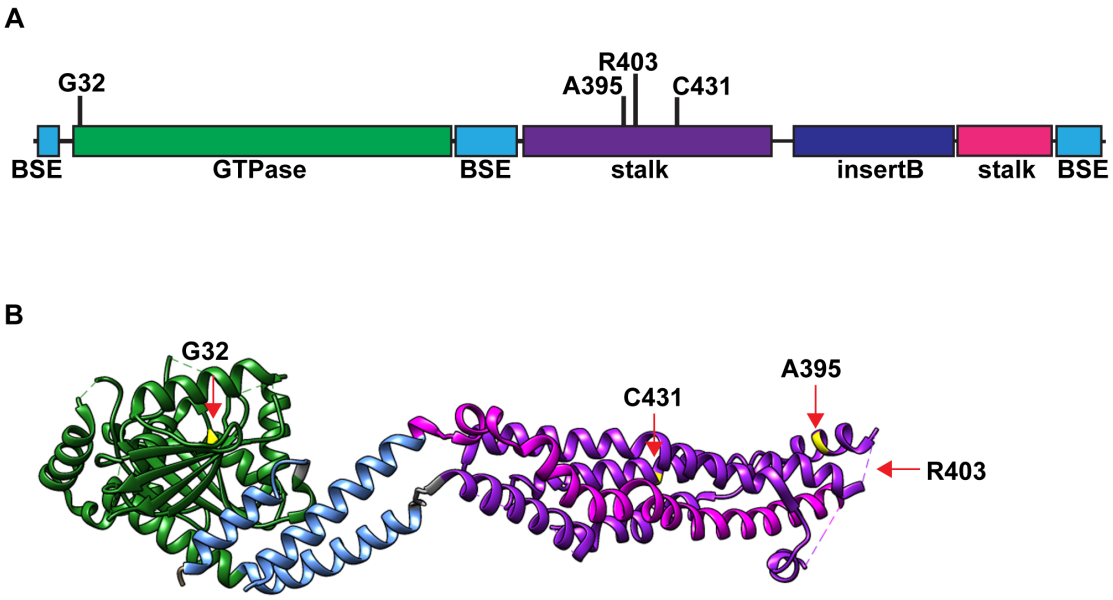

<u>Figure 2.1</u>. Schematic and structural representation of the position of the mutations identified in this study.

(A) Domain structure of Drp1 with mutations reported indicated above. (B) Drp1 structure (PDB 4BEJ) with position of mutations highlighted in yellow and red arrows. G32 is on a central beta-sheet of the globular GTPase domain. C431 is centrally located in the stalk domain. A395 is toward the bottom of the stalk. While R403 is absent from this structure, the approximate position in a predicted loop is indicated.

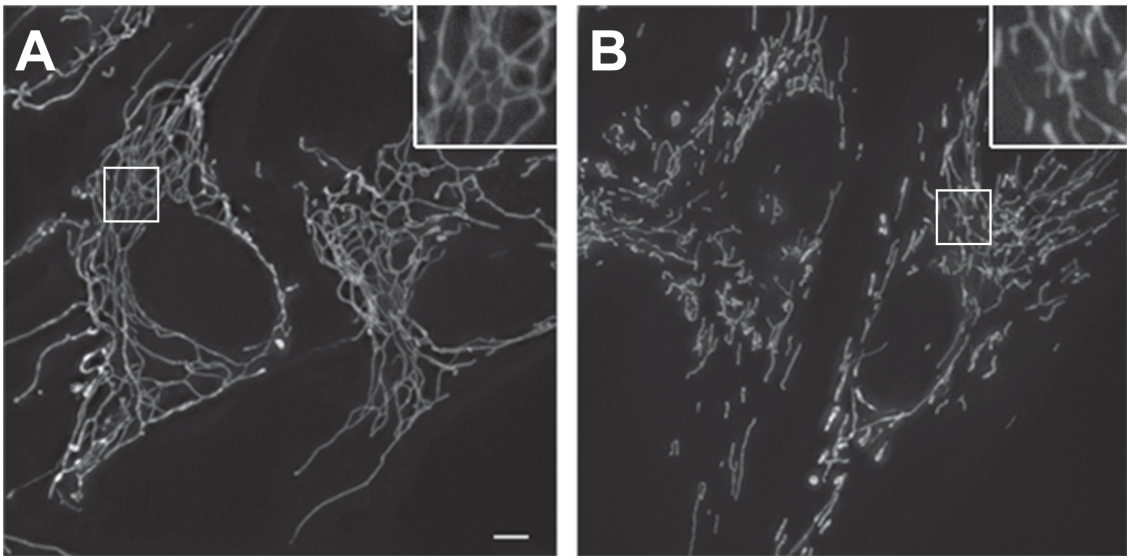

Figure 2.2. Patient 4 fibroblasts have an extensively connected mitochondrial network.

(A) Representative images of primary fibroblasts from Patient 4 (Drp1 G32A). (B) Representative image of primary fibroblasts from an age-matched control. Cells were stained with Mitotracker Red CMX Ros and visualized by fluorescence microscopy. Images represent maximum intensity projections. Scale bar 5um.

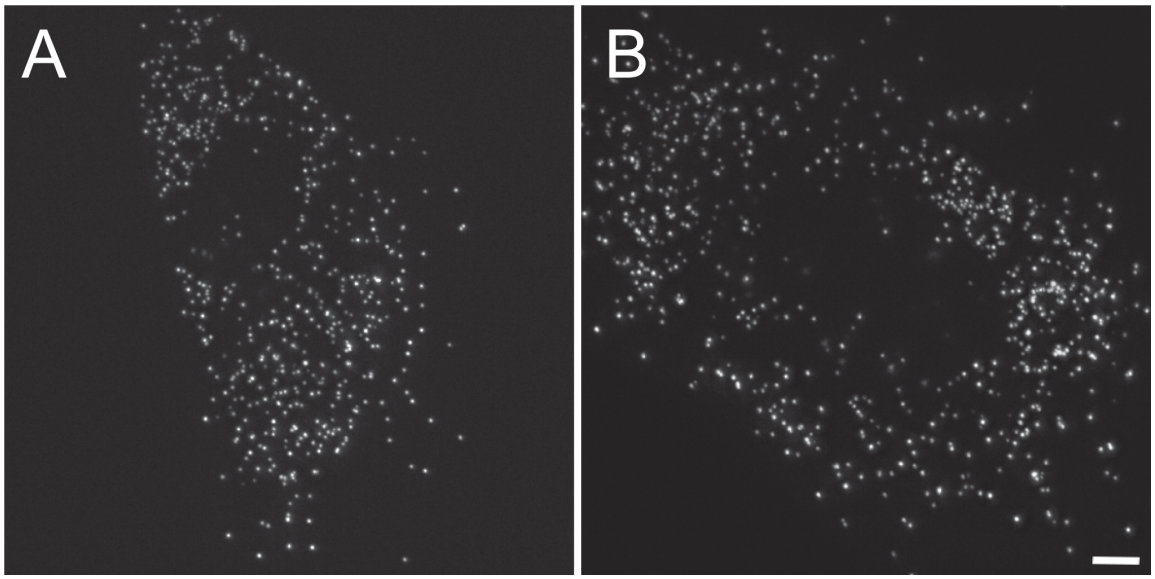

Figure 2.3. Patient 4 fibroblasts have normal peroxisome morphology.

Representative images of primary fibroblasts from Patient 4 (Drp1 G32A) (A) and an age-matched control (B). Cells were stained with CellLight Peroxisome-GFP (Molecular Probes) and visualized by fluorescence microscopy. Images represent maximum intensity projections. Scale bar 5 um.

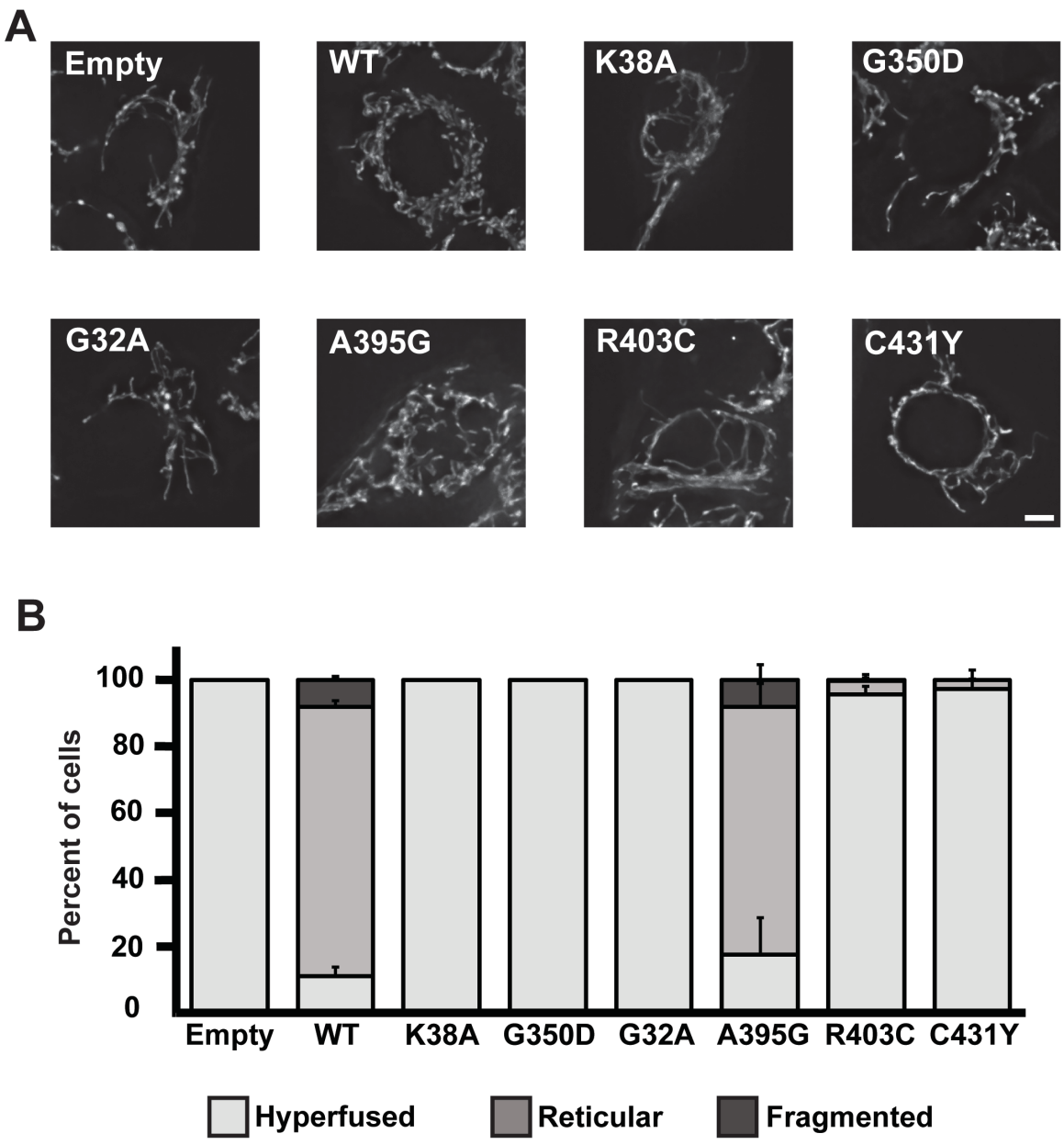

Figure 2.4. Expression of Drp1 mutants in Drp1 null cells.

(A) Representative images of Drp1$^{-/-}$ HCT116 cells transiently expressing Drp1-WT and mutant alleles are shown. Scale bar is 5um. (B) Quantification of mitochondrial morphology in Drp1$^{-/-}$ HCT116 cells expressing Drp1 mutants. Error bars indicate mean + standard deviation from three experiments (n>100 cells per mutant per experiment). "Hyperfused" indicates that the entire mitochondrial

network was highly connected, with few mitochondrial tips and lacking any mitochondrial fragments (defined as mitochondria less than 2 microns in length); reticular indicates that fewer than 30% of the mitochondria were fragments; fragmented indicates that more than 30% of the mitochondria were less than 2 microns in length.

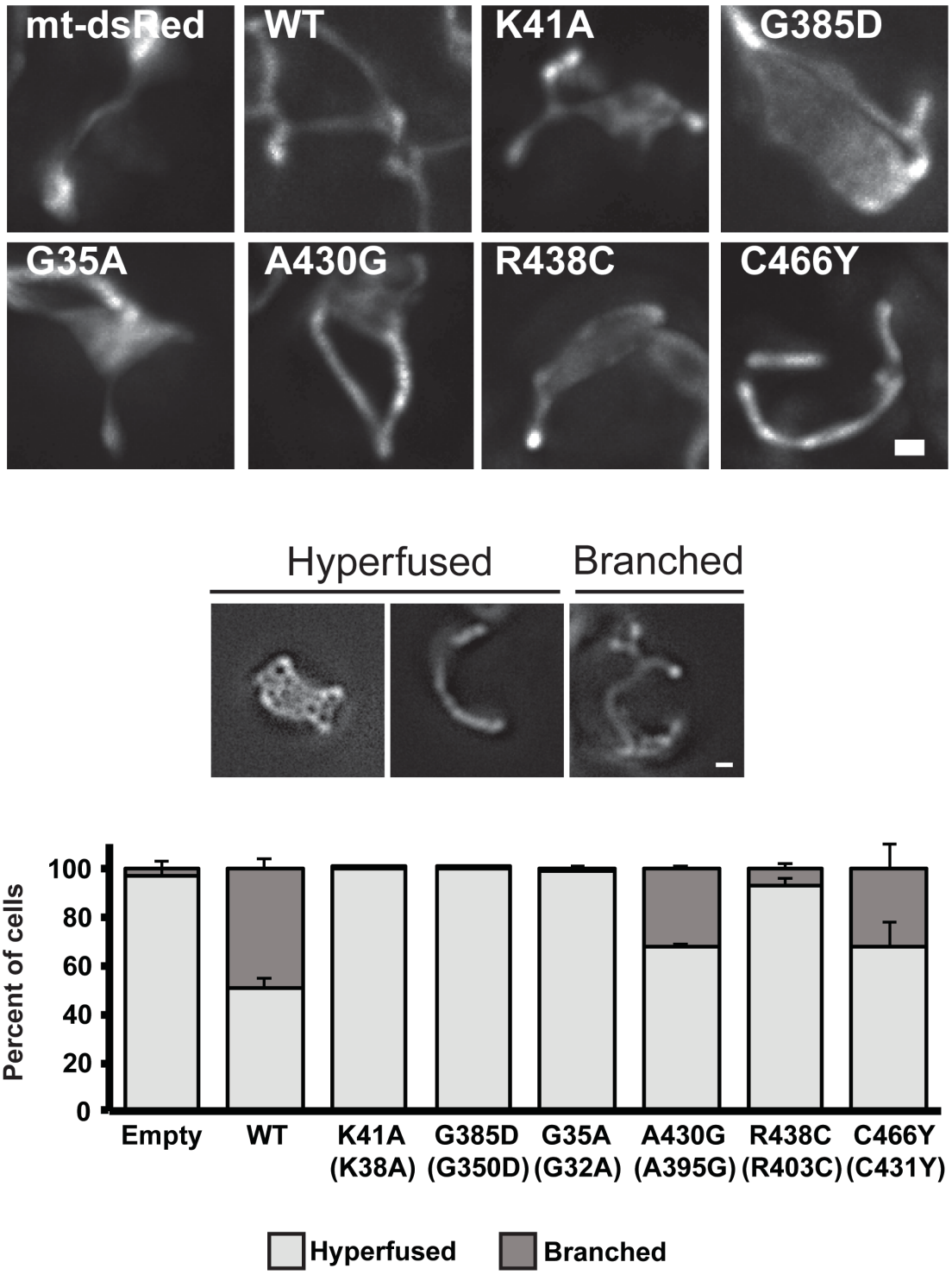

Figure 2.5. Expression of Dnm1 mutants in Dnm1 null cells to assess division activity.

Representative images of Δdnm1 yeast expressing mitochondrial targeted dsRed alone (mt-

dsRed) or mt-dsRed and the indicated Dnm1 variant are shown. Scale bar is 1 um. Representative images of different classes of Δdnm1 yeast used for morphological classification are shown. Hyperfused mitochondria include both net and elongated structures (left and middle) while branched mitochondria have more distinguishable tips (right). Scale bar is 1 μm. The graph represents quantification of mitochondrial morphology in Δdnm1 yeast expressing mitochondrial matrix-targeted dsRed and mutant alleles of Dnm1-GFP. Error bars show mean + standard deviation of three experiments. At least 100 cells counted per mutant in each experiment. Hyperfused mitochondria included single, elongated tubes and net structures; branched mitochondria indicate a multi-nodal connected network distributed throughout the cell with >2 mitochondria tips; and fragmented mitochondria were disconnected in short puncta of 0.5 microns or less.

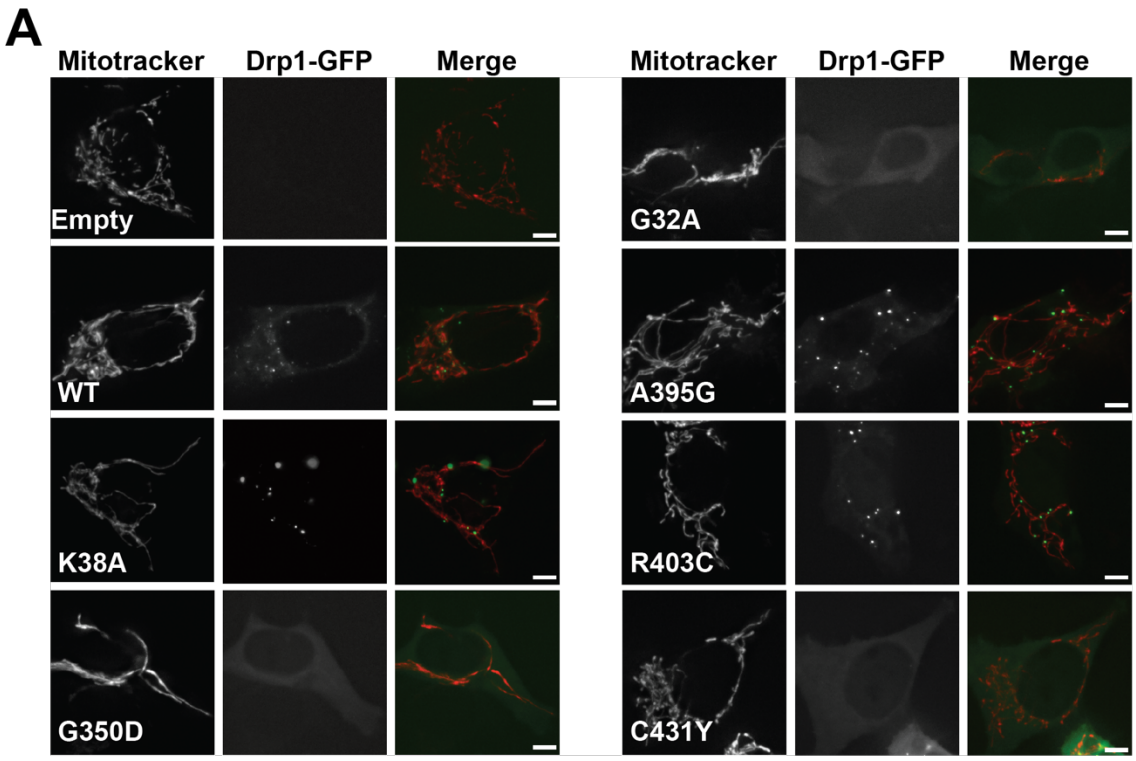
A
Mitotracker
Drp1-GFP
Merge
Mitotracker
Drp1-GFP
Merge
Empty
G32A
WT
A395G
K38A
R403C
G350D
C431Y

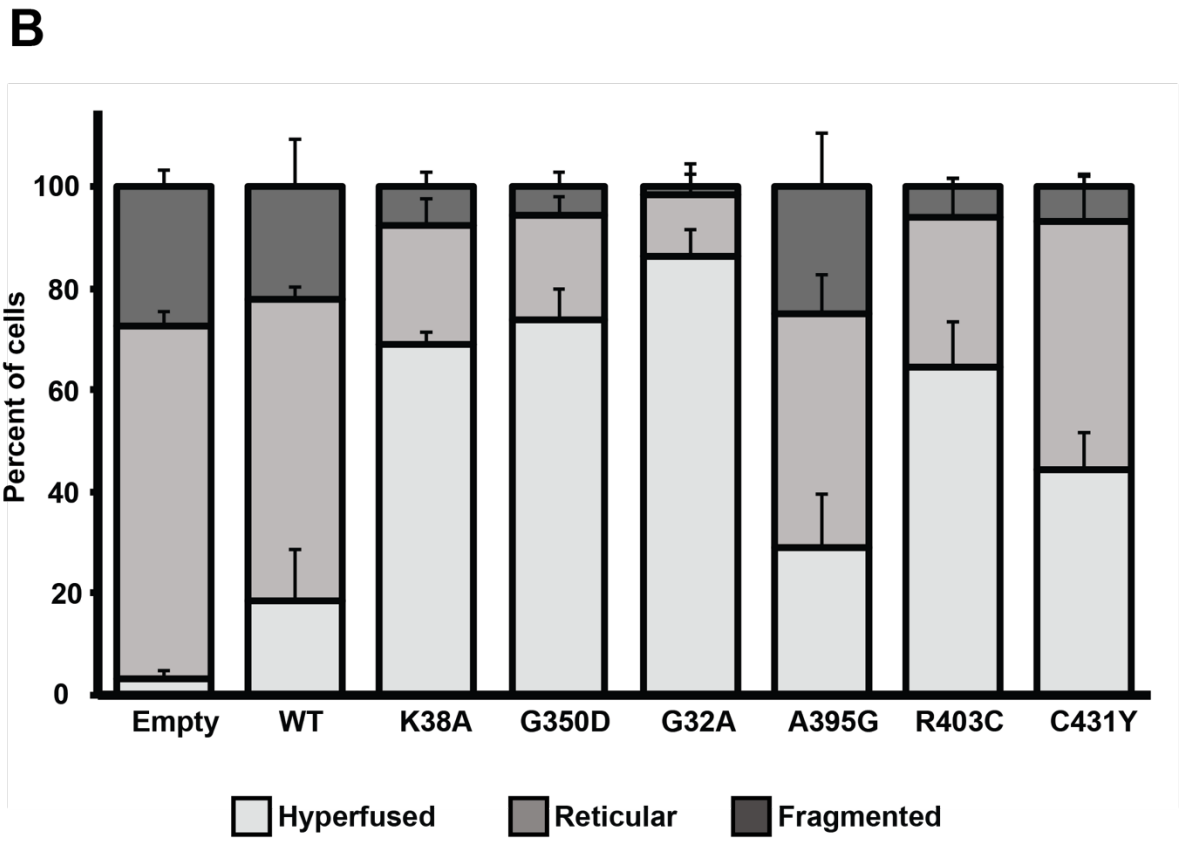
B
Percent of cells
100
80
60
40
20
0
Empty
WT
K38A
G350D
G32A
A395G
R403C
C431Y
Hyperfused
Reticular
Fragmented

Figure 2.6. Expression of Drp1 mutants in WT HCT116 cells to assess dominant negative effects. (A) Representative images of wild type HCT116 cells transiently expressing mitochondrial matrix-dsRed and GFP-Drp1 mutant alleles are shown. The mitochondrial signal (red), GFP-Drp1 (green) and merged signals from a single focal plane are shown. Scale bar is 5 μm. (B) Quantification of mitochondrial morphology in wild type HCT116 cells. Error bars indicate mean + standard deviation from three experiments (n>100 cells per mutant per experiment). "Hyperfused" indicates that the entire mitochondrial network was highly connected, with few mitochondrial tips and lacking any mitochondrial fragments (defined as mitochondria less than 2 microns in length); reticular indicates that fewer than 30% of the mitochondria were fragments; fragmented indicates that more than 30% of the mitochondria were less than 2 microns in length.

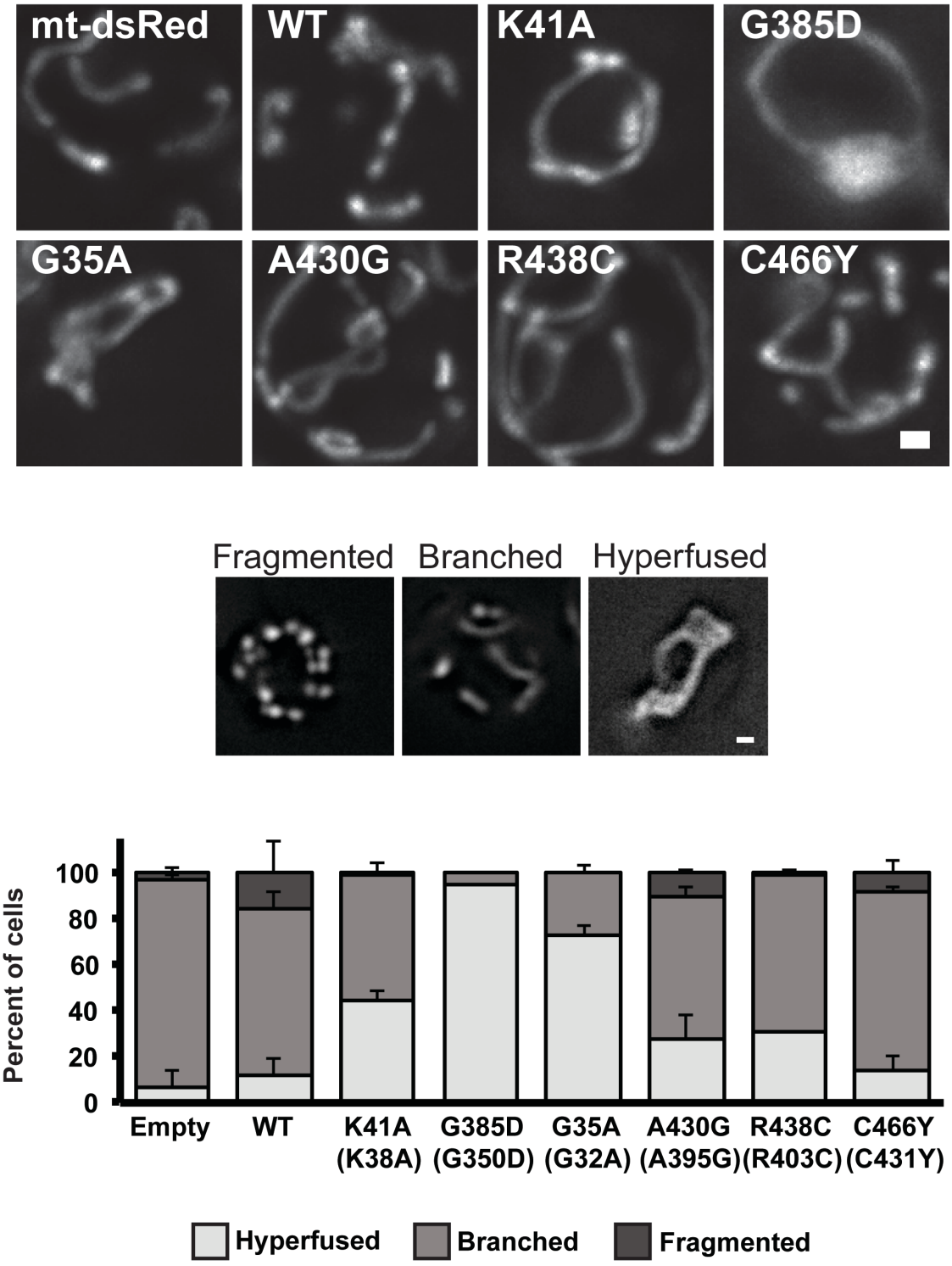

Figure 2.7. Expression of Dnm1 mutants in wild type yeast cells to assess dominant negative effects.

Representative images of wild type yeast expressing mitochondrial targeted dsRed alone (mt-

dsRed) or mt-dsRed and the indicated Dnm1 variant are shown. Scale bar is 1 um. Representative images used for morphological classification are also shown. Hyperfused mitochondria include both interconnected nets and elongated structures. Scale bar is 1 μm. The graph represents quantification of mitochondrial morphology in W303 yeast expressing mitochondrial matrix-dsRed and mutant alleles of Dnm1-GFP. Error bars show mean + standard deviation of three experiments (n>100 cells counted in each experiment). Hyperfused mitochondria included single, elongated tubes and net structures; branched mitochondria indicate a multi-nodal connected network distributed throughout the cell with >2 mitochondria tips; and fragmented mitochondria were disconnected in short puncta of 0.5 microns or less.

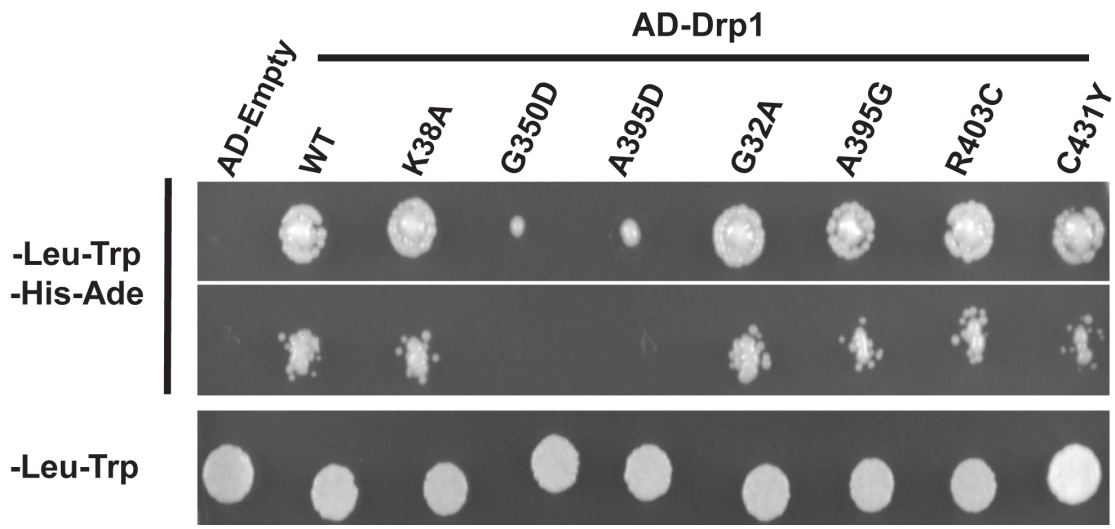

Figure 2.8. Interaction of Drp1 mutants with wild type Drp1 by yeast two hybrid analysis.

WT-Drp1 and Drp1 mutants were expressed as GAL4 activation domain (AD) fusions. AD-Drp1 constructs were tested for interaction with wild type Drp1 expressed as GAL4 DNA binding domain (BD) fusions. Growth at 30°C on adenine and histidine deficient plates indicates protein-protein interaction. The second row represents a tenfold serial dilution.

Acknowledgements

We would like to thank the patients and families for permission to publish this work. We thank Marijn Ford for critical discussion of the manuscript. We thank Richard Youle for sharing the Drp1 null cells. Funding: This work was supported by the National Institutes of Health (NIGMS grant R01GM118509 to SH); the National Science Foundation Graduate Research Fellowship Program (Grant No. DGE 1256082 to BW). Any opinions, findings, and conclusions or recommendations expressed in this material are those of the author(s) and do not necessarily reflect the views of the National Science Foundation. Dr. Tarnopolsky would like to acknowledge the donation of Warren Lammert, Kathy

Corkins and Dan Wright for support of the Neuromuscular and Neurometabolic Clinic and mitochondrial research.

Conflict of Interest Statement

Hong Cui, Katrina Haude, Renkui Bai are employees of GeneDx.

References

1. Mills, E. L., Kelly, B., O'Neill, L. A. J. (2017) Mitochondria are the powerhouses of immunity. Nat. Immunol. 18:488-498
2. Kasahara, A., Scorrano, L. (2014) Mitochondria: from cell death executioners to regulators of cell differentiation. Trends Cell Biol. 24:761-770
3. Chen, H., Chomyn, A., Chan, D. C. (2005) Disruption of fusion results in mitochondrial heterogeneity and dysfunction. J. Biol. Chem. 280:26185-26192
4. Chen, H., McCaffery, J. M., Chan, D. C. (2007) Mitochondrial fusion protects against neurodegeneration in the cerebellum. Cell 130:548-562
5. Kraus, F., Ryan, M. T. (2017) The constriction and scission machineries involved in mitochondrial fission. J. Cell Sci. 130:2953-2960
6. Phillips, M. J., Voeltz, G. K. (2016) Structure and function of ER membrane contact sites with other organelles. Nat. Rev. Mol. Cell. Biol. 17:69-82
7. Smirnova, E., Griparic, L., Shurland, D. L., van der Bliek, A. M. (2001) Dynamin-related protein Drp1 is required for mitochondrial division in mammalian cells. Mol Biol Cell 12:2245-2256
8. Osellame, L. D., Singh, A. P., Stroud, D. A., Palmer, C. S., Stojanovski, D., Ramachandran, R., Ryan, M. T. (2016) Cooperative and independent roles of the Drp1 adaptors Mff, MiD49 and MiD51 in mitochondrial fission. J. Cell Sci. 129:2170-2181
9. Shen, Q., Yamano, K., Head, B. P., Kawajiri, S., Cheung, J. T., Wang, C., Cho, J. H., Hattori, N., Youle, R. J., van der Bliek, A. M. (2014) Mutations in Fis1 disrupt orderly disposal of defective mitochondria. Mol. Biol. Cell 25:145-159
10. Yu, R., Liu, T., Jin, S. B., Ning, C., Lendahl, U., Nistér, M., Zhao, J. (2017) MIEF1/2 function as adaptors to recruit Drp1 to mitochondria and regulate the association of Drp1 with Mff. Sci. Rep. 7:880
11. Koirala, S., Guo, Q., Kalia, R., Bui, H. T., Eckert, D. M., Frost, A., Shaw, J. M. (2013) Interchangeable adaptors regulate mitochondrial dynamin assembly for membrane scission. Proc. Natl. Acad. Sci. U S A 110:E1342-51

12. Antonny, B., Burd, C., De Camilli, P., Chen, E., Daumke, O., Faelber, K., Ford, M., Frolov, V. A., Frost, A., Hinshaw, J. E., Kirchhausen, T., Kozlov, M. M., Lenz, M., Low, H. H., McMahon, H., Merrifield, C., Pollard, T. D., Robinson, P. J., Roux, A., Schmid, S. (2016) Membrane fission by dynamin: what we know and what we need to know. EMBO J. 35:2270-2284
13. Fröhlich, C., Grabiger, S., Schwefel, D., Faelber, K., Rosenbaum, E., Mears, J., Rocks, O., Daumke, O. (2013) Structural insights into oligomerization and mitochondrial remodelling of dynamin 1-like protein. EMBO J. 32:1280-1292
14. Francy, C. A., Clinton, R. W., Fröhlich, C., Murphy, C., Mears, J. A. (2017) Cryo-EM Studies of Drp1 Reveal Cardiolipin Interactions that Activate the Helical Oligomer. Sci. Rep. 7:10744
15. Mears, J. A., Lackner, L. L., Fang, S., Ingerman, E., Nunnari, J., Hinshaw, J. E. (2011) Conformational changes in Dnm1 support a contractile mechanism for mitochondrial fission. Nat. Struct. Mol. Biol. 18:20-26
16. Lee, J. E., Westrate, L. M., Wu, H., Page, C., Voeltz, G. K. (2016) Multiple dynamin family members collaborate to drive mitochondrial division. Nature 540:139-143
17. Schrader, M., Costello, J. L., Godinho, L. F., Azadi, A. S., Islinger, M. (2016) Proliferation and fission of peroxisomes - An update. Biochim. Biophys. Acta 1863:971-983
18. Mohanty, A., McBride, H. M. (2013) Emerging roles of mitochondria in the evolution, biogenesis, and function of peroxisomes. Front. Physiol. 4:268
19. Schrepfer, E., Scorrano, L. (2016) Mitofusins, from Mitochondria to Metabolism. Mol Cell 61:683-694
20. Mishra, P., Chan, D. C. (2014) Mitochondrial dynamics and inheritance during cell division, development and disease. Nat. Rev. Mol. Cell. Biol. 15:634-646
21. Ishihara, N., Nomura, M., Jofuku, A., Kato, H., Suzuki, S. O., Masuda, K., Otera, H., Nakanishi, Y., Nonaka, I., Goto, Y., Taguchi, N., Morinaga, H., Maeda, M., Takayanagi, R., Yokota, S., Mihara, K. (2009) Mitochondrial fission factor Drp1 is essential for embryonic development and synapse formation in mice. Nat. Cell Biol. 11:958-966
22. Wakabayashi, J., Zhang, Z., Wakabayashi, N., Tamura, Y., Fukaya, M., Kensler, T. W., Iijima, M., Sesaki, H. (2009) The dynamin-related GTPase Drp1 is required for embryonic and brain development in mice. J. Cell Biol. 186:805-816
23. Waterham, H. R., Koster, J., van Roermund, C. W., Mooyer, P. A., Wanders, R. J., Leonard, J. V. (2007) A lethal defect of mitochondrial and peroxisomal fission. N. Engl. J. Med. 356:1736-1741
24. Chao, Y. H., Robak, L. A., Xia, F., Koenig, M. K., Adesina, A., Bacino, C. A., Scaglia, F., Bellen, H. J., Wangler, M. F. (2016) Missense variants in the middle domain of DNM1L in cases of infantile encephalopathy alter peroxisomes and mitochondria when assayed in Drosophila. Hum. Mol. Genet. 25:1846-1856
25. Zaha, K., Matsumoto, H., Itoh, M., Saitsu, H., Kato, K., Kato, M., Ogata, S., Murayama, K., Kishita, Y., Mizuno, Y., Kohda, M., Nishino, I., Ohtake, A., Okazaki, Y., Matsumoto, N., Nonoyama, S. (2016) DNM1L-related encephalopathy in infancy with Leigh syndrome-like phenotype and suppression-burst. Clin. Genet. 90:472-474

26. Vanstone, J. R., Smith, A. M., McBride, S., Naas, T., Holcik, M., Antoun, G., Harper, M. E., Michaud, J., Sell, E., Chakraborty, P., Tetreault, M., Care4Rare, C., Majewski, J., Baird, S., Boycott, K. M., Dyment, D. A., MacKenzie, A., Lines, M. A. (2016) DNM1L-related mitochondrial fission defect presenting as refractory epilepsy. Eur. J. Hum. Genet. 24:1084-1088
27. Fahrner, J. A., Liu, R., Perry, M. S., Klein, J., Chan, D. C. (2016) A novel de novo dominant negative mutation in DNM1L impairs mitochondrial fission and presents as childhood epileptic encephalopathy. Am. J. Med. Genet. A 170:2002-2011
28. Gerber, S., Charif, M., Chevrollier, A., Chaumette, T., Angebault, C., Kane, M. S., Paris, A., Alban, J., Quiles, M., Delettre, C., Bonneau, D., Procaccio, V., Amati-Bonneau, P., Reynier, P., Leruez, S., Calmon, R., Boddaert, N., Funalot, B., Rio, M., Bouccara, D., Meunier, I., Sesaki, H., Kaplan, J., Hamel, C. P., Rozet, J. M., Lenaers, G. (2017) Mutations in DNM1L, as in OPA1, result indominant optic atrophy despite opposite effectson mitochondrial fusion and fission. Brain 140:2586-2596
29. Hogarth, K. A., Costford, S. R., Yoon, G., Sondheimer, N., Maynes, J. T. (2017) DNM1L Variant Alters Baseline Mitochondrial Function and Response to Stress in a Patient with Severe Neurological Dysfunction. Biochem. Genet. 56:56-77
30. Chang, C. R., Manlandro, C. M., Arnoult, D., Stadler, J., Posey, A. E., Hill, R. B., Blackstone, C. (2010) A lethal de novo mutation in the middle domain of the dynamin-related GTPase Drp1 impairs higher order assembly and mitochondrial division. J. Biol. Chem. 285:32494-32503
31. Li, X., Gould, S. J. (2003) The dynamin-like GTPase DLP1 is essential for peroxisome division and is recruited to peroxisomes in part by PEX11. J. Biol. Chem. 278:17012-17020
32. Burman, J. L., Pickles, S., Wang, C., Sekine, S., Vargas, J. N. S., Zhang, Z., Youle, A. M., Nezich, C. L., Wu, X., Hammer, J. A., Youle, R. J. (2017) Mitochondrial fission facilitates the selective mitophagy of protein aggregates. J. Cell Biol. 216:3231-3247
33. Zhu, P. P., Patterson, A., Stadler, J., Seeburg, D. P., Sheng, M., Blackstone, C. (2004) Intra- and intermolecular domain interactions of the C-terminal GTPase effector domain of the multimeric dynamin-like GTPase Drp1. J. Biol. Chem. 279:35967-35974
34. Ingerman, E., Perkins, E. M., Marino, M., Mears, J. A., McCaffery, J. M., Hinshaw, J. E., Nunnari, J. (2005) Dnm1 forms spirals that are structurally tailored to fit mitochondria. J. Cell Biol. 170:1021-1027
35. Bhar, D., Karren, M. A., Babst, M., Shaw, J. M. (2006) Dimeric Dnm1-G385D interacts with Mdv1 on mitochondria and can be stimulated to assemble into fission complexes containing Mdv1 and Fis1. J. Biol. Chem. 281:17312-17320
36. Naylor, K., Ingerman, E., Okreglak, V., Marino, M., Hinshaw, J. E., Nunnari, J. (2006) Mdv1 interacts with assembled dnm1 to promote mitochondrial division. J. Biol. Chem. 281:2177-2183
37. Zhu, P. P., Patterson, A., Stadler, J., Seeburg, D. P., Sheng, M., Blackstone, C. (2004) Intra- and intermolecular domain interactions of the C-terminal GTPase effector domain of the multimeric dynamin-like GTPase Drp1. J Biol Chem 279:35967-35974
38. Ford, M. G., Jenni, S., Nunnari, J. (2011) The crystal structure of dynamin. Nature 477:561-566

39. Sheffer, R., Douiev, L., Edvardson, S., Shaag, A., Tamimi, K., Soiferman, D., Meiner, V., Saada, A. (2016) Postnatal microcephaly and pain insensitivity due to a de novo heterozygous DNM1L mutation causing impaired mitochondrial fission and function. Am. J. Med. Genet. A 170:1603-1607
40. Huber, N., Guimaraes, S., Schrader, M., Suter, U., Niemann, A. (2013) Charcot-Marie-Tooth disease-associated mutants of GDAP1 dissociate its roles in peroxisomal and mitochondrial fission. EMBO Rep. 14:545-552
41. Trounce, I. A., Kim, Y. L., Jun, A. S., Wallace, D. C. (1996) Assessment of mitochondrial oxidative phosphorylation in patient muscle biopsies, lymphoblasts, and transmitochondrial cell lines. Methods Enzymol. 264:484-509
42. Kirby, D. M., Thorburn, D. R., Turnbull, D. M., Taylor, R. W. (2007) Biochemical assays of respiratory chain complex activity. Methods Cell Biol. 80:93-119
43. Retterer, K., Juusola, J., Cho, M. T., Vitazka, P., Millan, F., Gibellini, F., Vertino-Bell, A., Smaoui, N., Neidich, J., Monaghan, K. G., McKnight, D., Bai, R., Suchy, S., Friedman, B., Tahiliani, J., Pineda-Alvarez, D., Richard, G., Brandt, T., Haverfield, E., Chung, W. K., Bale, S. (2016) Clinical application of whole-exome sequencing across clinical indications. Genet. Med. 18:696-704
44. Richards, S., Aziz, N., Bale, S., Bick, D., Das, S., Gastier-Foster, J., Grody, W. W., Hegde, M., Lyon, E., Spector, E., Voelkerding, K., Rehm, H. L., ACMG, L. Q. A. C. (2015) Standards and guidelines for the interpretation of sequence variants: a joint consensus recommendation of the American College of Medical Genetics and Genomics and the Association for Molecular Pathology. Genet. Med. 17:405-424
45. Sesaki, H., Jensen, R. E. (1999) Division versus fusion: Dnm1p and Fzo1p antagonistically regulate mitochondrial shape. J. Cell Biol. 147:699-706

Chapter Three:

Characterization of a predicted Mfn1 phosphorylation site to better understand the mechanism and regulation of mitochondrial outer membrane fusion

Summary

This chapter begins with a discussion of the preliminary mass spectrometry screen used to identify candidate phosphorylation sites on Mfn1 and Mfn2. While much of my thesis research has specifically focused on an in-depth characterization of Mfn1 S228, I anticipate that future work in the lab will clarify the physiological roles of other phosphorylation sites identified in this screen. The Mfn1 and Mfn2 used in the preliminary mass spectrometry screen was purified by Emily Engelhart. Prepared samples were run on the mass spectrometer and analyzed by Gennifer Merrihew in the MacCoss lab at the University of Washington.

In the remainder of the chapter, I primarily discuss my thesis research focused on the characterization of mitochondrial fusion in cells expressing mutations in Mfn1 S228 that either block (S > A) or mimic phosphorylation (S > E). Ed Parker processed and imaged fixed cells for EM. Currently, another graduate student in the lab, Nyssa Samanas, is performing parallel reaction monitoring (PRM) mass spectrometry to identify changes in *in vivo* phosphorylation of Mfn1 S228 under various cellular stresses. Mfn1 S228 phosphorylation has been reliably detected in several early experiments, although the cellular conditions that promote or inhibit phosphorylation have not yet been identified. Once we have clarified the physiological role of Mfn1 S228 phosphorylation, we plan to reconcile this with my detailed biochemical and cellular characterization of Mfn1 S228 mutants in a publication that will be submitted for peer-reviewed publication by the end of the year.

Finally, in the mitofusin-specific assembly section, the results from blue native PAGE after incubation with GDP and GDP.BeF_3^- have been recently published in Molecular Biology of the Cell (*MBoC*; Sloat, Whitley, Engelhart & Hoppins, 2019). All chimera blue native PAGE experiments were done in collaboration with Emily Engelhart.

Introduction

Regulated changes in mitochondrial shape and position allow cells to maintain homeostasis and respond appropriately to changes in their environment (Eisner et al., 2018; Mishra and Chan, 2016; Zemirli et al., 2018). Prevalent neurodegenerative, cardiac and metabolic diseases are associated with imbalanced mitochondrial dynamics (reviewed in detail in Whitley et al., 2019). While mitochondrial fusion clearly plays a critical role in cellular function, we still understand very little about the mechanism by which mitochondrial membranes fuse. In general, cellular membrane fusion involves an early membrane tethering step, which can be mediated by either the fusion proteins themselves or by distinct protein tethers. Fusion proteins also promote membrane destabilization or curvature to overcome the energetic barrier required to fuse flat, tightly packed lipids (Martens and McMahon, 2008). Beyond these similarities, however, the mitofusin proteins that mediate mitochondrial outer membrane fusion are distinct from other well-studied fusion proteins like soluble N-ethylmaleimide-sensitive fusion protein attachment protein receptors (SNAREs) and viral fusion proteins (Han et al., 2017; Kielian, 2014). A more detailed understanding of the mitochondrial fusion mechanism will be essential to understand how fusion activity is regulated and could potentially be targeted in future therapeutic approaches.

Assembly across mitofusin GTPase domains (G-G interface)

Based on conserved properties across dynamin related proteins (DRPs), we expect that mitofusins remodel membranes in a process that couples protein assembly, nucleotide hydrolysis and conformational change (Daumke and Praefcke, 2016; Jimah and Hinshaw, 2018). Both fusion and division DRPs form an assembly interface across the GTPase domains of two proteins. Formation of the G-G interface is associated with GTP hydrolysis and the membrane remodeling activity of these proteins. Direct evidence for the presence of this assembly interface in mitofusins comes from recent crystal structures of a minimal construct of Mfn1 (MGD), which consists of the first half of Mfn1 linked to a single helix from the C-terminal domain (Cao et al., 2017; Qi et al., 2016; Yan et al., 2018). Mfn1 MGD assembles into a dimer that interacts across the GTPase domains of adjacent proteins after binding to nucleotide. Mutations blocking MGD dimerization also significantly decreased GTPase activity, suggesting that the enzymatic activity of Mfn1 requires the formation of the G-G interface (Cao et al., 2017).

Based on the existence of a G-G interface in Mfn1 MGD, most current models of mitofusin-mediated fusion predict that monomeric mitofusins dimerize across adjacent membranes to tether mitochondria (Cohen and Tareste, 2018; Tilokani et al., 2018; Yan et al., 2018). This model would resemble that of the endoplasmic reticulum (ER) fusion DRP, atlastin. Crystal structures and biochemical characterization show that atlastin forms homodimers across the GTPase domains of proteins on opposite membranes, leading to conformational changes that ultimately drive ER fusion (Bian et al., 2011; Byrnes et al., 2013; Byrnes and Sondermann, 2011). It is also important to note that while most models of mitofusin-mediated fusion predict that tethering occurs through the G-G

interface, alternative models suggest that dimerization across the C-terminal domains of mitofusins mediates membrane tethering (Franco et al., 2016; Rocha et al., 2018).

Additional assembly interfaces in full-length mitofusins

Structural homology to the bacterial dynamin-like protein BLDP suggests that full-length mitofusin dimers may form on the same membrane through back-to-back interactions across the helical stalk (Liu et al., 2018; Low and Löwe, 2006; Low et al., 2009). In the structurally similar dynamin-like proteins from Campylobacter jejuni (CJ-DLP1, CJ-DLP2), the N-terminal assembly domains of back-to-back CJ-DLP2 dimers promote membrane tethering through interactions across the GTPase domains of CJ-DLP1 proteins (Liu et al., 2018). Our lab recently identified a mitofusin-specific assembly region which is consistent with a back-to-back interface (Sloat et al., 2019). We predict that back-to-back mitofusin dimers on the same membrane (cis) can form G-G interfaces across membranes (trans) to tether mitochondria and initiate fusion.

Full-length mitofusins can also undergo nucleotide-dependent assembly into higher order oligomers (Engelhart and Hoppins, 2019; Ishihara et al., 2004; Sloat et al., 2019; Samanas et al., in preparation). While mitofusins are primarily dimeric in the absence of nucleotide, we observe complexes as large as 450kDa when mitochondria are incubated with GTP. Further analysis of the mitofusins is required to identify and characterize the domains required for nucleotide-dependent assembly.

Conformational changes

In addition to assembly-stimulated GTP hydrolysis, we also expect that the mitofusins will undergo conformational changes during membrane fusion to either disrupt lipids, pull membranes closer together or both. Based on homology to BDLP, we expect that full-length mitofusins adopt a linear, open conformation (**Figure 3.1A**), as well as a closed, V-shaped conformation (**Figure 3.1B**). In BDLP, this conformational change is mediated by a hinge region (Hinge 2) between the two helical bundles, HB1 and HB2 (Liu et al., 2018; Low et al., 2009; Low and Löwe, 2006). Evidence from our lab (Samanas et al., in preparation) and others (Franco et al., 2016; Rocha et al., 2018) suggests that a similar hinge exists in mitofusins. The Mfn1 GTPase domain is predicted to extend far from the membrane in the open conformation (**Figure 3.1A**) and come closer to the membrane and second helical bundle in the closed conformation (**Figure 3.1B**).

Nucleotide-dependent conformational changes in crystal structures of Mfn1 MGD further support the existence of these conformational states. In the absence of nucleotide (5GNU, 5GO4) or presence of GDP (5GNT, 5GOM), Mfn1 MGD dimers adopt a "straight" conformation in which the stalks of adjacent proteins are facing away from each other (Cao et al., 2017; Qi et al., 2016) (**Figure 3.1B**). When incubated with the transition-state mimicking nucleotide, GDP.BeF_3 (5YEW), Mfn1 undergoes a conformational change into a "bent" position in which the stalks of both proteins are facing the same direction (Yan et al., 2018) (**Figure 3.1A**). This conformational change occurs through a hinge region between the GTPase domain and HB1 (Hinge 1). Superimposition of Mfn1 MGD structures on predicted Mfn1 structures shows that the straight conformation of Mfn1 MGD corresponds to the closed full-length structure (**Figure 3.1B**), while the bent conformation of Mfn1 MGD corresponds to the open full-length structure (**Figure 3.1A**). We expect that the open

conformation would promote mitofusin tethering while the dramatic conformational change at the second hinge either destabilizes membranes and/or pulls them together to promote fusion.

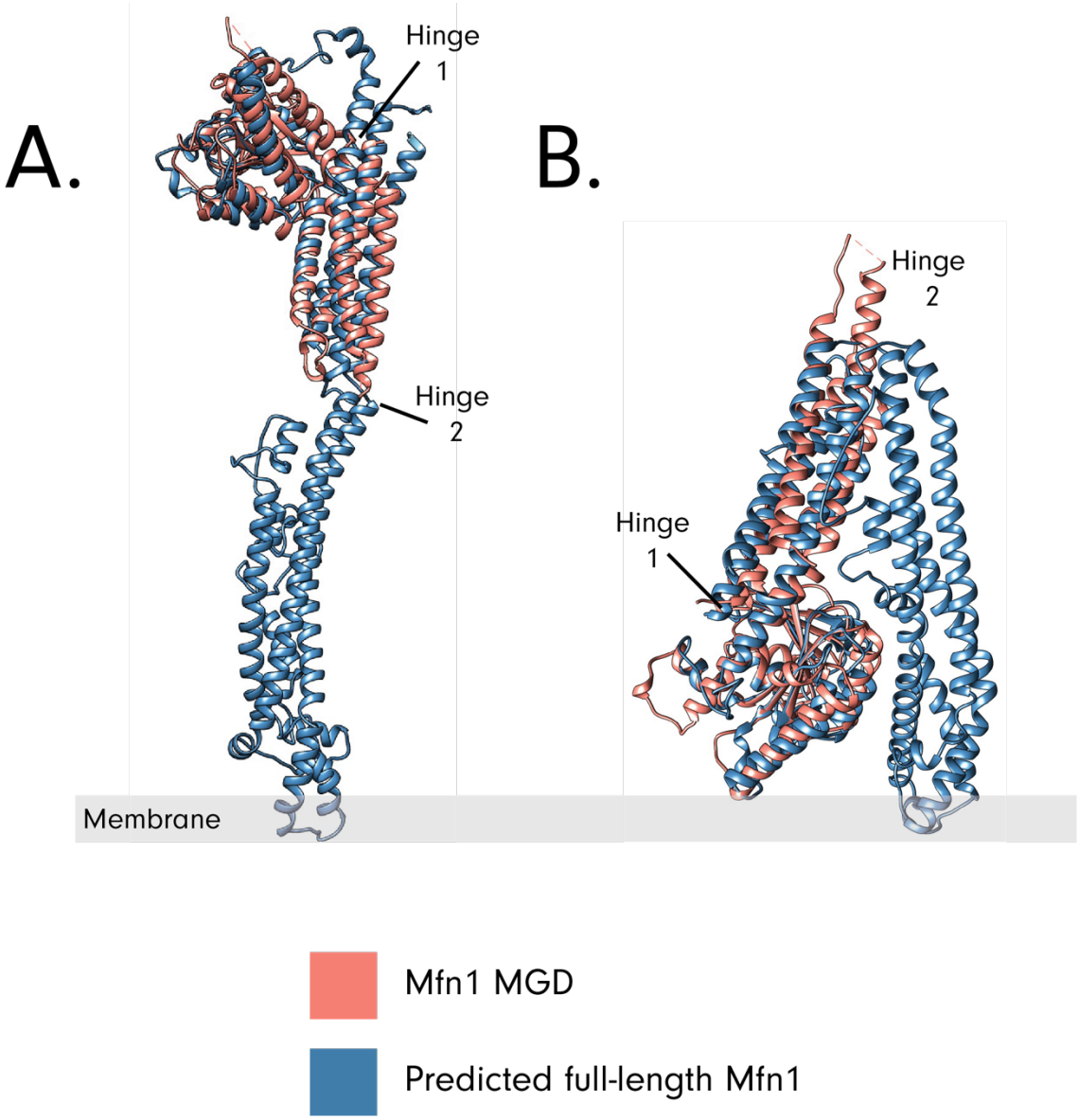

Figure 3.1. Superimposition of Mfn1 MGD onto the predicted structure of full-length Mfn1 highlights structural similarity and dramatic conformational changes at two proposed hinge regions. (A) Mfn1 MGD in the bent conformation (5YEW, pink) superimposed onto the predicted

structure of full-length Mfn1, modeled based on BDLP-GMPPNP (2W6D, blue). The predicted back-to-back interface is expected to form along the full-length Mfn1 stalk in this elongated conformation. (B) Mfn1 MGD in the straight conformation (5GOM, pink) superimposed onto the predicted structure of full-length Mfn1, modeled based on BDLP-GDP (2J68, blue). Structural predictions for full-length Mfn1 were created by modeling the sequence of murine Mfn1 protein (Q811U4) onto the indicated BDLP structures using I-TASSER.

Developing a fusion model

I predict that mitofusin assembly-stimulated hydrolysis and conformational changes drive mitochondrial outer membrane fusion. Mitofusins primarily form dimers at steady state (Engelhart and Hoppins, 2019; Ishihara et al., 2004; Sloat et al., 2019; Sugiura et al., 2013; Samanas et al., in preparation), which we predict to exist on the same membrane, or in *cis*. Based on structural homology to bacterial dynamin-like proteins and the identification of a mitofusin-specific assembly region in this area (Sloat et al., 2019), we hypothesize that *cis* dimers assemble via a back-to-back interface. In this position, the GTPase domains of dimers face away from each other and remain available to interact with mitofusins on other membranes, or in *trans* (**Figure 3.2A**). We hypothesize that these interactions promote mitochondrial tethering through the nucleotide-dependent assembly of mitofusin dimers across opposite membranes (**Figure 3.2B**). Conformational changes of mitofusin oligomers would then bring membranes together (**Figure 3.2C**) for membrane fusion (**Figure 3.2D**).

While this model represents higher-order mitofusin assemblies as tetramers, it remains possible that additional assembly is required to promote efficient membrane fusion. For example, recent electron

cryotomography of yeast mitochondria from an *in vitro* fusion assay suggests that multiple cycles of GTP hydrolysis in the yeast mitofusin homolog, Fzo, leads to the formation a protein ring that promotes fusion (Brandt et al., 2016). Within our model, I expect that a mitofusin ring would form through the creation of several *trans* assemblies (as in **Figure 3.2B**).

In addition to ambiguity in the size of mitofusin assemblies, it is also not possible to distinguish between Mfn1 and Mfn2 in our current fusion model. Because mitochondrial fusion is most efficient when Mfn1 and Mfn2 are present on opposite membranes (Hoppins et al., 2011; Ishihara et al., 2004), it is possible that Mfn1 and Mfn2 form homodimers on the same membrane that can then interact with the opposite mitofusin across membranes to promote fusion (blue vs. yellow proteins in **Figure 3.2**). Data from our lab suggests that both Mfn1 and Mfn2 can form nucleotide-dependent assemblies of similar sizes (**Figure 3.2B**), although the exact composition of these assemblies has not yet been verified.

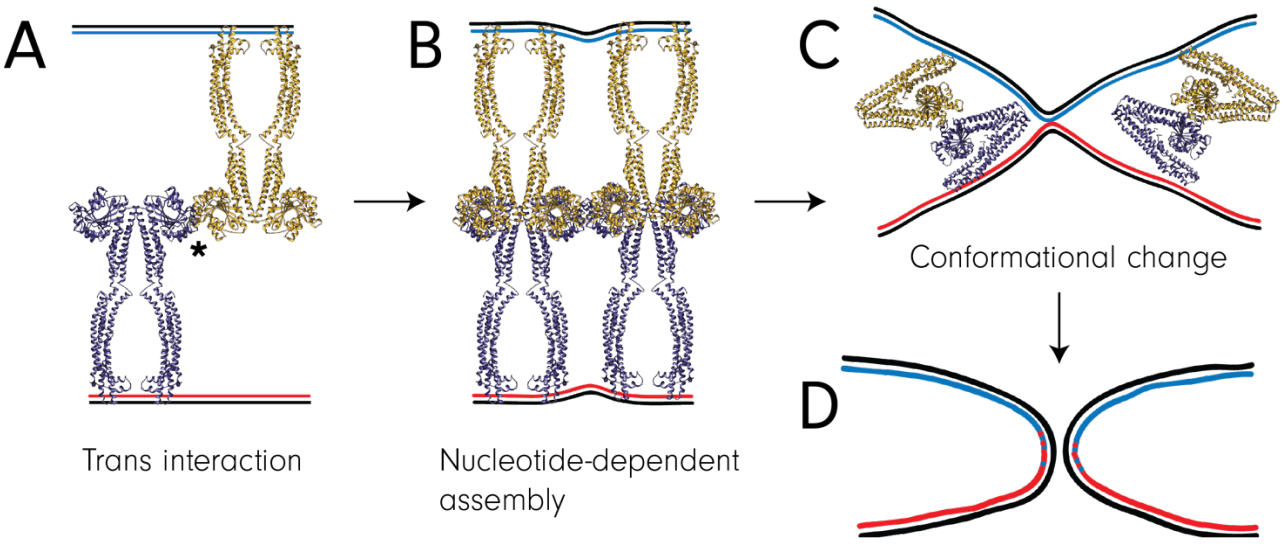

Figure 3.2: Current model of mitochondrial outer membrane fusion. We hypothesize that mitofusins assemble in both *cis* (same membrane) or *trans* (opposite membranes). In this model,

we predict that back-to-back *cis* dimers form tethers across GTPase domains with another mitofusin dimer in *trans* (A). The formation of the predicted G-G interface is noted with an asterisk (*). GTP binding and hydrolysis promote the higher order assembly of mitofusins (B). Dramatic conformational changes are then predicted to bring membranes together to complete fusion (C-D). [figure minorly adapted from Suzanne Hoppins]

Regulating mitochondrial fusion

Post- translational modification (PTM) of the proteins that mediate mitochondrial dynamics allows for rapid changes in mitochondrial shape in response to cellular conditions. While mitofusin modifications are relatively understudied compared to division protein PTMs, several modifications across both mitofusins have been reported to alter mitochondrial fusion and cellular outcomes (see discussion in Whitley et al., 2019). Ubiquitination of both Mfn1 and Mfn2, for example, has been implicated in increased protein turnover and mitochondrial fragmentation (reviewed in detail, Escobar-Henriques and Joaquim, 2019). Similarly, phosphorylation of Mfn2 at S27 by JNK (Leboucher et al., 2012) and at T111 and S442 by PINK1 (Chen and Dorn, 2013) have been implicated as signals that recruit ubiquitin ligases and stimulate mitochondrial turnover. In cases of increased mitofusin turnover, division activity can predominate and lead to mitochondrial fragmentation and mitophagy.

While the regulation of protein levels provides a critical mechanism for mediating protein activity, PTMs such as phosphorylation can also quickly and directly cause altered protein activity. Mitofusin phosphorylation might, for example, stimulate or inhibit mitofusin activity by directly affecting the

rate of nucleotide hydrolysis, the ability of the protein to dimerize in *cis*, tethering across G-G interfaces in *trans*, or the ability to undergo conformational changes. Phosphorylation of Mfn1 in particular has been implicated in the non-degradative, functional regulation of mitofusin activity. Phosphorylation of Mfn1 by PKC at S86 (Ferreira et al., 2019) or by ERK at T562 (Pyakurel et al., 2015) inhibits mitochondrial fusion and promotes mitochondrial fragmentation and cell death. Mfn1 S86 is positioned near the nucleotide binding region of the Mfn1 GTPase domain and would likely be accessible for phosphorylation only when GTPase domains are not interacting across the G-G interface. Based on our model, I predict that back-to-back *cis* dimers of Mfn1 are phosphorylated at S86 by PKC to either inhibit nucleotide binding or assembly of the G-G interface. This is consistent with *in vitro* data suggesting that Mfn1 S86 phosphorylation inhibits its GTPase activity and leads to increased mitochondrial fragmentation and dysfunction (Ferreira et al., 2019). The Mfn1 phosphorylation site at T562 is positioned near the predicted transmembrane domain of Mfn1 and predicted to be far from the GTPase domain in the open conformation of the full-length protein. In the closed conformation, however, T562 is predicted to come into close proximity with the GTPase domain. Based on our model for fusion, phosphorylation at Mfn1 T562 would be expected to interfere with the conformational changes required for membrane remodeling to complete fusion. Mitochondria from 1KO MEFs expressing Mfn1 T562D were also reported to have defective tethering and Mfn1 assembly, suggesting a possible role for this phosphorylation at multiple steps in the fusion process (Pyakurel et al., 2015).

Although other candidate phosphorylation sites have been identified in high throughput screens, there has not been a rigorous functional analysis of additional Mfn1 phosphorylation sites beyond Mfn1 S86 and T562. Validation of these sites and a better understanding of the conditions in which

mitofusins are phosphorylated will be important to further understand about how Mfn1 phosphorylation can regulate its activity. My work aims to understand the mechanism of mitochondrial outer membrane fusion by combining structural, biochemical and cellular tools to understanding how post-translational modification, or amino acid substitutions that alter the ability of a protein to be modified, changes mitofusin-mediated fusion activity. By modeling constitutive phosphorylation and dephosphorylation at Mfn1 S228 specifically, my work has uncovered a possible mechanism for the physiological regulation of Mfn1 assembly and fusion activity. Cellular and biochemical characterization of Mfn1 phospho-mutants suggests that phosphorylation at Mfn1 S228 could inhibit fusion activity by preventing Mfn1 from interacting with itself across mitochondria. Alternatively, dephosphorylation at this site could promote fusion in a normally inhibited population of Mfn1 dimers. Interestingly, the side chain of Mfn1 S228 faces the interface of the GTPase and HB1 domains, where mutations of several other residues are also associated with CMT2A. This suggests a common functional mechanism that could be relevant for understanding disease pathology in a subset of CMT2A patients.

Identification of candidate phosphorylation sites

Approach

Because mitofusin phosphorylation has thus far primarily been associated with reduced fusion activity, I originally set out to identify mitofusin phosphorylation(s) that stimulated fusion activity. During a phenomenon known as stress-induced mitochondrial hyperfusion (SIMH), mitochondrial morphology becomes elongated, or hyperfused, and mitochondria are resistant to turnover. At least some of the changes in mitochondrial shape during SIMH can be attributed to changes in the

phosphorylation status of Drp1. Mitochondria from starved cells expressing a phosphorylation blocking substitution (Drp1 S637A) had reduced levels of hyperfusion after starvation (Gomes et al., 2011). Phosphorylation by PKA at this residue has also been associated with reduced Drp1 activity (Chang and Blackstone, 2007) and mitochondrial recruitment (Cereghetti et al., 2008; Cribbs and Strack, 2007) in other contexts. While the role of Drp1 in SIMH has been well-described, Mfn1 has also been implicated in SIMH (Tondera et al., 2009). From this, I hypothesized that Mfn1 might also be regulated by PKA-mediated phosphorylation during SIMH. In this model, activation of PKA would simultaneously increase fusion activity and decrease division activity, protecting mitochondria from autophagy during the stress.

To test the hypothesis that Mfn1 is phosphorylated by PKA during SIMH, I incubated purified murine Mfn1 and Mfn2 protein with cytosol from wild type mouse embryonic fibroblasts (MEFs) at baseline, after SIMH-induction and after PKA stimulation. Promising mitofusin phosphorylation sites were then identified by mass spectrometry in collaboration with Gennifer Merrihew in the MacCoss lab and the Yeast Resource Center (YRC). While this experimental approach was specifically designed to optimize the probability of detecting a SIMH-induced phosphorylation, we also expected to identify non-SIMH phosphorylation sites with either inhibitory or stimulatory effects on mitofusin activity. This design also specifically allowed for the identification of PTM (phosphorylation, acetylation and methylation) sites across the entirety of both mitofusins, compared to sequence coverage of between 65-85% in immunoprecipitated protein (Samanas, personal communication; Pyakurel et al., 2015). I predict that the differences in coverage between recombinant and native proteins result from technical limitations in completely lysing native, membrane-bound protein.

The Mfn1 and Mfn2 used in this experiment were purified by another graduate student who confirmed the ability of these proteins to fold (Engelhart, 2019). Although no GTPase activity could be detected in either Mfn1 or Mfn2, it is likely that these proteins still represent at least one native conformation in which PTM can occur. If access to a phosphorylation site requires enzyme activity and conformational change, it is likely that such a site would be missed in this experiment.

Within the cytosol-enriched fraction isolated from MEFs, I expected to capture the cytosolic factors important for mediating phosphorylation of Mfn1 and Mfn2. During SIMH, I expected that cytosolic PKA could either directly interact with Mfn1 on the outer mitochondrial membrane or influence the activity of a downstream kinase to alter Mfn1 activity. To induce SIMH, wild type MEFs were treated with 10μM cycloheximide for 4hr (Tondera et al., 2009) or subjected to starvation in HBSS for 4hr (Rambold et al., 2011). Treatment with 20μM forskolin (FRSK) for one hour, which is known to promote Drp1 S637 phosphorylation, was used to stimulate PKA activity (Cribbs and Strack, 2007). To account for any possible additive or interacting effects between PKA signaling and SIMH, I tested an additional condition in which starved cells were treated with 20μM FRSK during the final hour. After treatment, a cytosol-enriched fraction was isolated from MEFs and incubated with recombinant Mfn1 and Mfn2 at 37C for 30 minutes to promote mitofusin phosphorylation. The protein was then bound to anti-FLAG beads, digested with either trypsin or chymotrypsin, and prepared for mass spectrometry analysis.

Analysis

Due to the relatively low abundance of phosphorylated compared to unphosphorylated peptides, our experimental approach did not provide the necessary resolution to detect any differences in

phosphorylation levels between treatment and untreated conditions. Since I was unable to detect Mfn1 phosphorylation(s) specific to a stressor, I chose at this point to shift focus toward a more general analysis of mitofusin phosphorylation across all treatments to identify candidate phosphorylation sites that could either increase or decrease fusion activity.

While low levels of total phosphorylation precluded a more detailed understanding of how phosphorylation changes during SIMH, we have recently resumed efforts to identify how phosphorylation at a specific site (Mfn1 S228) changes in cells across a variety of conditions. Another graduate student in the lab, Nyssa Samanas, is working with Dr. Priska von Haller at the UW Proteomics Resource to perform parallel reaction monitoring (PRM) mass spectrometry to identify conditions that increase or decrease Mfn1 S228 phosphorylation. While my research does not address phosphorylation during SIMH, similar PRM experiments can be performed to measure changes in phosphorylation at residues predicted to be phosphorylated by PKA.

The data-dependent acquisition (DDA) and data-independent acquisition (DIA) confirmed that this approach was indeed able to identify phosphorylations across almost all Mfn1 and Mfn2 peptides. From the DDA experiments, which identified highly abundant phosphorylated peptides based on a fixed set of precursor ions, I was able to identify several phosphorylated peptides, including an Mfn2 phosphorylation site (S27) which has been previously characterized in detail (Leboucher et al., 2012). Mass spectrometry also identified

Mfn1	Mfn2
S50	S27
T350	S151
S472	S177
S549	S283
T564	S455
	S489
	T492
	S726
	T742

Table 3.1: High abundance phospho-peptides identified using DDA approach. Mfn2 S27 and S726 were previously reported phosphorylation sites.

another Mfn2 phosphorylation site (S726) that was reported in a high throughput screen of the phosphoproteome in adipocytes (Humphrey et al., 2013). In two out of three phosphorylation prediction algorithms that use amino acid sequence to identify possible kinase targets (GPS 5.0, PPSP, KinasePhos 2.0), I confirmed that our analysis also identified two predicted PKA phosphorylation sites, Mfn1 S50 and Mfn2 S283. A complete list of phosphorylation sites identified from the DDA data is found in **Table 3.1**.

While DDA can identify highly abundant peptide species, we combined this analysis with DIA, which captures all ions within a sample, to more thoroughly analyze the range of lower abundance phosphorylated peptides in our samples. In a preliminary evaluation of the DIA data, Mfn2 S27 and Mfn2 T282/Mfn2 S283 were noted as the most compelling phosphorylation sites regardless of condition. Because Mfn2 T282 and S283 are immediately adjacent, it was not possible to determine which residue was phosphorylated. In addition to the single phosphorylation, a prevalent, double phosphorylation event of both T282 and S283 was also detected.

Due to unexpected delays in the development of a program to quickly extract and compare phosphorylated peptides across conditions, our collaborator developed a manual work-around to evaluate DIA data for the remaining sites of interest. DIA data was manually assessed to identify (1) if a peptide shifted mass consistent with a phosphorylation event and (2) what conditions phosphorylated protein is observed in. Because of the possible relationship to SIMH, I primarily emphasized the analysis of high-probability PKA phosphorylation sites based at least two phosphorylation prediction algorithms (GPS 5.0, PPSP, KinasePhos2.0): Mfn1 S50, S228, S421 and Mfn2 S249, T282, S283, S442. Based on the predicted full length Mfn1 or Mfn2 structures, all of the

candidate sites screened were also accessible for phosphorylation in either or both the open (**Figure 3.3A**) and closed (**Figure 3.3B**) conformation.

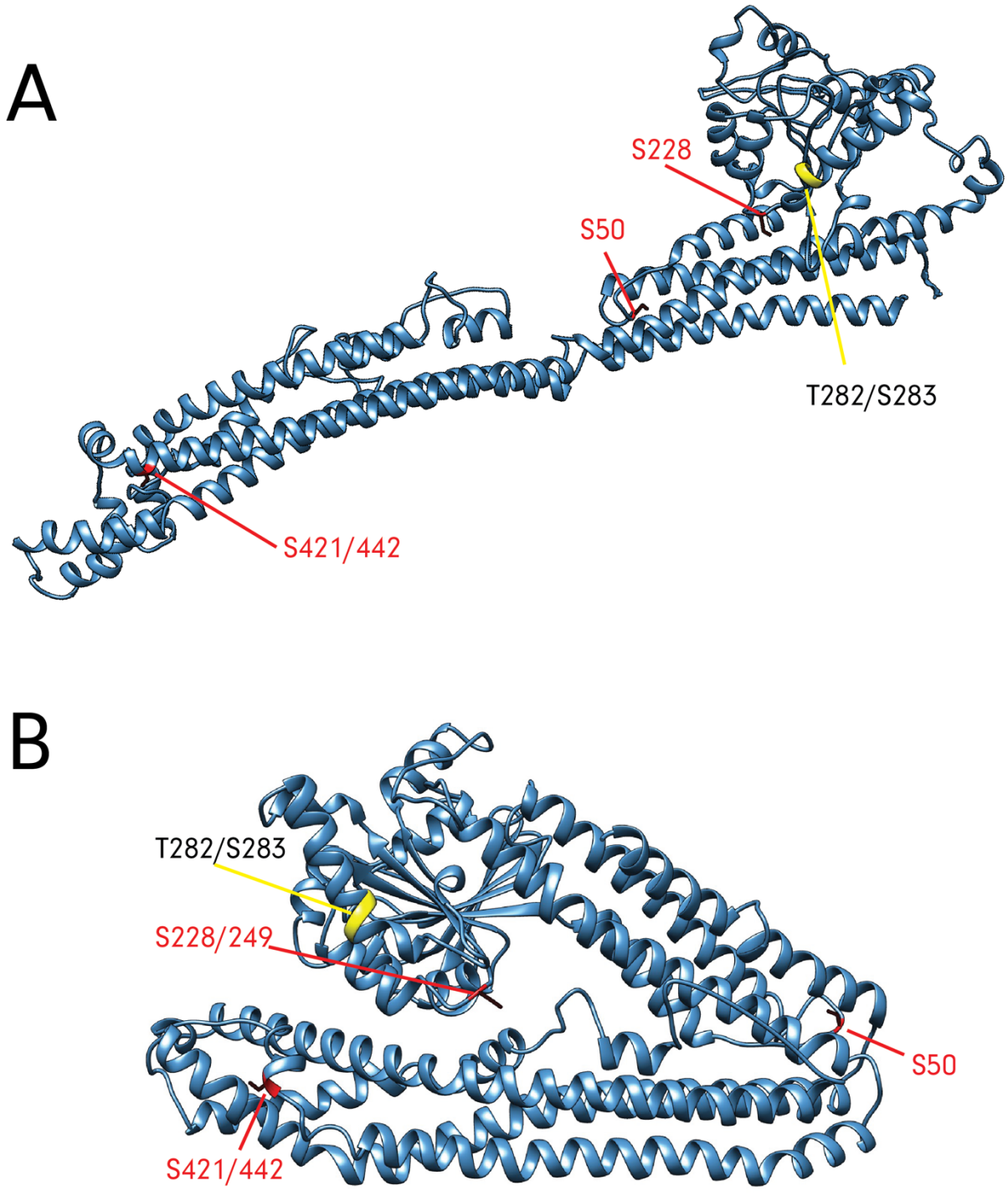

Figure 3.3: Candidate phosphorylation sites searched in DIA dataset. Since the overall fold is predicted to be similar between Mfn1 and Mfn2, the sites searched in the DIA set are mapped onto the predicted full-length structure of Mfn1 in its open (A) and closed (B) conformation. While Mfn2 T282/S283 are not conserved in Mfn1 (yellow), the residues are positioned at a similar location in a helix of the Mfn2 GTPase domain.

Within our samples over two independent experiments, only one site, Mfn2 S249, was not phosphorylated. There were no notable differences between the presence of phosphorylated protein across treatments. **Table 3.2** summarizes the differences in reported or predicted function of the residues evaluated.

		Conserved in other Mfn?	CMT2A mutation?	Annotated on Phosphosite?	Identified in MS?	Additional information
Mfn1	S50				x	
	S228	x	x	x	x	In stretch of five amino acids associated with CMT2A mutations.
	S421	x			x	
Mfn2	S249	x	x	x		In stretch of five amino acids associated with CMT2A mutations.
	T282				x	Not CMT2A mutation but in helix with cluster of CMT2A mutations
	S283				x	Not CMT2A mutation but in helix with cluster of CMT2A mutations
	S442	x		x	x	Predicted to be phosphorylated by PINK1 (Chen et al., 2003)

Table 3.2. Criteria for choosing candidate phosphorylation sites. For each site tested, an "x" indicates if that site is conserved across vertebrate mitofusins, associated with a CMT2A mutation, previously annotated in the Phosphosite phosphorylation database, and identified in this mass spectrometry screen. The additional information column identifies other potentially functionally relevant information about this region.

Screening predicted phosphomutants for altered mitochondrial morphology in cells

To screen the effect of predicted phosphorylation events on mitochondrial morphology, I created phosphorylation mimicking and blocking substitutions at most of the sites identified in **Table 3.2**. Phosphorylation adds a large, negatively charged phosphate group to serine, threonine or tyrosine via a reaction between the hydroxyl group of the amino acid and the relevant kinase. It is therefore possible to block phosphorylation by substituting the target residue with an alanine (A), which is structurally similar to serine but lacks the hydroxyl group. Similarly, substitution of serine with either aspartic acid (D) or glutamic acid (E) acts as a decent mimic of constitutive phosphorylation due primarily to the bulk and negative charge provided by these residues. Because D is the more commonly used phosphomimetic substitution, most original screens were performed primarily with using S/T to D substitutions. However, for a subset of sites, I also measured mitochondrial morphology after substitution from S/T to E.

I used a retroviral transduction system to express phosphomimetic and phosphoblocking substitutions at five of the seven candidate phosphorylation sites- Mfn1 S228/Mfn2 S249, Mfn2 S283, Mfn1 S421/Mfn2 S442 in mouse embryonic fibroblasts (MEFs) lacking Mfn1 (1KO) or Mfn2 (2KO). Clonal populations of cells expressing the relevant mitofusin at near-endogenous levels were isolated to ensure physiological levels of protein expression and prevent aberrant mitochondrial morphology due to mitofusin overexpression (Santel et al., 2003). While transduction with an empty vector control does not alter the fragmented mitochondrial morphology in KO MEFs, expression of WT Mfn1 or Mfn2 can rescue mitochondrial morphology in MEFs lacking Mfn1 (1KO) or Mfn2 (2KO), respectively. Based on this, I expected that Mfn1/Mfn2 variants with reduced fusion activity would not rescue mitochondrial fragmentation when expressed in KO MEFs. Variants that promote

increased fusion activity, however, were expected to cause mitochondrial hyperfusion. Below I briefly discuss the morphological trends observed in preliminary experiments from MEFs expressing C-terminally FLAG-tagged phosphoblocking and phosphomimicking variants.

Mfn1 S228/Mfn2 S249

I isolated three clonal populations of 1KO MEFs expressing Mfn1 S228A-FLAG or Mfn1 S228E-FLAG. While expression of Mfn1 S228A rescued mitochondrial morphology in 1KO MEFs, expression of Mfn1 S228E led to a dramatic clustering of mitochondria around the perinuclear space (**Figure 3.4**). Because Mfn1 S228 is conserved in Mfn2 (S249), I also measured mitochondrial morphology in a single blinded experiment of 2KO MEFs expressing Mfn2 S249A or S249E. Likely due to relatively low expression of Mfn2 in these isolates over time, I was unable to determine a consistent mitochondrial phenotype across clonal populations, although perinuclear clustering was rarely observed (**Figure 3.34**). Further morphological characterization in new clonal populations of 2KO MEFs expressing Mfn2 S249A and S249E will be important to determine a reliable mitochondrial phenotype in these cells.

Differences between mitochondrial morphology in 1KO MEFs expressing Mfn1 S228E and 2KO MEFs expressing Mfn2 S249E is consistent with previous experiments in our lab that have shown many different substitutions across Mfn2 were able to rescue mitochondrial morphology in 2KO MEFs, while the conserved substitution in Mfn1 has a dramatic phenotype. Because of its promise as a potential phosphorylation site (**Table 3.2**), combined with the mitochondrial morphology of 1KO MEFs expressing S228E and the availability of Mfn1 MGD to directly measure enzyme activity (Cao et al., 2017; Qi et al., 2016; Yan et al., 2018), I will focus primarily on the characterization of Mfn1

S228 in the subsequent section. This will be followed by a brief discussion of the mitochondrial phenotypes of 2KO MEFs expressing Mfn2 S249 at the end of this chapter.

Mfn2 S283

Two clonal populations were isolated from 2KO MEFs expressing Mfn2 S283A-FLAG or Mfn2 S283D-FLAG. In two unblinded experiments, expression of either Mfn2 S283A or S283D rescued mitochondrial morphology in 2KO MEFs (n>80 cells per experiment). Interestingly, in a preliminary experiment of cells treated with 10μM CHX, Mfn2 S283D but not S283A appeared to block SIMH. This suggests that Mfn2 S283 phosphorylation may impair fusion during SIMH conditions. This is surprising because of previous work suggesting that Mfn1, not Mfn2, is required for SIMH. However, based on the importance of the Mfn1-Mfn2 heterotypic interaction, it is possible that changes in Mfn2 can be translated into functional changes in Mfn1 through this interaction. Further blinded comparisons of mitochondrial morphology in control and SIMH conditions is required to better understand the physiological relevance of this predicted phosphorylation site.

Mfn1 S421/Mfn2 S442

I also isolated one clonal population of 1KO MEFs expressing Mfn1 S421A-FLAG and three clonal populations expressing Mfn1 S421D-FLAG. In three unblinded experiments, nearly half of the cells expressing either Mfn1 S421A or S421D were able to rescue mitochondrial morphology in 1KO MEFs and no obvious defects in SIMH were observed. Because the average Mfn1 expression level in these cells was around 75%, it is possible that the partial rescue is a result of insufficient Mfn1 expression. Further characterization of clonal populations expressing both variants at higher levels

will be important to better understand if and how phosphorylation of Mfn1 S421 affects mitochondrial morphology.

To determine how the same substitutions at this site affected the fusion activity of Mfn2, I isolated two clonal populations of 2KO MEFs expressing Mfn2 S442A and three clonal populations of 2KO MEFs expressing Mfn2 S442D. In two unblinded experiments, 2KO MEFs expressing Mfn2 S442A were primarily fragmented while 2KO MEFs expressing Mfn2 S442D had reticular mitochondria, with a small population of cells exhibiting mitochondrial hyperfusion. No obvious defects in the ability to undergo SIMH were observed. The inability of mitochondria to fuse in 2KO MEFs expressing Mfn2 S442A suggests that phosphorylation at this site may be important for normal mitochondrial dynamics. Phosphorylation at this site by PINK1 has also been implicated in parkin recruitment and mitochondrial turnover in the heart (Chen and Dorn, 2013).

Effects of Mfn1 S228 substitution in cells

Perinuclear clustering in 1KO MEFs expressing Mfn1 S228E

1KO MEFs transduced with an empty vector retain a fragmented mitochondrial morphology (**Figure 3.4A**), while expression of Mfn1 WT can rescue mitochondrial morphology in MEFs lacking Mfn1 (1KO) (**Figure 3.4B**). Similarly, expression of Mfn1 S228A (**Figure 3.4C, Table 3.3**) mostly rescues mitochondrial morphology in 1KO MEFs. Upon re-evaluation of the differences between clonal populations, I noted that in one clonal population, virtually all mitochondria were fragmented only during one technical replicate. Because removal of this replicate reduces variably and

fragmentation significantly, I propose that this replicate be removed and the experiment be repeated to verify the level of rescue in this population.

Expression of the phospho-mimetic Mfn1 S228E substitution causes a dramatic clustering of mitochondria around the perinuclear space (**Figure 3.4D, Table 3.3**). The "clustered" morphology classification indicates a mitochondrial network in which most, if not all mitochondria are localized in the perinuclear region. In addition to the dramatic, tight clusters observed in many cells (**Figure 3.4D**), clusters were also counted in cells where mitochondria were so close together that the morphology of individual mitochondrial structures could not be determined. Clustered mitochondria are distinct from hyperfused mitochondria, in which most organelles were over 5μm in length, with few or no short mitochondria present. Although hyperfused mitochondria sometimes have a tendency to concentrate in the perinuclear region, they are distinguished from clusters because specific, long mitochondria can be identified. The mitochondrial width also appeared thicker in clustered mitochondria, as if mitochondria fused in side-to-side interactions instead of tip-to-tip. While somewhat subjective, I performed all imaging and quantification while blinded to sample identity to ensure that similar mitochondrial morphologies were consistently grouped into the appropriate category. While not the objective of this project, future experiments to quantitatively distinguish between cluster subtypes can control for cell size and shape using micropattern adhesive cell substrates to more directly measure mitochondrial distribution (López-Doménech et al., 2018).

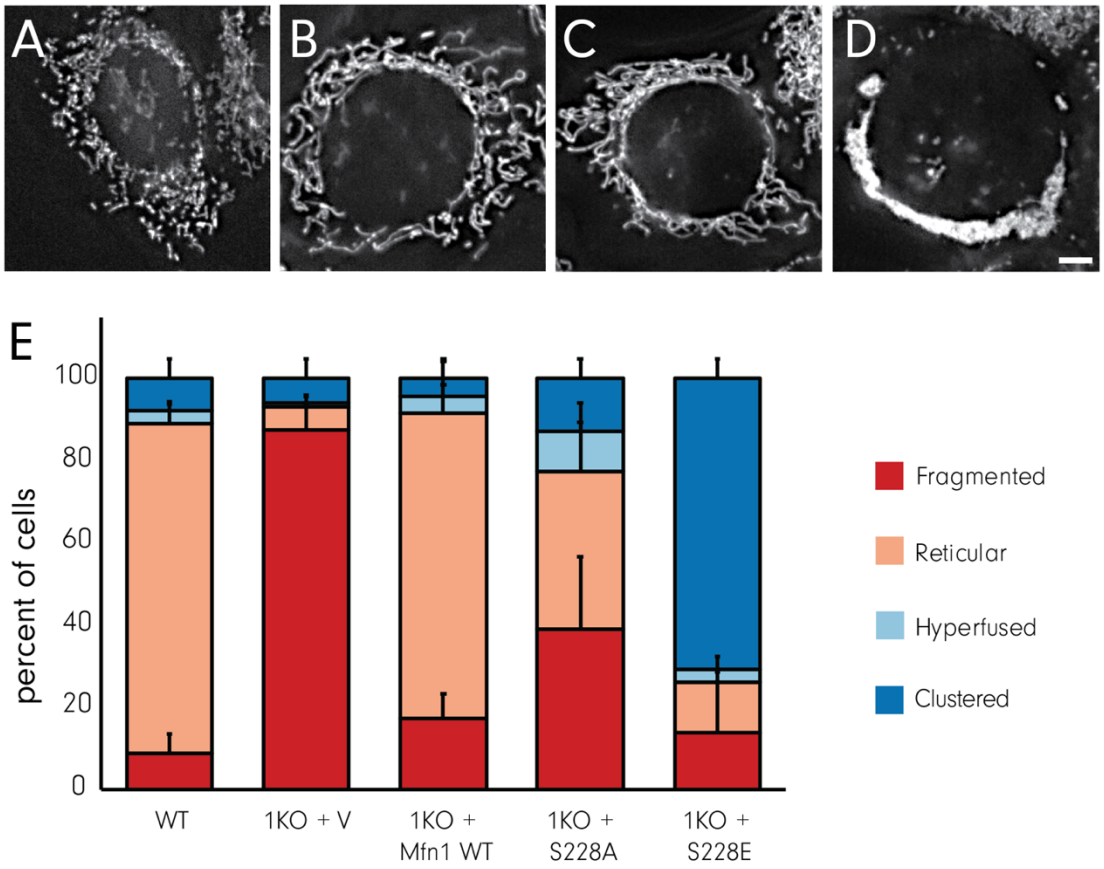

Figure 3.4: Mitochondrial morphology in Mfn1 S228-FLAG mutants expressed in 1KO MEFs. Representative images of clonal populations of 1KO MEFs transduced with either (A) empty vector, (B) wild type Mfn1, (C) Mfn1 S228A, or (D) Mfn1 S228E. Mitochondrial morphology was quantified based on mitochondrial length (fragmented, reticular, hyperfused) and location (aggregated). Quantification represents blinded counts from at least 100 cells in three independent experiments (error = SD). Scale bar is 5 microns.

I also used a C-terminal mNeonGreen tag to visualize Mfn1 localization in 1KO MEFs expressing Mfn1 S228A and S228E. mNeonGreen localization confirmed that both Mfn1 S228A and S228E were correctly targeted to the mitochondria. Expression of Mfn1 S228A-mNeonGreen in 1KO MEFs

resulted in reticular mitochondria, suggesting a wild type-like rescue (**Figure 3.5, Table 3.3**). When Mfn1 S228E-mNeonGreen was expressed in 1KO MEFs, a striking perinuclear mitochondrial clustering phenotype was observed, consistent with that observed in the similar FLAG-tagged variant (**Figure 3.4, Table 3.3**). Large foci of mNeonGreen signal were observed within some clustered mitochondria, and non-clustered mitochondria were primarily fragmented.

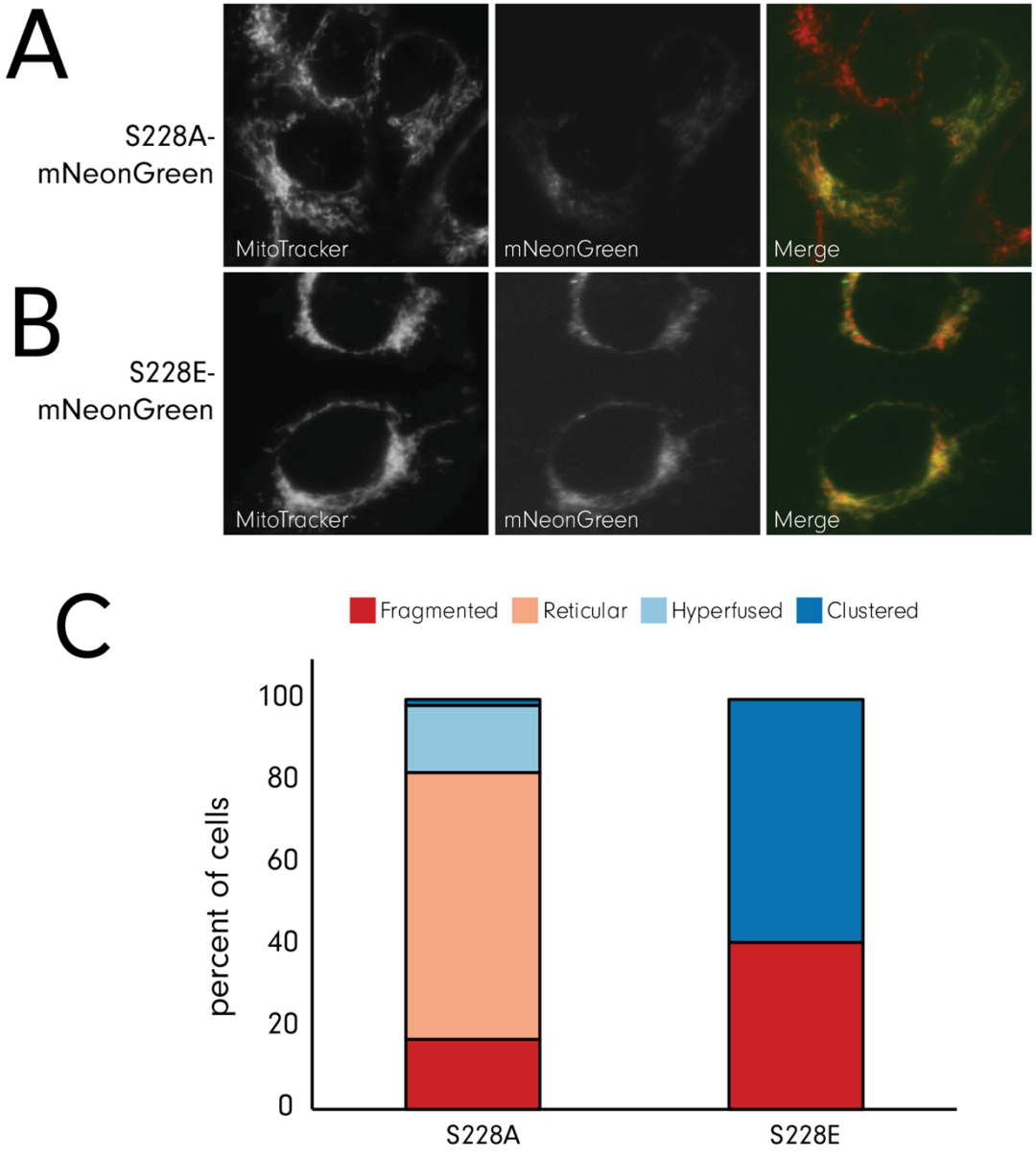

Figure 3.5. Mitochondrial morphology in 1KO MEFs expressing Mfn1 S228A or S228E-mNeonGreen. (A) Representative images from cells expressing either S228A-mNeonGreen or S228E-mNeonGreen. Mitochondrial morphology was observed using MitoTracker CMXRos, and Mfn1 localization was assessed by mNeonGreen signal. (B) Mitochondrial morphology was quantified based on mitochondrial length (fragmented, reticular, hyperfused) and location (aggregated). Quantification represents unblinded counts from two experiments (n=158 cells for S228A, n=96 cells for S228E).

The collapsed mitochondrial network in 1KO MEFs expressing Mfn1 S228E obscured the shape of individual mitochondria, making it difficult to infer how the Mfn1 S228E alters fusion activity. In other genetic backgrounds that cause mitochondrial clustering, such as overexpression of Drp1 dominant negative variants (Legros et al., 2002; Smirnova et al., 2001) or PINK1/parkin overexpression (Vives-Bauza et al., 2010), microtubule depolymerization with nocodazole caused mitochondria to spread throughout the cytosol to reveal the mitochondrial network morphology. Treatment with 5μM nocodazole for about one hour in WT MEFs and 1KO MEFs expressing an empty vector (**Figure 3.6A**) or wild type Mfn1-FLAG (**Figure 3.6B**), caused mitochondria to distribute throughout the cytosol as expected. A small portion of clusters (~20%) in 1KO MEFs expressing Mfn1 S228E-FLAG do not come apart with nocodazole (**Figure 3.6C**). In most cells, however, nocodazole treatment revealed a network of apparently highly connected mitochondria (**Figure 3.6D-F**).

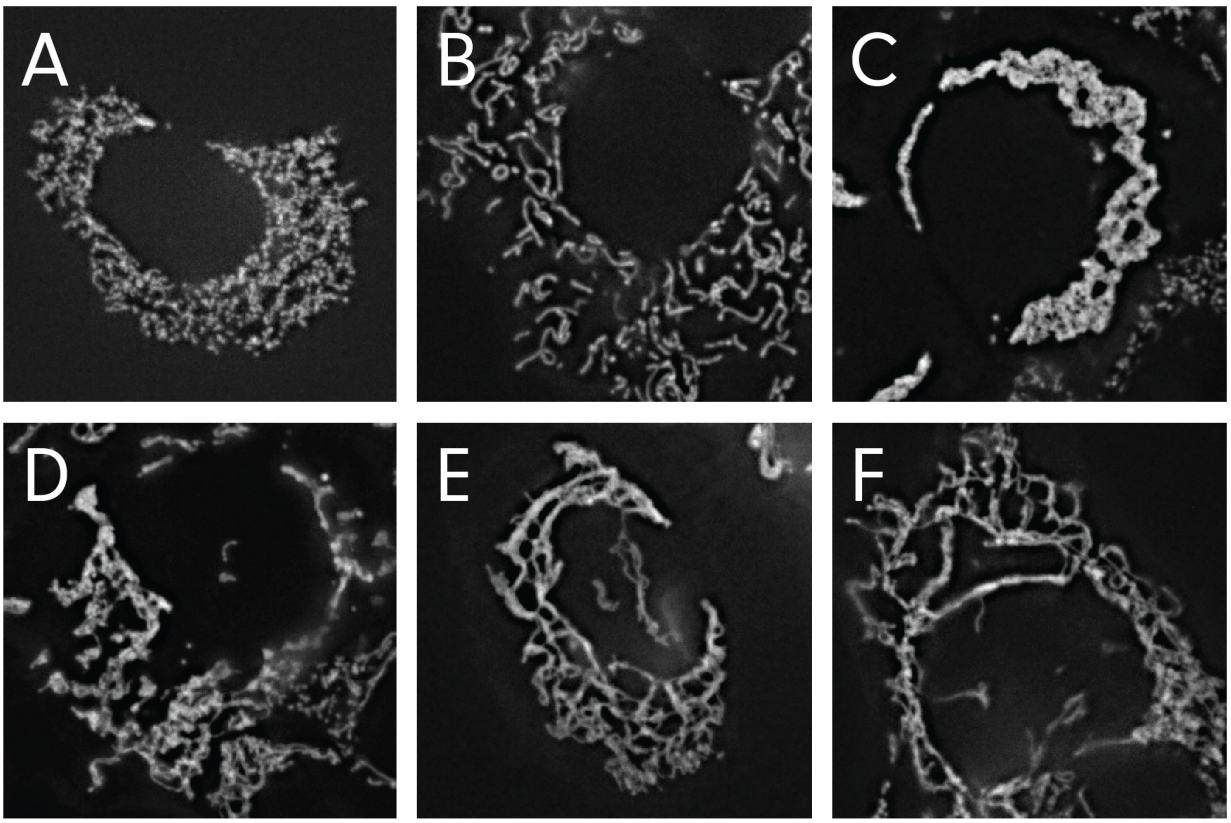

Figure 3.6. Mitochondrial morphology after nocodazole treatment of 1KO + Mfn1 S228-FLAG mutants. MEFs were incubated with 5μM nocodazole for 45min-1hr to depolymerize microtubules. Representative images of mitochondrial morphology are provided for 1KO MEFs transduced with (A) an empty vector, (B) WT Mfn1, and (C-E) 1KO + S228E.

Because fluorescence microscopy alone cannot confirm that the mitochondrial matrix in these cells is also connected, we are also planning to confirm mitochondrial connectivity using a matrix-targeted photoactivatable GFP (paGFP). I expressed a matrix-targeted photoactivatable GFP (paGFP) in 1KO MEFs transduced with a vector control, WT Mfn1, S228A or S228E. Based on experiments in a similar clustering mutant (Mfn1 F202L), I expect that the mitochondrial network in

1KO MEFs expressing Mfn1 S228E will be connected and capable of fusion. Alternatively, paGFP should not distribute through the mitochondrial network if clusters are composed of disconnected mitochondrial fragments. These experiments are currently being performed by another graduate student in the lab.

Highly connected mitochondrial networks could indicate increased fusion activity, reduced division activity or a combination of the two. Various mutations in the mitochondrial division protein Drp1 are associated with mitochondrial hyperfusion (for example, see Whitley et al., 2018) or mitochondrial clustering (Smirnova et al., 2001). To understand if the increased mitochondrial connectivity depended on altered fusion activity or impaired Drp1 recruitment to tight clusters, I measured the ability of Drp1 to be recruited to mitochondrial clusters using immunofluorescence. In all cells, Drp1 puncta were observed throughout the cytosol, as well as on the mitochondria, as we would expect for wild type mitochondria (**Figure 3.7**). This suggests that the network morphology cannot be explained simply by the inability of Drp1 to be recruited to these mitochondria. To fully understand changes in the balance between fusion and division in these cells, future work should confirm that Drp1 assemblies on mitochondria are functional and able to complete division.

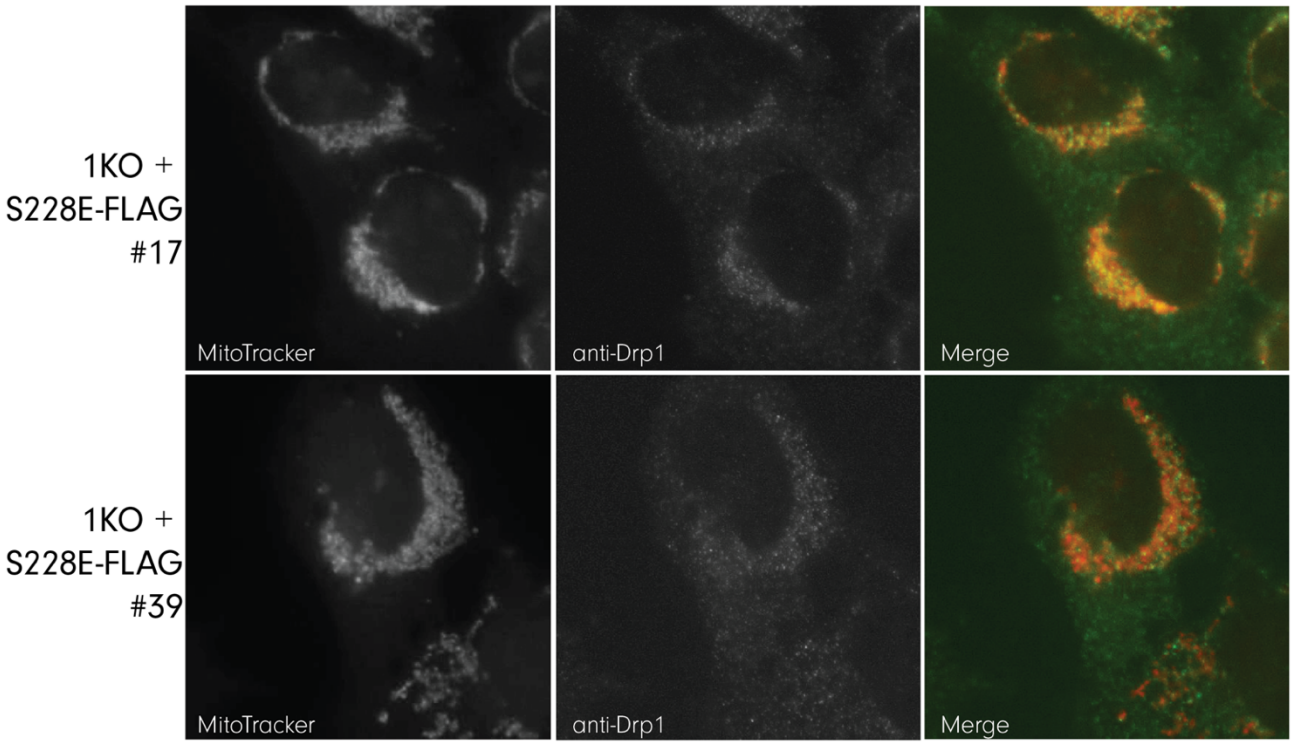

Figure 3.7. Drp1 localization in 1KO MEFs expressing Mfn1 S228E-FLAG. Representative images of cells incubated with MitoTracker and then fixed for immunofluorescence. Drp1 was detected using an anti-Drp1 antibody and around 60 cells were assessed for each isolate (n=60 cells for E17, n=66 cells for E39).

I also attempted to infer the ability of mitochondria to fuse by observing cluster formation. Clusters may form by short mitochondria being transported toward the nucleus, where they become fused. Alternatively, clusters may result from excessive mitochondrial hyperfusion that eventually leads to side-to-side fusion events and network collapse. To better understand cluster formation, I used the depolarizing agent, CCCP, to fragment mitochondria through the disruption of membrane potential, which lead to the separation of clusters. Treatment with 10μM CCCP for 3-4hr caused fragmentation

in most 1KO MEFs expressing Mfn1 S228E-FLAG. Morphology was evaluated while blinded to sample identity at baseline (**Figure 3.8A**), after CCCP treatment (**Figure 3.8B**) and after CCCP treatment followed by drug washout and recovery (**Figure 3.8C**).

Mitochondria in 1KO MEFs expressing an empty vector, Mfn1 WT and Mfn1 S228A were all primarily fragmented after CCCP treatment, as expected. CCCP treatment caused fragmentation in most 1KO MEFs expressing Mfn1 S228E. However, similar to cells treated with nocodazole (**Figure 3.6C**), approximately 20% of the mitochondrial clusters in these cells remained tightly connected after CCCP treatment (**Figure 3.8B**).

Following CCCP treatment, mitochondria can recover in normal cellular media to restore balanced mitochondrial dynamics. In WT MEFs and 1KO MEFs expressing Mfn1 WT, recovery in DMEM for 4hr restores a reticular mitochondrial morphology (**Figure 3.8C**), while 1KO MEFs transduced with an empty vector remain fragmented. 1KO MEFs expressing Mfn1 S228A restored a reticular mitochondrial network in around 40% of cells. This was fairly surprising but may suggest that the slight deficit in rescue observed in 1KO MEFs expressing Mfn1 S228A (**Figure 3.4**) could be due to moderately reduced fusion activity in this protein. In 1KO MEFs expressing Mfn1 S228E, the primary clustering phenotype was almost fully restored after 4hr, suggesting that clusters can form fairly quickly. Because cells expressing wild type Mfn1 are able to completely rescue mitochondrial morphology in the time period tested, it is still unclear if mitochondrial clusters form before or after mitochondrial fusion. To test this, mitochondrial morphology should be measured at earlier stages in recovery, before WT Mfn1 is able to restore a reticular mitochondrial network. Live imaging of

cluster re-formation during recovery can also elucidate how changes in mitochondrial fusion and transport lead to perinuclear cluster formation in 1KO MEFs expressing Mfn1 S228E.

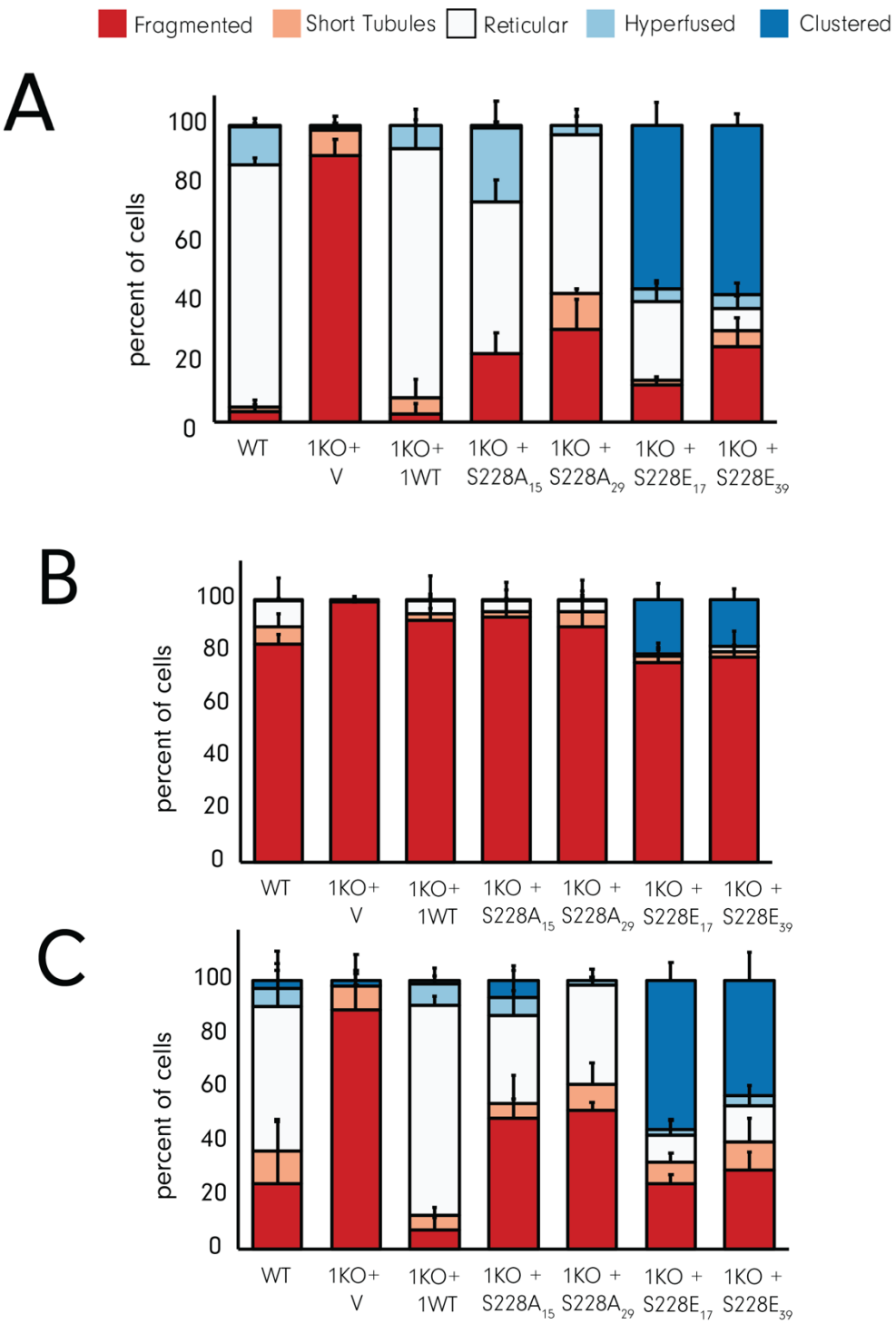

Figure 3.8. CCCP treatment and recovery in 1KO MEFs expressing Mfn1 S228A/E-FLAG. Morphology was quantified, blinded to sample identity at baseline (A), after 10μM CCCP for three hours (B) and after CCCP treatment followed by 4hr of recovery in normal media (C). Quantification represents data from 3-5 independent experiments, in which at least 100 cells were counted per condition.

To test the dependence of re-fusion or re-clustering after CCCP treatment on microtubule-based transport, I am also optimizing an experiment to measure mitochondrial shape and localization changes after CCCP washout into normal media with nocodazole. In the absence of microtubules, mitochondria are still able to fuse, likely by more random interactions between mitochondria (Legros et al., 2002). I predict that in 1KO MEFs expressing substitutions that inhibit Mfn1 activity, mitochondria remain fragmented and spread out after nocodazole treatment. In cells expressing variants of Mfn1 that increase its fusion activity, however, I would expect to see reticular or hyperfused mitochondria. Despite local mitochondrial clustering of various lengths, preliminary experiments provided no evidence for strong perinuclear clustering or excessive mitochondrial fusion in the absence of microtubules (**Figure 3.9B-F**). This suggests that the mitochondrial morphology in 1KO MEFs expressing Mfn1 S228E FLAG is not caused by increased fusion activity but rather the altered mitochondrial transport of primarily fragmented mitochondria. While the exact mechanism by which this occurs is unclear, I hypothesize that increased transport of mitochondria towards the nucleus locally concentrates mitochondria, allowing mitochondria with relatively low fusion activity to become highly fused.

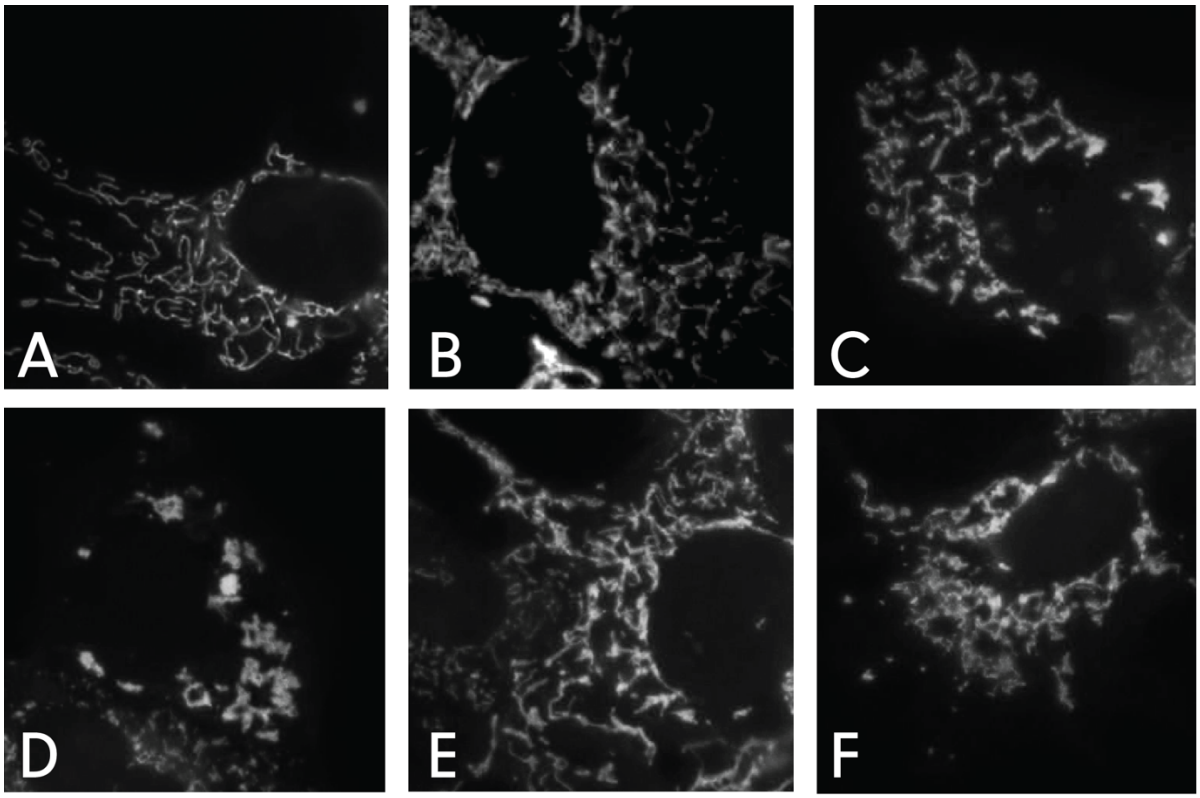

Figure 3.9. Representative images of CCCP recovery with nocodazole in 1KO MEFs expressing Mfn1 WT (A) or Mfn1 S228E-FLAG (B-F). After 10μM CCCP treatment, cells were recovered in DMEM containing 10μM nocodazole for two hours. Representative images in B-F reflect the range of mitochondrial morphologies observed, most of which involved some form of local clustering.

Influence of endogenous mitofusins on the mitochondrial phenotype of MEFs expressing Mfn1 S228E

To understand if mitochondrial clustering after expression of Mfn1 S228E was dominant, I expressed the same FLAG-tagged Mfn1 mutants in WT MEFs that expressed both Mfn1 and Mfn2. As we would expect for wild type Mfn1, expression of Mfn1 S228A in WT MEFs doesn't noticeably alter mitochondrial morphology (**Figure 3.10C**). However, due to difficulties obtaining clonal populations

expressing this variant at appropriate levels in the preliminary experiment, likely due to inefficient viral transduction, morphology in these cells was only measured on one occasion and requires the screening of additional FLAG-tagged populations to confirm the morphological phenotype. Expression of Mfn1 S228E-FLAG in WT MEFs caused mitochondrial clustering in around 40-50% of cells (**Figure 3.10**). Many of these cells appeared small and rounded, with preliminary observations that a substantial mitochondrial population concentrated near the top of the cell (**Figure 3.10B**). Additional characterization of these cellular populations should directly address if this morphological phenotype is associated with increased cell death or defects in cell division, both of which might be predicted by this abnormal cellular morphology.

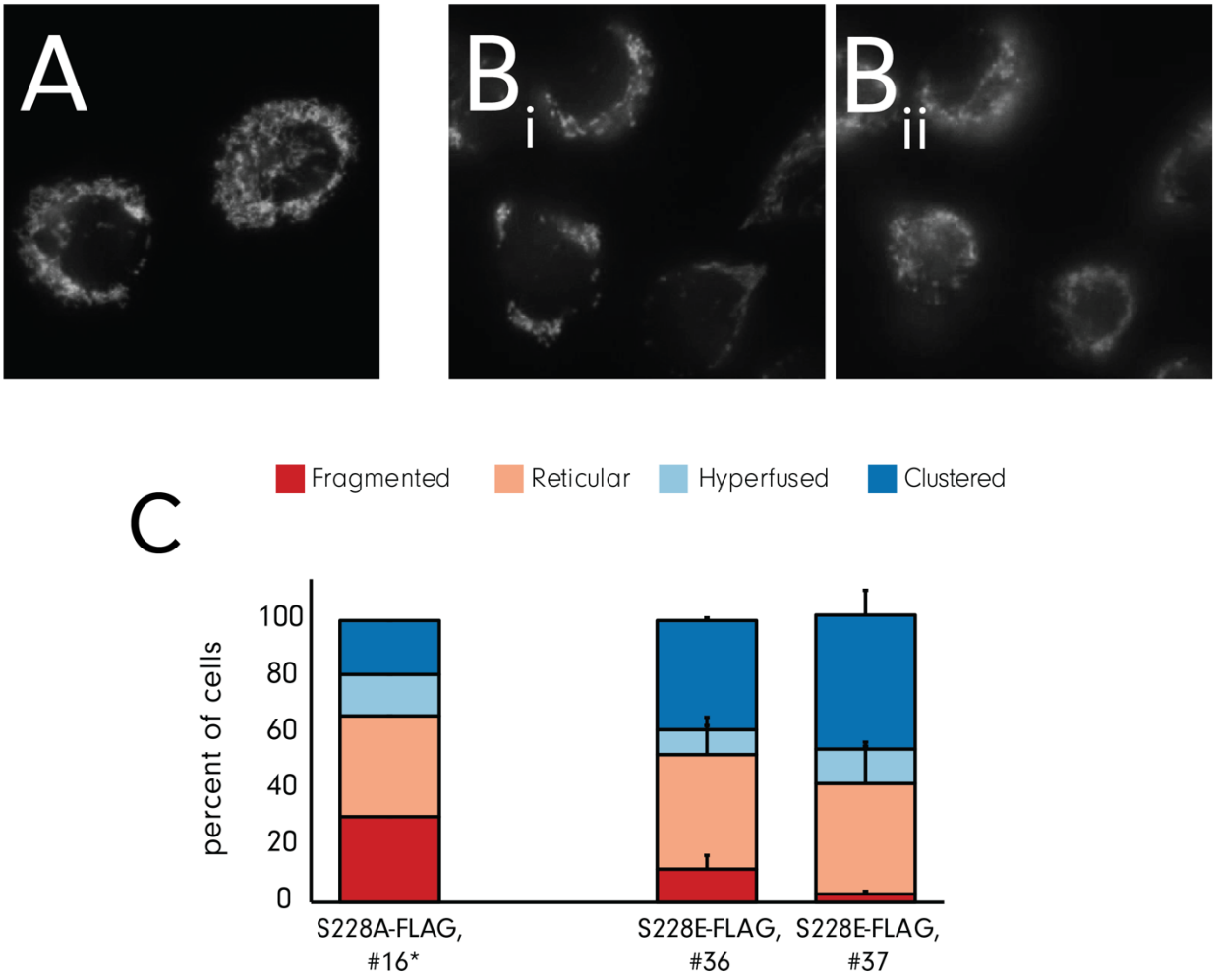

Figure 3.10. Mitochondrial morphology in WT MEFs expressing Mfn1 S228A or Mfn1 S228E-FLAG. (A-B) Representative images of 1KO MEFs expressing Mfn1 S228E. In B, two planes imaged at the bottom (B_i) and top (B_{ii}) of cells are shown to highlight mitochondrial distribution. (C) Mitochondrial morphology was quantified in clonal populations of WT MEFs expressing Mfn1 S228A-FLAG (1 experiment, n >100 cells) or Mfn1 S228E-FLAG (2 experiments, n >100 cells).

To detect mitofusin localization and ensure that the mitochondrial morphologies observed were not dependent on the protein tag, I also expressed the same Mfn1 variants with an mNeonGreen tag in WT MEFs. Mitochondrial morphology in WT MEFs expressing S228E-mNeonGreen was indistinguishable from the morphology observed in WT MEFs expressing S228A-mNeon Green (**Figure 3.11**). While morphology in WT MEFs expressing Mfn1 S228A was consistent with both tags, there were significantly fewer cells with clustered mitochondria in WT MEFs expressing Mfn1 S228E-mNeonGreen compared to Mfn1 S228E-FLAG (**Figure 3.10**). Because of the preliminary nature of this data, additional blinded replicates with both tags should be quantified to verify these differences. The comparable mitochondrial morphology observed in 1KO and WT MEFs expressing Mfn1 S228E-FLAG suggested that the S228E variant was dominant and could alter wild type Mfn1 fusion activity.

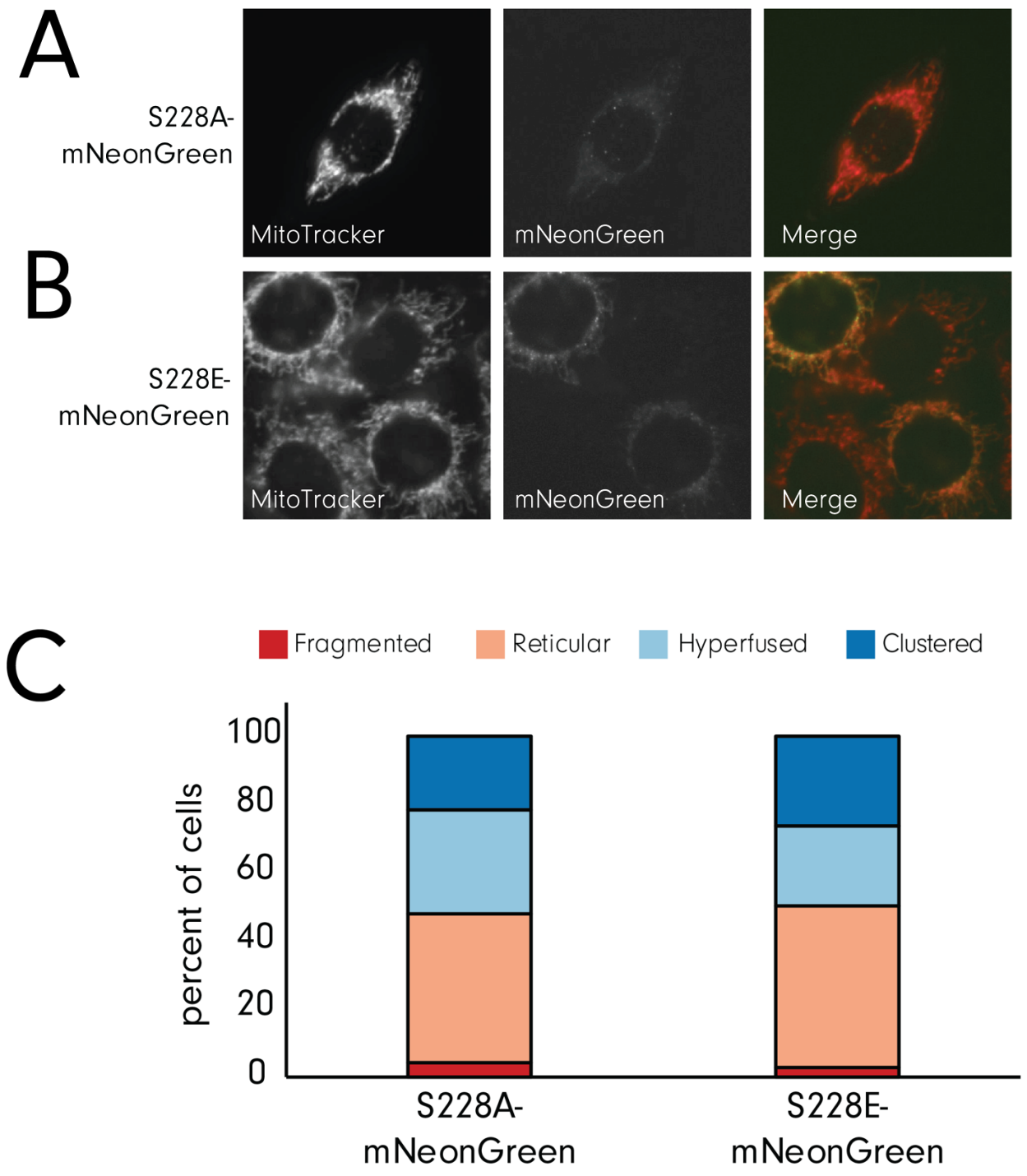

Figure 3.11. Mitochondrial morphology in WT MEFs expressing Mfn1 S228A or Mfn1 S228E-mNeonGreen. Representative images of WT MEFs expressing either (A) Mfn1 S228A or (B) Mfn1 S228E-mNeonGreen. (C) Mitochondrial morphology was quantified in clonal populations of WT

MEFs expressing Mfn1 S228A-mNeonGreen (2 experiments, n <50 cells) or Mfn1 S228E-mNeonGreen (3 experiments, n>100 cells).

While there is some functional redundancy between Mfn1 and Mfn2, there is also evidence that heterotypic interactions between Mfn1 and Mfn2 are the strongest drivers of mitochondrial fusion *in* vitro (Hoppins et al., 2011). To better understand how the presence of wild type Mfn1 and/or Mfn2 affected fusion in mitochondria expressing Mfn1 S228E, I measured mitochondrial morphology after expressing Mfn1 S228A and S228E mNeonGreen-tagged mutants in MEFs lacking Mfn2 (2KO). In 2KO MEFs expressing endogenous Mfn1 but not Mfn2, expression of Mfn1 S228A-mNeonGreen rescued mitochondrial morphology in half of Mfn2 (2KO) MEFs screened. There was less of a rescue in 2KO MEFs expressing Mfn1 S228E cells, with clustering only observed in cells with high mNeonGreen signal, suggesting that, like in WT MEFs, the presence of wild type Mfn1 is associated with reduced mitochondrial clustering. However, in the absence of wild type Mfn2, we would expect these cells to maintain a fragmented mitochondrial network due to reduced fusion activity. Because fewer than 50 cells were counted in each condition, follow-up experiments are required to understand if these data represent a repeatable phenotype in this background.

I also expressed Mfn1 S228A and S228E-mNeonGreen in DKO MEFs to understand how each Mfn1 S228 substitution affected protein activity in the absence of wild type Mfn1 and Mfn2. Preliminary, unblinded morphological analysis of DKO MEFs expressing Mfn1 S228A was inconclusive. In a small population (n<50 cells), mitochondrial morphology varied from fragmented to hyperfused to somewhat clustered. However, in a single experiment (n= 169 cells), expression of Mfn1 S228E

caused perinuclear clustering in 55% of cells, with most remaining cells having primarily fragmented mitochondria (**Figure 3.12**). The phenotype in DKO MEFs was similar to that observed in 1KO MEFs, although nocodazole treatment revealed that, in the few instances of cluster separation, clusters consisted of fragmented mitochondria. This suggests that in the absence of wild type protein, mitochondria expressing Mfn1 S228E can cluster but not fuse. Because Mfn1 S228E clusters in 1KO appear highly connected after nocodazole treatment, this also provides evidence that the presence of WT Mfn2 is required for mitochondrial connectivity in cells expressing Mfn1 S228E and perhaps fusion activity.

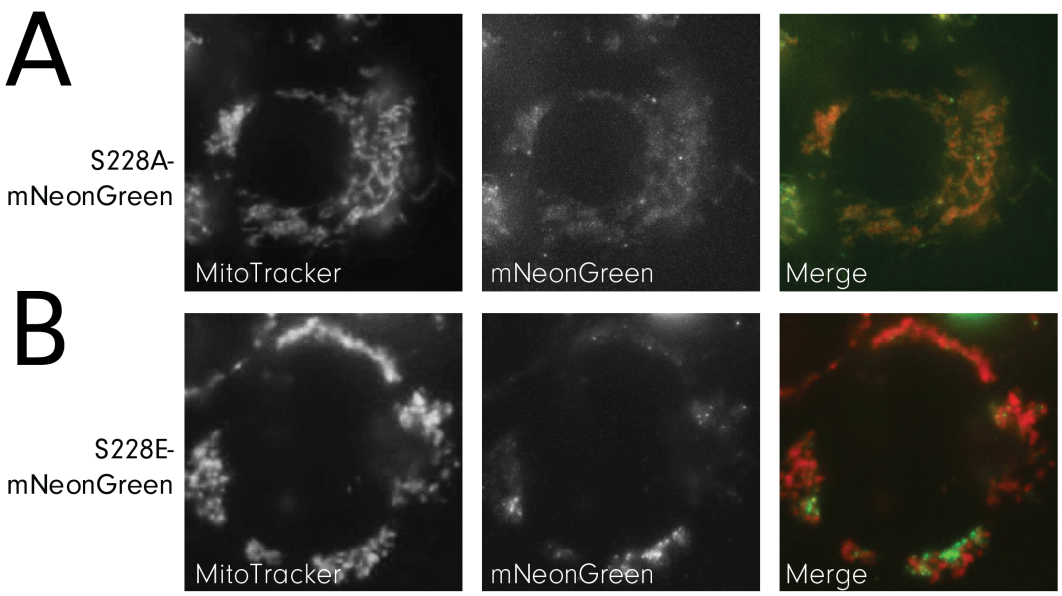

Figure 3.12. Mitochondrial morphology observed in DKO MEFs expressing Mfn1 S228-mNeonGreen variants. Representative images of DKO MEFs expressing either (A) Mfn1 S228A or (B) S228E in DKO MEFs. At least fifty cells were imaged from a single biological replicate.

Additional amino acid substitutions at Mfn1 S228

In addition to the phosphomimicking substitution of serine (S) to glutamic acid (E), aspartic acid (D) is frequently used as a phosphomimicking substitution. While we hypothesized that the larger side chain of glutamic acid would more closely represent the bulk of phosphorylation, I also measured mitochondrial morphology in clonal populations of 1KO MEFs expressing Mfn1 S228D. Unlike expression of Mfn1 S228E, expression of Mfn1 S228D appeared to partially rescue mitochondrial morphology and more closely resembles cells expressing S228A (**Figure 3.13, Table 3.3**).

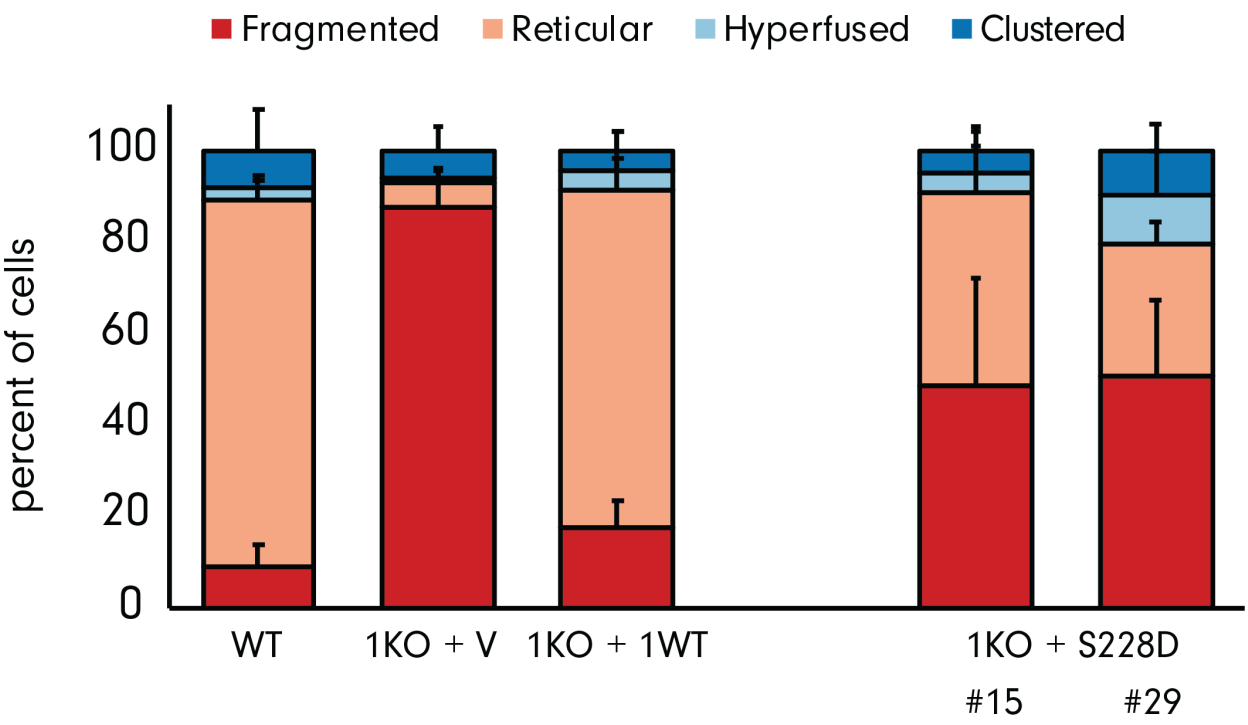

Figure 3.13. Expression of Mfn1 S228D-FLAG in 1KO MEFs. Two clonal populations of 1KO MEFs were isolated that expressed Mfn1 S228D at about 90% of wild-type levels. Mitochondria were quantified based on mitochondrial length (fragmented, reticular, hyperfused) and location (aggregated). Quantification represents blinded counts from at least 100 cells in three independent

experiments (error = SD). *Note that since these cells were counted on the same day as cells expressing Mfn1 S228A/E, the controls (WT, 1KO + V, 1KO + 1WT) are the same as in **Figure 3.4E**.

In an attempt to establish a positive control substitution that still allowed for Mfn1 phosphorylation at position 228, I also expressed Mfn1 S228T-FLAG in 1KO MEFs. Since threonine closely mimics serine structure and contains a phosphorylatable hydroxyl group, I expected that 1KO MEFs expressing Mfn1 S228T would retain the ability to be phosphorylated at Mfn1 S228. In three blinded experiments of three clonal populations expressing Mfn1 S228T at near-endogenous levels, I was unable to conclusively determine trends in mitochondrial morphology (**Figure 3.14, Table 3.3**). Significant mitochondrial fragmentation was consistently observed in one clonal population of 1KO MEFs expressing Mfn1 S228T (#38), while the other two clonal populations (#20, #30) possessed primarily reticular mitochondria. One explanation for the variable morphology across cells expressing identical substitutions is that Mfn1 expression varies across clonal populations, with #38 expressing at levels too low to rescue morphology. When Mfn1 expression was measured by western blot at the time of the microscopy experiments, 1KO MEFs were expressing Mfn1 S228T at between 90% (#38) and 160% (#20, 30) of wild type Mfn1 levels. While unlikely, it remains possible that these differences in expression levels could explain varying morphologies. Alternatively, it is possible that the variable results in 1KO MEFs expressing Mfn1 S228T is due to the differential specificity of kinases for serine vs. threonine. Confirmation of Mfn1 S228T expression levels and the isolation of additional clonal populations will be important to better understand the effects of this substitution and control for phenotypes due to protein levels or viral DNA integration site.

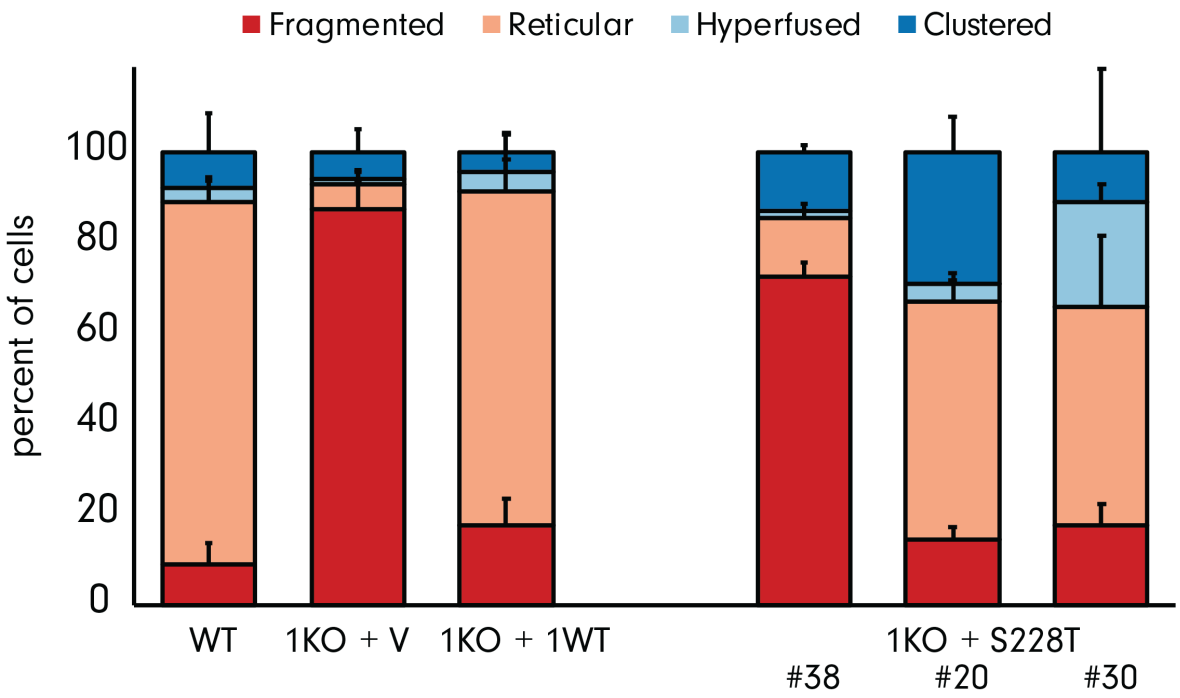

Figure 3.14. Mitochondrial morphology in 1KO MEFs expressing near-endogenous levels of Mfn1 S228T-FLAG. Three clonal populations of 1KO MEFs expressing Mfn1 S228T-FLAG were counted on three separate occasions, with over 100 cells counted per experiment. Imaging and quantification were performed blinded to sample identity. *Note that since these cells were counted on the same day as cells expressing Mfn1 S228A/E, the controls (WT, 1KO + V, 1KO + 1WT) are the same as in **Figure 3.4E**.

Next, I wanted to determine if the unique mitochondrial phenotype in 1KO MEFs expressing Mfn1 S228E was dependent on the size and/or charge of the substituted side chain. To determine if mitochondrial clustering specifically required Mfn1 S228 substitution with a large, negatively-charged residue, I substituted Mfn1 S228 with lysine (K), which has a similar size but opposite charge of glutamic acid. In a preliminary experiment of almost 200 1KO MEFs expressing Mfn1 S228K-FLAG

at near-endogenous levels, mitochondrial clustering was observed in about a third of cells, while the remaining cells had primarily fragmented or short mitochondria (**Figure 3.15A, Table 3.3**). In 1KO MEFs expressing Mfn1 S228K-mNeonGreen, perinuclear mitochondrial clustering was observed in approximately 55% of cells (**Figure 3.15B, Table 3.3**). Increased mitochondrial clustering in cells expressing S228K suggests that at least some of the changes in mitochondrial shape and distribution in cells expressing the phosphomimetic Mfn1 S228E substitution are caused by the addition of bulk, rather than specific charge, in this region of Mfn1.

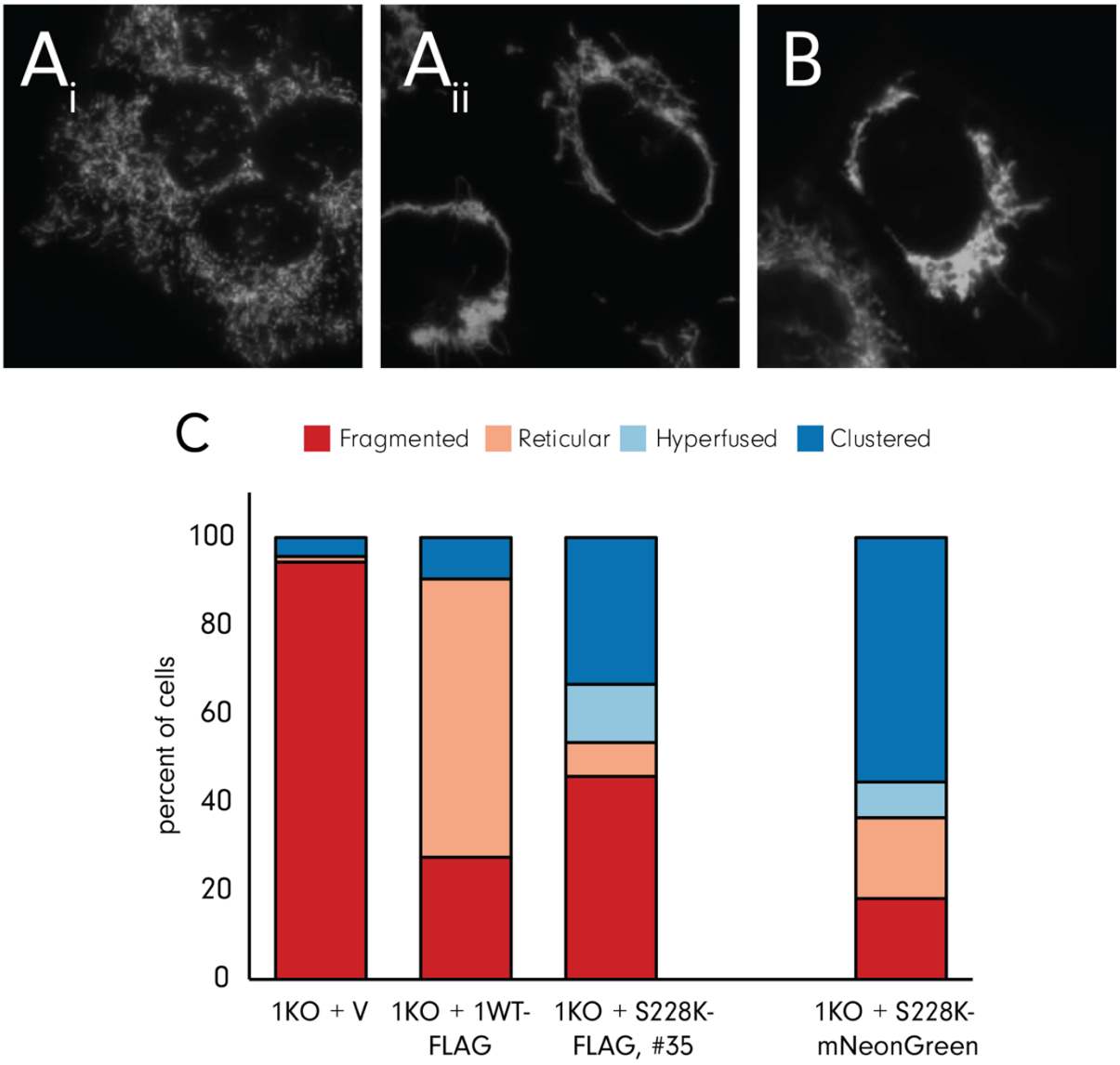

Figure 3.15. Mitochondrial morphology in 1KO MEFs expressing near-endogenous levels of Mfn1 S228K-FLAG. (A) Representative images of 1KO MEFs expressing Mfn1 S228K-FLAG with either (i) fragmented or (ii) clustered morphology. (B) Representative image of mitochondria in 1KO MEFs expressing Mfn1 S228K-mNeonGreen. (C) At least 130 cells were counted in one experiment of 1KO MEFs transduced with an empty vector, WT Mfn1-FLAG or Mfn1 S228K-FLAG (n=196 cells). Mitochondrial morphology was also quantified in one experiment of 1KO MEFs expressing Mfn1 S228K-mNeonGreen (n=99 cells). Imaging and quantification were performed blinded to sample identity.

To further understand the role of side chain size at Mfn1 S228, I am also making 1KO MEFs expressing FLAG and mNeonGreen-tagged Mfn1 S228F. The phenylalanine substitution represents a large, uncharged side chain that is also associated with the development of Charcot-Marie Tooth Type 2A (CMT2A) at the homologous site in Mfn2 (S249F) (Abe et al., 2011; Xie et al., 2016). Based on the phenotypes in 1KO MEFs expressing S228E, and to a lesser extent S228K, I expect that this substitution will also increase mitochondrial clustering.

While I do predict that bulky substitutions between the Mfn1 GTPase and HB1 domains affect protein structure, localization of Mfn1-mNeonGreen variants suggests that Mfn1 is properly localized to mitochondria. In data discussed in **Figures 3.28** and **3.29**, a truncated Mfn1 protein containing only the GTPase and HB1 domain of Mfn1 was able to fold, assemble and hydrolyze GTP, suggesting that the phenotypes observed here are not based solely on the expression of misfolded Mfn1.

Functional importance of the region surrounding Mfn1 S228

A set of mutations associated with CMT2A [Mfn2 L248V (Feely et al., 2011), R250Q/W (Feely et al., 2011; Verhoeven et al., 2006), P251R/L/A (Feely et al., 2011, Zuchner et al., 2004) and N252K (Casasnovas et al., 2010)] cluster around Mfn2 S249 (Mfn1 S228), suggesting that this region is important for mitofusin function (**Figure 3.16**). Specifically, close interactions between HB1 and both L227 and K229 in the bent conformation of Mfn1 MGD are predicted to be important for stabilizing the conformational changes that occur around Hinge 1 (Yan et al., 2018). I predicted that, as in 1KO MEFs expressing S228E, substitution of either L227 or K229 with glutamic acid will disrupt the intramolecular interactions between the GTPase domain and HB1.

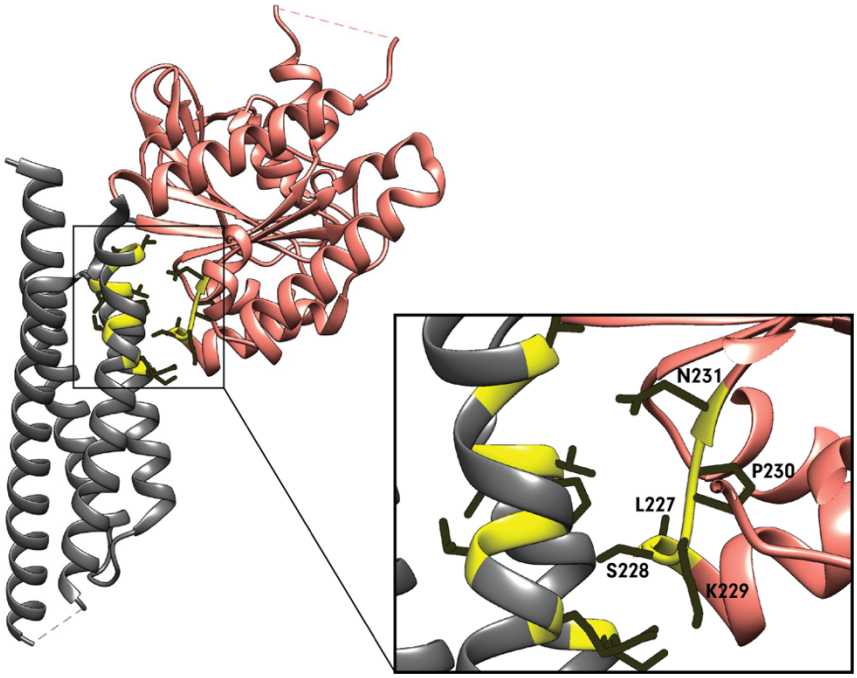

Figure 3.16. Residues associated with CMT2A disease-causing mutations. Mutation of several sites (yellow) at the interface of the GTPase domain (pink) and HB1 (gray) is associated with CMT2A.

To understand if the substitution of a large, negatively charged residue at these sites has similar effects on mitochondrial morphology compared to Mfn1 S228E, I evaluated morphology in 1KO MEFs expressing an mNeonGreen-tagged version of either L227E or K229E. Over 85% of L227E mNeonGreen-expressing cells had mitochondria that were clustered around the nucleus, a similar phenotype to cells expressing S228E (**Figure 3.17A,C, Table 3.3**). In the closed Mfn1 MGD structure (5YEW, **Figure 3.16**), Mfn1 L227 is predicted to interact with I66 and V70 on HB1. Addition of large, charged residue at this site is predicted to disrupt this interaction, and possibly protein function. Further analysis of the cellular and biochemical characteristics of 1KO MEFs expressing L227E-FLAG will be required to understand if this substitution alters mitofusin activity through a similar mechanism as S228E.

Unlike L227E, expression of K229E-mNeonGreen caused mitochondrial hyperfusion in approximately 60% of cells without any significant clustering observed (**Figure 3.17B,C, Table 3.3**). This was somewhat surprising because of the reported importance of interactions between K229 and Q346 in the bent conformation of Mfn1 MGD. One interpretation of this result is that the replacement of a positive charge with a negative charge at K229 still allows for the formation of stabilizing salt bridges with HB1 or changes them in such a way that contributes to increased fusion activity. This would be consistent with substitutions of uncharged residues at this site leading to CMT2A. Alternatively, if mitochondrial clusters result from mitochondrial hyperfusion, it is possible that K229E has a less severe mitochondrial phenotype compared to L227 and S228, possibly because of more flexibility of the K229 side chain to orient away from the GTPase-HB1 interface.

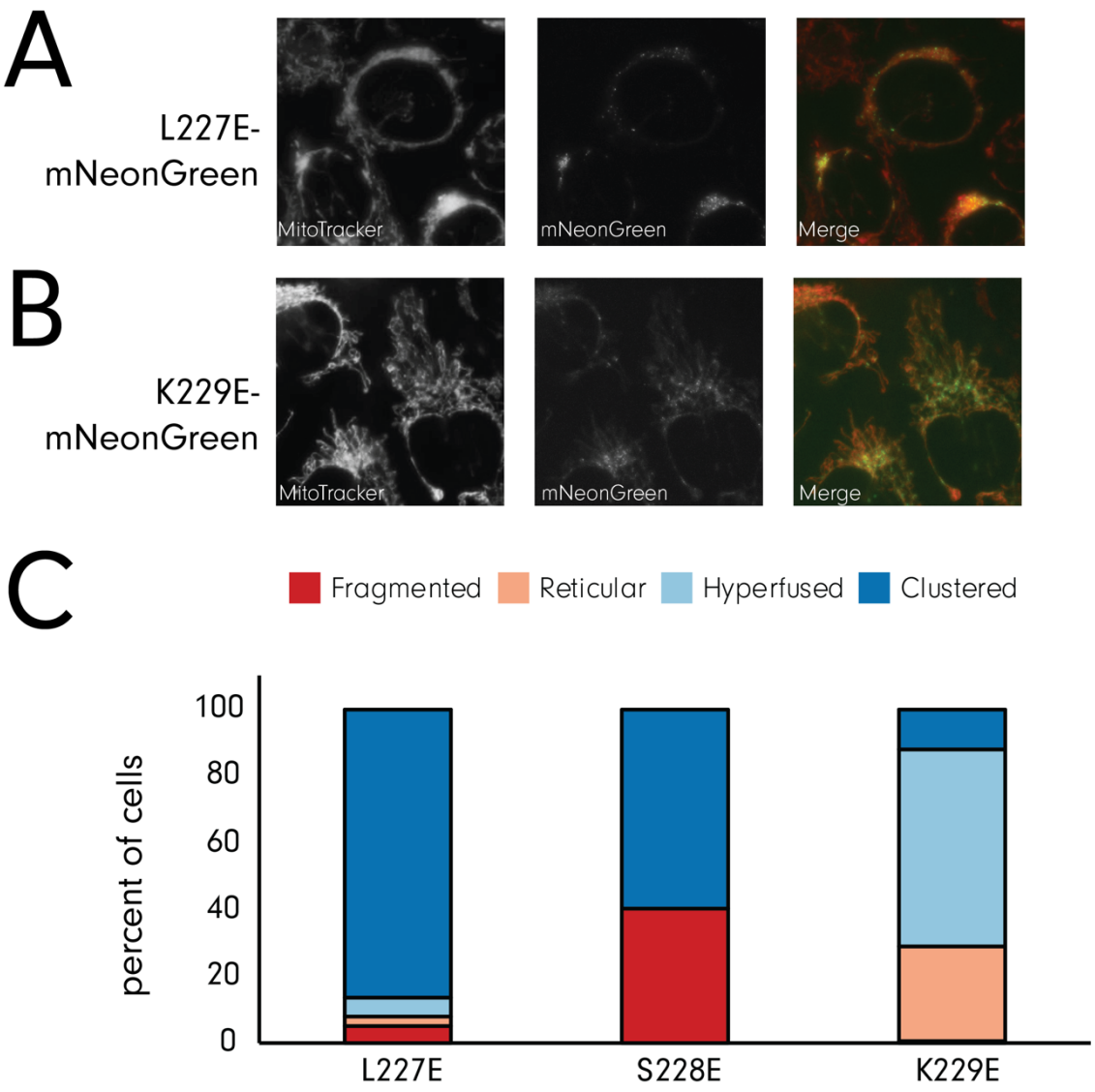

Figure 3.17. Mitochondrial morphology in 1KO MEFs expressing nearby CMT2A variants. Representative images of (A) Mfn1 L227E-mNeonGreen and (B) Mfn1 K229E-mNeonGreen expressed in 1KO MEFs. (C) Mitochondrial morphology was quantified, unblinded, in under 50 cells for L227E and over 100 cells in K229E.

Based on likely functional importance of this region, I predicted that Mfn1 S228 phosphorylation interfered with the stabilizing interactions between the GTPase domain and HB1 in the open conformation of the full-length protein (**Figure 3.1A**). Clash prediction based on van der Waals radii (UCSF Chimera) showed that the substitution of Mfn1 S228E is predicted to specifically interfere with the normal position of the H340 side chain in HB1. This residue is conserved in Mfn2, where it is associated with CMT2A variant H361Y (Feely et al., 2011; Verhoeven et al., 2006; Züchner et al., 2006). Characterization of cultured mouse neurons expressing Mfn2 H361Y suggest that mitochondria in these neurons are able to interact with the transport machinery but have significantly reduced mitochondrial motility, suggesting that substitutions in this region may affect mitochondrial transport (Misko et al., 2010). To test if large substitutions in this region contribute to the mitochondrial morphology in cells, I expressed Mfn1 H340Y-mNeonGreen in 1KO MEFs. In a single, preliminary experiment, mitochondria appeared to be primarily clustered or hyperfused, consistent with the importance of this region in Mfn1 function (**Figure 3.18, Table 3.3**). This suggests that defective mitochondrial transport could be a common phenotype between Mfn1 H340Y and S228E mutants.

Alternatively, based on the orientation of Mfn1 S228 in the closed conformation of the full-length protein (**Figure 3.1B**), phosphorylation at this site might impair or stabilize the closed conformation during the final steps of membrane fusion. Interestingly, structural predictions of full-length Mfn1 suggest that the side chain of S228 faces the side chain of T562, an annotated Mfn1 phosphorylation site (Pyakurel et al., 2015). The authors suggested that Mfn1 phosphorylation at T562 inhibited Mfn1 assembly and stimulates mitochondrial fragmentation, although they did not describe the mitochondrial morphology in MEFs expressing the phosphomimetic and blocking substitutions at

Mfn1 T562. In order to determine if Mfn1 S228E has a similar mitochondrial morphology to large substitutions at T562, I expressed several Mfn1 T562-mNeonGreen variants in 1KO MEFs. While there were a range of mitochondrial morphologies observed, the strongest effect appeared to be mitochondrial clustering in slightly under half of 1KO MEFs expressing Mfn1 T562E, and to a lesser extent in cells expressing Mfn1 T562D. Expression of Mfn1 T562A and T562K in 1KO MEFs mainly rescued mitochondrial morphology (**Figure 3.18, Table 3.3**).

Previous characterization of Mfn1 T562 shows that phosphorylation at this site is associated with reduced fusion activity, increased BAK oligomerization and apoptosis. If the mitochondrial phenotype in 1KO MEFs expressing Mfn1 T562D/E is repeatably similar to that of 1KO MEFs expressing Mfn1 S228E, this could indicate that both phosphorylations inhibit fusion activity. Alternatively, it remains possible that Mfn1 T562 phosphorylation operates under a distinct mechanism from that of Mfn1 S228 phosphorylation. Expression of Mfn1 T562K did not cluster mitochondria, suggesting that the negative charge at Mfn1 T562 might be specifically important for its function, such as mediating protein-protein interactions or promoting additional PTMs. Further comparisons between Mfn1 S228E and T562E could provide insight as to whether the phenotype in cells expressing Mfn1 S228E is mediated by conformational differences around Hinge 1 or 2.

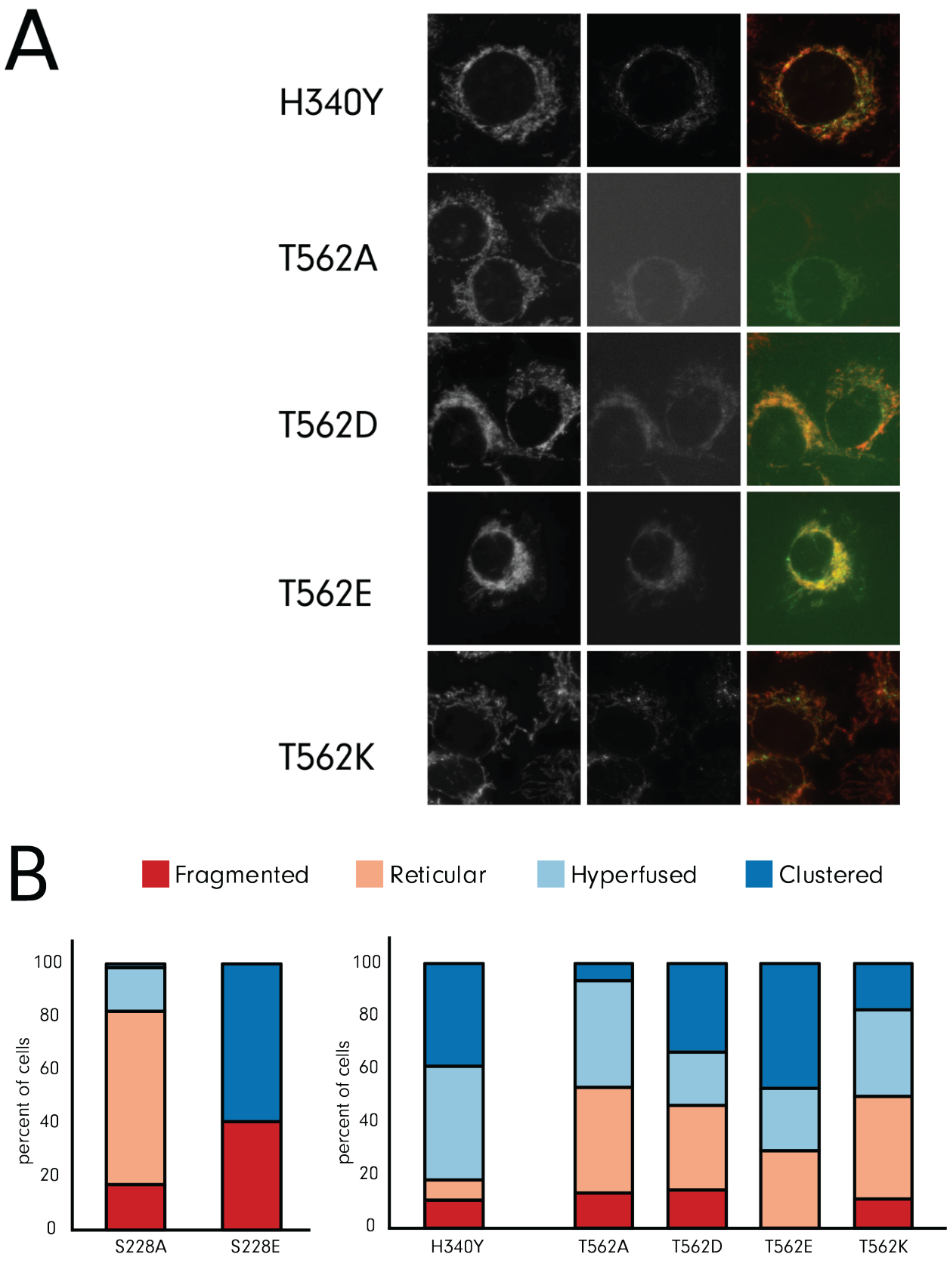
A
H340Y
T562A
T562D
T562E
T562K
B
Fragmented
Reticular
Hyperfused
Clustered
percent of cells
100
80
60
40
20
0
S228A
S228E
H340Y
T562A
T562D
T562E
T562K

Figure 3.18. Mitochondrial morphology in 1KO MEFs expressing HB1 and HB2 variants. (A) Representative images and (B) morphology quantification from one experiment in 1KO MEFs expressing mNeonGreen-tagged versions of H340Y (n=93 cells), T562A (n=30 cells), T562D (n=149 cells), T562E (n=34), and T562K (n=108).

Position (Mfn1)	Substitution	Tag	Mitochondrial morphology (1KO MEFs)	Position (Mfn2)	CMT2A-associated mutations
NO Mfn1			No rescue; mostly fragmented		
WT Mfn1			Complete rescue; mostly reticular		
S228	A	FLAG	Moderate rescue	Mfn2 S249	S249F
		mNeonGreen	Complete rescue		
	D	FLAG	Moderate rescue		
	E	FLAG	Signficant perinuclear clustering		
		mNeonGreen	Signficant perinuclear clustering		
	K	FLAG	Moderate perinuclear clustering		
		mNeonGreen	Signficant perinuclear clustering		
	T	FLAG	Moderate rescue but highly variable		
L227	E	mNeonGreen	Mostly clustered	Mfn2 L248	L248V
K229	E	mNeonGreen	Mostly hyperfused	Mfn2 R250	R250Q, R250W
H340	Y	mNeonGreen	Moderate perinuclear clustering	Mfn2 H361	H361Y
T562	A	mNeonGreen	Moderate hyperfusion		
	D	mNeonGreen	Moderate perinuclear clustering		
	E	mNeonGreen	Moderate perinuclear clustering		
	K	mNeonGreen	Moderate hyperfusion		

Table 3.3. Summary of mitochondrial morphology across Mfn1 variants. This table also indicates which variants were tested with which tag, conservation in Mfn2 and associated CMT2A variants, all of which are discussed in more detail throughout the main text.

Characterizing mitochondrial clusters in 1KO MEFs expressing Mfn1 S228E

It is not clear if mitochondrial clusters represent a change in mitochondrial fusion and/or transport activity. One explanation for the mitochondrial clustering observed in MEFs expressing Mfn1 S228E is that mitochondrial transport to the cell periphery is defective. Mitochondria in cells are moved along microtubules by the molecular motors, dynein and kinesin (Pilling et al., 2006; Schwarz, 2013). Dynein is responsible for mitochondrial transport toward the nucleus, while kinesin brings mitochondria to the cellular periphery. The mitochondrial outer membrane protein Miro is linked to molecular motors on microtubules through the adaptor proteins TRAK1/2 (Fransson et al., 2006; Glater et al., 2006). During the cell cycle, dynein and kinesin release from mitochondria, allowing for proper mitochondrial distribution and inheritance (Chung et al., 2016). Because MEFs expressing Mfn1 S228E had mitochondria that were clustered around the nucleus, I hypothesized that clustered mitochondrial structures resulted from overactive dynein-mediated transport or reduced kinesin-mediated transport.

First, I evaluated whether the molecular machinery required to transport mitochondria was found on mitochondria isolated from 1KO MEFs expressing Mfn1 S228E-FLAG. In two separate experiments, mitochondria isolated from 1KO + Mfn1 S228E-FLAG cells contained dynein, kinesin, Miro and TRAK (**Figure 3.19**). There did not appear to be obvious, repeatable, quantitative differences between wild type and mutant cells. Although all proteins were found on mitochondria in approximately normal levels, it is still possible that motors are defective. Other work in the lab is aimed at developing and applying better tools to understand mitochondrial distribution after motor inhibition. This work should also emphasize differences in mitochondrial transport in neurons, as well as fibroblasts.

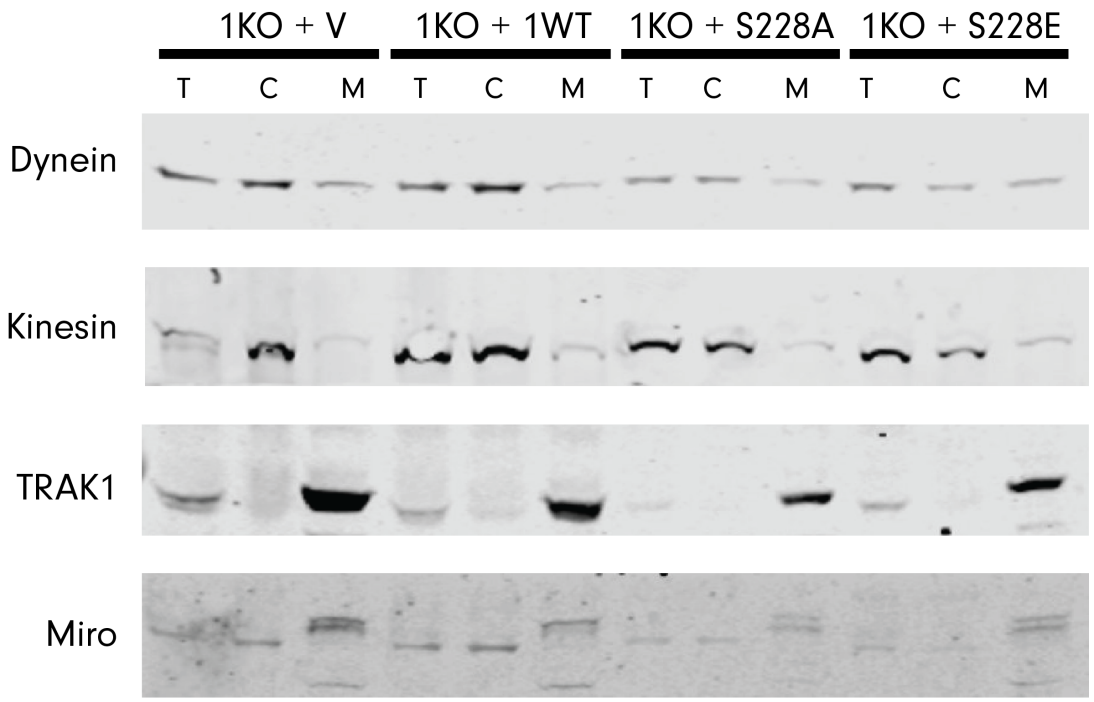

Figure 3.19. Recruitment of transport proteins to mitochondria in 1KO MEFs expressing Mfn1-FLAG. Mitochondrial and cytosolic fractions were isolated from 1KO MEFs expressing an empty vector, wild type Mfn1, Mfn1 S228A or Mfn1 S228E. Western blots of mitochondrial (M) and cytosolic (C) fractions, as well as total cell lysate (T) were probed for dynein, kinesin, TRAK1 or Miro.

Mitochondrial clusters in 1KO MEFs expressing Mfn1 S228E appear to be held together by microtubules (**Figure 3.6**) and able to recruit the fundamental transport machinery to the mitochondria (**Figure 3.19**). If active transport processes are indeed holding mitochondrial clusters together, I reasoned that changes in mitochondrial shape might be observed during the cell cycle, when both mitochondria and microtubules undergo dramatic remodeling events. To determine if

the mitochondria in perinuclear clusters persist throughout the cell cycle, I used low-serum media to synchronize 1KO MEFs expressing Mfn1 S228E-mNeonGreen.

While I have not yet been able to reliably capture synchronized MEF populations at later stages in the cell cycle, I was able to characterize mitochondrial morphology at the G1/S transition. Arrested cells were released in either normal media (serum release) for 18hr or the reversible DNA replication inhibitor, aphidicolin for 10-14hr, the proportion of cells with clustered mitochondria significantly decreased (**Figure 3.20**). During this stage of the cell cycle, wild type mitochondria are highly connected in order to produce sufficient energy for the subsequent stages of growth and division **(Mitra et al., 2009)**. While almost 60% of 1KO MEFs expressing Mfn1 S228E-mNeonGreen have clustered mitochondria at baseline, less than 15% of cells have clustered mitochondria at this stage in the cell cycle (**Figure 3.20**).

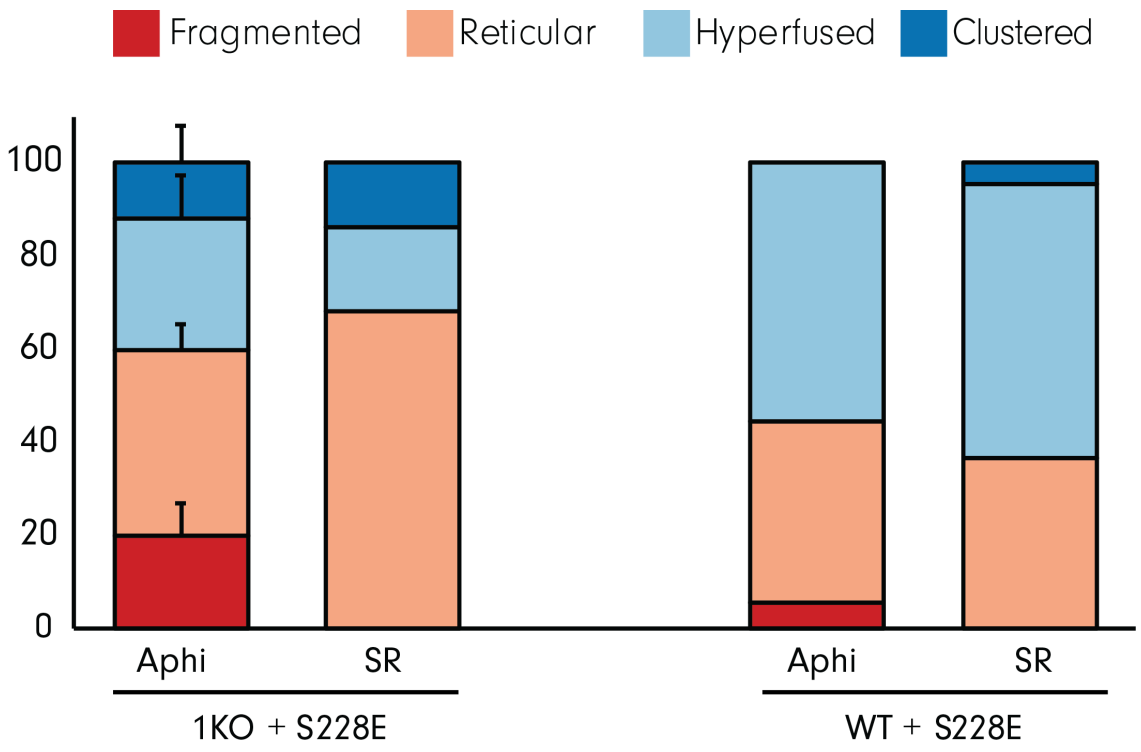

Figure 3.20. G1/S morphology of 1KO and WT MEFs expressing Mfn1 S228E-mNeonGreen. Mitochondrial morphology was measured in cells at the G1/S transition, as established by either aphidicolin treatment (Aphi) or serum release (SR). Morphology was measured on two independent occasions for 1KO + S228E (Aphidocolin), while all other conditions represent one replicate, n<50 cells counted per condition.

Preliminary data in 1KO and WT MEFs expressing Mfn1 S228E-mNeonGreen (**Figure 3.20**) suggests that mitochondria within these clusters may still undergo regulated changes. To substantiate these preliminary observations in clonal populations with the appropriate controls, I next screened mitochondrial morphology during G1/S in clonal populations of 1KO MEFs that express Mfn1 S228A-FLAG and S228E-FLAG. The mitochondrial morphology in 1KO MEFs expressing Mfn1 S228A was extremely variable but did exhibit larger populations of both fragmented and clustered mitochondria compared to wild type Mfn1. Mitochondrial clustering in 1KO MEFs expressing Mfn1 S228E-FLAG, however, decreased by about half during the G1/S transition (**Figure 3.21**). While around twice as many mitochondria remain clustered in the Mfn1 FLAG vs. mNeonGreen-expressing cells, the loss of mitochondrial clusters during the cell cycle in both cases suggests that mitochondrial shape and distribution in 1KO MEFs expressing Mfn1 S228E can be regulated and likely do not represent a nonfunctional endpoint structure. These experiments should be repeated with both Mfn1 tags to better understand how small differences at the C-terminal portion of the protein can affect mitochondrial distribution.

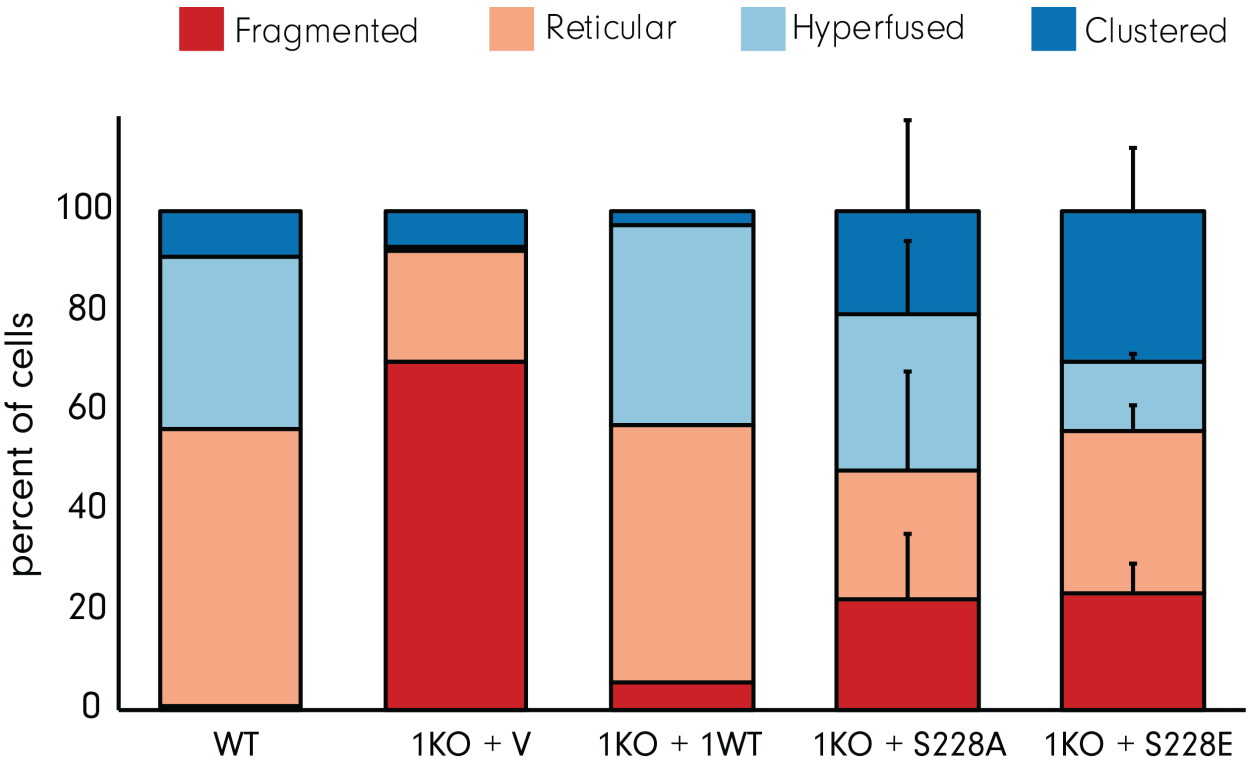

Figure 3.21. G1/S morphology of 1KO MEFs expressing Mfn1 S228A or S228E-FLAG. In a single, blinded experiment, at least 90* (except A15, n=60; E17, n=87) cells were counted. Error bars represent the standard deviation between two clonal populations.

Because mitochondria undergo similar changes in shape during the G1/S transition and SIMH, I also measured mitochondrial morphology after four hours of starvation or cycloheximide (CHX) treatment in 1KO MEFs expressing Mfn1 S228A or Mfn1 S228E-mNeonGreen and WT MEFs expressing Mfn1 S228E-mNeonGreen. In response to CHX treatment, 1KO MEFs expressing Mfn1 S228A underwent robust hyperfusion. 1KO and WT MEFs expressing Mfn1 S228E remained primarily clustered (**Figure 3.22**). In contrast, clusters were decreased by about half in both WT and 1KO MEFs expressing Mfn1 S228E after starvation but not CHX. Surprisingly, mitochondria in 1KO MEFs

expressing Mfn1 S228A-mNeonGreen did not become significantly hyperfused during starvation but did hyperfuse dramatically after CHX treatment. These results should be repeated alongside wild type controls to determine if the mitochondrial phenotype in 1KO MEFs expressing S228A represents a defect in starvation-induced SIMH or an overall, less dramatic effect of starvation on inducing hyperfusion relative to CHX. If Mfn1 S228A can repeatably inhibit SIMH, this would suggest that Mfn1 S228 phosphorylation might be involved in the mitochondrial hyperfusion observed after specific SIMH conditions. Future experiments should also determine if the persistence of mitochondrial clusters in depends on a common mechanism across SIMH and the cell cycle or if there are drug-specific differences.

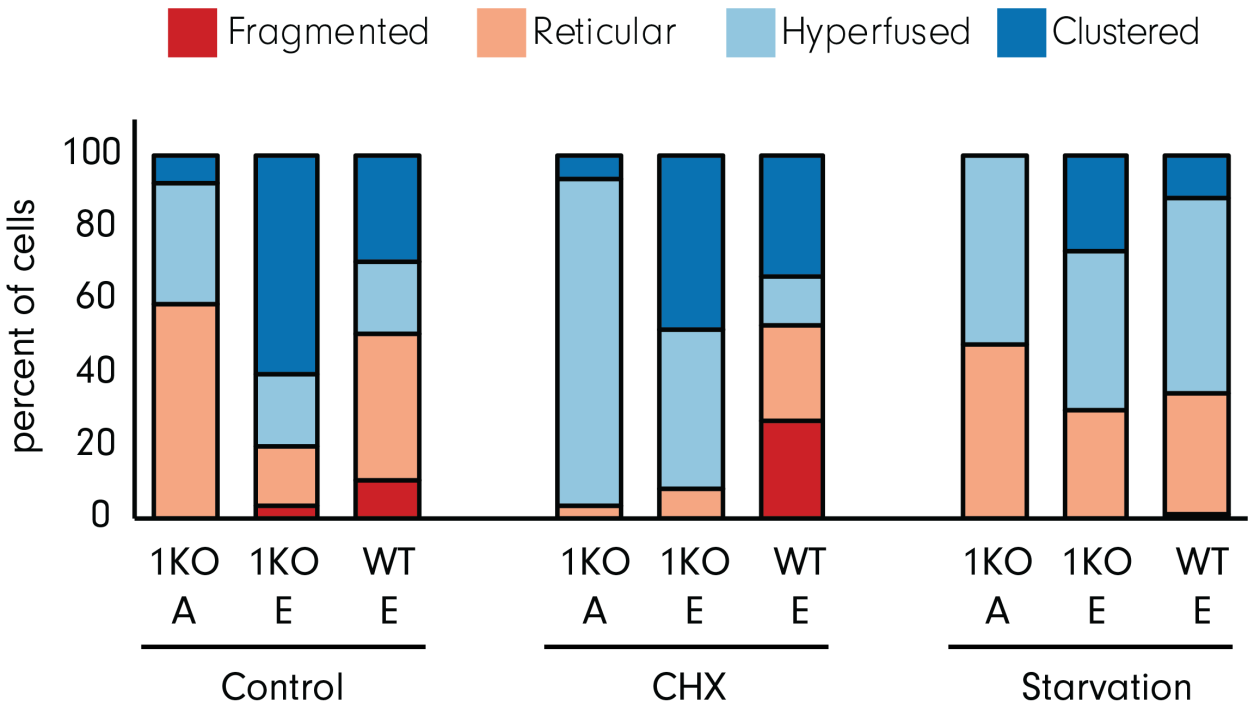

Figure 3.22. SIMH in 1KO MEFs expressing Mfn1 S228A-mNeonGreen and 1KO and WT MEFs expressing Mfn1 S228E-mNeonGreen. In a single, preliminary experiment, 1KO MEFs expressing Mfn1 S228A or Mfn1 S228E (n ~40 cells per condition) or WT MEFs expressing Mfn1 S228E (n~70

cells per condition) were stained with Mitotracker Red to visualize mitochondrial morphology. SIMH-treated cells were incubated with 10μM CHX or starved in HBSS for four hours before imaging.

Since fewer mitochondrial clusters were observed in cells expressing Mfn1-S228E with an mNeonGreen tag compared to a FLAG tag during the G1/S transition, I also verified the starvation-induced SIMH phenotype in clonal populations of 1KO MEFs expressing Mfn1 S228A-FLAG and S228E-FLAG. All experiments were performed and quantified blinded to sample identity and run alongside the appropriate wild type and knockout controls (**Figure 3.23**). As in G1/S, the unclustering phenotype was less obvious and highly variable in cells expressing Mfn1 S228E-FLAG compared to the equivalent substitution with an mNeonGreen tag (**Figure 3.23**). Further, the mitochondrial morphology was not repeatable in identical blinded experiments performed recently.

The variation in mitochondrial morphology between identical variants with different C-terminal tags in several experiments suggests that protein tags could have differential effects on mitofusin activity. Because the FLAG tag is smaller and experiments were performed in clonal populations of similar expression levels, these results seem more likely to mimic wild type mitofusin changes than those in the larger mNeonGreen. Further characterization of mitochondrial morphology throughout the cell cycle and SIMH response is required to determine possible mechanisms for changes in mitochondrial clustering.

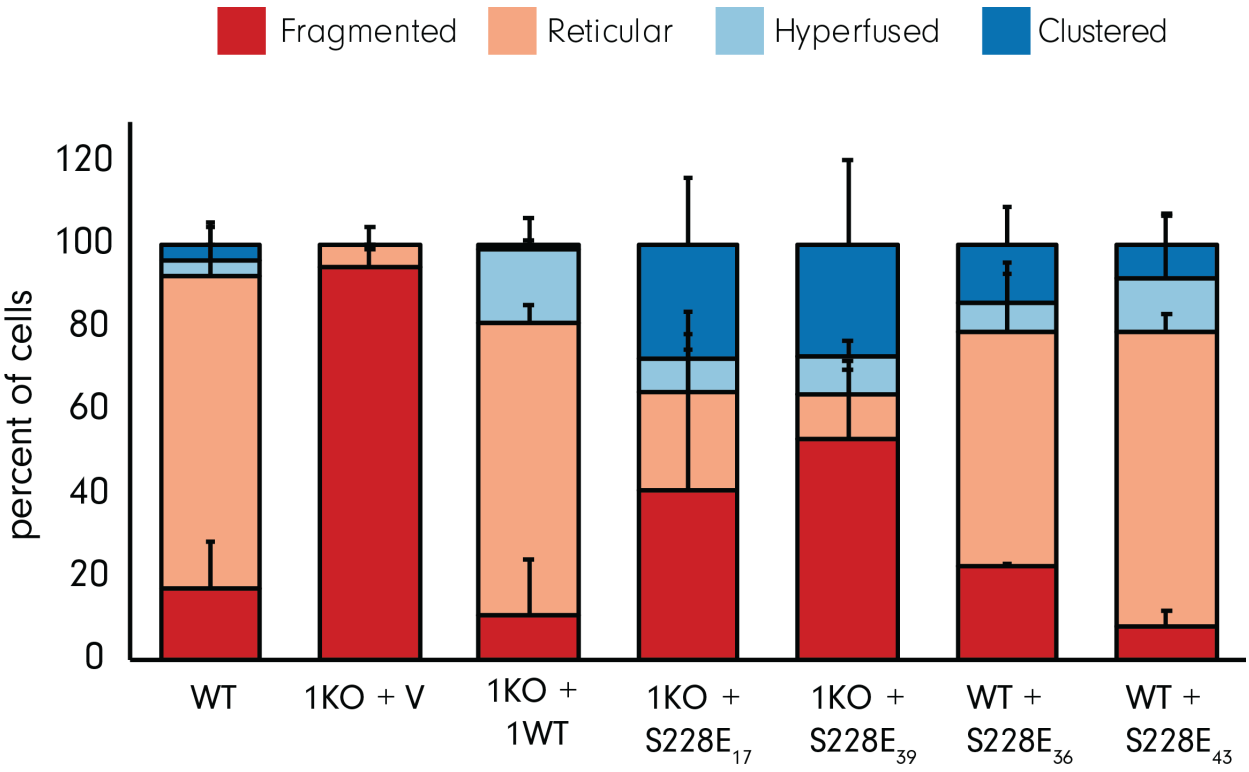

Figure 3.23. SIMH in 1KO and WT MEFs expressing Mfn1 S228E- FLAG. In two blinded replicates, at least 100 cells were counted. Error bars represent the standard deviation between replicates.

While mitofusin overexpression is known to cause mitochondrial clustering around the nucleus, our experimental system ensures that we do not overexpress mitofusins, making that an unlikely explanation of the clustering observed here. Mitochondrial aggregation is also associated with the defective proteasomal turnover of ubiquitinated proteins, which causes increased autophagy and mitochondrial accumulation in the perinuclear space (Narendra et al., 2010; 2008). A single, preliminary visualization of lysosomes in 1KO MEFs expressing Mfn1 S228E-FLAG, however, did not show a significantly different lysosomal distribution between WT Mfn1 and Mfn1 S228E. Additional

work to measure autophagic flux or autophagasome localization should be performed to clarify 1KO cells expressing S228E have defective autophagy.

Ultimately, our lab hopes to understand how mitochondrial clustering occurs and what it reveals about normal fusion and transport activity. For the purposes of this project, however, I will not full explore this question but do expect future research in the lab will address this in more depth, across mitofusin variants.

Additional cellular characteristics of Mfn1 S228E mitochondria

Because of the unusual mitochondrial clustering, I also visualized the mitochondrial ultrastructure using electron microscopy (EM). While I expected to identify the characteristics of mitochondria within clusters, I was unable to detect mitochondrial clusters in two clonal populations of 1KO MEFs expressing Mfn1 S228E-FLAG. The apparent disappearance of mitochondrial clusters in EM images was suprising but not unique to cells expressing Mfn1 S228E. Similar findings were reported for another Mfn1 GTPase domain variant, F202L, that also had perinuclear clusters that were primarily detectable by fluorescence microscopy instead of EM. Despite no obvious clustering, a distinguishing feature of the mitochondria in 1KO MEFs expressing Mfn1 S228E was significant inner membrane swelling and deformities (**Figure 3.24**). Swollen mitochondrial matrices and abnormal cristae organization are frequently associated with mitochondrial dysfunction (Zick et al., 2009). This would suggest that Mfn1 S228E alters mitochondrial respiration and inner membrane morphology. To directly measure this, future experiments could directly measure oxygen consumption in MEFs expressing different Mfn1 mutations.

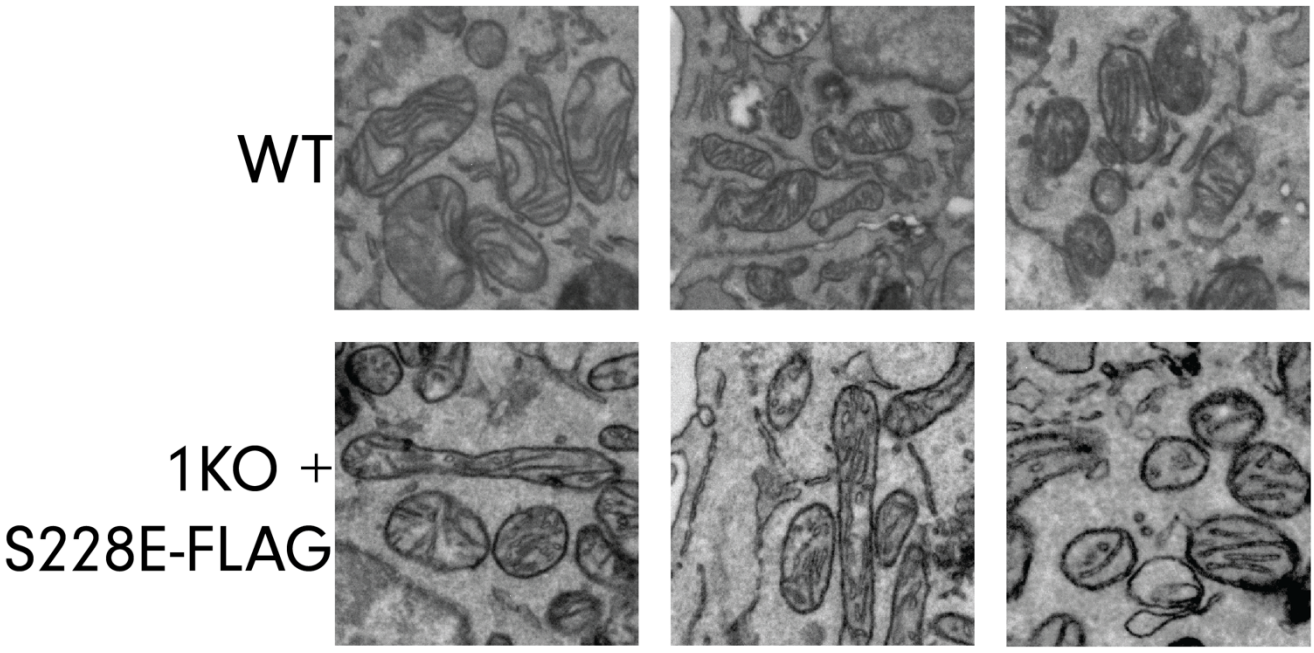

Figure 3.24: Mitochondrial ultrastructure in 1KO MEFs expressing WT Mfn1 or Mfn1 S228-FLAG. 1KO MEFs expressing Mfn1 WT-FLAG (top) or Mfn1 S228E-FLAG (bottom) were fixed and imaged using transmission electron microscopy. Thirty images were taken per condition, and two clonal populations of 1KO MEFs expressing Mfn1 S228E were tested.

The abnormal cristae structure in 1KO MEFs expressing Mfn1 S228E mutants could result from abnormal inner membrane fusion or cristae remodeling, which are mediated by the dynamin-related protein Opa1 (Frezza et al., 2006; Glytsou et al., 2016). I measured Opa1 processing by western blot in wild type and mutant cells and did not see any significant difference in processing between wild type Mfn1 and Mfn1 S228E (**Figure 3.25**). The relative levels of long and short Opa1 isoforms varied significantly across experimental replicates, obscuring the detection of any subtle differences in Opa1 processing by this method.

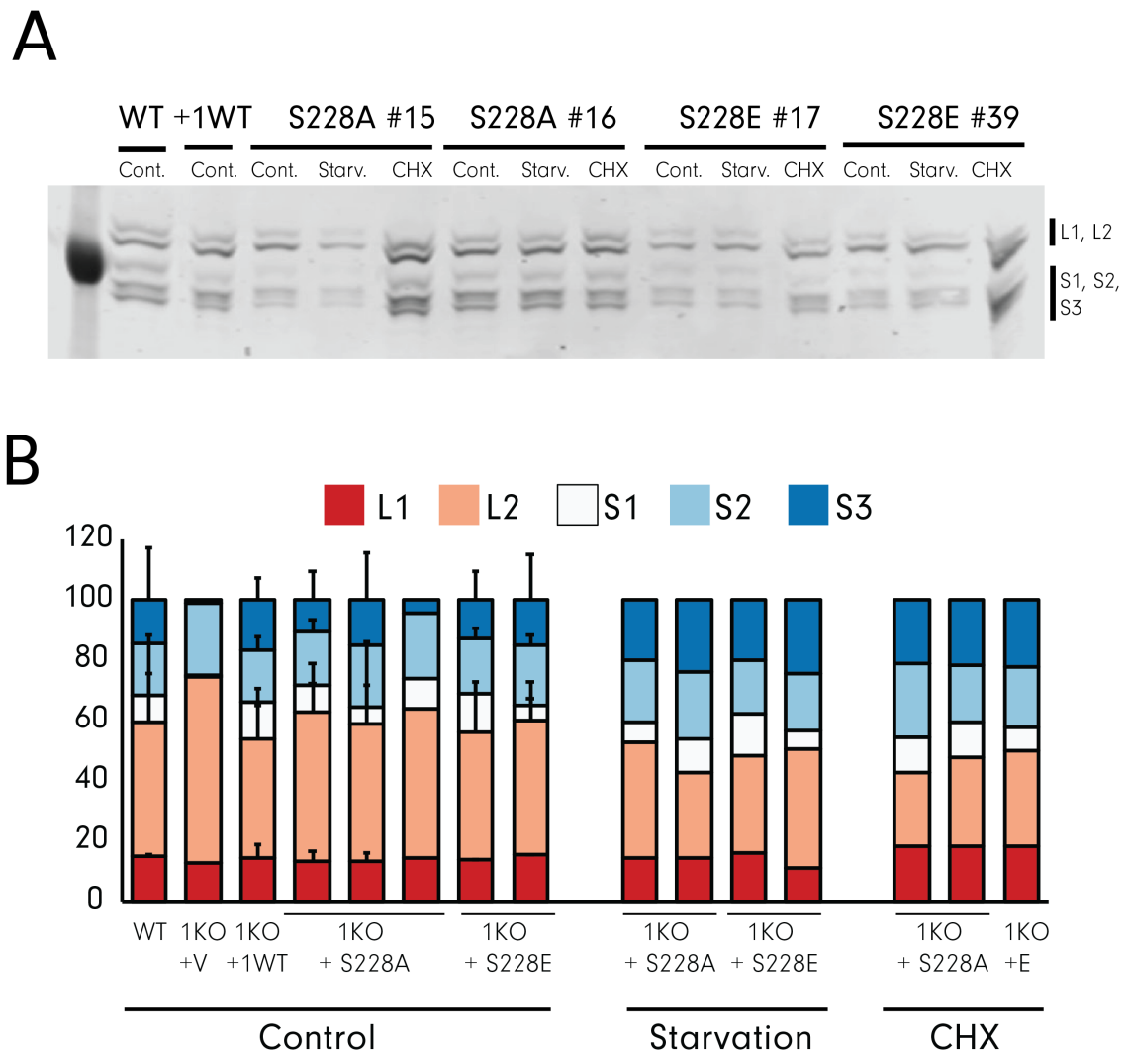

Figure 3.25. Opa1 processing at baseline and during SIMH in 1KO MEFs expressing Mfn1 S228A/E-FLAG. SIMH was induced by either 4hr. of starvation in HBSS or 4hr. 10μM CHX treatment. Cells lysates were collected from WT MEFs or 1KO MEFs transduced with an empty vector, WT Mfn1, Mfn1 S228A and Mfn1 S228E. Two long (L1, L2) and three short (S1, S2, S3) forms of Opa1 were identified by western blot and quantified in (B). Baseline processing was repeated in two experiments (error bars = standard deviation between days), while SIMH was done on one occasion.

Rather than resulting from dysfunctional inner membrane dynamics, it is possible that the abnormal structures observed by EM resulted from mitochondrial damage and membrane swelling due to fixation. This seems somewhat less likely because this abnormal morphology was less prevalent in 1KO MEFs expressing Mfn1 WT. However, if cells expressing Mfn1 S228E are slightly more susceptible to stress, a harsh fixation may have a more dramatic on them than controls. If this experiment is repeated in the future, an alternative fixative should be tried in parallel to ensure that any morphological defects observed are due to the indicated substitutions and not sample preparation.

Biochemical characterization of Mfn1 S228.

One explanation for the highly connected mitochondrial network in 1KO MEFs expressing Mfn1 S228E is that the Mfn1 S228E substitution increases Mfn1-mediated fusion activity. Alternatively, increased retrograde mitochondrial transport might be a mechanism to concentrate mitochondria with low fusion activity around the nucleus, increasing the probability of successful fusion events. To more directly assess how phosphorylation of Mfn1 S228 alters mitofusin activity, I biochemically characterized Mfn1 S228A and S228E in the Mfn1 MGD construct and full-length protein. Together, this analysis revealed that Mfn1 S228E had reduced levels of mitochondrial fusion, which was associated with reduced interactions with Mfn1 in *trans* (**Figure 3.31**). and a loss of nucleotide-dependent assembly (**Figure 3.32**). These data are consistent with a model in which aberrant transport activity, rather than increased Mfn1 activity, drives the increased mitochondrial fusion that we observe in cells.

In vitro fusion

I utilized an *in vitro* mitochondrial fusion assay to understand the effect of Mfn1 S228E substitution on the fusion activity of Mfn1 **(Hoppins et al., 2011)**. Using this approach, I was able to directly measure the ability of the mitofusins to fuse membranes in the absence of additional cellular cofactors, such as the transport machinery or modifying cytosolic proteins. Mitochondria from wild type MEFs and 1KO MEFs expressing an empty vector, S228A or S228E were labeled with either a matrix-targeted RFP or CFP fluorophore and isolated to measure *in vitro* fusion activity. Fusion reactions consisted of 12.5µg each of RFP and CFP-labeled mitochondria, which were incubated in the presence of either GTP or GTP and cytosol, which has been previously shown to stimulate fusion activity **(Hoppins et al., 2011)**. Fusion reactions were imaged by fluorescence microscopy and quantified by calculating the proportion of mitochondria in which the red and blue fluorophores were colocalized in three dimensions.

Compared to wild type cells, 1KO MEFs expressing an empty vector had significantly reduced but measurable fusion activity due to Mfn2-mediated fusion (**Figure 3.26, gray bar**). Mitochondria isolated from 1KO + S228A MEFs had near-wild type levels of *in vitro* fusion activity (**Figure 3.26, gray bar**), consistent with the significant but not total rescue of mitochondrial morphology in these cells. Surprisingly, mitochondria isolated from 1KO + S228E MEFs had similar fusion activity to 1KO cells, suggesting that Mfn1 S228E mutants cannot fuse mitochondria *in vitro* (**Figure 3.26, gray bar**). In the in vitro fusion assay, incubation of mitochondria supplemented with cytosol stimulates fusion around 20%, suggesting that proteins in the cytosol can stimulate mitofusin activity (**Figure 3.26, black bar**). To understand if cytosolic stimulation was sufficient to restore fusion activity in mitochondria expressing Mfn1 S228E, I measured *in vitro* mitochondrial fusion in mitochondria from

1KO MEFs expressing Mfn1 S228E and one isolate of Mfn1 S228A. Cytosol was able to stimulate fusion to a similar extent across all reactions except one isolate of Mfn1 S228E (**Figure 3.26, black bar**). In both Mfn1 S228E isolates, however, cytosol was not able to restore wild type-like levels of fusion in mitochondria expressing S228E, suggesting a significant fusion defect in these mitochondria equivalent to complete loss of Mfn1. While this was especially surprising based on the highly connected mitochondrial morphology observed following the release of clusters with nocodazole, it would support a model in which altered transport and Mfn2-mediated fusion is the main driver of mitochondrial clustering.

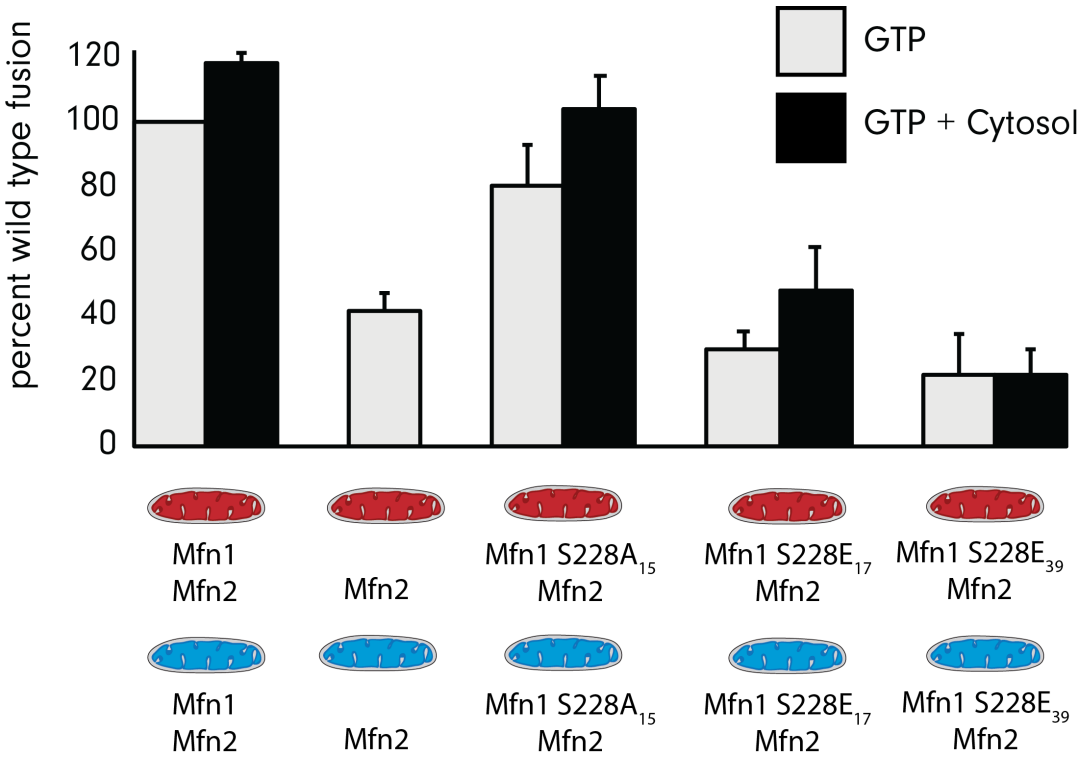

Figure 3.26. In vitro fusion of mitochondria from 1KO MEFs expressing Mfn1 S228A and S228E. Mitochondria were isolated from wild type cells ($Mfn1^{+/+}Mfn2^{+/+}$), a clonal population of 1KO cells transduced with an empty vector ($Mfn1^{-/-}Mfn2^{+/+}$), a clonal population of 1KO cells expressing Mfn1

S228A, and two clonal populations of 1KO cells expressing Mfn1 S228E. The indicated mitochondrial combinations were incubated under *in vitro* fusion conditions at 37C for 30 minutes.

Given the striking defect in mitochondrial fusion observed in 1KO MEFs expressing Mfn1 S228E, I next wanted to evaluate if this was a dominant variant that interfered with the fusion activity of wild type Mfn1. When wild type Mfn1 and Mfn2 are present on the opposite mitochondria, fusion of mitochondria expressing Mfn1 S228A reached wild type levels, and fusion in mitochondria expressing Mfn1 S228E significantly increased (**Figure 3.27, gray bar**). This near-wild type fusion activity can most likely be attributed to interactions between WT Mfn2 on mutant mitochondria with WT Mfn1 on the opposing membrane, which is the main complex driving outer membrane fusion. This also suggests that the Mfn1 S228E substitution does not interfere with the ability of wild type mitofusins to interact. Future *in vitro* fusion reactions could test this by measuring fusion in mitochondria isolated from wild type cells expressing Mfn1 S228E.

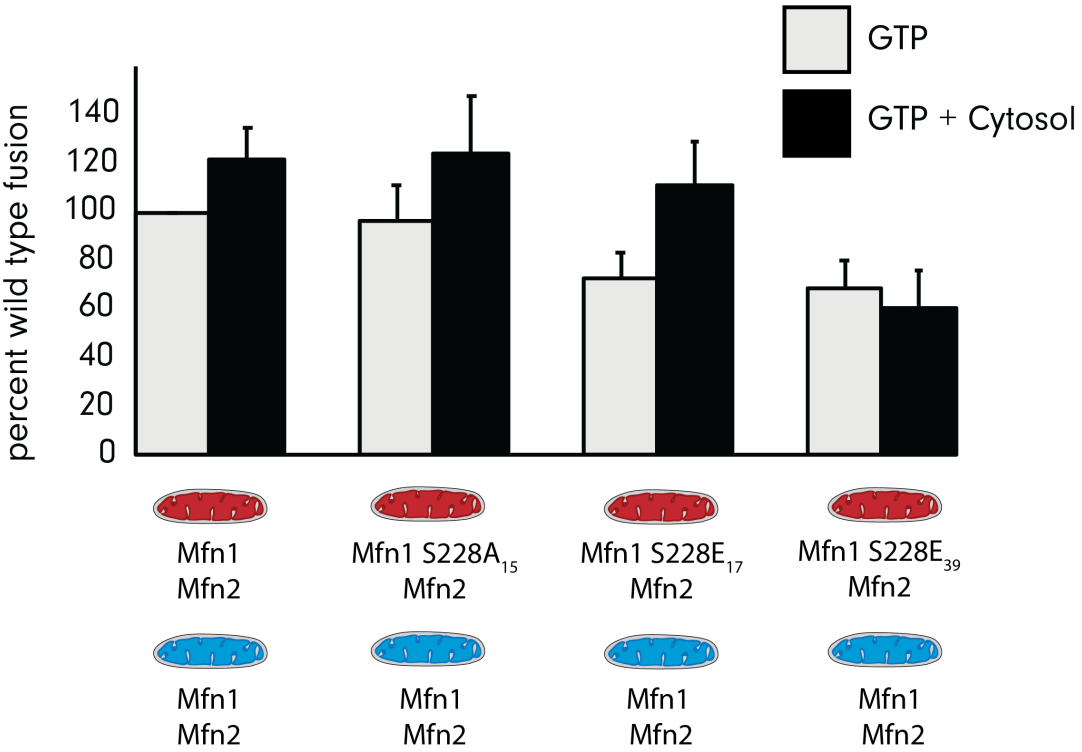

Figure 3.27. In vitro fusion of Mfn1 S228A and S228E mutants in 1KO background. Mitochondria were isolated from wild type cells ($Mfn1^{+/+}Mfn2^{+/+}$), a clonal population of 1KO cells expressing Mfn1 S228A, and two clonal populations of 1KO cells expressing Mfn1 S228E. The indicated mitochondrial combinations were incubated under *in vitro* fusion conditions at 37C for 30 minutes.

GTPase activity

The significantly inhibited fusion activity of Mfn1 S228E mutants could be a consequence of dysfunction at multiple points in the fusion process- nucleotide binding or hydrolysis, membrane tethering, or protein assembly. To first understand the basic enzymatic properties of the protein, I purified the partial Mfn1 construct (MGD) as well as Mfn1 MGD with S228A and S228E substitutions. As previously reported, wild type Mfn1 MGD was able to hydrolyze GTP (Cao et al., 2017; Qi et al., 2016; Yan et al., 2018). Both Mfn1 S288A and S228E had comparable GTPase activity to the wild type protein (**Figure 3.28**), suggesting that both substitutions do not inhibit GTP binding and hydrolysis within the core enzymatic machinery. This is consistent with the positioning of Mfn1 S228 far from the dimerization interface and nucleotide binding region. Additionally, most reported mutants that block nucleotide binding or hydrolysis are unable to rescue mitochondrial fusion due to protein inactivity, leading to mitochondrial fragmentation that is clearly distinct from the phenotype that I observe in cells expressing Mfn1 S228E. Together, these data suggest impaired fusion activity by Mfn1 S228E is not because the enzyme is dysfunctional.

A

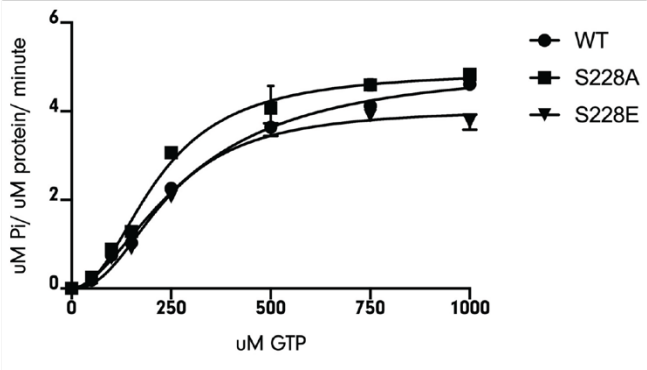

B

	WT	S228A	S228E
Vmax	5.039	4.907	4.056
h	1.771	2.181	2.345
K_m	293.4	215.6	239.1

Figure 3.28. GTPase activity of Mfn1 MGD with Mfn1 S228 substitutions. Kinetic analysis of GTP hydrolysis in wild type Mfn1 MGD and Mfn1 S228A/E MGD. (A) A representative kinetic plot fit to an allosteric sigmoidal equation is shown. (B) Kinetic parameters for Mfn1 MGD constructs tested.

Assembly of Mfn1 MGD

GTPase activity in Mfn1 S228E MGD suggested that Mfn1 S228E MGD could still form a G-G interface, as this is required for activity. To confirm this, I incubated WT, Mfn1 S228A and Mfn1 S228E MGD proteins with or without GDP.BeF3 and separated the proteins by size using sucrose gradient density centrifugation. All proteins showed a similar increase in size after GDP.BeF_3^- incubation, consistent with the size of a predicted dimer (**Figure 3.29A-B**). This was repeated independently for S228E on several occasions, suggesting that assembly of the G-G interface was unaffected in the MGD protein. These results were further confirmed by size exclusion chromatography (SEC) (**Figure 3.29C**).

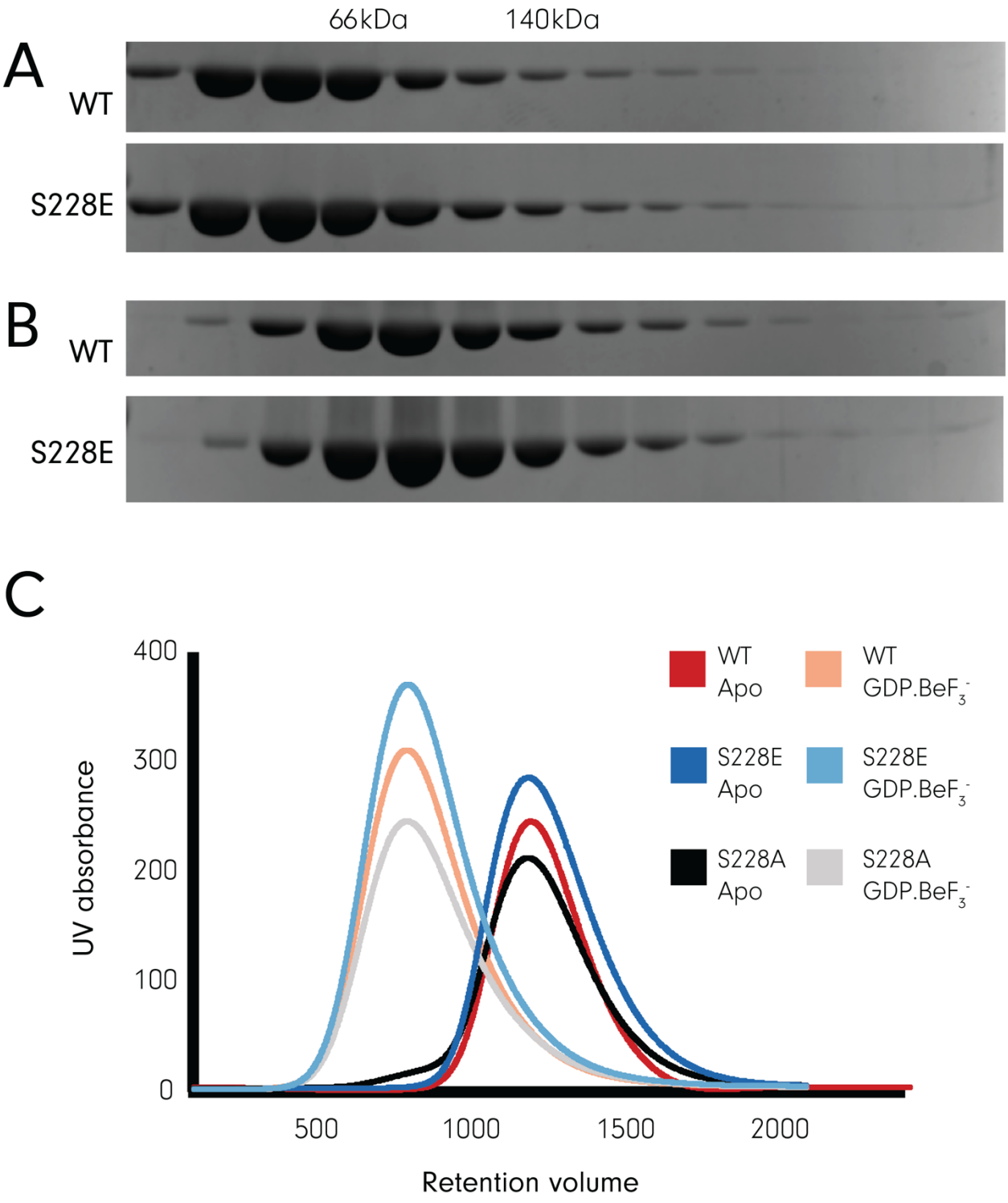

Figure 3.29. Sucrose gradients and SEC of Mfn1 MGD incubated with GDP.BeF3. (A) WT Mfn1 MGD or Mfn1 S228E-MGD were incubated in the absence of nucleotide (A) or presence of GDP.BeF_3-

(B) for 30min at 37C. Reactions were subjected to 5-20% continuous sucrose density gradient centrifugation. (C) The relative sizes of wild type, S228A and S228E Mfn1 MGD constructs were determined using size exclusion chromatography (SEC). Nucleotide incubation was performed as in B.

Because these assays cannot distinguish relative positions of the GTPase domain and HB1, it remains possible that the Mfn1 S228E construct has conformational differences between the GTPase domain and stalk domain that we cannot detect. If a further, more detailed characterization of the predicted conformational changes in this protein is required, another graduate student in the lab has been able to successfully crystallize a mutant variant of the MGD protein.

Trans mitochondrial interactions

Based on results in Mfn1 MGD, I predicted that full-length Mfn1 S228E was able to dimerize across the G-G interface. To directly test this, I isolated mitochondria from 1KO MEFs expressing Mfn1 WT (FLAG or GFP-tagged) and 1KO MEFs expressing Mfn1 S228E (FLAG or GFP-tagged) and incubated mitochondria from differentially-tagged populations with GDP.BeF3 to promote assembly across the G-G interface. FLAG-tagged Mfn1 was then immunoprecipitated, run on an SDS-PAGE gel and subjected to western blotting to detect Mfn1. The presence of two bands suggests that Mfn1-FLAG can interact with itself on the same membrane (lower band) or with Mfn1-GFP on another membrane (higher band). Without nucleotide, Mfn1 FLAG does not pull down any Mfn1 GFP. However, with the presence of the transition state mimic, GDP.BeF_3^-, Mfn1 does pull down a small amount of Mfn1 in *trans* (**Figure 3.30**).

Surprisingly, Mfn1 S228E-FLAG was unable to pull down Mfn1 S228E-mNeonGreen. From this, we can conclude that Mfn1 S228E cannot interact with itself across membranes and likely has defective tethering activity. There is also evidence that Mfn1 S228E also has impaired interactions with wild type Mfn1 in one clonal population of 1KO MEFs expressing S228E, although those experiments should be repeated to confirm this observation. Additional experiments are underway to determine if and how Mfn1 S228E affects the *trans* interaction between Mfn1 and Mfn2 which we expect to be important for fusion. A stronger understanding of the role of Mfn2 in the fusion process could also explain differences between in vitro fusion and mitochondrial morphology in cells expressing Mfn1 S228E.

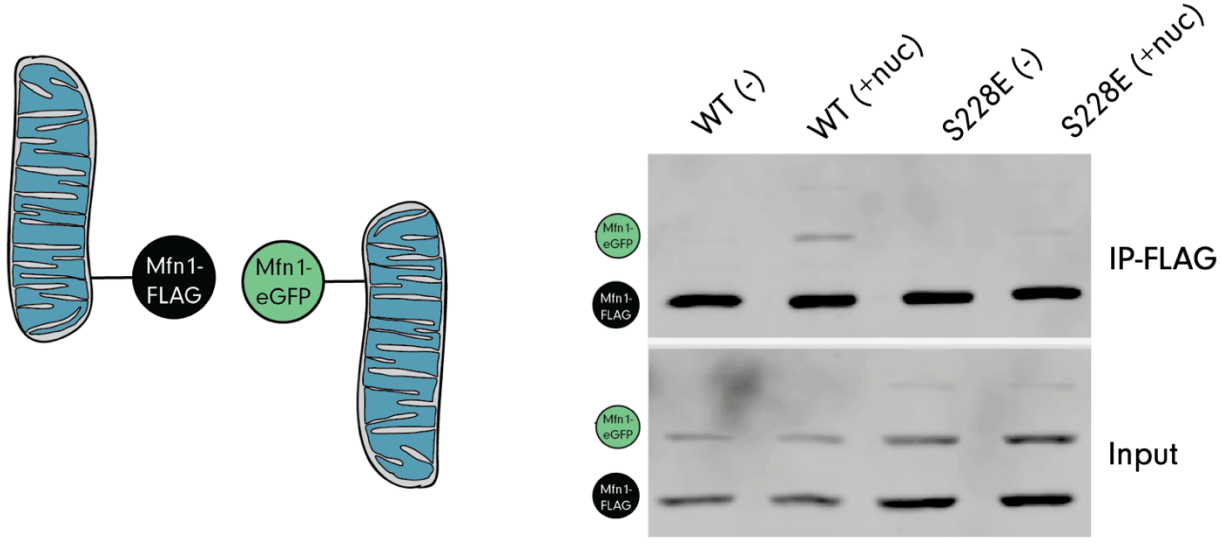

Figure 3.30. Interactions between Mfn1 S228E in trans. Mitochondria were isolated from clonal populations of 1KO MEFs expressing Mfn1 WT-FLAG, Mfn1 WT-eGFP, Mfn1 S228E-FLAG or Mfn1 S228E-eGFP and incubated with BeF3 in the presence or absence of GDP. Following lysis, immunoprecipitation was performed with α-FLAG magnetic beads. Proteins eluted from the beads were subjected to SDS-PAGE and immunoblotted with α-Mfn1. Arrowhead indicates the eGFP protein

eluted from FLAG beads. Experiment was repeated twice using two different clonal populations of MEFs expressing Mfn1 S228E.

Assembly of full-length Mfn1

Because this is inconsistent with the results in Mfn1 MGD, I next wanted to characterize native, full-length protein assembly in 1KO MEFs expressing S228E. While Mfn1 S228E does not directly affect the ability of the GTPase domain to bind and hydrolyze GTP, impaired Mfn1 trans interactions in 1KO MEFs expressing Mfn1 S228E suggest that Mfn1 nucleotide-dependent assembly is impaired compared to wild type Mfn1. Because there is not yet a way to rigorously measure the GTPase activity of cellular Mfn1, I used sucrose gradient density centrifugation to evaluate the assembly of Mfn1 following detergent solubilization of mitochondria isolated from 1KO MEFs expressing either Mfn1 WT (**Figure 3.31A**) or Mfn1 S228E (**Figure 3.31B)**. While Mfn1 S228E was indistinguishable from wild type Mfn1 in the apo state, assembly of Mfn1 S228E was not stimulated by incubation with $GDP.BeF_3^-$.

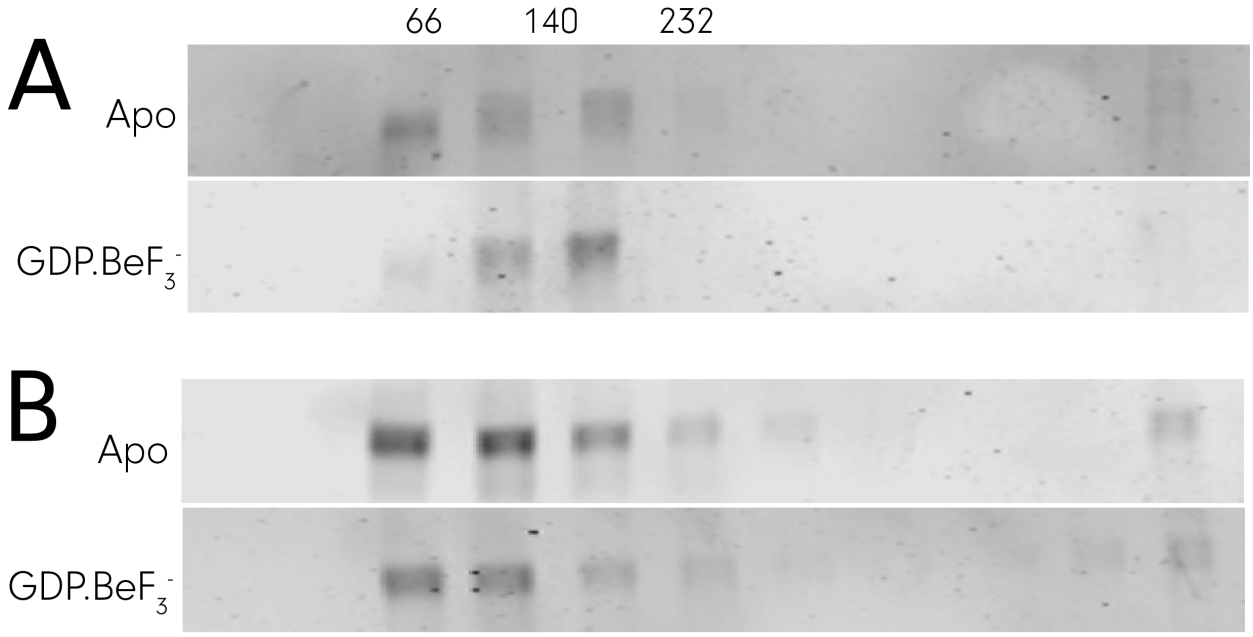

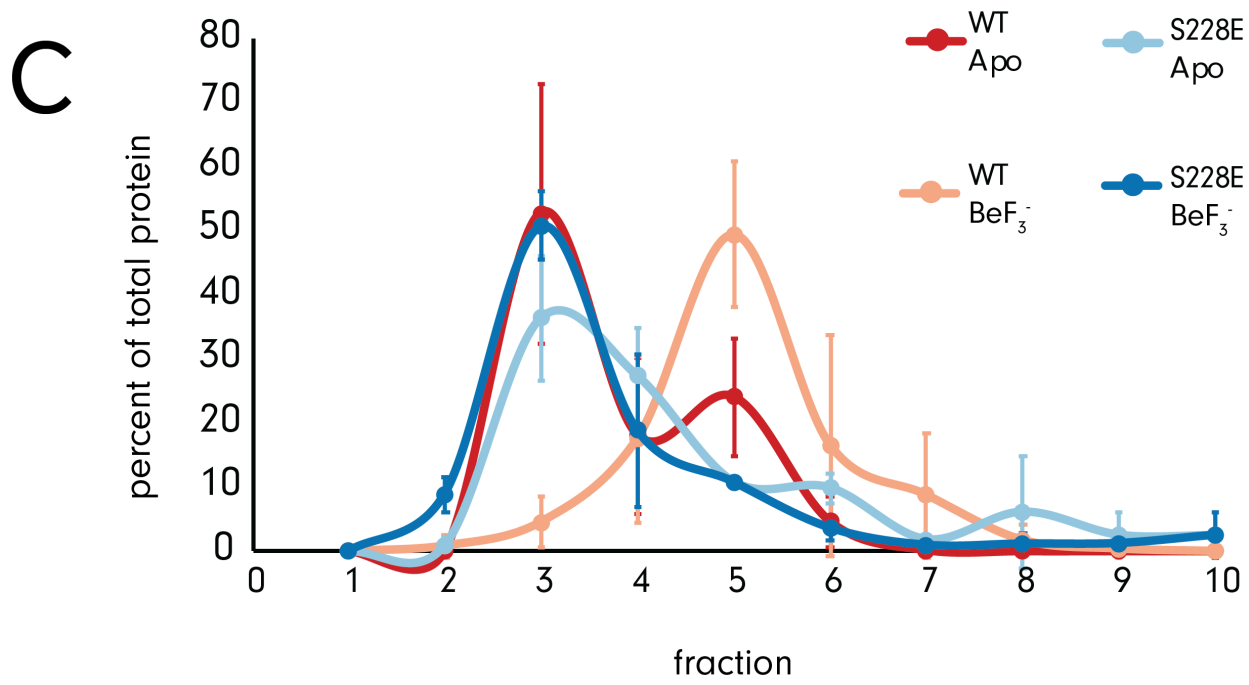

Figure 3.31. Sucrose gradients of full length Mfn1 from isolated mitochondria. (A) Mitochondria were isolated from 1KO MEFs expressing Mfn1 WT (A) or Mfn1 S228E (B). Mitochondria were incubated in the absence or presence of GDP.BeF_3- for 30min at 37C. Reactions were subjected to 5-20% continuous sucrose density gradient centrifugation. Bands around 66kDa are expected to represent monomeric Mfn1, while bands slightly larger than 140kDa are expected to represent dimeric Mfn1. (C) The distribution of protein through the sucrose gradient was quantified using densitometric analysis (ImageJ).

Blue native PAGE

To determine if the observations in sucrose gradients are consistent with the assembly of native Mfn1, I also evaluated assembly using blue native PAGE, which separates protein complexes based on their molecular weight and native protein structure. Based on previous BN-PAGE experiments in the lab, I expected that dimeric Mfn1 would assemble into larger structures after incubation with

GTP, the non-hydrolysable GTP analog- GMPPNP or the transition state mimetic, GDP.BeF_3^- (Engelhart and Hoppins, 2019; Sloat et al., 2019; Samanas et al., *in preparation*). In 1KO MEFs expressing WT Mfn1-FLAG, most of the protein exists as a species around 180kDA, consistent with a dimer (**Figure 3.32, straight line**). After incubation with GTP, protein shifts out of the dimer band and into higher order species around 320kDa (**Figure 3.32, double headed arrow**) and 450kDa (**Figure 3.32, single headed arrow**). A similar shift into higher-order species was observed after incubation with a nonhydrolyzable GTP analog, GMPPNP. In 1KO MEFs expressing Mfn1 S228A, protein assembly mostly mirrored wild type protein, with slightly less protein assembling into higher order species. Strikingly, expression of Mfn1 S228E in 1KO MEFs completely blocked the assembly of these higher order structures. Rather, Mfn1 S228E remained predominantly as a dimer. Additionally, a faint band was detected in between the predominant 320kDa and 450kDa bands, which was also present in low levels in wild type samples. It is not yet clear if this represents an assembly of a different size, formed as a transient intermediate during fusion, or if it represents one of the more common assemblies at an intermediate conformation.

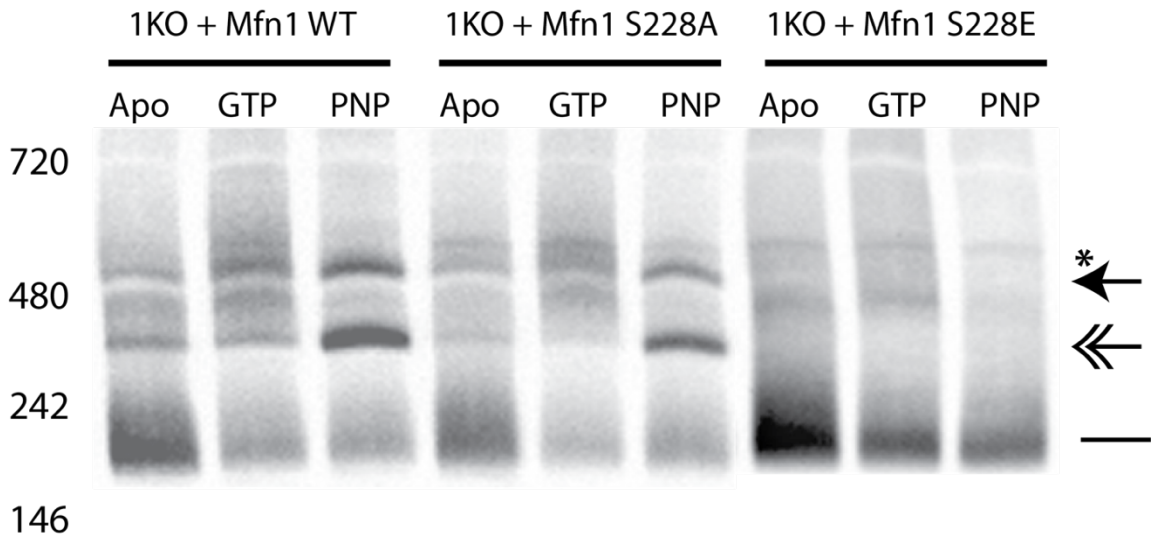

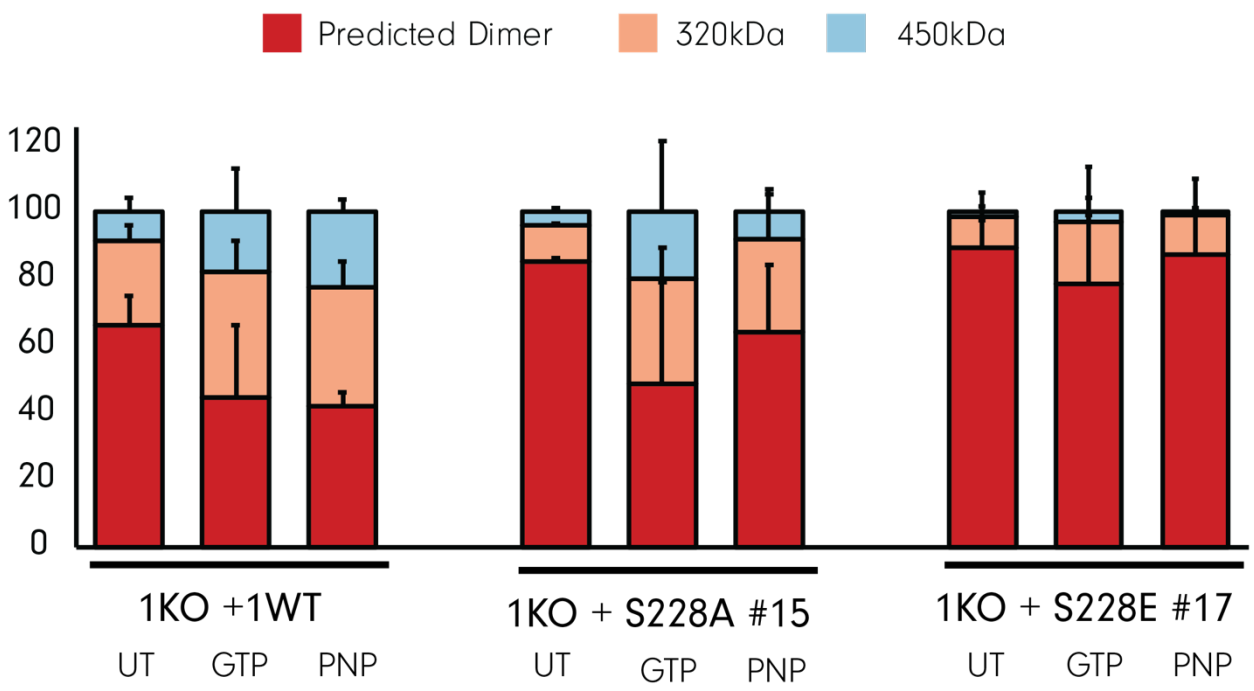

Figure 3.32. BN-PAGE of full length, native Mfn1 from isolated mitochondria. Mitochondria were isolated from clonal populations of 1KO MEFs expressing Mfn1 WT, Mfn1 S228A and Mfn1 S228E. Untreated mitochondria (UT) were incubated on ice for 30min while treated mitochondria were incubated with the specified nucleotide at 30C for 30min. Mitochondria were then lysed, subjected to BN-PAGE, and immunoblotted with an anti-FLAG antibody. Asterisk indicates a non-specific band from the anti-FLAG antibody. Protein complexes are indicated with lines/arrows as follows: predicted dimer (straight line), ~320kDa (double arrowhead), and ~450kDa (arrowhead). The distribution of protein is represented in the bar graph as mean + standard deviation of two independent experiments.

Together, the assembly data supports the hypothesis that Mfn1 S228E cannot undergo nucleotide-dependent assembly-stimulated hydrolysis, leading to decreased fusion activity. These results also highlight the importance of evaluating mitofusin function using both the MGD construct and full-

length protein. The MGD construct has provided detail structural information that allows us to test hypotheses about enzyme function and G-G interface formation. A complete assessment of protein oligomerization, however, must include an evaluation of assembly in the full-length protein.

Additional work to understand Mfn1 S228 should emphasize reconciling the biochemical fusion defects with apparent mitochondrial hyperfusion and clustering in cells. Because 1KO MEFs expressing Mfn1 S228E are meant to represent cells in which 100% of Mfn1 S228 is phosphorylated, it is possible that physiological levels of Mfn1 S228 phosphorylation do not cause mitochondrial clustering. Consistently, across preliminary PRM mass spectrometry experiments less than 50% of Mfn1 S228 is phosphorylated in cells. Based on the CCCP and nocodazole experiments, it seems unlikely that mitochondrial hyperfusion occurs in these cells without clustering, suggesting that Mfn2 may be the primary driver of fusion in a concentrated, perinuclear mitochondrial pool. This could be tested by more directly elaborating the dependence of cellular phenotypes on Mfn2, as well as determining concentration-dependent effects of mitochondrial *in vitro* fusion.

Additional characterization of assembly: Mitofusin-specific functions

In a separate project to determine if mitofusin-specific function is associated with a specific region of the protein, I worked with another graduate student to characterize the assembly of Mfn1, Mfn2 and two chimeric proteins that substituted the HB1 region of Mfn1 for Mfn2, and vice versa **(Sloat et al., 2019)**. The chimeric protein Chi3 consists primarily of Mfn1, with the region of Mfn2 corresponding to amino acids Mfn2 348-534 substituted for Mfn1 327-513 (**Figure 3.33A**). The opposite chimeric protein, Chi5, is primarily Mfn2 with the region of Mfn1 corresponding to amino

acids Mfn1 327-513 substituted for Mfn2 348-534 (**Figure 3.33A**). The substituted regions are 75% similar and 56% identical.

First, we evaluated native assembly of FLAG-tagged protein in 1KO MEFs. In the absence of nucleotide, Mfn1 was primarily dimeric, as were samples incubated with GDP (**Figure 3.33B**). When incubated with a transition state mimic, GDP.BeF3, more than half of the wild type mitofusin shifted out of the predicted dimer in 1KO MEFs expressing Mfn1 or Mfn2. Notably, Mfn1 formed a higher order species around 450kDa that was never observed in 1KO MEFs expressing Mfn2-FLAG (**Figure 3.33B**). Some of these differences, however, can likely be explained by specific experimental conditions, including salt concentration and temperature during nucleotide incubation. In a similar experiment where mitochondria were incubated with GDP, GTP or GMPPNP with increased salt, both Mfn1 and Mfn2 seem able to make this large oligomeric structure, but to varying degrees (**Figure 3.33C**). In DKO cells only expressing wild type Mfn1 or Mfn2, a similar proportion of protein shifts into higher order species (50-60%) (**Figure 3.33C**). While DKO MEFs expressing Mfn2 can form some Mfn2 oligomers around 450kDa, DKO MEFs expressing Mfn1 form significantly more of these species, suggesting differences in nucleotide-induced assembly between Mfn1 and Mfn2.

To associate activity with assembly, we measured the assembly of chimeric proteins Chi3 and Chi5. In the presence of GTP, GMPPNP or GDP.BeF3-, Chi3 was able to shift a significant portion of dimeric protein to higher order oligomers. Interestingly, in DKO MEFs, Chi3 can assemble beyond a dimer, but is unable to form the large amount of the 450kDa species observed in wild type Mfn1 (**Figure 3.33D**). This suggests that Mfn1 HB1 is important for tetramer formation. DKO and 1KO MEFs

expressing Chi5 have similar assembly defects, indicating a defect in assembly-stimulated hydrolysis in this chimeric protein.

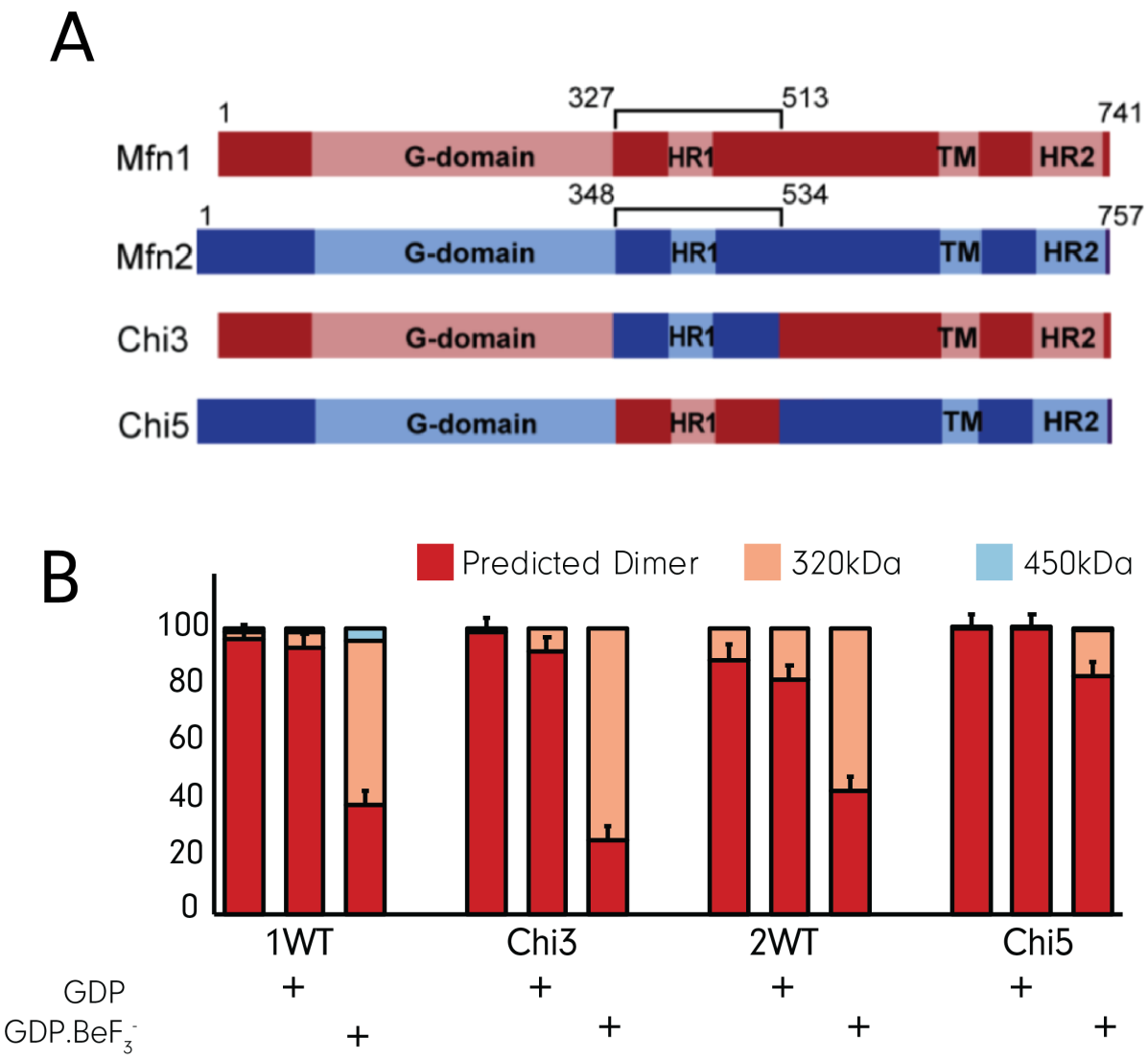

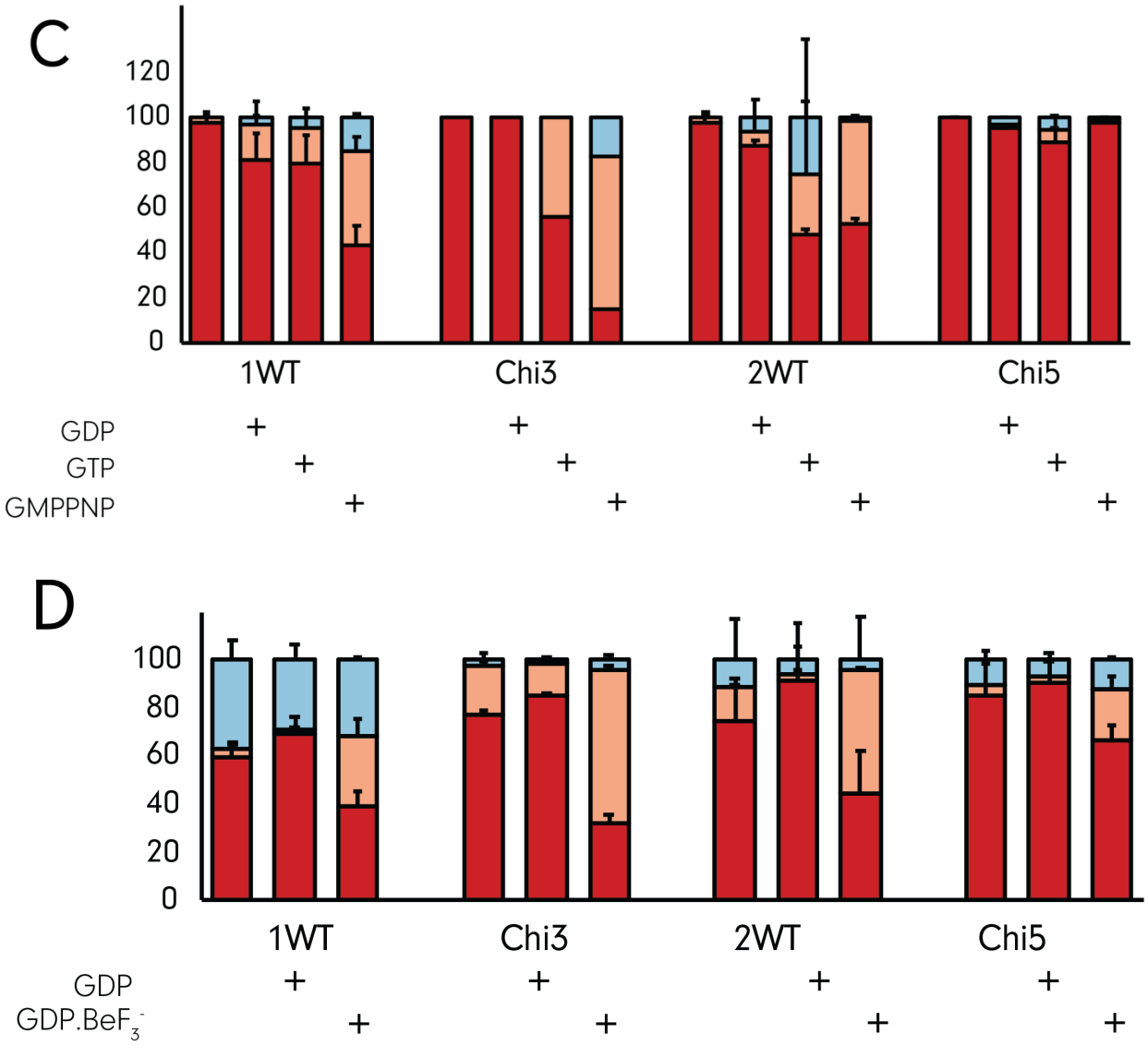

Figure 3.33. Chimera BN-PAGE in 1KO MEFs (B,C) and DKO MEFs (D). (A) Organization of chimeric proteins [figure credit: Suzanne Hoppins]. (B-D) For each condition, at least three independent experiments were performed. Quantifications of B and D were published in Sloat et al., 2019, while quantification in C was done under revised conditions (same as those used for Mfn1 BN-PAGE in Figure 3.32).

Preliminary characterization of Mfn2 S249.

Because Mfn2 S249 phosphorylation was not observed in either of the early mass spectrometry experiments, I hypothesized that phosphoregulation at this site was specific to Mfn1. I did, however, use the same substitutions in Mfn2 S249 (S249A, S249E) to briefly evaluate conserved mitofusin features and mitofusin-specific functions of Mfn2. Based on the preliminary screen of mitochondrial morphology in 2KO MEFs expressing Mfn2 S249A and S249E with a C-terminal Neon tag, both mutants appeared to at least partially rescue mitochondrial morphology. Notably, no clustering was observed in Mfn2 S249E mutants. To confirm this observation, I also expressed C-terminally FLAG-tagged Mfn2 S249A and S249E in 2KO MEFs. At least three clonal isolates expressing at near wild type levels were obtained for each mutant. 2KO MEFs transduced with an empty vector have primarily fragmented mitochondria, while expression of wild type Mfn2 restores a reticular mitochondrial morphology. A blinded screen of mitochondrial morphology in Mfn2 S249 mutants showed a surprisingly variable range of morphologies between different isolates of the same mutant. Importantly, there was no clustering observed in any cells, suggesting that substitution of the same residue of Mfn1 and Mfn2 has distinct effects on mitochondrial morphology (**Figure 3.34**). The variability in this preliminary data set, however, suggests that additional work is needed to more completely understand the effects of Mfn2 S249 on mitochondrial morphology. Isolates with high proportions of cells with fragmented mitochondria were especially surprising, as previous work in the lab has suggested that expression of most Mfn2 disease-associated mutants can rescue mitochondrial morphology in 2KO MEFs. Since one isolate for each mutant had wild type rescue, it is possible that differences in Mfn2 expression levels could explain the variability in the cells tested. If this were the case, I would expect that MEFs expressing Mfn2 S249A #1, 16 and Mfn2 S249E #28, #30 actually express much lower levels of Mfn2, while Mfn2 S429A #5 and Mfn2 S249E #31 are

closer to the intended expression level. It will be important to repeat this experiment after verifying expression levels of Mfn2.

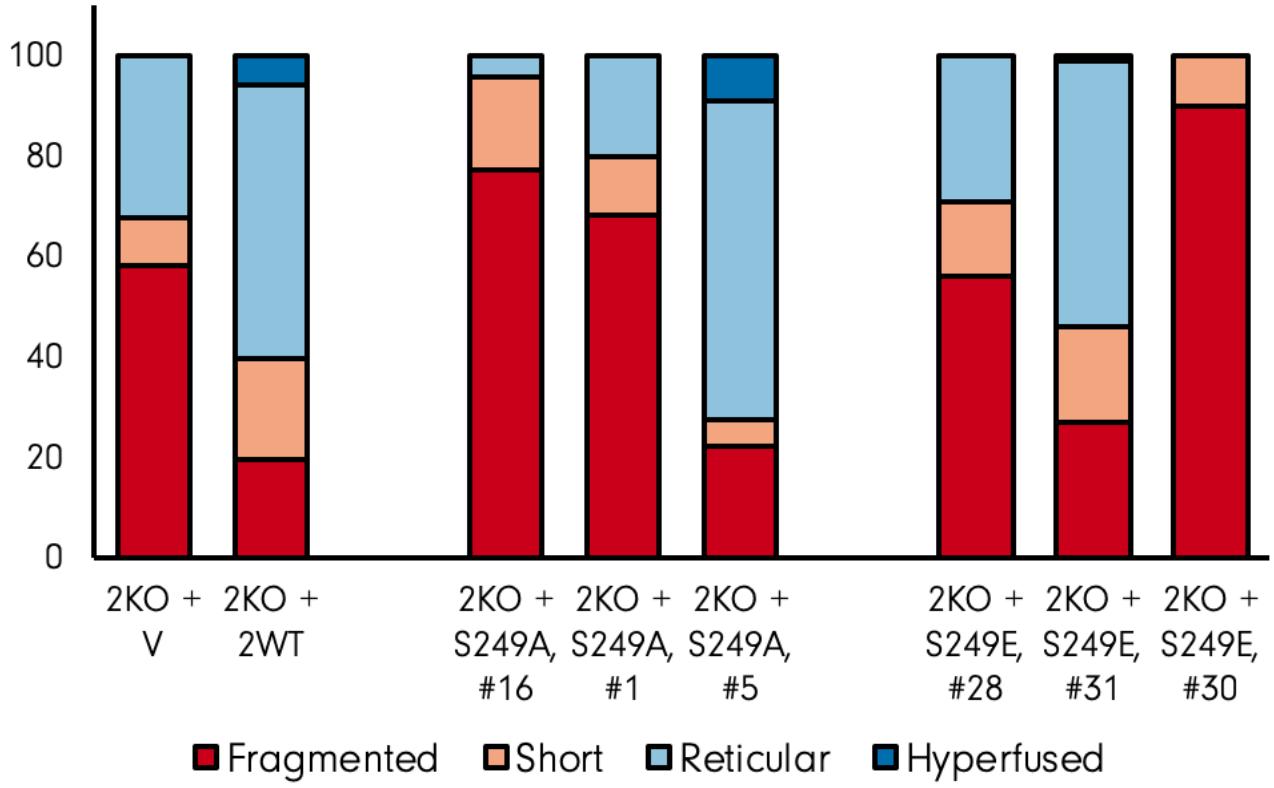

Figure 3.34. Morphology of Mfn2 S249A/E-FLAG in 2KO MEFs. Mitochondrial morphology was quantified in Mfn2 KO MEFs expressing either an empty vector, wild type Mfn2, or Mfn2 S249A/E FLAG-tagged mutants. Graph represents at least 100 cells per condition, imaged and quantified while blinded to the sample identity.

One explanation for the lack of mitochondrial clustering in Mfn2 S249E mutants is that Mfn2 S249E impacts Mfn2 fusion activity differently from how Mfn1 S228E inhibits Mfn1 fusion activity. If defective assembly and *in vitro* fusion activity are related to clustering in Mfn1 S228E mutants, a lack of

clustering and the presence of reticular mitochondria in Mfn2 S249E might be associated with normal fusion and assembly. Alternatively, since mitochondrial morphology serves as a macro-level readout of fusion activity, it is possible that both substitutions impair protein function but clustering only occurs with Mfn1 mutants for reasons we do not yet understand. To test this alternative explanation, I also measured the native assembly of Mfn2 S249 mutants after nucleotide incubation. Higher order assembly of Mfn2 S249E in 2KO MEFs was significantly reduced after incubation with either GTP or the nonhydrolyzable GTP analog, GMPPNP. Surprisingly, Mfn2 S249A assembly was also impaired after GMPPNP incubation (**Figure 3.35**). For the reasons discussed above, this experiment should also be repeated after expression levels in these mutants is confirmed. If these observations hold, however, this suggests that both Mfn1 S228E and Mfn2 S249E mutant variants have impaired mitofusin assembly. Unlike in Mfn1 S228E, however, Mfn2 S249E does appear to form complexes of the appropriate sizes, just at a much lower frequency than wild type Mfn2.

Proteins bound to GMPPNP represent those bound but not hydrolyzing GTP and may stabilize the higher order structures that form after nucleotide binding but prior to hydrolysis. Impaired assembly of Mfn2 mutants with GMPPNP has been reported for several other Mfn2 mutants (Samanas et al., in preparation; Englehart et al., 2019). It remains unclear how an alanine substitution would alter assembly in this region, emphasizing the need for additional characterization

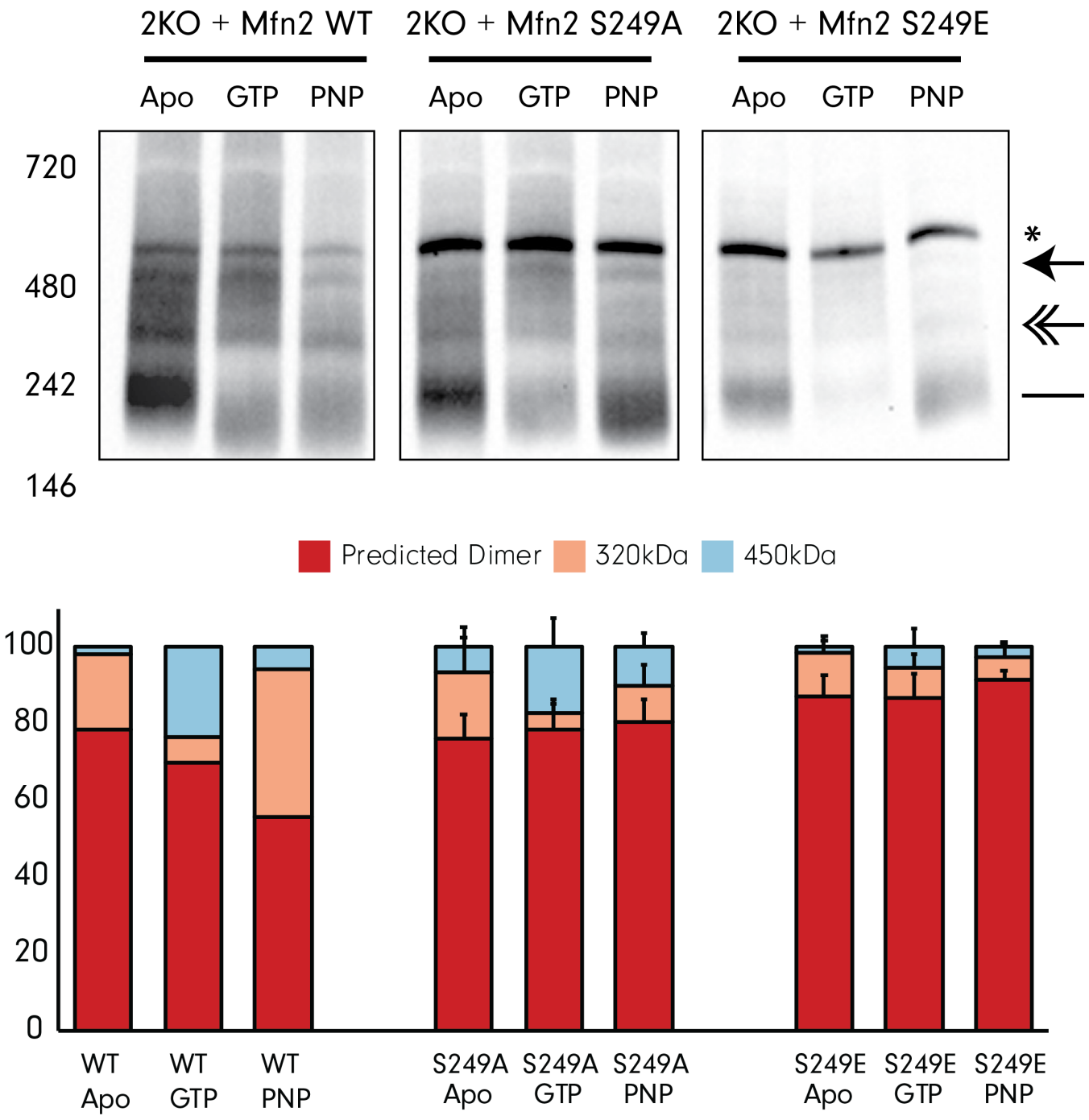

Figure 3.35. BN-PAGE of Mfn2 S249A/E in 2KO MEFs. Native protein assembly was evaluated by blue-native PAGE and imaged using an anti-FLAG antibody. Quantifications represent approximate densitometry of primary bands. Error bards represent standard deviation across three clonal isolates.

Discussion

Together, the biochemical data support a model in which Mfn1 phosphorylation at S228 inhibits fusion activity. I predict that Mfn1 S228 phosphorylation disrupts the interactions between the GTPase domain and HB1 causing the GTPase domain to assume an alternate conformation that is less favorable for membrane tethering. While this still allows for back-to-back dimerization on the same membrane, I hypothesize that Mfn1 S228 phosphorylation constrains the conformational changes around Hinge 1, ultimately leading to impaired nucleotide-dependent assembly and membrane fusion (**Figure 3.2B-D**).

Future work in the lab is addressing the signaling pathway(s) that mediate changes in mitofusin activity through PTM of Mfn1 S228. While it remains possible that PKA mediates phosphorylation at this site, I no longer expect that phosphorylation at this site promotes mitochondrial fusion. Rather, I predict that phosphorylation quickly inhibits fusion activity by reducing the availability of *cis* dimers to tether. Because mitochondria cluster and connect, rather than fragment due to no fusion activity, additional work should also evaluate how Mfn1 S228 phosphorylation affects mitochondrial transport.

Methods

Plasmids and reagents

The following plasmids were purchased from Addgene: pBABE-hygro (#1765), pBABE-puro (#1764), mito-PAGFP (#23348), pclbw-mito TagRFP (#58425), pclbw-mitoCFP (addgene #58426). The Mfn1 MGD plasmid was a kind gift from Song Gao (Cao et al., 2017). Mutations were made by Gibson assembly and confirmed by sequencing. For SIMH, cycloheximide (CHX) was purchased from Fisher Scientific and HBSS with 5mM glucose was purchased from Invitrogen. For cell cycle arrest, aphidicolin was purchased from Sigma.

Cell culture

Mouse embryonic fibroblasts of all mitofusin knockout backgrounds (1KO, 2KO, DKO and WT) were purchased from ATCC. Cells were grown at 37C and 5% CO_2 and cultured in Dulbecco's modified eagle medium (DMEM) containing 1x GlutaMAX (Invitrogen) and was supplemented with 10% FBS (Seradigm).

Mass spectrometry

Reactions were performed in cytosol buffer (20mM PIPES, 150mM KOAc, 5mM MgOAc, 0.2M sorbitol) with cytosol, creatine kinase, and creatine phosphatase. 6µg of purified protein was added to 100µL cytosol and incubated at 37C for 90 minutes. Samples were then bound to anti-FLAG beads and washed in IPL buffer (50mM HEPES-KOH pH7.4, 2mM $MgCl_2$, 300mM KCl, 1mM TCEP). Protein was then treated with 1mM DTT, followed by 3mM iodoacetamide (IAA) before trypsin digestion and elution in 2M urea and 50mM TrisCl.

Viral infection and establishment of clonal populations

platE cells (Cell Biolabs) were cultured in complete media (DMEM + 10% FBS) with 1µg/mL puromycin and 10µg/mL blasticidin. Transfections were performed when cells were around 75% confluent in 6-well dishes. 3µg of Mfn1 or 1.5µg of Mfn2 were transfected using FuGene HD (Promega), according to manufacturer instructions. The viral supernatant was collected and added to MEFs, along with 8µg/mL polybrene, at 48- and 72-hours post-transfection. Approximately 16hr after the final viral transduction, MEF cells were split and selection was added (1µg/mL puromycin for Neon, 200µg/mL hygromycin for FLAG).

Clonal populations of MEFs expressing mutant mitofusins were generated by plating MEFs, after selection, at a low density to generate small, distinct populations of cells generated from a single precursor. Clonal populations were collected using sterile filter paper dots in trypsin. After clonal populations are collected, whole cell extract is collected and lysed. Western blot analysis was performed to screen populations for those expressing the mutant mitofusin at wild type levels.

Microscopy

Cells for microscopy were plated on No. 1.5 glass-bottomed dishes (MatTek) to be approximately 75% confluence on the day of imaging. Prior to imaging, MEFs were incubated with 0.1µg/mL Mitotracker Red CMX Ros (Invitrogen) for 15-30 minutes at 37C with 5% CO_2. After incubation, MitoTracker was removed and cells were incubated in complete media for at least 45 minutes before imaging. Images were obtained using Nikon Ti-E widefield microscope with 63X NA 1.4 oil objective (Nikon) with a solid-state light source (Spectra X, Lumencor) and an sCMOS camera (Zyla

5.5 Megapixel). Z series were collected with a step size of 0.3μm. Each cell line was imaged on at least three separate occasions (n>100 cells per experiment) at 37C with 5% CO_2.

For nocodazole treatments, cells were incubated with 0.1μg/mL Mitotracker Red CMX Ros for 15-30 minutes, rinsed and then incubated in complete DMEM with 5μM nocodazole for 45 minutes to one hour before imaging.

For CCCP treatments, 10μM CCCP (Fisher Scientific) was incubated in DMEM for 4 hours at 37C. After CCCP treatment, cells were rinsed in 1x PBS and then replaced with DMEM or DMEM with 10μM nocodazole.

Transmission electron microscopy (EM)

1KO MEFs transduced with an empty vector, wild type Mfn1, or Mfn1 S228E were trypsinized and pelleted before fixation in 4% glutaraldehyde in NaCaCo (pH 7.3) at room temperature overnight. Samples were stored at 4C before pre-imaging processing by Ed Parker.

Image Analysis

Images obtained by fluorescent microscopy were deconvolved using 8-15 iterations of the 3D Landweber deconvolution. Images were then exported, and maximum intensity projections were made using ImageJ (NIH). Mitochondria is scored based on the following criteria: Mitochondrial fragmentation indicates that most mitochondria are <2μm in length and a reticular morphology is defined as <30% fragmented mitochondria per cell with the average mitochondrial length >2μm. Hyperfusion indicated that most mitochondria were connected as a single structure and clusters

indicate mitochondria that were not distributed throughout the cytosol and whose morphology is not immediately obvious.

Matrix-targeted photoactivatable GFP (mito-paGFP)

Cells transduced with mito-PAGFP were plated in No. 1.5 glass-bottomed dishes (MatTek) and incubated with 0.1µg/mL Mitotracker CMX Ros (Invitrogen) for 15-30 minutes at 37C with 5% CO_2, washed and incubated with complete media for at least 45 minutes prior to imaging. MEFs were imaged at 37C with 5% CO_2. A region that was approximately 1µm was activated using a 405nm laser and the same cell was imaged after 50 minutes. Images were collected with a Nikon Ti-E widefield microscope with a 63X NA 1.4 oil objective (Nikon), a solid-state light source (Spectra X, Lumencor), and an sCMOS camera (Zyla 5.5 Megapixel).

Mitochondrial isolation

Cells for mitochondrial isolation were grown on 15cm plates (3-5 plates harvested total) to approximately 90% confluency and then harvested by scraping. Cells were pelleted at 500xg and washed in MIB (0.2M sucrose, 10mM Tris MOPS [pH 7.4], 1mM EGTA). The cell pellet was resuspended in approximately one cell pellet volume of cold MIB. Sample was then homogenized by 10-14 strokes at 400 RPM on ice with a Kontes Potter-Elvehjem tissue grinder. Lysed sample was then spun at 500xg for 5-10min to remove nuclei and unbroken cells. Homogenization and centrifugation were repeated once and supernatant was then transferred to a clean tube. This was then spun at 7,400 xg at 4C for 10min to pellet a crude mitochondrial fraction. The mitochondrial pellet was next suspended in a small volume of MIB and the protein concentration was measured using a Bradford assay (Bio-Rad Laboratories).

In vitro fusion

MEFs that stably expressed a mitochondria-targeted RFP or CFP were grown to 90% confluency in 15cm dishes and grown to confluency. Mitochondria were isolated as described above and mitochondrial concentrations were determined using Bradford Reagent. For fusion reactions, mitochondria were mixed such that 10µg of RFP and CFP-labeled mitochondria were present in each sample. Mitochondria were then washed in MIB and spun at 7,400xg for 10min to recover the mitochondrial pellet. Pellets were resuspended in 10µL fusion buffer (20mM PIPES-KOH [pH 6.8], 150mM KOAc, 5mM MgOAc2, 0.4M sorbitol, 0.12mg/mL creatine phosphokinase, 40mM creatine phosphate, 1.5mM ATP, 1.5mM GTP), with or without wild type cytosol. Fusion reactions were incubated at 37C for 60 minutes and reactions were stopped on ice. For imaging, 4µL of the fusion reaction was pipetted onto a 3% low-melt agarose bed for image acquisition with a Nikon Ti-E widefield microscope with a 100X NA 1.4 oil objective (Nikon), solid stage light source (Spectra X, lumencor) and a sCMOS camera (Zyla 5.5 Megapixel). For each condition, at least 300 mitochondria were counted from at least four images. Fusion was scored based on the colocalization of red and cyan fluorophores as measured in three dimensions.

Co-IP

50µg of FLAG-tagged and 50µg of Neon-tagged mitochondria of the indicated mutants were combined at a concentration of 6µg/µL and incubated at 37C for 30 minutes with beryllium fluoride (2.5mM BeSO4, 25mM NaF) with or without 2mM GDP in fusion buffer (20mM PIPES-KOH [pH 6.8], 150mM KOAc, 5mM MgOAC2, 0.4M sorbitol with 0.12 mg/mL creatine kinase, 40mM creatine phosphate, 1.5mM ATP). Mitochondria were then solubilized in lysis buffer (20mM HEPES-KOH [pH 7.4], 50mM KCl, 5mM MgCl2) with 1.5% w/v n-dodecyl B-D-maltoside (DDM), and 1x Halt Protease

inhibitor (Thermo Scientific) for 30 minutes on ice. Lysates were cleared at 10,000xg for 15 minutes at 4C.

Supernatants were then incubated with 50µL magnetic uMACS anti-DYKDDDDK MicroBeads (Miltenyi Biotech) for 30 minutes on ice. Samples were then applied to the MACS column (Miltenyi Biotec) and placed in the magnetic field using a uMACS Separator (Miltenyi Biotec). After washing once in 400µL 20mM HEPES-KOH [pH 7.4], 50mM KCl, 5mM MgCl2, 0.1% DDM, columns were washed in 200µL 20mM HEPES-KOH [pH 7.4], 50mM KCl, 5mM MgCl2. Samples were then incubated samples in one column volume (25µL) SDS-PAGE loading buffer (60mM Tris-HCl [pH 6.8], 2.5% sodium dodecyl sulfate, 5% BME, 5% sucrose, 0.1% bromophenol blue) for 15 minutes at room temperature and then eluted in 35µL of SDS PAGE loading buffer.

Samples were run on SDS PAGE and transferred onto nitrocellulose at 100V for 1 hour in 1x transfer buffer (25 mM Tris, 192mM glycine, 20% methanol). Membranes were blocked in 4% milk for at least 30 minutes and then probed with anti-Mfn1 (rabbit polyclonal, gift from Jodi Nunnari, University of California, Davis; 1:500) or anti-Mfn2 (mouse monoclonal, Sigma clone 4H8; 1:1000) for 4 hours at RT or overnight at 4C. Membranes were incubated with DyLight secondary antibody (Invitrogen) at room temperature for 30 minutes to one hour and then imaged on a LICOR Imaging system (LI-COR Biosciences).

BN-PAGE

Mitochondria were isolated and concentrations were determined as described above. Nucleotide reactions were set up in MIB containing 10mM MgOAc and 100mM KOAc, with PMSF and 1x Halt

protease inhibitor. Samples were incubated with 2mM nucleotide at 30C for 30 minutes or incubated on ice in the "untreated" condition. While this does not represent a true "apo" control, this condition is used to represent the assembly of native Mfn1 in untreated cells. Samples were lysed in NativePAGE™ sample buffer with 1% digitonin (Sigma) for 15 minutes on ice. Cell lysate was spun at 16,000xg for 30 minutes and the supernatant was added to G250 sample buffer (Sigma) at a 0.25% final concentration.

10µg of protein was loaded per well. Gels were run in dark blue buffer (0.05% Coomassie G250) at 40V for 30 minutes, followed by 100V for 30 minutes. At this point, gels were moved to light blue buffer (0.005% Coomassie G250) and run at 100V for 30 minutes, followed by 250V for 70 minutes. Samples were transferred onto PVDF membranes at 30V for 16 hours. After transfer, samples were fixed in 8% acetic acid for 15 minutes, rinsed in water and dried. Membranes were rehydrated in methanol, rinsed in water and then 4% milk. Samples were incubated with a mouse monoclonal anti-FLAG antibody (Sigma; 1:1000), followed by anti-HRP secondary antibody (Cell Signaling Technology) and detected using a SuperSignal Femto (HRP peroxidase-based) kit imaged on an iBright.

Immunofluorescence (IF)

Cells were fixed in 4% paraformaldehyde with 0.5% glutaraldehyde and permeabilized in 0.01% TritonX-100. Samples were blocked in 10% FBS with 0.1% TritonX-100 before incubation with anti-mouse Drp1 antibody (BD Biosciences, #611112), followed by incubation with a rabbit anti-mouse secondary antibody conjugated to AlexaFluor488 (Fisher Scientific).

Mfn1 MGD purification

Mfn1 constructs were expressed in Escherichia coli Rosetta (DE3) cells cultured in Luria- Bertani medium with 150 µg/mL ampicillin and 25 µg/mL chloramphenicol at 37C. Cells were grown to an OD_{600} of ~0.6 and protein expression was induced by the addition of 100µM isopropyl-1-thio-β-d- galactopyranoside (IPTG). Induced cultures were grown overnight at approximately 17–18C. The cells were harvested by centrifugation at 6,000 x g for 10 minutes. Cell pellets expressing Mfn1 MGD were resuspended in 5mL phosphate buffered saline, pelleted by centrifugation at 6,000 x g for 5 minutes, frozen in liquid nitrogen and stored at - 80C.

Cells were thawed in a room temperature water bath and resuspended in 50mL lysis buffer (50mM HEPES-KOH [pH 7.4], 400mM NaCl, 5mM $MgCl_2$, 30mM imidazole, 1mM phenylmethanesulfonylfluoride (PMSF), 1x protease inhibitor cocktail (Thermo Scientific), 2.5mM β-mercaptoethanol (β-ME) and lysed using a microfluidizer (Avestin). The lysate was subjected to centrifugation at 14,000 RPM for 45 minutes. The supernatant was applied to 2.5mL HisPur™ Ni-NTA beads (Thermo Scientific) equilibrated with Binding buffer 1 (20mM HEPES-KOH [pH 7.4], 400mM NaCl, 5mM $MgCl_2$, 30mM imidazole [pH 8.0], 2.5mM β- ME) and nutated at 4C for 30 minutes. Ni-NTA beads bound to protein were washed with 20 column volumes of Binding buffer 1 and proteins were eluted with 2.5mL Elution buffer (20mM HEPES-KOH [pH 7.4], 400mM NaCl, 5mM $MgCl_2$, 300mM imidazole, 2.5mM β-ME). Mfn1 MGD-containing elutions were incubated with 800µg glutathione S-transferase (GST)-fused PreScission protease (PSP) to remove the amino-terminal His_6-tag. This was dialyzed overnight against Binding buffer 2 (20mM HEPES-KOH [pH 7.4], 400mM NaCl, 5mM $MgCl_2$, 2.5mM β-ME). After dialysis, PSP was removed using a GST column. The protein was re-applied to a second Ni-NTA column equilibrated with Binding buffer 2. Binding buffer 1 was used to elute the protein, which were subsequently loaded onto a Superdex200 16/60 column (GE Healthcare) equilibrated with gel filtration buffer containing 20mM HEPES-KOH [pH

7.4], 150mM NaCl, 5mM $MgCl_2$ and 1mM dithiothreitol. The protein eluted in a discrete peak corresponding to a molecular mass of approximately 50kDa. Protein was concentrated on an Amicon Ultra Centrifugal Filter (MWCO 30) (Millipore) to 30mg/mL and glycerol was added to 20% before the protein was aliquoted and stored at -80C. Protein purification was performed at 4C. Protein concentration was determined by Laboratories).

SEC

Samples were incubated in SEC Buffer (20mM Tris-HCl pH 8.0, 150mM KCl, 4mM MgCl2, 3mM DTT) and separated on a Superose 6 Increase 10/300 GL column. GDP.BeF incubation was done with 2.5mM GDP, 2.5mM BeSO4, and 25mM NaF.

GTPase assay

Frozen protein was thawed on ice and diluted to 2.5µM in 20 mM HEPES-KOH [pH 7.4], 50mM KCl, 5mM MgCl2, 1mM dithiothreitol. Protein concentrations were confirmed by Bradford assay (Bio Rad Laboratories). Reactions were set up in triplicate in a 96 well plate on ice. Variable concentrations of GTP were added and reactions were incubated at 37°C for 15 minutes. Reactions were stopped by adding 200 mM EDTA on ice. Concentrations of free inorganic phosphate were measured by malachite green reagent. Malachite green reagent was added, and reactions were incubated at room temperature for 15 minutes (Leonard et al., 2005). The optical density at 650nM was measured and a potassium phosphate standard curve was used to determine the amount of GTP hydrolyzed.

Sucrose gradient- Mfn1 MGD

200µg purified wild type Mfn1 MGD or Mfn1 S228E MGD protein was added to 150µL buffer containing 20mM Tris HCl (pH 8), 150mM KCl, 4mM $MgCl_2$. For nucleotide incubation with GDP.BeF_3, protein was incubated with 2mM GDP, 2.5mM $BeSO_4$ and 25mM NaF for 15 minutes on ice, followed by 30 minutes at 37C, and 15 minutes on ice. Untreated protein was incubated under the same conditions with 2.5mM $BeSO_4$ and 25mM NaF in the absence of GDP. Protein was added to the top of a 5-20% (w/v) linear sucrose gradient. Gradients were centrifuged at 32,500xg for 16 hours at 4C (L70 Ultra, Beckman). After centrifugation, samples were taken down in 14 fractions. Since a majority of the protein was found in fractions 2-9, these fractions were separated at half the volume of the remaining fractions to increase resolution. Laemmli buffer was added to 20µL of each fraction, run on SDS-PAGE gel and resolved with Coomassie Blue.

Sucrose gradient- full length Mfn1-FLAG

Mitochondria were isolated as described above, and 50 µg of mitochondria were incubated in the absence or presence of GDP.BeF_3 in buffer containing 20mM HEPES pH 7.8, 50mM KCl, and 5mM MgCl2 for 30min at 37C. Mitochondria were lysed in 1% DDM for 1.5 hours and then added to a 5-20% continuous sucrose gradient. Gradients were spun at 32500 rpm for 16 hours at 4C. Fractions were collected and protein was extracted using TCA precipitation.

References

Abe, A., Numakura, C., Kijima, K., Hayashi, M., Hashimoto, T., Hayasaka, K., 2011. Molecular diagnosis and clinical onset of Charcot-Marie-Tooth disease in Japan. J. Hum. Genet. 56, 364–368. doi:10.1038/jhg.2011.20

Bian, X., Klemm, R.W., Liu, T.Y., Zhang, M., Sun, S., Sui, X., Liu, X., Rapoport, T.A., Hu, J., 2011. Structures of the atlastin GTPase provide insight into homotypic fusion of endoplasmic reticulum membranes. Proc. Natl. Acad. Sci. U.S.A. 108, 3976–3981. doi:10.1073/pnas.1101643108

Brandt, T., Cavellini, L., Kühlbrandt, W., Cohen, M.M., 2016. A mitofusin-dependent docking ring complex triggers mitochondrial fusion in vitro. Elife 5, 36634. doi:10.7554/eLife.14618

Byrnes, L.J., Singh, A., Szeto, K., Benvin, N.M., O'Donnell, J.P., Zipfel, W.R., Sondermann, H., 2013. Structural basis for conformational switching and GTP loading of the large G protein atlastin. EMBO J 32, 369–384. doi:10.1038/emboj.2012.353

Byrnes, L.J., Sondermann, H., 2011. Structural basis for the nucleotide-dependent dimerization of the large G protein atlastin-1/SPG3A. Proc. Natl. Acad. Sci. U.S.A. 108, 2216–2221. doi:10.1073/pnas.1012792108

Cao, Y.-L., Meng, S., Chen, Y., Feng, J.-X., Gu, D.-D., Yu, B., Li, Y.-J., Yang, J.-Y., Liao, S., Chan, D.C., Gao, S., 2017. MFN1 structures reveal nucleotide-triggered dimerization critical for mitochondrial fusion. Nature 542, 372–376. doi:10.1038/nature21077

Casasnovas, C., Banchs, I., Cassereau, J., Gueguen, N., Chevrollier, A., Martínez-Matos, J. A., ... Volpini, V. (2010). Phenotypic spectrum of MFN2 mutations in the Spanish population. Journal of Medical Genetics, 47(4), 249–256. https://doi.org/10.1136/jmg.2009.072488

Cereghetti, G.M., Stangherlin, A., Martins de Brito, O., Chang, C.R., Blackstone, C., Bernardi, P., Scorrano, L., 2008. Dephosphorylation by calcineurin regulates translocation of Drp1 to mitochondria. Proc. Natl. Acad. Sci. U.S.A. 105, 15803–15808. doi:10.1073/pnas.0808249105

Chang, C.-R., Blackstone, C., 2007. Cyclic AMP-dependent protein kinase phosphorylation of Drp1 regulates its GTPase activity and mitochondrial morphology. J Biol Chem 282, 21583–21587. doi:10.1074/jbc.C700083200

Chen, Y., Dorn, G.W., 2013. PINK1-phosphorylated mitofusin 2 is a Parkin receptor for culling damaged mitochondria. Science 340, 471–475. doi:10.1126/science.1231031

Chung, J.Y.-M., Steen, J.A., Schwarz, T.L., 2016. Phosphorylation-Induced Motor Shedding Is Required at Mitosis for Proper Distribution and Passive Inheritance of Mitochondria. Cell Rep 16, 2142–2155. doi:10.1016/j.celrep.2016.07.055

Cohen, M.M., Tareste, D., 2018. Recent insights into the structure and function of Mitofusins in mitochondrial fusion. F1000Res 7. doi:10.12688/f1000research.16629.1

Cribbs, J.T., Strack, S., 2007. Reversible phosphorylation of Drp1 by cyclic AMP-dependent protein kinase and calcineurin regulates mitochondrial fission and cell death. EMBO Rep 8, 939–944. doi:10.1038/sj.embor.7401062

Daumke, O., Praefcke, G.J.K., 2016. Invited review: Mechanisms of GTP hydrolysis and conformational transitions in the dynamin superfamily. Biopolymers 105, 580–593. doi:10.1002/bip.22855

Eisner, V., Picard, M., Hajnóczky, G., 2018. Mitochondrial dynamics in adaptive and maladaptive cellular stress responses. Nat. Cell Biol. 20, 755–765. doi:10.1038/s41556-018-0133-0

Englehart, EA, Insights into the molecular mechanisms of mitochondrial outer membrane tethering and fusion, PhD dissertation, University of Washington, 2019,http://hdl.handle.net/1773/44051

Engelhart, E.A., Hoppins, S., 2019. A catalytic domain variant of Mitofusin requiring a wildtype paralog for function uncouples mitochondrial outer-membrane tethering and fusion. J Biol Chem jbc.RA118.006347. doi:10.1074/jbc.RA118.006347

Escobar-Henriques, M., Joaquim, M., 2019. Mitofusins: Disease Gatekeepers and Hubs in Mitochondrial Quality Control by E3 Ligases. Front Physiol 10, 517. doi:10.3389/fphys.2019.00517

Feely, S.M.E., Laura, M., Siskind, C.E., Sottile, S., Davis, M., Gibbons, V.S., Reilly, M.M., Shy, M.E., 2011. MFN2 mutations cause severe phenotypes in most patients with CMT2A. Neurology 76, 1690–1696. doi:10.1212/WNL.0b013e31821a441e

Ferreira, J.C.B., Campos, J.C., Qvit, N., Qi, X., Bozi, L.H.M., Bechara, L.R.G., Lima, V.M., Queliconi, B.B., Disatnik, M.-H., Dourado, P.M.M., Kowaltowski, A.J., Mochly-Rosen, D., 2019. A selective inhibitor of mitofusin 1-βIIPKC association improves heart failure outcome in rats. Nat Commun 10, 329. doi:10.1038/s41467-018-08276-6

Franco, A., Kitsis, R.N., Fleischer, J.A., Gavathiotis, E., Kornfeld, O.S., Gong, G., Biris, N., Benz, A., Qvit, N., Donnelly, S.K., Chen, Y., Mennerick, S., Hodgson, L., Mochly-Rosen, D., Dorn, G.W., 2016. Correcting mitochondrial fusion by manipulating mitofusin conformations. Nature 540, 74–79. doi:10.1038/nature20156

Fransson, S., Ruusala, A., Aspenström, P., 2006. The atypical Rho GTPases Miro-1 and Miro-2 have essential roles in mitochondrial trafficking. Biochem. Biophys. Res. Commun. 344, 500–510. doi:10.1016/j.bbrc.2006.03.163

Frezza, C., Cipolat, S., Martins de Brito, O., Micaroni, M., Beznoussenko, G.V., Rudka, T., Bartoli, D., Polishuck, R.S., Danial, N.N., De Strooper, B., Scorrano, L., 2006. OPA1 controls apoptotic cristae remodeling independently from mitochondrial fusion. Cell 126, 177–189. doi:10.1016/j.cell.2006.06.025

Glater, E.E., Megeath, L.J., Stowers, R.S., Schwarz, T.L., 2006. Axonal transport of mitochondria requires milton to recruit kinesin heavy chain and is light chain independent. J. Cell Biol. 173, 545–557. doi:10.1083/jcb.200601067

Glytsou, C., Calvo, E., Cogliati, S., Mehrotra, A., Anastasia, I., Rigoni, G., Raimondi, A., Shintani, N., Loureiro, M., Vazquez, J., Pellegrini, L., Enriquez, J.A., Scorrano, L., Soriano, M.E., 2016. Optic Atrophy 1 Is Epistatic to the Core MICOS Component MIC60 in Mitochondrial Cristae Shape Control. Cell Rep 17, 3024–3034. doi:10.1016/j.celrep.2016.11.049

Gomes, L.C., Di Benedetto, G., Scorrano, L., 2011. During autophagy mitochondria elongate, are spared from degradation and sustain cell viability. Nat. Cell Biol. 13, 589–598. doi:10.1038/ncb2220

Han, J., Pluhackova, K., Böckmann, R.A., 2017. The Multifaceted Role of SNARE Proteins in Membrane Fusion. Front Physiol 8, 5. doi:10.3389/fphys.2017.00005

Hoppins, S., Edlich, F., Cleland, M.M., Banerjee, S., McCaffery, J.M., Youle, R.J., Nunnari, J., 2011. The soluble form of Bax regulates mitochondrial fusion via MFN2 homotypic complexes. Molecular Cell 41, 150–160. doi:10.1016/j.molcel.2010.11.030

Humphrey, S.J., Yang, G., Yang, P., Fazakerley, D.J., Stöckli, J., Yang, J.Y., James, D.E., 2013. Dynamic adipocyte phosphoproteome reveals that Akt directly regulates mTORC2. Cell Metabolism 17, 1009–1020. doi:10.1016/j.cmet.2013.04.010

Ishihara, N., Eura, Y., Mihara, K., 2004. Mitofusin 1 and 2 play distinct roles in mitochondrial fusion reactions via GTPase activity. J Cell Sci 117, 6535–6546. doi:10.1242/jcs.01565

Jimah, J.R., Hinshaw, J.E., 2018. Structural Insights into the Mechanism of Dynamin Superfamily Proteins. Trends Cell Biol 29, 257–273. doi:10.1016/j.tcb.2018.11.003

Kielian, M., 2014. Mechanisms of Virus Membrane Fusion Proteins. Annu Rev Virol 1, 171–189. doi:10.1146/annurev-virology-031413-085521

Koshiba, T., Detmer, S.A., Kaiser, J.T., Chen, H., McCaffery, J.M., Chan, D.C., 2004. Structural basis of mitochondrial tethering by mitofusin complexes. Science 305, 858–862. doi:10.1126/science.1099793

Leboucher, G.P., Tsai, Y.C., Yang, M., Shaw, K.C., Zhou, M., Veenstra, T.D., Glickman, M.H., Weissman, A.M., 2012. Stress-induced phosphorylation and proteasomal degradation of mitofusin 2 facilitates mitochondrial fragmentation and apoptosis. Molecular Cell 47, 547–557. doi:10.1016/j.molcel.2012.05.041

Legros, F., Lombès, A., Frachon, P., Rojo, M., 2002. Mitochondrial fusion in human cells is efficient, requires the inner membrane potential, and is mediated by mitofusins. Mol. Biol. Cell 13, 4343–4354. doi:10.1091/mbc.e02-06-0330

Liu, J., Noel, J.K., Low, H.H., 2018. Structural basis for membrane tethering by a bacterial dynamin-like pair. Nat Commun 9, 3345. doi:10.1038/s41467-018-05523-8

Low, H.H., Löwe, J., 2006. A bacterial dynamin-like protein. Nature 444, 766–769. doi:10.1038/nature05312

Low, H.H., Sachse, C., Amos, L.A., Löwe, J., 2009. Structure of a bacterial dynamin-like protein lipid tube provides a mechanism for assembly and membrane curving. Cell 139, 1342–1352. doi:10.1016/j.cell.2009.11.003

López-Doménech, G., Covill-Cooke, C., Ivankovic, D., Halff, E.F., Sheehan, D.F., Norkett, R., Birsa, N., Kittler, J.T., 2018. Miro proteins coordinate microtubule- and actin-dependent mitochondrial transport and distribution. EMBO J 37, 321–336. doi:10.15252/embj.201696380

Martens, S., McMahon, H.T., 2008. Mechanisms of membrane fusion: disparate players and common principles. Nat Rev Mol Cell Biol 9, 543–556. doi:10.1038/nrm2417

Mishra, P., Chan, D.C., 2016. Metabolic regulation of mitochondrial dynamics. J. Cell Biol. 212, 379–387. doi:10.1083/jcb.201511036

Misko, A., Jiang, S., Wegorzewska, I., Milbrandt, J., Baloh, R.H., 2010. Mitofusin 2 is necessary for transport of axonal mitochondria and interacts with the Miro/Milton complex. J Neurosci 30, 4232–4240. doi:10.1523/JNEUROSCI.6248-09.2010

Mitra, K., Wunder, C., Roysam, B., Lin, G., Lippincott-Schwartz, J., 2009. A hyperfused mitochondrial state achieved at G1-S regulates cyclin E buildup and entry into S phase. Proc. Natl. Acad. Sci. U.S.A. 106, 11960–11965. doi:10.1073/pnas.0904875106

Miyazono, Y., Hirashima, S., Ishihara, N., Kusukawa, J., Nakamura, K.-I., Ohta, K., 2018. Uncoupled mitochondria quickly shorten along their long axis to form indented spheroids, instead of rings, in a fission-independent manner. Sci Rep 8, 350. doi:10.1038/s41598-017-18582-6

Narendra, D., Kane, L.A., Hauser, D.N., Fearnley, I.M., Youle, R.J., 2010. p62/SQSTM1 is required for Parkin-induced mitochondrial clustering but not mitophagy; VDAC1 is dispensable for both. Autophagy 6, 1090–1106. doi:10.4161/auto.6.8.13426

Narendra, D., Tanaka, A., Suen, D.-F., Youle, R.J., 2008. Parkin is recruited selectively to impaired mitochondria and promotes their autophagy. J. Cell Biol. 183, 795–803. doi:10.1083/jcb.200809125

Pilling, A.D., Horiuchi, D., Lively, C.M., Saxton, W.M., 2006. Kinesin-1 and Dynein are the primary motors for fast transport of mitochondria in Drosophila motor axons. Mol. Biol. Cell 17, 2057–2068. doi:10.1091/mbc.e05-06-0526

Pyakurel, A., Savoia, C., Hess, D., Scorrano, L., 2015. Extracellular regulated kinase phosphorylates mitofusin 1 to control mitochondrial morphology and apoptosis. Molecular Cell 58, 244–254. doi:10.1016/j.molcel.2015.02.021

Qi, Y., Yan, L., Yu, C., Guo, X., Zhou, X., Hu, X., Huang, X., Rao, Z., Lou, Z., Hu, J., 2016. Structures of human mitofusin 1 provide insight into mitochondrial tethering. J. Cell Biol. 215, 621–629. doi:10.1083/jcb.201609019

Rambold, A.S., Kostelecky, B., Elia, N., Lippincott-Schwartz, J., 2011. Tubular network formation protects mitochondria from autophagosomal degradation during nutrient starvation. Proc. Natl. Acad. Sci. U.S.A. 108, 10190–10195. doi:10.1073/pnas.1107402108

Rocha, A.G., Franco, A., Krezel, A.M., Rumsey, J.M., Alberti, J.M., Knight, W.C., Biris, N., Zacharioudakis, E., Janetka, J.W., Baloh, R.H., Kitsis, R.N., Mochly-Rosen, D., Townsend, R.R., Gavathiotis, E., Dorn, G.W., 2018. MFN2 agonists reverse mitochondrial defects in preclinical models of Charcot-Marie-Tooth disease type 2A. Science 360, 336–341. doi:10.1126/science.aao1785

Santel, A., Frank, S., Gaume, B., Herrler, M., Youle, R.J., Fuller, M.T., 2003. Mitofusin-1 protein is a generally expressed mediator of mitochondrial fusion in mammalian cells. J Cell Sci 116, 2763–2774. doi:10.1242/jcs.00479

Schwarz, T.L., 2013. Mitochondrial trafficking in neurons. Cold Spring Harb Perspect Biol 5, a011304–a011304. doi:10.1101/cshperspect.a011304

Sloat, S.R., Whitley, B.N., Engelhart, E.A., Hoppins, S., 2019. Identification of a Mitofusin specificity region that confers unique activities to Mfn1 and Mfn2. Mol. Biol. Cell mbcE19050291. doi:10.1091/mbc.E19-05-0291

Smirnova, E., Griparic, L., Shurland, D.L., van der Bliek, A.M., 2001. Dynamin-related protein Drp1 is required for mitochondrial division in mammalian cells. Mol. Biol. Cell 12, 2245–2256. doi:10.1091/mbc.12.8.2245

Sugiura, A., Nagashima, S., Tokuyama, T., Amo, T., Matsuki, Y., Ishido, S., Kudo, Y., McBride, H.M., Fukuda, T., Matsushita, N., Inatome, R., Yanagi, S., 2013. MITOL Regulates Endoplasmic Reticulum-Mitochondria Contacts via Mitofusin2. Molecular Cell 51, 20–34. doi:10.1016/j.molcel.2013.04.023

Tilokani, L., Nagashima, S., Paupe, V., Prudent, J., 2018. Mitochondrial dynamics: overview of molecular mechanisms. Essays Biochem. 62, 341–360. doi:10.1042/EBC20170104

Tondera, D., Grandemange, S., Jourdain, A., Karbowski, M., Mattenberger, Y., Herzig, S., Da Cruz, S., Clerc, P., Raschke, I., Merkwirth, C., Ehses, S., Krause, F., Chan, D.C., Alexander, C., Bauer, C., Youle, R., Langer, T., Martinou, J.-C., 2009. SLP-2 is required for stress-induced mitochondrial hyperfusion. EMBO J 28, 1589–1600. doi:10.1038/emboj.2009.89

Verhoeven, K., Claeys, K.G., Züchner, S., Schröder, J.M., Weis, J., Ceuterick, C., Jordanova, A., Nelis, E., De Vriendt, E., Van Hul, M., Seeman, P., Mazanec, R., Saifi, G.M., Szigeti, K., Mancias, P., Butler, I.J., Kochanski, A., Ryniewicz, B., De Bleecker, J., Van den Bergh, P., Verellen, C., Van Coster, R., Goemans, N., Auer-Grumbach, M., Robberecht, W., Milic Rasic, V., Nevo, Y., Tournev, I., Guergueltcheva, V., Roelens, F., Vieregge, P., Vinci, P., Moreno, M.T., Christen, H.-J., Shy, M.E., Lupski, J.R., Vance, J.M., De Jonghe, P., Timmerman, V., 2006. MFN2 mutation distribution and genotype/phenotype correlation in Charcot-Marie-Tooth type 2. Brain 129, 2093–2102. doi:10.1093/brain/awl126

Vives-Bauza, C., Zhou, C., Huang, Y., Cui, M., de Vries, R.L.A., Kim, J., May, J., Tocilescu, M.A., Liu, W., Ko, H.S., Magrané, J., Moore, D.J., Dawson, V.L., Grailhe, R., Dawson, T.M., Li, C., Tieu, K., Przedborski, S., 2010. PINK1-dependent recruitment of Parkin to mitochondria in mitophagy. Proc. Natl. Acad. Sci. U.S.A. 107, 378–383. doi:10.1073/pnas.0911187107

Whitley, B.N., Engelhart, E.A., Hoppins, S., 2019. Mitochondrial dynamics and their potential as a therapeutic target. Mitochondrion. doi:10.1016/j.mito.2019.06.002

Whitley, B.N., Lam, C., Cui, H., Haude, K., Bai, R., Escobar, L., Hamilton, A., Brady, L., Tarnopolsky, M.A., Dengle, L., Picker, J., Lincoln, S., Lackner, L.L., Glass, I.A., Hoppins, S., 2018. Aberrant Drp1-mediated mitochondrial division presents in humans with variable outcomes. Hum Mol Genet 27, 3710–3719. doi:10.1093/hmg/ddy287

Xie, Y., Li, X., Liu, L., Hu, Z., Huang, S., Zhan, Y., Zi, X., Xia, K., Tang, B., Zhang, R., 2016. MFN2-related genetic and clinical features in a cohort of Chinese CMT2 patients. J. Peripher. Nerv. Syst. 21, 38–44. doi:10.1111/jns.12159

Yan, L., Qi, Y., Huang, X., Yu, C., Lan, L., Guo, X., Rao, Z., Hu, J., Lou, Z., 2018. Structural basis for GTP hydrolysis and conformational change of MFN1 in mediating membrane fusion. Nat. Struct. Mol. Biol. 25, 233–243. doi:10.1038/s41594-018-0034-8

Zemirli, N., Morel, E., Molino, D., 2018. Mitochondrial Dynamics in Basal and Stressful Conditions. Int J Mol Sci 19, 564. doi:10.3390/ijms19020564

Zick, M., Rabl, R., Reichert, A.S., 2009. Cristae formation-linking ultrastructure and function of mitochondria. Biochim. Biophys. Acta 1793, 5–19. doi:10.1016/j.bbamcr.2008.06.013

Züchner, S., De Jonghe, P., Jordanova, A., Claeys, K.G., Guergueltcheva, V., Cherninkova, S., Hamilton, S.R., Van Stavern, G., Krajewski, K.M., Stajich, J., Tournev, I., Verhoeven, K., Langerhorst, C.T., de Visser, M., Baas, F., Bird, T., Timmerman, V., Shy, M., Vance, J.M., 2006. Axonal neuropathy with optic atrophy is caused by mutations in mitofusin 2. Ann. Neurol. 59, 276–281. doi:10.1002/ana.20797

Chapter Four:

Conclusions and contributions

Balanced and regulated mitochondrial dynamics are critical for cellular function. Imbalanced mitochondrial dynamics have been implicated as either a cause or consequence of various neurodegenerative, cardiac and metabolic diseases (**Chapter 1**). While most reviews discussing mitochondrial dynamics during disease emphasize the clinical features within a particular tissue system, our review took a uniquely mechanistic approach to understand the role of imbalanced mitochondrial dynamics across a range of diseases.

The importance of connecting basic biochemistry research to clinical observations was also highlighted in the evaluation of disease-causing variants of Drp1 (**Chapter 2**). By evaluating mitochondrial morphology and Drp1 localization in yeast, mouse and human cells, I was able to connect patient data with a functional understanding of mitochondrial division. Because most reports of disease-causing Drp1 variants only describe the phenotypes observed in patient cells (Gerber et al., 2017; Hogarth, Costford, Yoon, Sondheimer, & Maynes, 2018; Vanstone et al., 2016; Waterham et al., 2007; Zaha et al., 2016), it is difficult to conclude with certainty that mutations in *DNM1L* cause aberrant mitochondrial morphology and disease progression. Our approach uniquely combined an evaluation of mitochondrial morphology in patient cells with experimental determination of the effect of Drp1 mutation in mouse and yeast cells with or without wild type Drp1. Only two other Drp1 variants have been evaluated in mammalian cells (Chao et al., 2016; Fahrner et al., 2016), and our evaluation in yeast is particularly novel. As whole exome sequencing has resulted in an exponential increase in the number of *DNM1L* mutations associated with disease,

similar experiments to determine if mutations are necessary and sufficient to cause the changes in mitochondrial morphology associated with disease will be a good first step.

Our work specifically identified and characterized Drp1 G32A, showing that mitochondrial recruitment can be inhibited by a substitution in the highly conserved GTP binding region **(Whitley et al., 2018)**. This was fairly surprising, as a similar, well-characterized mutation- Drp1 K38A- affects GTP hydrolysis but does not abolish the mitochondrial recruitment of Drp1. To date, only two additional heterozygous Drp1 mutations in the GTPase domain have been reported **(Gerber et al., 2017)**, both of which have similar effects on mitochondrial and peroxisomal morphology as G32A. Additional cellular characterization to understand the mitochondrial recruitment of Drp1 in these cells is required to determine if these Drp1 variants mediate changes in mitochondrial morphology via a similar mechanism to G32A or K38A. A strong mechanistic understanding of disease-associated mutations can then be used to develop personalized therapeutic interventions that are optimally suited to rebalance mitochondrial dynamics.

In a second project discussed in **Chapter 3**, I established a model for the inhibitory role of Mfn1 S228 phosphorylation. While the physiological role of Mfn1 S228 phosphorylation is currently being investigated, here I present data outlining the functional effects of phosphoblocking (S→A) or phosphomimicking (S→E) substitutions at Mfn1 S228. Based on our fusion model (**Figure 3.2**), I expect that Mfn1 S228 phosphorylation blocks the interaction of Mfn1 S228 with itself in *trans* (prevents interaction in Figure 3.2A). This is consistent with primarily dimeric Mfn1 S228E, regardless of nucleotide incubation, and reduced *in vitro* fusion activity.

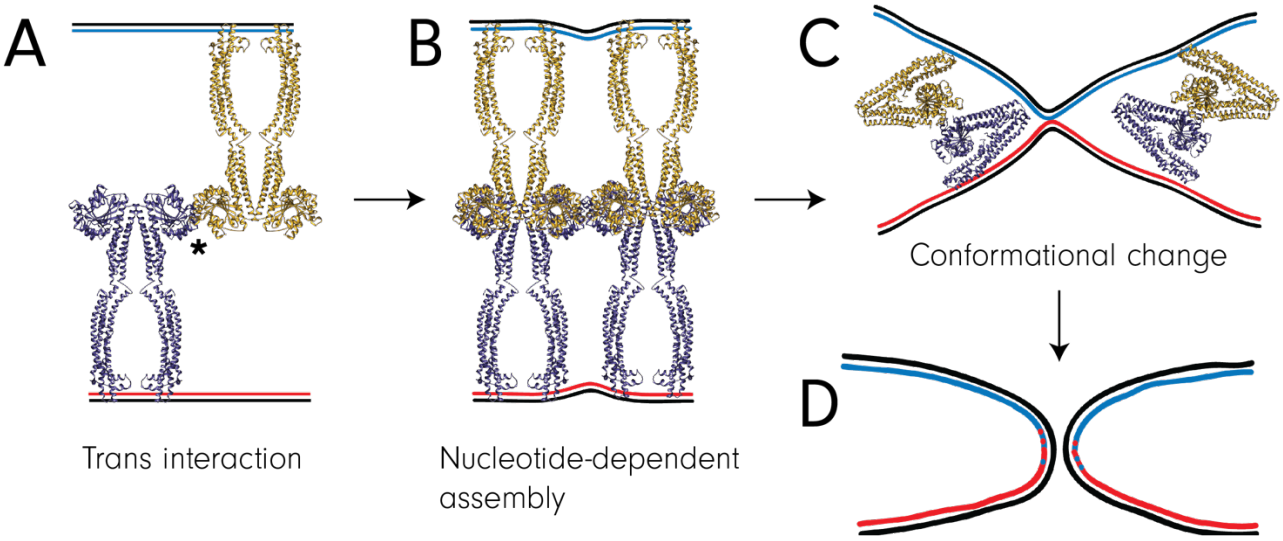

Figure 3.2, from Chapter 3: Current model of mitochondrial outer membrane fusion. We hypothesize that mitofusins assemble in both *cis* (same membrane) or *trans* (opposite membranes). In this model, we predict that back-to-back *cis* dimers form tethers across GTPase domains with another mitofusin dimer in *trans* (A). The formation of the predicted G-G interface is noted with an asterisk (*). GTP binding and hydrolysis promote the higher order assembly of mitofusins (B). Dramatic conformational changes are then predicted to bring membranes together to complete fusion (C-D). [figure minorly adapted from Suzanne Hoppins]

Additional work is required to strengthen and expand our current model of mitochondrial outer membrane fusion. Recent evidence suggests that most mitochondrial contacts do not result in membrane fusion, but rather serve to reduce mitochondrial motility and are followed by untethering events (Wong et al., 2019). While Rab7-Fis1 interactions have been associated with mitochondrial contact untethering (Wong et al., 2019), we do not yet understand the specific characteristics of a mitochondrial contact site that promote fusion. Future studies should elaborate the composition of fusion-competent assemblies, including size and the relative roles of Mfn1 vs. Mfn2. Another area

of active work is reconciling cellular phenotypes with *in vitro* effects. Based on the impaired mitochondrial fusion phenotype in 1KO MEFs expressing Mfn1 S228E, I expected mitochondria in these cells to be primarily fragmented. Surprisingly, mitochondria became predominantly clustered around the nucleus and appear to be connected rather than fragmented. One possible mechanism for mitochondrial clustering could be due to altered mitochondrial transport and mitophagy (Shlevkov et al., 2016; Narendra et al., 2010). I hypothesize that physiological levels of Mfn1 S228 phosphorylation, less than fifty percent of the total cellular Mfn1 based on preliminary PRM mass spectrometry, inhibit mitochondrial fusion to promote the turnover of dysfunctional Mfn1 and/or mitochondria. In this model, expression of only Mfn1 S228E would cause the excessive mitochondrial clustering phenotype observed in cells, leading to Mfn2-dependent fusion among locally concentrated mitochondria. This hypothesis could be directly tested by measuring concentration-dependent increases in *in vitro* fusion activity and confirming Mfn2 interactions and assembly through Co-IP and BN-PAGE, respectively. This would also require connectivity in Mfn1 S228E-expressing cells to depend on Mfn2, which appears to be the case based on our preliminary morphology data in WT, 2KO and DKO backgrounds (**Figures 3.10-12**).

The characterization of Mfn1 S228E has also allowed for the comparison between mutants with similar cellular phenotypes. When compared another Mfn1 variant that causes perinuclear clustering in 1KO MEFs, F202L, Mfn1 S228E has a similar defect in nucleotide-dependent assembly but a distinct defect in *trans* Mfn1 interactions. Additionally, while Mfn1 S228E was completely unable to form the expected species at 320kDa and 450kDa, Mfn1 F202L could form assemblies of these sizes but at far reduced frequencies than wild type Mfn1. The ability for Mfn1 F202L to interact in *trans* suggests that Mfn1 F202L and S228E likely alter fusion through distinct mechanisms, which

both ultimately result in blocked nucleotide-dependent assembly and reduced *in vitro* fusion activity. In her characterization of Mfn1 F202L, Emily also showed that fusion activity depended on Mfn2, consistent with a role for increased, Mfn2-dependent fusion in mitochondrial clusters (Engelhart et al., 2019).

Finally, future work should also emphasize a better understanding of the physiological relevance of phosphorylation at Mfn1 S228. As disease-associated variants related to mitochondrial fusion and division are identified, mechanistic understanding of how these mutations alter protein function will be an important tool to understand normal mitochondrial function, as well as to treat diseases characterized by imbalanced mitochondrial dynamics. We anticipate that continued work in our lab to understand the mechanism of mitochondrial fusion could eventually contribute to the design of more specific, effective therapeutics to address imbalanced mitochondrial dynamics.

References

Chao, Y.-H., Robak, L. A., Xia, F., Koenig, M. K., Adesina, A., Bacino, C. A., et al. (2016). Missense variants in the middle domain of DNM1L in cases of infantile encephalopathy alter peroxisomes and mitochondria when assayed in Drosophila. Human Molecular Genetics, 25(9), 1846–1856. http://doi.org/10.1093/hmg/ddw059

Engelhart, E.A., Hoppins, S., 2019. A catalytic domain variant of Mitofusin requiring a wildtype paralog for function uncouples mitochondrial outer-membrane tethering and fusion. J Biol Chem jbc.RA118.006347. doi:10.1074/jbc.RA118.006347

Fahrner, J. A., Liu, R., Perry, M. S., Klein, J., & Chan, D. C. (2016). A novel de novo dominant negative mutation in DNM1Limpairs mitochondrial fission and presents as childhood epileptic encephalopathy. American Journal of Medical Genetics Part A, 170(8), 2002–2011. http://doi.org/10.1002/ajmg.a.37721

Gerber, S., Charif, M., Chevrollier, A., Chaumette, T., Angebault, C., Kane, M. S., et al. (2017). Mutations in DNM1L, as in OPA1, result in dominant optic atrophy despite opposite effects on mitochondrial fusion and fission. Brain : a Journal of Neurology, 140(10), 2586–2596. http://doi.org/10.1093/brain/awx219

Hogarth, K. A., Costford, S. R., Yoon, G., Sondheimer, N., & Maynes, J. T. (2018). DNM1L Variant Alters Baseline Mitochondrial Function and Response to Stress in a Patient with Severe Neurological Dysfunction. Biochemical Genetics, 56(1-2), 56–77. http://doi.org/10.1007/s10528-017-9829-2

Narendra, D., Kane, L.A., Hauser, D.N., Fearnley, I.M., Youle, R.J., 2010. p62/SQSTM1 is required for Parkin-induced mitochondrial clustering but not mitophagy; VDAC1 is dispensable for both. Autophagy 6, 1090–1106. doi:10.4161/auto.6.8.13426

Shlevkov, E., Kramer, T., Schapansky, J., LaVoie, M. J., & Schwarz, T. L. (2016). Miro phosphorylation sites regulate Parkin recruitment and mitochondrial motility. Proceedings of the National Academy of Sciences, 113(41), E6097–E6106. https://doi.org/10.1073/pnas.1612283113

Vanstone, J. R., Smith, A. M., McBride, S., Naas, T., Holcik, M., Antoun, G., et al. (2016). DNM1L-related mitochondrial fission defect presenting as refractory epilepsy. European Journal of Human Genetics : EJHG, 24(7), 1084–1088. http://doi.org/10.1038/ejhg.2015.243

Waterham, H. R., Koster, J., van Roermund, C. W. T., Mooyer, P. A. W., Wanders, R. J. A., & Leonard, J. V. (2007). A lethal defect of mitochondrial and peroxisomal fission. The New England Journal of Medicine, 356(17), 1736–1741. http://doi.org/10.1056/NEJMoa064436

Whitley, B. N., Lam, C., Cui, H., Haude, K., Bai, R., Escobar, L., … Hoppins, S. (2018). Aberrant Drp1-mediated mitochondrial division presents in humans with variable outcomes. Human Molecular Genetics, 27(21), 3710–3719. https://doi.org/10.1093/hmg/ddy287

Wong, Y. C., Peng, W., & Krainc, D. (2019). Lysosomal Regulation of Inter-mitochondrial Contact Fate and Motility in Charcot-Marie-Tooth Type 2. Developmental Cell, 50(3), 339-354.e4. https://doi.org/10.1016/j.devcel.2019.05.033

Zaha, K., Matsumoto, H., Itoh, M., Saitsu, H., Kato, K., Kato, M., et al. (2016). DNM1L-related encephalopathy in infancy with Leigh syndrome-like phenotype and suppression-burst. Clinical Genetics, 90(5), 472–474. http://doi.org/10.1111/cge.12805